



UNIVERSITY OF
LEICESTER

DOCTORAL THESIS

Feeding Supermassive Black Holes through collisional cascades

Author:

Christian FABER

Supervisor:

Prof. Walter DEHNEN

*A thesis submitted in fulfilment of the requirements
for the degree of Doctor of Philosophy*

**Theoretical Astrophysics Group
Department of Physics and Astronomy
University of Leicester**

April 13, 2019

Declaration of Authorship

I, Christian FABER, declare that this thesis titled, “Feeding Supermassive Black Holes through collisional cascades” and the work presented in it are my own. I confirm that:

- This work was done wholly or mainly while in candidature for a research degree at this University.
- Where any part of this thesis has previously been submitted for a degree or any other qualification at this University or any other institution, this has been clearly stated.
- Where I have consulted the published work of others, this is always clearly attributed.
- Where I have quoted from the work of others, the source is always given. With the exception of such quotations, this thesis is entirely my own work.
- I have acknowledged all main sources of help.
- Where the thesis is based on work done by myself jointly with others, I have made clear exactly what was done by others and what I have contributed myself.

Signed:

Date:

UNIVERSITY OF LEICESTER

Abstract

College of Science and Engineering
Department of Physics and Astronomy

Doctor of Philosophy

Feeding Supermassive Black Holes through collisional cascades

by Christian FABER

The processes driving gas accretion on to supermassive black holes (SMBHs) are still poorly understood. Angular momentum conservation prevents gas within ~ 10 pc of the black hole from reaching radii $\sim 10^{-3}$ pc where viscous accretion becomes efficient.

In this thesis I present simulations of the collapse of a clumpy shell of swept-up isothermal gas, which is assumed to have formed as a result of feedback from a previous episode of AGN activity. The gas falls towards the SMBH forming clumps and streams, which intersect, collide, and often form a disc. These collisions promote partial cancellations of angular momenta, resulting in further infall and more collisions. This continued collisional cascade generates a tail of gas with sufficiently small angular momenta and provides a viable route for gas inflow to sub-parsec scales. The efficiency of this process hardly depends on details, such as gas temperature, initial virial ratio and power spectrum of the gas distribution, as long as it is not strongly rotating.

In order to assess the result more quantitatively, I reduce the numerically motivated inner boundary and find that the inner structure is affected to about 4 times the inner boundary radius in the case of eccentric inflows. In this context I also discuss some tentative evidence that the collisional cascade may minimise any pre-existing preferential orientation of the angular momentum.

Finally I present a preliminary analysis on the prevalence of disc disruption and destructions and the affect of dense, self-gravitating clumps in discs. These findings may provide an explanation for the missing star formation disc of the O-stars inside the central parsec of our Milky Way and the discrepancy between the total mass required to form the observed stars and the at least by a magnitude higher mass that must have eventually fed Sgr A*, created an wide-angle outflow and subsequently caused the Fermi bubbles.

Acknowledgements

I thank my supervisor Walter Dehnen for giving me the opportunity of undertaking the work in the first place, providing me with his high-performance SPH-code SPHINX and discussing a plethora of ideas regarding how to approach the various aspects of my research. In particular I like to thank Hossam Aly, Martin Bourne and Sergei Nayakshin for having always an open ear and their enthusiasm for discussions surrounding everything that touches supermassive black holes. I further like to thank the so far not mentioned staff members of the theory group: Andrew King (my second supervisor), Richard Alexander, Graham Wynn, Mark Wilkinson and Chris Nixon for many interesting discussion during the weekly group meetings and the (not quite) weekly AstroPh sessions. A special thanks goes out to Lisa Brant, especially for organising everything surrounding my travel to conferences, and the IT staff for their swift responses -in particular Gary Gilchrist and Jon Wakelin.

I am also grateful to all the post-docs and students, who made the four years in the "bat cave" so interesting and enjoyable: Stuart, Stephen, Giovanni, Cas, Bec and Hastyar, Hossam, Martin, Tom, Hasan, Mark, Lilian, Amery, Rob, Elen, Jack, Anagha, Giulia and "new" Tom.

Finally I would like to extend my heartfelt thanks in particular to Keziah, my family and Liam, who provided me with much support and encouragement throughout my PhD and the writeup of this thesis.

Research in Theoretical Astrophysics at Leicester is supported by STFC grant ST/M503605/1. Some calculations presented in this paper were performed using the ALICE/ALICE2 High Performance Computing Facility at the University of Leicester. Some resources on ALICE form part of the DiRAC Facility jointly funded by STFC and the Large Facilities Capital Fund of BIS. This work used the DiRAC Data Analytic system at the University of Cambridge, operated by the University of Cambridge High Performance Computing Service on behalf of the STFC DiRAC HPC Facility (www.dirac.ac.uk). This equipment was funded by BIS National E-infrastructure capital grant (ST/K001590/1), STFC capital grants ST/H008861/1 and ST/H00887X/1, and STFC DiRAC Operations grant ST/K00333X/1. DiRAC is part of the National E-Infrastructure.

Contents

Declaration of Authorship	i
Abstract	ii
Acknowledgements	iii
1 Introduction	1
1.1 Across time and space	1
1.2 The black hole	3
1.2.1 Theoretical predictions	3
1.2.2 Observational evidence	5
1.3 Stellar mass black holes	9
1.3.1 Accretion disc	10
1.4 Supermassive black holes	13
1.4.1 Formation	15
1.4.2 Growth and feedback	16
1.5 Structure of thesis	24
2 Smoothed Particle Hydrodynamics	26
2.1 The theoretical laboratory	26
2.2 Smoothed Particle Hydrodynamics	27
2.2.1 Smoothing kernel	27
2.2.2 Gravity	28
2.2.3 Artificial viscosity	30
2.2.4 Timesteps	31
3 Feeding SMBHs by gaseous collapse	32
3.1 Introduction	32
3.2 Modelling approach	36
3.2.1 The hydrodynamical method	36

3.2.2	Generation of turbulence	36
3.2.3	Initial conditions and model setup	37
3.3	The reference simulations	40
3.3.1	A detailed look at a representative simulation	47
3.3.2	Simulations differing only by the random seed	51
3.4	Effects of varying the parameters	53
3.4.1	Sound speed	53
3.4.2	Power spectrum of the turbulent velocity field	55
3.4.3	Balance between rotation and turbulence	57
3.4.4	Solenoidal velocity field	59
3.4.5	Mass of the initial gas shell	59
3.4.6	Width of the initial gas shell	61
3.4.7	The initial kinetic energy of the gas	61
3.5	Discussion	63
3.6	Conclusion	65
4	Collisional cascades enhance feeding of SMBHs	68
4.1	Introduction	68
4.2	Simulation setup	73
4.3	Convergence	74
4.4	The collisional cascade	81
4.5	Will gaseous infall always be chaotic?	84
4.6	Discussion and conclusion	91
5	Application to the Galactic Centre	93
5.1	Introduction	93
5.2	Initial conditions	99
5.3	Disc destruction	102
5.4	Self-gravity	107
5.5	Discussion and conclusion	114
6	Conclusions	118
6.1	Feeding of SMBHs via collisional cascades	118
6.2	Comparison to the Centre of Milky Way	121
6.3	Future work	122

Bibliography

List of Figures

1.1	Momentum driven feedback diagram taken from King, 2010	21
1.2	$M_{\bullet} - M_{bulge}$ and $M_{\bullet} - \sigma$ relation taken from Kormendy and Ho, 2013	23
3.1	Distribution of r_{circ} over <i>eccentricity</i> for Seed A at $t = 0$	41
3.2	Overview plots for Seed A at $t = 0.5$	42
3.3	Overview plots for Seed A at $t = 1.0$	43
3.4	Overview plots for Seed A at $t = 1.5$	44
3.5	Overview plots for Seed A at $t = 2.0$	45
3.6	Overview plots for Seed A at $t = 3.0$	46
3.7	Density plots of different seeds at $t = 1$	49
3.8	Distribution of e over r_{circ} for different seeds at $t = 3$	50
3.9	Time over mean r_{circ} and e of a range of gas fractions for different seeds	52
3.10	Time over mean r_{circ} and e of a range of gas fractions for different soundspeeds, c_s	54
3.11	Time over mean r_{circ} and e of a range of gas fractions for different power spectra, k	56
3.12	Time over mean r_{circ} and e of a range of gas fractions for different balances between rotation and turbulence, χ	58
3.13	Time over mean r_{circ} and e of a range of gas fractions for a solenoidal velocity field	60
3.14	Time over mean r_{circ} and e of a range of gas fractions for different widths of the initial shell, r_{width}	62
4.1	Schematic of how the inner boundary affects the orbit of SPH particles	71
4.2	Density plot for Seed A at $t = 1.5$ for varying r_{sink}	75
4.3	Distributions over r_{circ} and e for different r_{sink}	76

4.4	Convergence test for $r_{\text{sink}} = 0.005$	78
4.5	Convergence test for $r_{\text{sink}} = 0.0025$	79
4.6	Convergence test for $r_{\text{sink}} = 0.001$	80
4.7	Time evolution of mean r_{circ} and e for different r_{sink}	82
4.8	Distributions over initial and final r_{circ} for different r_{sink}	83
4.9	Cumulative distribution over the final r_{circ} for three initial values	85
4.10	Density plot for Seed D at $t = 1.5$	87
4.11	$\cos \theta$ over time for $\chi = 0.5$	88
4.12	$\cos \theta$ over time for $\chi = 0.75$	89
4.13	$\cos \theta$ over time for $\chi = 1$	90
5.1	Finding chart of the mini-spiral taken from Tsuboi et al., 2017	98
5.2	Density plot for Seed B at $t = 1$ for varying ϵ	101
5.3	Time over mean r_{circ} and e of a range of gas fractions for different ϵ	103
5.4	Density plots for Seed B at $t = 0.65 - 0.81$	104
5.5	Distribution of r_{circ} over time for absorbed particles	106
5.6	Density plots with self-gravity of Seed A at $t = 1.21$	109
5.7	Density plots with self-gravity of Seed B at $t = 1.21$	110
5.8	Time over mean r_{circ} and e of a range of gas fractions for different M_{shell} with self-gravity	112
5.9	Time over mean r_{circ} and e of a range of gas fractions for different M_{shell} with self-gravity	113
5.10	Distribution of r_{circ} over time for absorbed particles with self-gravity	115

List of Tables

3.1 Table providing an overview of the various physical parameters tested	38
---	----

List of Abbreviations

AGN	Active Galactic Nucleus
AV	Artificial Viscosity
BAL QSO	Broad Absorption Line Quasars
BH	Black Hole
BLR	Broad emission Line Region
CDM	Cold Dark Matter
CND	Circum-Nuclear Disc
CNR	Circum-Nuclear Ring
CMB	Cosmic Microwave Background
HST	Hubble Space Telescope
IMBH	Intermediate Mass Black Hole
ISCO	Inner Most Stable Orbit
ISM	InterStellar Medium
LINER	Low-Ionisation Nuclear Emission Region
MRI	Magneto-Rotational Instability
SMBH	Super Massive Black Hole
SPH	Smoothed Particle Hydrodynamics
UFO	Ultra-Fast Outflows

To my family and especially my grandpa.

Chapter 1

Introduction

1.1 Across time and space

Across time and space human kind has been, is and likely will continue gazing up to the sky. This fascination is stirred by the sparkle that represents both stars close and far, part of clusters and even whole galaxies -in short: The Universe itself. However, it is not just the ancient light from galaxies far, far away that transcends this time and space. Looking back throughout our history and across the world we discover evidence of this allure that often went beyond mere philosophical (e.g. the Greek philosophers, see Runes, 2001) or even religious practices (e.g. Egyptian pyramids positioning, see Shaltout and Antonio Belmonte, 2005; Waziry, 2016). The Aztecs used the perceived changes in position of the stars to guide their harvest (Šprajc, 2016) and sailors operated increasingly complex tools to navigate across the oceans successfully (Swanick, 2006).

The realisation of its various practical purposes together with the unquenchable desire to satisfy human curiosity has elevated Astronomy; from relatively simple observation with the eye (diameter < 1 cm) to telescope projects like the AstronRadio. The latter combine telescopes both on Earth and in space into a virtual one that spans more than half the distance between Earth and the Moon (diameter $\sim 250,000$ km) thanks to clever use of interferometry (Kardashev et al., 2017). Equally, the associated techniques have changed considerably from incredulous noting down of the observed positions of planets and stars to the strong predictive power of mathematical theory (e.g. Newton's *Principia*, Kepler's *Astronomia Nova* or the theories of relativity by Einstein; see Newton, Motte, and

Cajori, 1966; Kepler and Donahue, 1992; Einstein, 1905; Einstein, 1915) and simulations solved by huge clusters of computers (e.g. Angulo et al., 2012; Vogelsberger et al., 2014; Schaye et al., 2015; Potter, Stadel, and Teyssier, 2017) based on the curious interplay of formulas, observational data and a degree of sophisticated guessing to ensure the fine balance between feasible computation times and avoiding oversimplifications of the physics involved.

Progress has been made not only by using advanced technology (e.g. to find the eight planets of the Solar system like Galileo's work in the 16-17th century), but also by re-evaluating and consequently changing existing theories (e.g. moving from the geocentric model standardised by Ptolemy to the heliocentric modern view brought to wider attention by Copernicus). While these classic examples of scientific progress appear to be part of a bygone era, one has to go back only a few decades to find that the multitude of galaxies we analyse in great detail nowadays were referred to as mere nebulae (Curtis, 1988) and Venus was thought to be a lush jungle-covered planet (Mayer, McCullough, and Sloanaker, 1958) and not the smouldering, toxic wasteland we know it is today (Hashimoto et al., 2008).

It seems fitting to begin with the perceived beginning of the Universe -at least as we know it. It is thought to have started with the Big Bang about 13.7×10^9 yr (Planck Collaboration et al., 2016). The theoretical possibility of an expanding Universe was first derived, based on Einstein's general relativity theory (Einstein, 1915), by Friedmann, 1922. The first observational evidence confirming this suggestion was discovered by measuring how fast surrounding galaxies are accelerating away from us (Hubble, 1929). Lemaître, who already proposed a link between the earlier findings of Friedmann and Hubble, concluded that any expansion must have an origin (Lemaître, 1931) -the Big Bang as it was called two decades later. Work on stellar nucleosynthesis (Burbidge et al., 1957) led to good agreements between measured and predicted abundances of elements like hydrogen, helium and lithium (Hoyle and Tayler, 1964), which further supported the idea of an expanding Universe. The theory became widely accepted with the discovery of the Cosmic Microwave Background (CMB; see Penzias and Wilson, 1965). Modern measurements provide some of the most accurate estimates of the cosmological constants, which form the standard picture of Universe called the Lambda cold dark matter (λ -CDM) model (Planck Collaboration et al., 2014; Planck Collaboration et al., 2016).

In the last decade a number of observations of galaxies with high redshift

have indicated that some of the earliest examples have formed in the first 1×10^9 years after the Big Bang (e.g. Oesch et al., 2015; Zitrin et al., 2015; Oesch et al., 2016) potentially coinciding with the start of the re-ionisation era (Oesch et al., 2016), which made the Universe transparent and allows Astronomers to detect such extremely old objects in the first place. The web-like appearance of the CMB is imprinted on the large scale structures of galaxy clusters in which galaxies form in a hierarchical fashion (e.g. Geller and Huchra, 1989; Dubinski, 1998; Cole et al., 2000). Following the top-down model the large-scale collapse of gaseous matter (Eggen, Lynden-Bell, and Sandage, 1962), however see (Searle and Zinn, 1978) for an alternative model, leads eventually to the formation and evolution of common features like galactic discs and bulges (e.g. Noguchi, 1999; Tonini et al., 2016; Nelson et al., 2016; Clauwens et al., 2018).

The aforementioned galaxies or more precisely the object at their heart shall be the focus of this thesis: A supermassive black hole.

1.2 The black hole

Nowadays the existence of black holes is widely accepted in the scientific community and it has spread to common knowledge thanks to a plethora of cameos in films and literature often depicting it as an all-consuming void. As the theory and impact of these objects has gained importance in the last hundred years, it is worth noting that the concept is more than twice as old.

1.2.1 Theoretical predictions

Combining Newton's work both on the theory of gravity (Newton, Motte, and Cajori, 1966) and the idea that light could be made out of minuscule, but distinct bodies led John Michell in 1783 and Pierre-Simon Laplace in 1796 to the argument that even light must feel the gravitational attraction of massive bodies (see Schaffer, 1979).

The problem can be simplified by assuming a system of two spherical bodies. Body A is more massive and the only gravitational relevant source for body B , which itself is moving radially away from the former at the escape velocity v_{esc} . Therefore the velocity of B will reach zero at an infinite distance leading to

both the kinetic and potential energy of the system to be zero at this final state. Utilising the conservation of energy, one obtains the following expression:

$$\frac{1}{2}mv_{\text{esc}}^2 + \frac{-GMm}{R} = 0 + 0 \quad (1.1)$$

$$v_{\text{esc}} = \sqrt{\frac{2GM}{R}}, \quad (1.2)$$

where m is the mass of the escaping object, v_{esc} the minimum velocity to escape the object with mass M , r the distance between both objects and G the gravitational constant.

While the measurement of the speed of light has been attempted before (including by Galileo), Rømer successfully used the the time difference of the period of the moon Io caused by the Earth apparent movement towards or away from Jupiter to conclude that light travelled at a finite velocity in 1676 (see Cohen, 1940). Newton in his "Opticks" work in 1704 and later John Bradley in 1729 based on the aberration of light refined the value close to its modern value of $c \sim 3 \times 10^5$ km/s. Using Equation 1.1 and c for v_{esc} , it immediately follows that there might be objects so massive that not even light can escape -the object would appear dark. Michell came to the same conclusion more than 2 centuries ago and indeed referred to these objects as "dark stars". In fact he argued that there might be many such "dark stars" and that one may detect these objects by their interaction with a visible companion star (see Schaffer, 1979) -later on it will be described how these suggestions indeed turned out to be true.

Equation 1.1 can be also reformulated given a known mass to define the radius at which point nothing can escape:

$$R_S = \frac{2GM_{\bullet}}{c^2}, \quad (1.3)$$

where R_S is the Schwarzschild (1916) radius. Incidentally Schwarzschild derived this formula despite its Newtonian appearance as part of the first exact solution of Albert Einsteins general relativity equations (Einstein, 1915). However, Equation 1.3 holds only for non-rotating and spherically symmetric objects. The other three solutions are for a charged, non-rotating black hole (Reissner, 1916; Nordström, 1918); a purely rotating black hole (Kerr, 1963) and finally a charged, rotating one (Newman and Janis, 1965). It is worth noting, that all black holes can

be described by only three previously mentioned properties: a mass M , angular momentum (often parameterised as spin a or more commonly its dimensionless form computed by a/M_{\odot}) L and an electric charge Q (see e.g. Israel, 1967; Robinson, 1975).

With the spreading realisation that these objects might exist, the question how and under what conditions they may form arose naturally. The precursor to a potential formation channel was the work on dense stars and how degeneracy pressures may resist collapse e.g. for white dwarfs (Stoner, 1930) leading to the conclusion by Chandrasekhar, 1931 of the maximum stable mass for a white dwarf of slightly more than a solar mass. Shortly after the discovery of neutrons (Chadwick, 1932) a higher value was calculated for the upper mass limit for neutron stars in which neutron degeneracy pressure counteracts the increased density (Oppenheimer and Volkoff, 1939). Consequently black holes were theorised to be the end product, if those mass limits were exceeded (Oppenheimer and Snyder, 1939) and current estimates, thanks to the great success of gravitational wave astronomy in recent years, put the limit to $\sim 2.2M_{\odot}$ (e.g. Shibata et al., 2017; Ruiz, Shapiro, and Tsokaros, 2018; Cho, 2018).

1.2.2 Observational evidence

In hindsight observational signatures of (super massive) black hole activity can be found even before the Schwarzschild solution was derived: for example both Fath (1909) and Slipher (1917) observed an unexplained bright feature in the centre of some galaxies. It took several decades before it was realised that these were examples of an entire group called Seyfert galaxies (e.g. Seyfert, 1943; Burbidge, Burbidge, and Prendergast, 1963; Maiolino and Rieke, 1995).

A further decade later, as a result of the development of radio telescopes, a few bright radio sources were matched with optical counterparts, which in turn were identified as galaxies (e.g. Baade and Minkowski, 1954; Burbidge and Burbidge, 1962). Assuming the strong polarisation of the emission is caused by synchrotron radiation (Elder et al., 1947), an electromagnetic radiation produced by charged, relativistic particles with a radial acceleration, it was suggested that the energy output of M87 could be as large as $\sim 10^{61}$ erg/s (compared to the Sun output of merely $\sim 10^{19}$ erg/s, see Burbidge, 1956) and later concluded based on further

similar findings in other galaxies that some kind of powerful process must be associated with the nuclei of these galaxies (e.g. Burbidge, Burbidge, and Sandage, 1963; Rees, 1975).

So called quasars (shortened from quasi-stellar) are another type of bright radio objects, however, at first they were only detected as radio source before their optical counterpart was discovered contrary to the detection of Seyfert galaxies. Even after they were identified, the objects appeared as an unresolved, stellar like spectrum due to their large redshifts (e.g. Schmidt, 1963; Greenstein, 1963; Schmidt and Matthews, 1964), which led to the aforementioned name. Equipped with the knowledge of the nature of the optical counterparts, even more galaxies were discovered that featured the stellar like spectra in their centre, however, many featured no strong radio emission and therefore were called radio-quiet in opposite to the radio-loud mentioned above (Sandage, 1965). Further noteworthy types of active galaxies are low-ionisation nuclear emission line regions (LINER, e.g. Heckman, 1980; Ho, Filippenko, and Sargent, 1997). However, see e.g. Terlevich and Melnick, 1985, for a different interpretation. Another type are Blazars of which the original discovered quasar belongs (e.g. Schmidt, 1963; Urry et al., 2000) to. There are many more subcategories and often the border between the classes are fluid. Attempts have been made to unify the different groups by essentially arguing that different viewing angles produce the plethora of Active Galactic Nuclei (AGN) types including those based on the properties of the associated radio jets (e.g. Fanaroff and Riley, 1974; Barthel, 1989; Antonucci, 1993; Urry and Padovani, 1995; Podigachoski et al., 2015; Chen et al., 2015).

The name "quasi-stellar" already reveals that those first observations were resolution limited placing the source of the luminosity only to small sizes centred on the nuclei of the galaxies (e.g. Morris, Palmer, and Thompson, 1957; Allen et al., 1962). However, with an increased catalogue of follow-up observations, short variabilities of about a year were recognised, which in turn can be used together with the speed of light to reduce the source size estimate to ~ 1 pc (e.g. Smith and Hoffleit, 1961; Smith and Hoffleit, 1963; Manwell and Simon, 1966; Usher et al., 1969) and in fact X-ray observations place the timescales even to minutes suggesting source sizes of ~ 0.3 pc and smaller (e.g. Bowyer et al., 1970; Ives, Sanford, and Penston, 1976; Yang et al., 2016) -for review see e.g. (Ulrich, Maraschi, and Urry, 1997).

The compactness of the source producing these vast amounts of energy quickly

led to several theories about how it could be produced: at first mergers, which later will be shown to play an important role in funnelling gas towards the centre of the galaxy (Heckman et al., 1986), were suggested in form of the colliding gas as a radio source (e.g. Burbidge et al., 1957; Burbidge, 1958; Harrower, 1960). Further suggestions presented stellar sources (typically their explosive end, see e.g. Burbidge, 1961; Hoyle and Fowler, 1963; Terlevich and Melnick, 1985, however, see Cameron, 1962, for a different interpretation) or even intergalactic clouds with weak magnetic fields to account for the measured polarisation (Burbidge, 1958). It became quickly apparent that these ideas were incorrect partly due to the limited resolution of the available observational data or unphysical assumptions like a too high rate of supernovae explosions required by those models (Cameron, 1962).

Instead it was argued that the accretion upon a massive, compact object and the associated release of the vast quantities of gravitational energy might be both creating those central objects and power the observed emissions (e.g. Salpeter, 1964; Zel'dovich, 1964; Lynden-Bell, 1969). Lynden-Bell further suggested that supermassive black holes (SMBHs) also reside in nearby galaxies in form of "dead quasars" and that Seyfert (1943) galaxy emission was powered as well by the process of accretion upon a SMBH (Lynden-Bell, 1969). Subsequent work confirmed this type of source of the observed luminosities (e.g. Wolfe and Burbidge, 1970; Lynden-Bell and Rees, 1971; Pringle and Rees, 1972; Bardeen, Press, and Teukolsky, 1972).

Finally, Soltan (1982) assumed the count of quasars and their respective luminosity density and a 10 percent converting mass into radiation efficiency leading to the suggestions that there should be $10^5 - 10^6$ SMBHs (with a mass of $10^8 - 10^9 M_{\odot}$) per 1 Gpc^3 . Hence it is strongly suggested that every massive galaxy contains a SMBH at its centre (e.g. Soltan, 1982; Kormendy and Richstone, 1995; Kormendy and Ho, 2013).

Galaxies that produce these vast amounts of energy are called active galaxies while their innermost region, which is the source of the energy output, is called an active galactic nucleus (AGN). These AGN include the just introduced quasar and Seyfert galaxies. However, astronomers sometimes refer to AGN as the whole galaxy as well and not exclusively to the active SMBH for the sake of simplicity.

As the existence of these massive objects at the centre of galaxies became commonly accepted, attempts were naturally made to observe them and measure

their masses, although this is typically achieved only by indirect means. The first successful measurement of SMBH mass was achieved by determining the velocity dispersion of stars, which appeared to not fit the models for the central part. This led to the requirement of a "dark mass" of $\sim 5 \times 10^9 M_{\odot}$ at the centre of M87 (e.g. Sargent et al., 1978; Dressler and Richstone, 1988; Dressler and Richstone, 1990; Kormendy and Richstone, 1992). The application of theoretical models of luminosity profiles to the same data resulted in a similar result (Young et al., 1978; for other examples see e.g. van der Marel et al., 1997). The angular resolution limiting seeing that plagues ground-based observations could be avoided with the availability of the Hubble Space Telescope (HST) and consequently a small disc of ionised gas in the centre of M87 was revealed (e.g. Ford et al., 1994; Bahcall, Kirhakos, and Schneider, 1994; Lauer et al., 1995; Ferrarese, Ford, and Jaffe, 1996; van der Marel and van den Bosch, 1998). The spectra of the disc indicated Keplerian rotation with measured velocities of hundreds of km/s suggesting a slightly lower mass (Harms et al., 1994). Modern estimates, however, find a mass of $\sim 7 \times 10^9 M_{\odot}$ using a combination of different tracers (Oldham and Auger, 2016). Besides the use of Doppler shift measurements of stellar absorption or gas emission lines, reverberation mapping is another important technique to measure SMBHs. The flux variations of the broad emission line region (BLR) is used to measure its size, which leads together with measurements of the root-mean-square velocity of the gas contained in this region to a mass estimate of the SMBH (e.g. Blandford and McKee, 1982; Peterson et al., 2002; Homayouni et al., 2018).

I previously alluded to prevalence of SMBHs in most if not all galaxies - naturally this should include our own Milky Way as well and due to its relative proximity should provide an unique testbed both for theory and observational techniques. The first hints of a radio source at the centre of the Milky Way was discovered by Jansky, 1933. After attributing different patterns to local sources like thunderstorms, he realised that one signal was repeating just under 24 hours. This value agreed well with the rotation time of the Earth with respect to a fixed source in the sky. In fact the results suggested that the source of these radio signals originates from the centre of the Milky Way (Jansky, 1933). Decades later Balick and Brown, 1974, identified the source as Sgr A*, however, whether this was identical to a SMBH was debated until measurements of the velocity variations of fine structure emissions inside the sphere of influence (the volume gravitationally dominated by the SMBH) indicated a central mass of up to $4 \times 10^6 M_{\odot}$ (e.g.

Serabyn and Lacy, 1985; Miyoshi et al., 1995). Thanks to the increasing ability to resolve smaller and smaller scales, noticeably larger velocity dispersions were found for stars inside 0.1 pc compared to those further out. This led to the suggestion of compact dark mass of up to $\sim 3 \times 10^6 M_{\odot}$, which was argued to be either a SMBH or a cluster of stellar black holes (Genzel et al., 1996). Monitoring of stars even closer to the proposed SMBH (S2's pericentre is ~ 120 AU, see Gravity Collaboration et al., 2018), the orbit of a star named "S2" could be predicted with good certainty leading to a new mass estimate close to the originally suggested value by Serabyn and Lacy, 1985; Boehle et al., 2016. However, this time the data excluded the option of a dense cluster of stellar objects and therefore confirming the existence of SMBH (e.g. Schödel et al., 2002; Ghez et al., 2008). More recently the same star allowed the successful test of Einstein's theories of relativity (Einstein, 1905; Einstein, 1915) as it passed its pericentre producing a measurable relativistic Doppler effect (Gravity Collaboration et al., 2018).

A more direct observational signature could potentially arise from the event horizon shadow (e.g. Falcke, Melia, and Agol, 2000; Pu and Broderick, 2018) targeting a central area as small as $\sim 10^{-6}$ pc. Projects (e.g. the Event Horizon Telescope, see for example Fish et al., 2011) utilising very long baseline interferometry (like telescopes placed across different countries) have struggled to achieve this impressive feat (e.g. Doeleman et al., 2008; Fish et al., 2011). More recent work, however, is based on resolved structures (e.g. Johnson et al., 2015; Fish et al., 2016; Broderick et al., 2016). Given the extreme resolutions required, observations like these are currently limited to our own SMBH and M87, which is further away, but also significantly more massive and therefore larger. At the point of writing this thesis, about one petabyte of data produced in the 2017 observation run is still being analysed and no data potentially showing the inner accretion disc has been published yet.

1.3 Stellar mass black holes

While this thesis considers mainly a simulated abstraction of a SMBH, it is worth discussing their (significantly) smaller relative: the stellar mass black hole with masses typically not exceeding $100 M_{\odot}$. Recalling Michells predictions earlier, one may expect many stellar mass black holes, however, even if because of this some are noticeably closer to us, their size or rather their impact on its environment is

also smaller. Hence we are once again left with Michell's other prediction, that those objects might be best inferred by their interaction with a companion.

Similar to the detection of the first hints of the existence of SMBHs, observations of high energy producing systems have been used to guide the search for stellar mass black holes. X-ray binaries are such systems and their emission is thought to be caused by the accretion onto a potential stellar mass black hole (Shklovsky, 1967). The first such candidate was Cygnus X-1 thanks to its appearance as one of the strongest X-ray sources in the sky (e.g. Prendergast and Burbidge, 1968; Webster and Murdin, 1972; Bolton, 1972) with a mass of $\sim 15M_{\odot}$ and a slightly more massive companion star (Orosz et al., 2011). The recent success of detecting gravitational waves emitted from a merger event provides another channel of observations including systems featuring two black holes, that would be otherwise very likely invisible (Abbott et al., 2016).

Detailed observations of stellar mass black holes have paved the way to a better understanding of the process involved with SMBH (e.g. Frank, King, and Raine, 2002; King and Pounds, 2003).

1.3.1 Accretion disc

The concept of the accretion disc may well be one of the most widely applicable ones in astrophysics ranging from proto-planetary disc (e.g. Joy, 1945; Herbig, 1960; Armitage and Hansen, 1999; Rice et al., 2003; Dipierro et al., 2015), Roche-lobe overflow in binary star systems (e.g. Prendergast and Burbidge, 1968; Webster and Murdin, 1972) all the way up to the accretion discs around SMBHs (e.g. Ford et al., 1994; Fish et al., 2016; Broderick et al., 2016).

The fundamental ingredients for the formation of such a disc is a gravitationally dominant central body and bound gaseous material with enough angular momentum to not be able to fall in straight away. If the gas can radiate away its energy, angular momentum conservation leads to the formation of a circular disc at the circularisation radius r_{circ} (e.g. Prendergast and Burbidge, 1968; Pringle, 1981). Furthermore, if a process exists that can transport angular momentum outwards, material can be accreted by the central object leading to the name accretion disc (e.g. Shakura and Sunyaev, 1973; Lynden-Bell and Pringle, 1974).

As everything in space is in motion, everything must have momentum and angular momentum with respect to the gravitational dominant source. For example the collapse of molecular gas clouds due to efficient cooling or shocks caused by wind of e.g. other stars or even supernovae can lead to the formation of stars (e.g. Larson, 1981; Kennicutt, 1998; Jog and Solomon, 1992; Keto, Ho, and Lo, 2005). Using ammonia line emissions, the specific angular momentum of such a cloud was measured to be $10^{21} \lesssim j_{core} \lesssim 10^{22} \text{ g}^2/\text{cm}$, where j_{core} is the specific angular momentum of the core region (Goodman et al., 1993). If one considers the core to be the gravitationally dominant region, one can assume roughly Keplerian orbits for the outer parts using

$$j_{Kepler} = \sqrt{GM_{\bullet}R} \quad (1.4)$$

one obtains a radius about 6 magnitudes too large assuming $M_{\bullet} \sim M_{\odot}$. The only consequence of that much angular momentum can be the formation of an accretion disc and in fact this is true not just for stars, but also for stellar and supermassive black holes (see Section 1.4.2).

More complex interactions with the disc -may it be by a body perturbing the disc directly (e.g. Goldreich and Tremaine, 1979; Armitage and Hansen, 1999; Tanaka, Takeuchi, and Ward, 2002) or gas falling onto it (e.g. Nixon et al., 2011; Zubovas, 2015; Faber and Dehnen, 2018)- cannot be solved analytically and require numerical simulations to match observations and further the theory (see Section 2.1).

Gas that crossed the innermost stable orbit (ISCO, see Bardeen, Press, and Teukolsky, 1972) will essentially fall straight into the black hole producing large amounts of energy in the form of X-rays (Shklovsky, 1967). This concept remains the same, if one accounts for the deeper gravitational potential caused by the SMBH resulting in larger amounts of liberated energy (see Section 1.2.2).

Once a disc has formed, mass is transported inwards and angular momentum outwards by viscosity (proposed for differentially rotating stars by Goldreich and Schubert, 1967). The viscous time can be given as:

$$t_{\nu} \sim \frac{R^2}{\nu}, \quad (1.5)$$

where ν is the kinematic viscosity and R the radius.

The transport might be facilitated via turbulence and while this suggestion remains uncertain, Shakura and Sunyaev (1973) were able to show that the physics of the viscosity can be "hidden" inside a parameter α allowing one not to know the precise source of the viscosity, as the formula depends on c_s and H , which are functions of temperature. The resulting viscosity, therefore, depends on local disc properties:

$$\nu = \alpha c_s H = \alpha H^2 \Omega, \quad (1.6)$$

where α is the parameterised viscosity, c_s the sound speed and H the scale height of the disc. Equation 1.6 holds true, if one assumes that the eddies of the turbulence are subsonic and smaller than H .

The viscous torque between two radii of a disc is proportional to the gradient of the respective radial velocity resulting in an outward flow of the angular momentum and inward flow of material for a disc of decreasing radial velocity with increasing distance (e.g. as is the case for a Keplerian disc, see Lynden-Bell and Pringle, 1974). An early physical representation for this viscosity was the suggestion of molecular viscosity, but it was immediately ruled out on grounds that the estimate for the viscous timescale is orders of magnitudes larger than any estimates for disc lifetimes (Pringle, 1981). Other models suggested that convection might be enough to explain the low conductivity of T Tauri discs (e.g. Cameron, 1978; Lin and Papaloizou, 1980) or non-magnetic hydrodynamic (e.g. thermal) instabilities (e.g. Shakura, Sunyaev, and Zilitinkevich, 1978; Dubrulle, 1992). However, flaws with the idea were quickly pointed out like the perturbations arising in a Keplerian disc may be to a degree stabilised by Coriolis forces disfavouring the convective case (Ryu and Goodman, 1992).

This physics behind this parameterisation is commonly thought (although by no means certain or even properly understood) magneto-rotational instability (MRI) causing ionised parts of the disc to exert a force due to the differential motion at different radii inside a weak magnetic field (Balbus and Hawley, 1991). The MRI slows down the inner, faster moving parts of the disc, while it speeds up the outer, slower moving ones leading to an outward angular momentum transport as described earlier. The instability results in turbulence and consequent mixing of the material, which allows the process to remain active.

Simulations of MRI show that it can produce an α (see Equation 1.6) between

$10^{-3} \lesssim \alpha \lesssim 10^{-1}$ (e.g. Hawley, Gammie, and Balbus, 1995; Stone et al., 1996). However, observational evidence suggests 10^{-2} for protoplanetary discs (e.g. Gullbring et al., 1998; Hartmann et al., 1998) and of order 10^{-1} for black holes (e.g. Smak, 1999; Lasota, 2001; King, Pringle, and Livio, 2007).

Over the years a number of results highlighted the potential restrictions or even downfalls of the models as its requirement for disc to be (partially) ionised. While this might be true for a hot enough disc ($T_{crit} \sim 800$ K, see Umebayashi and Nakano, 1988), colder discs may require external sources like cosmic X-rays (Glassgold, Najita, and Igea, 2004). It might be unlikely that the whole disc can be ionised and there might be shielded zones in the midplane, where MRI should not have any effect (e.g. Gammie, 1996; Gressel et al., 2013; Perna, Lazzati, and Giacomazzo, 2016; Martin et al., 2018).

1.4 Supermassive black holes

It is widely agreed upon that most, if not all massive galaxies contain a SMBH in their centre (see reviews e.g. by Kormendy and Richstone, 1995; Richstone et al., 1998; Kormendy and Ho, 2013). More recent observations extend this statement to some dwarf galaxies as well (e.g. Greene and Ho, 2004; Reines, Greene, and Geha, 2013; Mezcua et al., 2018), but due to the increased difficulties associated with observing these often low luminosity objects, the topic is still a matter of debate and intermixed with claims for intermediate mass black holes (e.g. Mezcua et al., 2018; Pacucci et al., 2018). This immediately suggests a close connection with the host galaxy and one may be intuitively drawn to imagine parallels to our own Solar system by replacing the Sun with the SMBH and instead of planets the galaxy has a myriad of stars swirling around its core. However, gravity follows an inverse square-law and therefore the SMBH dominates only a tiny fraction (of order pc) of the galaxy (of order kpc). The volume a massive object dominates is referred to as the sphere of influence: Its extend is described by the velocity dispersion $\sigma(r)$ of the surrounding matter having to be equal to the orbital speed v_{orb} resulting from the gravity of the massive object like a SMBH (e.g. Peebles, 1972; Frank, King, and Raine, 2002)

$$|v_{orb}| = \sqrt{\frac{GM_{\bullet}}{r}} = \sigma(r). \quad (1.7)$$

If one assumes typical values for M_\bullet and σ (Frank, King, and Raine, 2002; Merritt, 2004), one obtains:

$$r_{inf} = \frac{GM_\bullet}{\sigma_\bullet^2} \sim 10.8\text{pc} \left(\frac{M_\bullet}{10^8 M_\odot} \right) \left(\frac{\sigma(r_\bullet)}{200\text{kms}^{-1}} \right)^{-2}. \quad (1.8)$$

Accordingly r_{inf} changes to ~ 0.1 pc for a smaller SMBH comparable to the Sgr A* (accounting for more applicable values for σ this value approaches roughly 1 pc). Another definition of this quantity is the mass of stars inside the sphere of influence is $M_\star(r < r_{inf}) = 2M_\bullet$, which is equivalent to Equation 1.8 assuming a singular isothermal sphere (distribution of the stars with constant velocity dispersion and density proportional to $1/r^2$). The advantage of defining the mass of the stars inside the radius r_{inf} to be twice the mass of the SMBH, is that it can be adapted for other stellar density power laws (Merritt, 2004).

Another commonly used reference radius is named after Bondi (1952) for which the gravitational potential (e.g. the escape velocity) is set equal to the specific thermal energy of the gas (e.g. the sound speed), which leads to (e.g. Frank, King, and Raine, 2002)

$$r_{Bondi} = \frac{2GM_\bullet}{c_s^2}. \quad (1.9)$$

The definition in conjunction with work by Hoyle and Lyttleton (1941) and Bondi and Hoyle (1944) is frequently used especially in cosmological simulations (e.g. Di Matteo et al., 2008; DeGraf and Sijacki, 2017; Grand et al., 2017; Stevens et al., 2017) to obtain sub-grid models that compute the mass accretion rate onto the SMBH as the required scales are often beyond the resolution limit to compute the rates directly. Essentially the flow outside of the radius is treated as subsonic, while beyond the radius it becomes supersonic (comparable to a pure free fall solution). As the simulation reach higher and higher resolutions, its properties of not accounting for the background gravitational potential of the bulge of the galaxy, the likely existence of shocks inside, the effect of angular momentum to form accretion discs instead of falling directly into the SMBH and the potential impact of self-gravity, have resulted in more focus on the differences that may arise from a more thorough treatment (e.g. Negri and Volonteri, 2017; Beckmann, Slyz, and Devriendt, 2018).

1.4.1 Formation

Galaxies grow in dark matter halos (see Section 1.1) allowing material to fall into the potential, shock heat and cool by radiation. Therefore, if the cooling time is less than the Hubble time and the dynamical time, a galaxy can form (e.g. Hoyle, 1953; Sunyaev and Zeldovich, 1972; Silk, 1977; Rees and Ostriker, 1977; Cole et al., 2000). From observations of the most distant AGN (e.g. Willott, McLure, and Jarvis, 2003; Riechers et al., 2009; Mortlock et al., 2011), it follows that the SMBHs not only already existed at these redshifts, but must have also grown to their observed size. While it will be argued in Section 1.4.2 that the growth rates required to achieve those masses are compatible with stellar mass sized seeds (e.g. King et al., 2005; King, Pringle, and Hofmann, 2008; Fanidakis et al., 2011), the black hole formation channels might still be important for extreme examples (for overviews see e.g. Volonteri, 2010; Latif and Ferrara, 2016).

The most commonly suggested source for black hole seeds are the result of the end of the theorised population III stars (e.g. Begelman and Rees, 1978; Bond, Arnett, and Carr, 1984; Heger and Woosley, 2002; Umeda and Nomoto, 2003; Ricarte and Natarajan, 2018), which are thought to have been the first stars. They grow more massive than their successors (population II and I stars) as the absence of metals likely contributed significantly to the cooling process and allowing stars of the order $10^2 M_{\odot}$ to potentially form (e.g. Tegmark et al., 1997; Fosbury et al., 2003; Greif et al., 2011; Stacy, Greif, and Bromm, 2012; Sobral et al., 2015; Murphy et al., 2018). If the formation of such massive stars is indeed possible, the collapse of gaseous matter may yield a black hole directly as well following similar arguments as for the population III stars (e.g. Haehnelt and Rees, 1993; Loeb and Rasio, 1994; Bromm and Loeb, 2003; Koushiappas, Bullock, and Dekel, 2004; Lodato and Natarajan, 2006; Latif et al., 2016; Barrow, Aykutaalp, and Wise, 2018). Other theories like the "bar within bars" mechanism that funnels gas efficiently into a slowly collapsing core until cooling becomes efficient leading to runaway infall that grows even a stellar mass seed quickly enough have been suggested as well as direct collapse scenarios (e.g. Shlosman, Frank, and Begelman, 1989; Begelman, Volonteri, and Rees, 2006).

However, even if the conditions do not allow a collapse into a single massive object, the infalling matter may form several gravitational instabilities instead that result in a high density star cluster in the nucleus of a galaxy (e.g. Schneider

et al., 2006). The compactness may lead to collisions (e.g. Sanders, 1970; Begelman and Rees, 1978) that could provide both massive seeds, fuel the rapid growth (e.g. Portegies Zwart et al., 2004; Stone, Küpper, and Ostriker, 2017) and potentially suggest the existence of intermediate black holes (IMBH, see e.g. Ebisuzaki et al., 2001; Portegies Zwart and McMillan, 2002; Kızıltan, Baumgardt, and Loeb, 2017).

All formation channels require extremely fast ways of cooling and a efficient mechanism to remove angular momentum. How such a mechanism for the latter requirement may look like and how well it performs in a simulated environment is at the heart of this thesis.

1.4.2 Growth and feedback

In principal two modes of growth can be discerned (e.g. Berti and Volonteri, 2008): The merger of two black holes (e.g. Begelman, Blandford, and Rees, 1980; Berti and Volonteri, 2008; further divided by the mass ratio as it impacts their spin contribution, see e.g. Hughes and Blandford, 2003) and the accretion of gaseous material (e.g. Salpeter, 1964; Soltan, 1982). The latter is thought be dominant as the coalescence of two SMBHs is typically the result of a major (galaxy) merger, which funnels gas towards the central region as well (e.g. Searle and Zinn, 1978; Heckman et al., 1986; Barnes and Hernquist, 1991; Hernquist and Mihos, 1995; Springel, Di Matteo, and Hernquist, 2005b; King, Pringle, and Livio, 2007; Sparre and Springel, 2016), although some more recent simulations suggest that these mergers are not the statistically prevailing fuelling mechanism in line with some observational studies (Steinborn et al., 2018). Nevertheless, the growth rate of SMBHs is thought to be linked with the stellar mass build up (e.g. Richstone et al., 1998; Wang et al., 2009) for redshifts at least up to $z \sim 2$.

Recent measurements of the time lag between the SMBHs ability to photoionise significant fractions of its host galaxy and when it becomes active in the first place, have yielded that each active phase lasts $\sim 10^5$ yr (Schawinski et al., 2015) -see also e.g. (Sanders, 1981; Novak, Ostriker, and Ciotti, 2011; Bland-Hawthorn et al., 2013; Oppenheimer et al., 2018). Comparing the result to the estimated growth time of $10^7 - 10^9$ yr (e.g. Soltan, 1982; Yu and Tremaine, 2002), it follows that the luminous part of the accretion must happen in multiple events (e.g. Salpeter, 1964; Lynden-Bell, 1969; Shakura and Sunyaev, 1973; Soltan, 1982;

Ulrich, Maraschi, and Urry, 1997; Schawinski et al., 2015). The resulting variations in output luminosity may be up scaled versions of those in X-ray binaries (see Section 1.3) (e.g. Maccarone, Gallo, and Fender, 2003; Falcke, K rding, and Markoff, 2004; McHardy et al., 2006). Further evidence for this AGN lifetime is given by considering the radius ($r_{sg} \sim 10^{-2}$ pc) at which self-gravity dominates the disc and cannot directly contribute to the accretion process as it is prone to fragmentation (e.g. Pringle, 1981; Frank, King, and Raine, 2002). Therefore an accretion disc can only be smaller than said radius (King, Pringle, and Livio, 2007). This provides an upper limit for an individual event and can be shown to be of the same order of $\sim 10^5$ yr (King and Nixon, 2015) providing an independently derived theoretical result. Hence, if the accretion happens in many individual episodes, it is very likely that the angular momentum orientation of those events is uncorrelated -a process that is commonly referred to as chaotic accretion (e.g. Sanders, 1981; Moderski, Sikora, and Lasota, 1998; King and Pringle, 2006; King and Nixon, 2015).

In Section 1.2.2 I have mentioned the tremendous energies involved when a SMBH is active and growing. However, the radiation itself will produce a pressure. In fact, it can be shown that if the mass accretion rate becomes too large, the radiation pressure can overcome the gravitational pull of the SMBH, push out the gaseous infall and consequently self-regulates its growth rate. Assuming a mass growth limit by the Eddington (1916) limit (which originally considered the hydrostatic equilibrium of a star, however, the same principle applies to SMBHs) defining the balance of the radiation pressure and the gravitational attraction of matter towards the massive object and assuming the latter to infall spherically and steady, one can write down:

$$\dot{M}_{Edd} = \frac{L_{Edd}}{\eta c^2}, \quad (1.10)$$

where $\eta = GM_{\bullet}/Rc^2$ is the accretion efficiency (essentially based on how compact an object is) and can take values between 0.0057 – 0.42 for the spin parameter between 0 – 1, for which the widely used average is $\eta \sim 0.1$ (e.g. Soltan, 1982; Yu and Tremaine, 2002; Elvis, Risaliti, and Zamorani, 2002; King and Nixon, 2015). The limit on the accretion rate can be used together with η to calculate the starting mass in order to grow SMBHs to size we observe them now (e.g. Salpeter, 1964; Shapiro, 2005).

It has been suggested that SMBHs spin up during the growth phases (e.g. Bardeen, 1970; Scheuer and Feiler, 1996; Gammie, Shapiro, and McKinney, 2004; Volonteri et al., 2005) and as more matter is converted into energy (up to $\sim 40\%$), less mass is available for the growth of the SMBH. Hence its e-folding time exceeds 300 Myr (e.g. King and Pringle, 2006), which requires that black hole seeds have to be more massive than a stellar mass (see Section 1.4.1), especially for very massive SMBHs (e.g. $10^9 M_\odot$) at high redshifts ($\gtrsim 6$, see e.g. Willott, McLure, and Jarvis, 2003; Riechers et al., 2009; Mortlock et al., 2011). Further evidence for high spins are provided by estimates based on observations at large redshifts (Elvis, Risaliti, and Zamorani, 2002), however, it is argued that the spin may change significantly with redshift (Wang et al., 2009). By connecting the radiative efficiency η with redshift dependent quantities like the luminosity density and the duty cycle, the authors obtain $\eta \sim 0.3$ at $z \sim 2$, but $\eta \sim 0.003$ at $z \sim 0$ implying a spin down over time (Wang et al., 2009). Furthermore, it was shown on analytical grounds that the Lense-Thirring effect does not necessarily align an initially misaligned accretion disc (caused by chaotic accretion with the black hole spin, see Bardeen and Petterson, 1975) and in fact may counteralign half of the time (e.g. King et al., 2005; King and Pringle, 2006; King, Pringle, and Hofmann, 2008; Fanidakis et al., 2011; Hopkins et al., 2012). The resulting accretion from counteraligned discs reduces the e-folding times to $\lesssim 25$ Myr allowing the black hole seeds to be as low as stellar mass seeds.

Using the efficiency noted in Section 1.4.1, the energy liberated in these accretion events can be computed (King and Pounds, 2015):

$$E_\bullet = \eta M_\bullet c^2 \sim 2 \times 10^{61} \left(\frac{M_\bullet}{10^8 M_\odot} \right) \text{ erg.} \quad (1.11)$$

This value can be further compared to the binding energy of a typical galaxy bulge (King and Pounds, 2015):

$$E_{\text{bulge}} \sim M_{\text{bulge}} \sigma^2 \sim 8 \times 10^{58} \left(\frac{M_{\text{bulge}}}{10^{11} M_\odot} \right) \left(\frac{\sigma}{200 \text{ km s}^{-1}} \right)^2 \text{ erg.} \quad (1.12)$$

The larger E_\bullet therefore might be used to explain the impact on the host galaxy, which as argued in Section 1.4 cannot stem from the influence of the gravitational potential of the SMBH. However, the discrepancy of a factor of a few hundreds is large enough, that it should unbind the whole galaxy going against the notion

of repeated accretion events described earlier and perhaps even against the existence of galaxies full stop. Clearly most of the radiation appears to escape the galaxy for us to be observed, but the coupling of the energy to the host galaxy must still be weak.

The interaction of the released energy is communicated in form of radiation and wind (potentially collimated in the form of jets, see e.g. Silk and Rees, 1998; Fabian, 1999; Pounds et al., 2003; King and Pounds, 2003; King and Pounds, 2015) and is generally referred to as AGN feedback (e.g. Fabian, 2012; King and Pounds, 2015). Low accretion rates are thought to produce jets and appear as radio loud sources, often referred to as maintenance mode since the jet potentially heats up the gas that may otherwise fall onto the galaxy and therefore suppresses star formation (e.g. Quilis, Bower, and Balogh, 2001; McNamara et al., 2005; Sijacki and Springel, 2006; Fabian, 2012). High accretion close to the Eddington limit is thought to eventually cause strong enough outflows to remove the gas reservoir for star formation of the galaxy (e.g. Halpern, 1984; Reynolds and Fabian, 1995; McKernan, Yaqoob, and Reynolds, 2007; Spilker et al., 2018), referred to as quasar mode feedback and appears to be radio quiet as described in Section 1.2.2. However, both simulations and observations suggest that this feedback may also induce star formation (referred to as positive feedback compared to the negative feedback just described, see e.g. Nayakshin and Zubovas, 2012; Zubovas et al., 2013; Nayakshin, 2014; Bieri et al., 2016).

Observation of these outflows and their interaction with the host galaxy provide direct evidence for the importance of the connection between these objects. Outflows of neutral and ionised gas have been observed to reach velocities of $\sim 10^3$ km/s (e.g. Anderson and Kraft, 1969; Crenshaw, Kraemer, and George, 2003; Feruglio et al., 2010; Cicone et al., 2014; Tadhunter et al., 2014; Tombesi et al., 2015). Even faster winds reaching velocities of $\sim 0.1c$ and more are found in broad absorption line quasars (BAL QSOs, see e.g. Clowes et al., 1979; Drew and Boksenberg, 1984; Turnshek et al., 1988; Gibson et al., 2009; Reeves et al., 2009; Moe et al., 2009; Reeves et al., 2016) or in the form of ultra-fast outflows (UFOs, see e.g. Begelman, McKee, and Shields, 1983; Pounds et al., 2003; King and Pounds, 2003; Pounds and Reeves, 2009; Kraemer, Tombesi, and Bottorff, 2018). These (mildly) relativistic outflows match the theoretical models of close to Eddington accretion onto a SMBH (e.g. Shakura and Sunyaev, 1973; Pounds et al., 2003; King and Pounds, 2003) by measuring the absorption column density of the

winds, which were realised to be Compton thick (e.g. $\gtrsim 10^{24} \text{ cm}^{-2}$, the inverse of the Thomson cross-section, see e.g. Maiolino et al., 1998; Risaliti, Maiolino, and Salvati, 1999; Malizia et al., 2009) allowing the computation of the implied mass outflow rate (e.g. Pounds et al., 2003; King and Pounds, 2003; King, 2010). Similarly to the attempts to unify the different types of AGNs (see Section 1.2.2), it has been proposed the differences are down to different mass accretion rates of the same underlying physical model (Zubovas and King, 2013). The launching mechanism itself is commonly thought to be the radiation pressure facilitated by spectral lines or continuum radiation exerting force on mainly free electrons (larger cross-section than protons, but typically drag their paired up proton along as well) (e.g. Lucy and Solomon, 1970; Proga, Stone, and Drew, 1998; Frank, King, and Raine, 2002; King and Pounds, 2003), however, arguments inspired by the Solar wind propose a hydromagnetic processes as well (e.g. Lovelace, 1976; Blandford and Payne, 1982; Contopoulos and Lovelace, 1994; Fukumura et al., 2010).

Theoretical predictions suggest based on the high inferred densities that every photons scatters only once transferring its complete momentum to the wind (King, 2010) leading to reduction of the coupling energy to the wind by $\eta/2$ (King, 2010; Faucher-Giguère and Quataert, 2012), however, still leaving a significant amount to impact the host galaxy (see energy comparison of Equation 1.12 and Equation 1.11). To reduce the coupling efficiency even further (and subsequently avoid blowing the whole galaxy apart after one large accretion even), rapid cooling of the wind is invoked (King and Pounds, 2003; King, 2010).

The wind interacts with the ISM causing shocks both reverse back into the wind and forward into the ISM (see Figure 1.1) with Inverse Compton (IC) scattering thought to be the most important cooling mechanism (Rees, 1967; King and Pounds, 2003; King, 2010; Kraemer, Tombesi, and Bottorff, 2018). If the shocked wind can cool quickly enough compared to the flow time of the velocity of the shock pattern, it is known as momentum driven feedback (e.g. King and Pounds, 2003; King, 2010; King, Zubovas, and Power, 2011), while otherwise the thermal pressure keeps driving the shock (known as energy driven feedback) potentially clearing the host galaxy of its gas (e.g. Silk and Rees, 1998; King, 2010; Zubovas and King, 2012; Faucher-Giguère and Quataert, 2012; Baron et al., 2018), however, there are some suggestions that the outflows may always be energy driven (e.g. Ciccone et al., 2014; Costa, Sijacki, and Haehnelt, 2014; Costa et al., 2018). The latter so far has been only observed in ultra luminous infrared galaxies, however, a

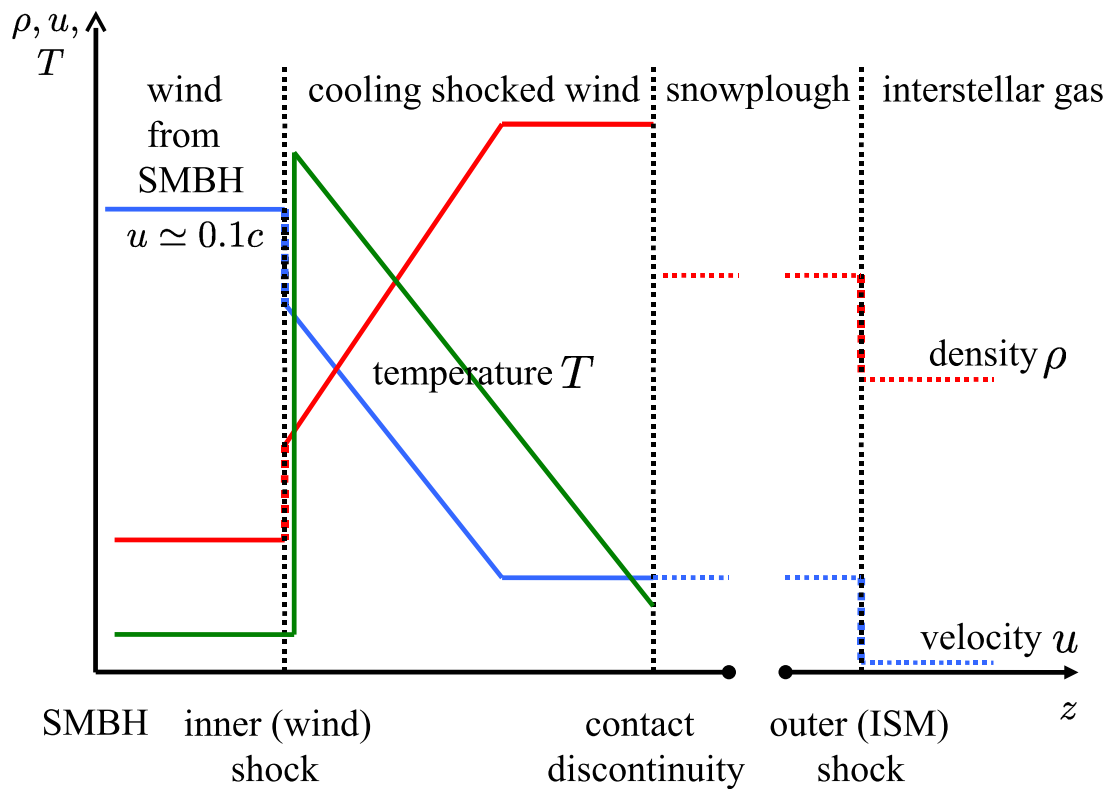


FIGURE 1.1: A schematic representation of the temperature T (green), gas density ρ (red) and velocity u (blue) for increasing radius z . The respective solid lines refer to the wind properties and the dotted to the ambient ISM. The outflow slows down due to a reverse (inner) shock when it interacts with the ISM. The shocked gas is quickly cooled by the inverse Compton effect. The shocked wind sweeps-up ("snowploughs") the ISM, which in itself causes a (outer) shock. The cooling region is significantly smaller than the "snowplough" region. The figure is taken from King, 2010.

recent observation of a comparably low power AGN shows evidence of an energy driven outflow as well (Longinotti et al., 2018). Assuming a single temperature regime (King and Pounds, 2003) the resulting cooling time can be shown to be equated together with an estimate of the momentum driven flow time to find an approximate switch-over radius from momentum driven to energy driven feedback (Zubovas and King, 2012). However, this assumption might not be accurate and some suggest that feedback might be always energy driven (e.g. Faucher-Giguère and Quataert, 2012; Bourne and Nayakshin, 2013). On the other hand, a non-uniform ISM may allow additional energy to escape in such a scenario to avoid quenching star formation too early (e.g. Nayakshin and Zubovas, 2012; Zubovas et al., 2013; Nayakshin, 2014; Bieri et al., 2016). Both improved observational data and more detailed simulation may lead to a better estimation of the coupling efficiency based on the dependence of black hole accretion rate and the star formation rate on the galactic stellar mass and could in turn provide insight which of the feedback models are more prevalent (Zubovas, 2018).

Finally, the arguably strongest indirect indicator of the interaction between the SMBH and the host galaxy is the realisation that the mass of the former is proportional to the mass of the bulge of the latter (e.g. Dressler, 1989; Kormendy and Richstone, 1995; Ferrarese and Merritt, 2000; Kormendy and Ho, 2013). From the originally 8 data points (Kormendy and Richstone, 1995), the available data has increased by more than a magnitude and found $M_{\bullet} / M_{bulge} \sim 0.001 - 0.003$ (e.g. Magorrian et al., 1998; Ferrarese and Merritt, 2000; Merritt and Ferrarese, 2001; McLure and Dunlop, 2002; Kormendy and Ho, 2013; McConnell and Ma, 2013; DeGraf et al., 2015; Larkin and McLaughlin, 2016; Bentz and Manne-Nicholas, 2018).

In Figure 1.2 the disc galaxies have been removed as their pseudo bulges are thought to be formed over an extended time (Kormendy, Bender, and Cornell, 2011; Kormendy and Ho, 2013), while elliptical galaxies and classical bulges form by merger events (e.g. Toomre, 1977; Springel, Di Matteo, and Hernquist, 2005a; Boylan-Kolchin, Ma, and Quataert, 2006; Kormendy and Ho, 2013), leading to ratio more similar to the original findings of ~ 0.005 (e.g. Magorrian et al., 1998). The right hand side of Figure 1.2 shows an even tighter relation by displaying the mass of the SMBH against the velocity dispersion σ of the host spheroid. Gebhardt et al., 2000; Kormendy and Ho, 2013 find the exponent to be ~ 4.38 excluding again pseudo bulges, while the earlier findings indicated values between

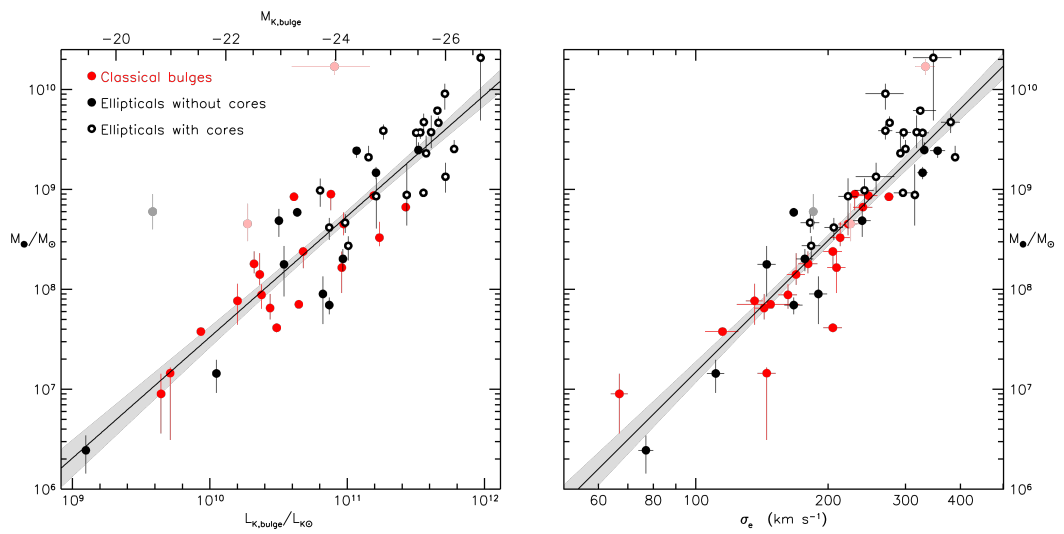


FIGURE 1.2: The left-hand side show the classic $M_\bullet - M_{bulge}$ relation, while the right-hand side displays the better correlated $M_\bullet - M_\sigma$ relation. The red dots indicate SMBHs associated with classical bulges and the black dots the association with elliptical host galaxies. The lines represents a symmetry least-squares fit and the shaded area its 1σ range. The figure is taken from Kormendy and Ho, 2013.

$\sim 3.75 - 4.8$ (e.g. Ferrarese and Merritt, 2000; Gebhardt et al., 2000). The scatter is typically lower than the observational error underlining the relevance of the relation between the SMBH and its host (Kormendy and Ho, 2013), however, some argue that the ratio is only an artefact of averaging merger events (Peng, 2007; Hirschmann et al., 2010; Jahnke and Macciò, 2011).

The $M_{\bullet} - \sigma$ relation could be thought as an upper limit for SMBH masses, where SMBHs grow until they reach a mass indicated by the relation and their feedback becomes strong enough to clear out the gas of the bulge preventing further growth (King, 2003; King, 2010; Zubovas and King, 2012). Therefore the previously mentioned outflows are theorised to drive the scaling relation (Silk and Rees, 1998; Haehnelt, Natarajan, and Rees, 1998; King and Pounds, 2003; King, 2003; King, 2010; Zubovas, 2018).

Furthermore, work to find a potentially fundamental correlation for all galaxies with the respective dark matter halos is not resolved yet (Ferrarese, 2002; Kormendy, Bender, and Cornell, 2011; Kormendy and Ho, 2013), however, simulations indicate that such a correlation may exist (Booth and Schaye, 2010; Treuhardt et al., 2012; Bogdán and Goulding, 2015).

Some further evidence of the necessity of feedback can be seen by considering the galaxy stellar mass function, which requires a double Schechter (1976) function to fit observations (Baldry, Glazebrook, and Driver, 2008; Peng et al., 2010; Baldry et al., 2012). The behaviour can be explained by considering the effects of AGN feedback like the quenching of star formation (Peng et al., 2010). Simulations indicate that AGN feedback is required as well to reproduce the observations in halos with masses of $\gtrsim 10^{11} M_{\odot}$ at which point the free-fall time is smaller than the cooling time (Bower et al., 2006). Cosmological simulations also require AGN feedback to match the observable especially at the high mass end (Springel, Di Matteo, and Hernquist, 2005b; Dubois et al., 2012; Schaye et al., 2015; Costa et al., 2018).

1.5 Structure of thesis

This thesis contains six chapters that cover a scientific introduction, a short introduction to the numerical method used here, three science chapters and a conclusion.

The science chapters focus on the chaotic infall scenario proposed by Dehnen and King, 2013. Chapter 3 presents a detailed view of the behaviour of the simulations, in particular the effect of the seed of the turbulent velocity field, and shows the robustness of the qualitative result for a range of physical parameters. In Chapter 4 I analyse follow-up simulations that investigate the effect of the numerically motivated inner boundary, discuss implications and show how this can be used to improve the quantitative results of my previously run simulations. Furthermore, I provide some preliminary evidence that shows how collisional cascades remove at least partly any preferential direction of the angular momentum of the infalling gas. Finally, in Chapter 5 I explore how discs influence the depositing of low angular momentum material through streams and present simulations with self-gravity turned on. I compare the preliminary results of these with conditions found in the central parsec of our Milky Way.

The entirety of Chapter 3 and sections of Chapter 4 that concern the simulations, discussion and results related to the numerical boundary problem have been published (Faber and Dehnen, 2018). The investigation into the prevalence of chaotic accretion in the same chapter and Chapter 5 are based on unpublished research, although some comments concerning self-gravity were made in the paper based on the simulations in the last science chapter.

Chapter 2

Smoothed Particle Hydrodynamics

2.1 The theoretical laboratory

I already alluded in Section 1.1 to the vast amount of available computing power even though many research projects struggle with the (sometimes) debilitating effects of resolution or rather their lack of. While the time spans involved in Astrophysics often exceed the lifetime of a human by many magnitudes, the myriad of stars and galaxy we can observe somewhat alleviates this problem. Humanity may never see how the "Antennae Galaxies" merger will conclude, but we can observe other merging galaxies, which will likely be at a different stage of this complex process. While this allows us to obtain a more complete picture of the merger process (e.g. Begelman, Blandford, and Rees, 1980; Merritt and Ferrarese, 2001), the nature of observing potentially fundamentally different systems and the inherent observational challenges associated with e.g. telescopes, limit the scope of the conclusions and extend of the predictions. When the processes become too complex to be expressed analytically, simulation may offer a way out.

An example of a non-computer based laboratory used light bulbs to model the gravitational interactions between two galaxies. The light bulbs represented the mass elements and their luminosity was set to be proportional to the simulated mass (Holmberg, 1941). Computer based simulations started with as little as 4 particles per simulation, which tried to solve a N-body problem, however, already featured for example a variable time-step (von Hoerner, 1960). Modern examples use in extreme cases up to 303×10^9 particles to simulate typically dark matter structures on scales of Gpc (Angulo et al., 2012).

However, it was quickly realised that the abundant gas had significant impact

on physical processes involved, which led to the rise of hydrodynamical simulations. These can be categorised into Eulerian and Lagrangian codes. The former discretises space and is typically used in grid codes, while the latter discretises mass and is used in Smoothed Particle Hydrodynamics (SPH) codes, which is utilised in this thesis. Modern codes are even capable of combining the two aspects (Springel, 2010a).

2.2 Smoothed Particle Hydrodynamics

The smoothed-particle hydrodynamics (SPH) computational method, developed by Lucy, 1977; Gingold and Monaghan, 1977, uses a Lagrangian description in which the particles follow the flow and serve as interpolation points for the fluid properties. The specifics, advantages and issues of such a simulation setup are broadly discussed in the literature and I refer the interested reader to reviews on the subject (Springel, 2010b; Dehnen and Read, 2011; Monaghan, 2012; Price, 2012). However, I shall discuss some details that are relevant for the here presented simulations.

2.2.1 Smoothing kernel

The key ingredient of the SPH approach is the smoothing as it allows the approximation of a potentially complex physical system as one particle. The property of a particle can subsequently be determined by adding up the weighted contributions of all particles that are inside the range of the kernel. By allowing the kernel range (smoothing length h) to vary based on the surrounding of each particle, high resolution (small h) can be achieved in dense regions, while more sparsely populated regions (large h) provide benefits for the required computation time. The density of the SPH particle can be estimated using the following expression:

$$\rho(\mathbf{x}_i) = \sum_j m_j W(|\mathbf{x}_i - \mathbf{x}_j|, h_i), \quad (2.1)$$

where m is the mass, W the kernel function, \mathbf{x} the position vector and h the smoothing length. The adaptive properties can be achieved by modifying h such that the product of h and the estimated density is always constant. Further relevant quantities like the internal energy can be computed based on the above described procedure to obtain local estimations of fields.

Typically a cubic spline (e.g. Monaghan and Lattanzio, 1985) is used as the kernel function (essentially a weighing function), which fulfils the critical requirements for a kernel like it is symmetric in radius in the sense that $W(|\mathbf{r}_i - \mathbf{r}_j|, h_a) \equiv W(|\mathbf{r}_j - \mathbf{r}_i|, h_a)$, where r cannot be negative. Furthermore, h must decrease monotonically with r while at small separations it must be flat to avoid unphysical density computations. Finally it must feature a smooth derivative as otherwise the density estimate would feature discontinuities.

Principally a Gaussian complies with these conditions as well, but it behaves asymptotically at large r and therefore it would always encompass all particles of a simulation however little their impact might be on the estimates. A more selective approach offered by for example said cubic spline saves significant computation time, while minimising the impact on the accuracy of the simulation.

Higher neighbour numbers in principal reduce random force errors, which can be caused by for example shear flows. Turbulence produces such flows, which are generally common in galaxy, star or planet formation, but are of particular interest in the here presented simulations as turbulence can be the main driver for the cancellation of angular momentum (see Chapter 3). The equally prevalent shocks provide another source that changes the typically isotropic distribution of particles (resulting in significantly lower Poisson noise compared to e.g. a random distribution) to be condensed in a direction leading to an anisotropic arrangement of the particles (still better than shot noise, but convergence becomes an issue). Larger neighbour numbers and a larger smoothing length h can overcome the error at the cost of a lowered resolution. However, at high neighbour numbers a pairing instability will reduce accuracy (Dehnen and Aly, 2012; Price, 2012) as they reduce the effective neighbour number. This can be avoided, if the Fourier transform of the kernel is not negative. This is true for a Wendland (1995) kernel (Dehnen and Aly, 2012), which I utilise in the here presented simulations.

2.2.2 Gravity

The gravitational force per SPH particle is computed based on the smoothed mass distribution of the remaining particles, which can be expressed with the help of the Poisson equation:

$$\nabla^2\Phi = 4\pi G\rho, \quad (2.2)$$

where Φ is the gravitational potential and ρ the smoothed density of the particles. In reality every particle would be affected by all other N particles (e.g. $N - 1$) leading to

$$m_i\ddot{\mathbf{x}}_i = -G \sum_{i \neq j}^N m_i m_j \frac{\mathbf{x}_i - \mathbf{x}_j}{|\mathbf{x}_i - \mathbf{x}_j|^3}, \quad (2.3)$$

where m is the mass of the particle, $\ddot{\mathbf{x}}$ the acceleration and \mathbf{x} the position. While this approach would not be an issue for the first careful steps in the realms of N -body simulations (e.g. von Hoerner, 1960), this approach becomes rapidly prohibitively expensive as the loop has to go through all particles as well leading to a scaling of N^2 . As gravity follows an inverse square law, an approximation can be made by reducing the number of particles a single particle is affected by.

One way is to divide the space into successfully smaller cubic cells (typically 8 in number) as part of the Tree method (Barnes and Hut, 1986). The "root" is referred to as the cell that contains the whole simulation and subsequent "branches" until the smallest cell, the "leaf", is reached, which however, may still contain more than one particle (Dehnen and Read, 2011). The here utilised code SPHINX actually goes up the tree until it contains all the neighbours. This method saves about 10% time in comparison to going down from the very top. SPHINX utilises an explicit vectorisation, where the particles are sorted along the tree in memory. This means that blocks of 8 (with the new Skylake machines it is 16) can be read at once. On average 5 particles out of the memory block are neighbours, however, tests have shown with the new Skylake machines that this number only goes up to 8 out 16. This results in a noticeably smaller speed up than expected.

Given the smoothing mentioned in Section 2.2.1, each particle represents the mass distribution of potentially many physical objects (e.g. stars). Close encounters would cause clumping, that may not only be unphysical, but also slows down the simulation as the integration of the movement of the particles would require smaller and smaller timesteps the closer the particles get. Therefore gravity is softened to reduce the gravitational attraction of close objects (Dehnen and Read, 2011). For example the use of a cubic spline kernel (see Section 2.2.1) keeps the

gravitational force calculation unchanged unless a group of particles moves inside a given radius that is smaller than the smoothing length. At these close distances the gravitational pull does not diverge as r^{-2} , but is gradually reduced to zero. The benefits of this method is the simpler integration of the equations of motions due to the continuous and smooth function estimating the physical properties of the particles and the avoidance of large angle deflections for sufficiently large smoothing length. However, as a consequence of the softening, the analysis of scales smaller than a few times the smoothing length is inaccurate (Dehnen and Read, 2011). Hence while it may be desirable in some cases to increase the softening length above the minimum value in order to reduce the computational cost, one has to ensure that the results are not affected significantly (see Section 5.1).

The softening of gravity becomes particularly important in Chapter 5, where self-gravity is turned on allowing massive clumps to interact with each other via gravity instead of being gravitationally influenced only by the sink particle at the centre of the simulation (see Chapter 3 and 4).

2.2.3 Artificial viscosity

The utilisation of a symplectic integrator and the Euler-Lagrangian nature (see Section 2.2.4) of the derived SPH equations result in an inherent conservation of the energy, total mass, entropy and both momentum and angular momentum with the latter being one of the main motivations to use the SPH simulations for the work presented in this thesis. However, for example shocks should result in an increase of entropy and therefore a method is required to dissipate local differences in velocity.

In order for SPH to deal with shocks that feature discontinuities, an artificial viscosity (AV) is used to avoid particles moving across each other faster than the time step and therefore avoid the calculation of a collision and the existence of multi-valued momentum values (Cullen and Dehnen, 2010). AV is typically implemented as an acceleration to the equations of motion and an additional entropy term at the shock front to keep the energy conserved (Read and Hayfield, 2012). A switch is used to minimise AV away from shocks returning the flow into an essentially inviscid fluid. The switch uses an improved indicator to distinguish for example between pre-shocks and post-shocks and allows the setting

of appropriate local values for the artificial viscosity leading to better modelling of weak shocks and convergent flows (Cullen and Dehnen, 2010).

2.2.4 Timesteps

The most straightforward method to compute the evolution of a simulation is the Euler integration, but it features a significant scaling error as high order terms are increasingly expensive. The energy can be conserved over longer periods by using a symplectic integrator instead (Dehnen and Read, 2011). Such an integrator is the commonly used leapfrog method, where the particles are kick-drift-kicked (which is superior to drift-kick-drift in terms of the energy error).

Each particle has an individual timestep to speed up the computation as particles in a low mass distribution do not require the same precise integration (smaller timesteps) as particles at high densities. Timesteps differ by a factor of two (the different levels are called rungs), which allows all particles to be synchronised at the largest timestep.

A wake mechanism enforces that neighbouring particles may not differ by more than a factor of two to avoid unphysical situations where e.g. a shock (high density, small timestep) moves through a low density volume (large timestep) and therefore does not capture the interactions as the properties of the low density region would not be computed as frequently as the high density particles.

Chapter 3

Feeding SMBHs by gaseous collapse

The processes driving gas accretion on to supermassive black holes (SMBHs) are still poorly understood. Angular momentum conservation prevents gas within ~ 10 pc of the black hole from reaching radii $\sim 10^{-3}$ pc where viscous accretion becomes efficient. Here I present simulations of the collapse of a clumpy shell of swept-up isothermal gas, which is assumed to have formed as a result of feedback from a previous episode of AGN activity. The gas falls towards the SMBH forming clumps and streams, which intersect, collide, and often form a disc. These collisions promote partial cancellations of angular momenta, resulting in further infall and more collisions. This continued collisional cascade generates a tail of gas with sufficiently small angular momenta and provides a viable route for gas inflow to sub-parsec scales. The efficiency of this process hardly depends on details, such as gas temperature, initial virial ratio and power spectrum of the gas distribution, as long as it is not strongly rotating. Adding star formation to this picture might explain the near-simultaneous formation of the S-stars (from tidally disrupted binaries formed in plunging gas streams) and the sub-parsec young stellar disc around Sgr A*.

3.1 Introduction

It is commonly accepted that most massive galaxies contain a supermassive black hole (SMBH) in their centre (see reviews e.g. by Kormendy and Richstone, 1995; Kormendy and Ho, 2013). The observed M_{\bullet} - σ relation linking the mass M_{\bullet} of the SMBH to the stellar velocity dispersion σ in the bulge of the galactic host (Ferrarese and Merritt, 2000; Gebhardt et al., 2000), or for more recent analysis (McConnell and Ma, 2013; Kormendy and Ho, 2013), provides a compelling

argument that the black hole presents a critical component of the galaxy and a crucial ingredient for its evolution (e.g. Haehnelt, Natarajan, and Rees, 1998; Silk and Rees, 1998; King and Pounds, 2003; Sijacki et al., 2015), or for reviews (e.g. Frank, King, and Raine, 2002; Fabian, 2012). However, the gravitational influence of the SMBH is negligible, since its mass $M_{\bullet} \ll M_{\text{host}}$, the mass of the hosting bulge/spheroid, and hence cannot cause the M_{\bullet} - σ relation.

A comparison of the total quasar luminosity density to the mass density of SMBHs shows that the dominant mode of SMBH growth is through gas accretion (Soltan, 1982). The total energy released from an accreting SMBH exceeds the binding energy of the host, e.g. $\eta M_{\bullet} c^2 \gg M_{\text{host}} \sigma^2$, even if one assumes only a $\eta = 10\%$ efficiency for converting gravitational energy of the accreted gas into radiation. This radiation probably drives powerful gas outflows (Silk and Rees, 1998; Fabian, 1999; Pounds et al., 2003; King and Pounds, 2003; King and Pounds, 2015), which are much more efficient at communicating their energy to the host's interstellar medium (ISM) than the original radiation. These outflows can be highly collimated (jets, often associated with low accretion rates), when some form of isotropisation is required to affect most of the host (e.g. Quilis, Bower, and Balogh, 2001; McNamara et al., 2005; Sijacki and Springel, 2006; Fabian, 2012). Conversely, the outflows generated by accretion rates close to the Eddington (1916) limit are usually associated with near-spherical ionised winds (e.g. Halpern, 1984; Reynolds and Fabian, 1995; McKernan, Yaqoob, and Reynolds, 2007). Once the SMBH reaches the M_{\bullet} - σ relation, the outflows become efficient in expelling most of the gas from the galaxy, inhibiting further SMBH growth and star formation (King, 2005). This picture suggests, independently of the Soltan (1982) argument, that SMBHs grow predominantly by gas accretion.

This scenario of SMBH growth by gas accretion has been challenged by the observation of a number of black holes with masses $M_{\bullet} \gtrsim 10^9 M_{\odot}$ at redshifts $z \sim 6$ (e.g. Willott, McLure, and Jarvis, 2003; Riechers et al., 2009; Mortlock et al., 2011), which require an e-folding time of $\lesssim 50$ Myr to grow from stellar-mass seeds. If the SMBH is spinning near the maximum, as initially thought (Volonteri et al., 2005) based on the assumption that accretion always spins the hole up (Bardeen, 1970; Scheuer and Feiler, 1996), the e-folding time exceeds 300 Myr (e.g. King and Pringle, 2006), and therefore requires more massive, non-stellar black-hole seeds (e.g. Haehnelt and Rees, 1993; Latif and Ferrara, 2016). However, if the SMBH grows from consecutive accretion discs generated by randomly

orientated inflows ('stochastic accretion'), the black-hole spin remains low (King et al., 2005; King, Pringle, and Hofmann, 2008; Fanidakis et al., 2011) implying e-folding times of $\lesssim 25$ Myr. Hence the observed SMBHs at $z \sim 6$ are compatible with stellar mass seeds, if the holes maintain an accretion duty cycle of $\gtrsim 50\%$. Consequently these high-redshift SMBHs may well originate from the extreme end of the distribution of SMBH growth by gas accretion from stellar-mass seeds.

However, the process(es) responsible for the transportation of gas to the hole are still unclear. The main obstacle is the conservation of angular momentum within the gravitational influence of the SMBH, which prevents the gas from approaching the black hole. Instead the gas is likely to dissipate energy and form a disc at the circularisation radius dictated by its angular momentum content. Once a disc has formed, mass is transported inwards and angular momentum outwards by viscosity (proposed for differentially rotating stars by Goldreich and Schubert, 1967). The widely used parameterisation of Shakura and Sunyaev, 1973 for this process gives a viscous accretion time scale of

$$\begin{aligned}
 t_{\text{visc}} &= \frac{1}{\alpha} \left(\frac{R}{H} \right)^2 \left(\frac{R^3}{GM_{\bullet}} \right)^{1/2} \\
 &\sim 3 \times 10^5 \text{ yr} \left(\frac{0.1}{\alpha} \right) \left(\frac{H/R}{0.002} \right)^{-2} \left(\frac{R}{0.002 \text{ pc}} \right)^{3/2} \left(\frac{M_{\bullet}}{10^8 M_{\odot}} \right)^{-1/2},
 \end{aligned} \tag{3.1}$$

where R and H are the size and vertical extent of the disc respectively. α is a dimensionless viscosity parameter, for which observational evidence gives $\alpha \sim 0.1 - 0.4$ (Smak 1999; Dubus, Hameury, and Lasota 2001, for review see e.g. King, Pringle, and Livio 2007). There are two lines of evidence that SMBH accretion discs are restricted to very small scales. First, self-gravity limits the discs (e.g. Kolykhalov and Syunyaev, 1980; Pringle, 1981; Lodato, 2007) to $R \lesssim 10^{-2}$ pc (King and Pringle, 2007). Second, since $H/R \lesssim 0.002$ for AGN discs (e.g. King, Pringle, and Hofmann, 2008; Poindexter, Morgan, and Kochanek, 2008; Bate et al., 2008), t_{visc} becomes comparable to the observationally inferred duration $\sim 10^5$ yr of AGN phases (Schawinski et al., 2015) only at $R \lesssim 0.002$ pc (King and Nixon, 2015). However, there are claims that the accretion disc might be thicker than the proposed value based on observations (Floyd, Bate, and Webster, 2009). On the other hand, the region containing $\sim 10^8 M_{\odot}$ of accretable material is $r_{\text{acc}} \gtrsim 10$ pc in radius (assuming a SMBH host on the $M_{\bullet}-\sigma$ relation and with $M_{\bullet} = 10^8 M_{\odot}$). Within this region most gas will have some (mostly random) angular

momentum preventing it from reaching the required 10^{-3} pc scale. Therefore some other mechanism is required to bridge the gap of a factor $\gtrsim 10^4$ in radius (or $\gtrsim 10^2$ in angular momentum).

Dehnen and King, 2013 suggested a mechanism for driving gas into the immediate vicinity of the hole. This is based on the picture of stochastic accretion described above, where SMBH growth results from many accretion events (King et al., 2005; King, Pringle, and Hofmann, 2008). These events correspond to quasar-like activity and generate a radiation-driven wind. As long as the hole is still in its infancy, i.e. below the M_{\bullet} - σ relation, this quasi-spherical outflow is not powerful enough to clear the galaxy of gas, but strong enough to push most of the ambient gas away from the hole and sweep it up into a shell of radius $r_{\text{shell}} \sim 1\text{-}10$ pc. The sweeping up of the gas may have caused some cancellation of orbital angular momentum (Zubovas, 2015), generating a tail of low-angular momentum material in the shell. More importantly, the shell of gas has gained gravitational potential energy by the outflow and, if anything, lost kinetic energy by dissipation. It is thus prevented from falling back only by the ongoing outflow. But as soon as the outflow ends, the gas must fall back in the form of clouds and streams on plunging orbits. The infall of multiple streams from different directions increases the likelihood of collisions near pericentre with the potential of further angular momentum cancellation. This in turn promotes further infall, and results in a cascade of collisions at continually decreasing radii, generating a significant tail of very low angular momentum material, from which eventually an accretion disc forms. In this chapter I shall test this idea by using smoothed particle hydrodynamics (SPH) simulations.

This chapter is organised as follows: In Section 3.2 I describe the initial conditions and the parameter choices for the different simulations. I choose a suite of simulations for my default choice of the physical parameters in Section 3.3 to outline the general evolution of the infalling gas. I study the effects of varying the physical parameters in Section 3.4. The results are summarised and discussed in Section 3.5, while Section 3.6 concludes.

3.2 Modelling approach

3.2.1 The hydrodynamical method

The smoothed-particle hydrodynamics (SPH) computational method, developed by Lucy, 1977; Gingold and Monaghan, 1977, uses a Lagrangian description in which the particles follow the flow and serve as interpolation points for the fluid properties. The simulations reported here have been performed with the SPH code SPHINX (utilised by e.g. Aly et al., 2015), which implements fully conservative SPH with individually adaptive smoothing length (for review e.g. Price, 2012). SPHINX features the widely used method of Cullen and Dehnen, 2010 for suppressing artificial viscosity away from shocks and employs as smoothing kernel the fourth-order Wendland (1995) function as proposed by Dehnen and Aly, 2012 to improve numerical convergence.

The time integration is performed using individually adaptive particle time steps organised in the standard block-step scheme with hierarchically ordered time steps differing by a factor of two (e.g. Hayli, 1967; Makino, 1991). Individual steps are done with the second-order accurate leapfrog integrator implemented as a predictor-corrector scheme. In order to resolve cloud-cloud/stream-stream and similar collisions, a wake-up mechanism ensures that the time steps of neighbouring particles differ no more than a factor of 4.

The implementation uses a “one-sweep” algorithm, which requires only a single neighbour search per particle and time step and avoids storing of neighbour lists. The code uses explicit vectorisation and multi-threading for shared-memory hardware.

3.2.2 Generation of turbulence

An isotropic Gaussian random vector field $v(\boldsymbol{x})$ with a given power spectrum

$$P(k) = \left\langle |\hat{v}(\mathbf{k})|^2 \right\rangle_{|\mathbf{k}|=k} \quad (3.2)$$

can be created simply as three independent Gaussian random scalar fields (e.g. see Efstathiou et al., 1985) with the same power spectrum divided by a factor 3. In order to generate a Gaussian random scalar field $f(\boldsymbol{x})$, its Fourier transform

$\hat{f}(\mathbf{k})$ is sampled as complex random variable with uniform phase and normally distributed amplitude with zero mean and variance equal to the power $P(k)$.

In practice, I taper the velocity power spectrum at some maximum wave length by replacing $P(k) \propto k^{-n}$ with

$$P(k) \propto (k^2 + k_{\min}^2)^{-n/2}, \quad (3.3)$$

where $k_{\min} = 2\pi/\lambda_{\max}$ (as suggested by Dubinski, Narayan, and Phillips, 1995). In my simulations λ_{\max} is set equal to the initial radius r_{shell} of the gas shell.

In order to obtain a velocity field satisfying $\nabla \cdot \mathbf{v} = 0$, one may obtain \mathbf{v} as the curl of a Gaussian random field $\mathbf{u}(\mathbf{x})$ with power spectrum steeper by a factor k^2 or, equivalently set $\hat{\mathbf{v}} = i\mathbf{k} \times \hat{\mathbf{u}}$ where the variance of $\hat{\mathbf{u}}(\mathbf{k})$ equals $k^{-2}P(k)$. Another method that allows the adjustment of partial contributions from a solenoidal and divergent field can be achieved by projecting a general Gaussian random vector field onto its divergent free part. This can be achieved in Fourier space by replacing $\hat{\mathbf{v}}$ with

$$\hat{\mathbf{v}} - \frac{\mathbf{k}\mathbf{k} \cdot \hat{\mathbf{v}}}{k^2}. \quad (3.4)$$

I used the first of these methods in the simulations.

3.2.3 Initial conditions and model setup

All initial conditions are based on a spherical shell of gas modelled by SPH particles with normally distributed radii of mean r_{shell} and a standard deviation $0.2r_{\text{shell}}$ centred on a massive sink particle at the origin representing the SMBH (plus unresolved material at $\lesssim r_{\text{sink}}$). I employ units such that $G = 1$, $M_{\bullet} = 1$ and $r_{\text{shell}} = 1$.

The initial positions of the gas particles are sampled using a quasi-random generator, which provides a low-discrepancy sequence of numbers (for review see e.g. Niederreiter, 1992). Unlike the common pseudo-random numbers, quasi-random numbers avoid shot noise and therefore create more glass-like initial conditions suitable for SPH simulations. This shell models the gas swept-up by a feedback event, which itself is not modelled. The beginning of the simulation

TABLE 3.1: Summary of the initial conditions and parameters used in the simulations presented. I use model units in which Newton’s constant of gravity $G = 1$, the mass of the SMBH $M_{\bullet} = 1$, and the initial radius of the gas shell $r_{\text{shell}} = 1$. M_{shell} is the total amount of gas and is modelled by $N_{\text{shell}} = 2 \times 10^6$ SPH particles initially placed in a spherical shell of radius r_{shell} and Gaussian width r_{width} . The initial gas velocities are set according to equations (3.5-3.7) and are controlled by the parameters η and χ as described in the text. c_s is the sound speed of the gas (in units of the circular speed at the shell radius $\sqrt{GM/r_{\text{shell}}}$). r_{sink} is a computationally motivated boundary region around the SMBH; Particles inside the radius are removed from the simulation. The penultimate column specifies whether gas self-gravity was included, and the final column indicates the Gaussian width of the initial shell.

Section	M_{shell}	v_{turb}	power n	η	χ	c_s	r_{width}
3.3	0.01	$\nabla \cdot v_{\text{turb}} \neq 0$	-11/3	0.9	0.75	0.1	0.01
3.4.1	0.01	$\nabla \cdot v_{\text{turb}} \neq 0$	-11/3	0.9	0.75	0.05, 0.2	0.01
3.4.2	0.01	$\nabla \cdot v_{\text{turb}} \neq 0$	-5/2, -9/2	0.9	0.75	0.1	0.01
3.4.3	0.01	$\nabla \cdot v_{\text{turb}} \neq 0$	-11/3	0.9	0.25, 0.5, 1.0	0.1	0.01
3.4.4	0.01	$\nabla \cdot v_{\text{turb}} = 0$	-11/3	0.9	0.75	0.1	0.01
3.4.5	0.1, 1	$\nabla \cdot v_{\text{turb}} \neq 0$	-11/3	0.9	0.75	0.1	0.01
3.4.6	0.01	$\nabla \cdot v_{\text{turb}} \neq 0$	-11/3	0.9	1.0	0.1	0.01
3.4.7	0.01	$\nabla \cdot v_{\text{turb}} \neq 0$	-11/3	0.5, 1.1	0.75	0.1	0.01

coincides with the end of an accretion-driven outflow (responsible for sweeping up the gas) and the start of subsequent gas infall.

Clearly a smooth and symmetric gas shell is not realistic in view of the turbulent motion and a non-uniform distribution of the swept-up ISM. Hence I add some turbulence to the initial velocity field. In particular, the velocity of each particle is the weighted sum of a turbulent and a purely rotational velocity field, i.e.

$$\mathbf{v}_i = \chi \mathbf{v}_{\text{turb}}(\mathbf{r}_i) + (1 - \chi) \mathbf{v}_{\text{rot}}(\mathbf{r}_i), \quad (3.5)$$

where the mixture parameter χ equals 0.75 for most of my simulations. The turbulent velocity field is a Gaussian random field with a Kolmogorov (1941)¹ power spectrum $P \propto k^n$, where $n = -11/3$ for most of my simulations (see Section 3.2.2 for details of how the velocities are generated) and scaled such that

$$\sum_i m_i \mathbf{v}_{\text{turb}}^2(\mathbf{r}_i) = \eta_{\text{turb}} \sum_i \frac{Gm_i M_\bullet}{|\mathbf{r}_i|}, \quad (3.6)$$

i.e. η_{turb} is the virial ratio in the case $\chi = 1$ (when only the turbulent velocity component contributes to \mathbf{v}_i). In general, \mathbf{v}_{turb} is not divergence free, though I also study the case where $\mathbf{v}_{\text{turb}}(\mathbf{r})$ is constructed to satisfy $\nabla \cdot \mathbf{v}_{\text{turb}} = 0$ everywhere. \mathbf{v}_{rot} corresponds to solid-body rotation with a fraction η_{rot} of the circular speed at the shell radius, i.e.

$$\mathbf{v}_{\text{rot}}(\mathbf{r}) = \eta_{\text{rot}} \mathbf{r} \times \hat{\mathbf{e}}_z \sqrt{GM_\bullet / r_{\text{shell}}^3}. \quad (3.7)$$

In all my simulations the numerical values for η_{turb} and η_{rot} are identical and set to $\eta = 0.9$ for most simulations. This implies that the virial ratio for my initial conditions satisfies

$$\frac{2E_{\text{kin}}}{-E_{\text{pot}}} = \frac{\sum_i m_i \mathbf{v}_i^2}{\sum_i Gm_i M_\bullet / |\mathbf{r}_i|} \approx \chi^2 \eta_{\text{turb}} + \frac{2}{3} (1 - \chi)^2 \eta_{\text{rot}}^2. \quad (3.8)$$

This relation would be exact, if the shell was infinitely thin and the turbulent and rotational velocities were uncorrelated over the particles such that $\sum_i m_i \mathbf{v}_{\text{turb},i} \cdot \mathbf{v}_{\text{rot},i} = 0$. For my default parameter setting of $\chi = 0.75$ and $\eta = 0.9$, this evaluates to $-2E_{\text{kin}}/E_{\text{pot}} \approx 0.54$, i.e. the system is sub-virial, but not excessively so. By varying both χ and η any combination for the contributions of rotation and

¹English translation as Kolmogorov, 1991.

turbulence to the velocity field can be obtained, but I only investigate changes in one or the other parameter.

Finally, I assume an isothermal equation of state for the gas with sound speed c_s , which for most simulations equals 0.1 times the circular speed at the initial shell radius, $\sqrt{GM_\bullet/r_{\text{shell}}}$.

Particles coming closer to the central sink particle than r_{sink} , which defaults to $0.01r_{\text{shell}}$, are absorbed, i.e. their mass, momentum, and angular momentum is added to the sink particle, which carries a spin for this purpose. This effectively implements an inner boundary condition to the model and is necessary to avoid excessively short time steps.

The total gas mass is set to be $M_{\text{shell}} = 0.01M_\bullet$ for most of my simulations, but I run a set of simulations with ten or hundred times more gas as well. The simulations presented all contain $N_{\text{gas}} = 2 \times 10^6$ gas particles. I experimented with larger numbers (4×10^6 and 8×10^6) and found no significant difference in the results presented below in contrast to simulations with $N_{\text{gas}} = 10^6$ or less.

Although by default I would normally ignore the self-gravity of the gas, it has been included in a few sets of simulations (see Section 5.4). However, I ignore the gravity from the galactic host, because the gravity in the simulated volume is dominated by the hole (also the dynamics studied are not critically dependent on the Keplerian nature of ballistic trajectories).

The random nature of the initial turbulent velocities implies that details of the simulated flows (e.g. position and angular momentum of the gas clumps) are random, too. Indeed I find variations between simulations when I utilise different random seeds to generate the turbulent velocities, but keep the other parameters identical. In order to assess this variation and the main trends, I ran for each set of physical parameters considered a set of six simulations differing only in the random seed for the turbulent velocities.

Table 3.1 gives an overview over all simulations and their parameters presented here.

3.3 The reference simulations

In view of the lack of detailed observational data and the huge parameter space, I chose to pick typical physical parameters to define a reference simulation. In this section I present the results from this reference simulation (and its random

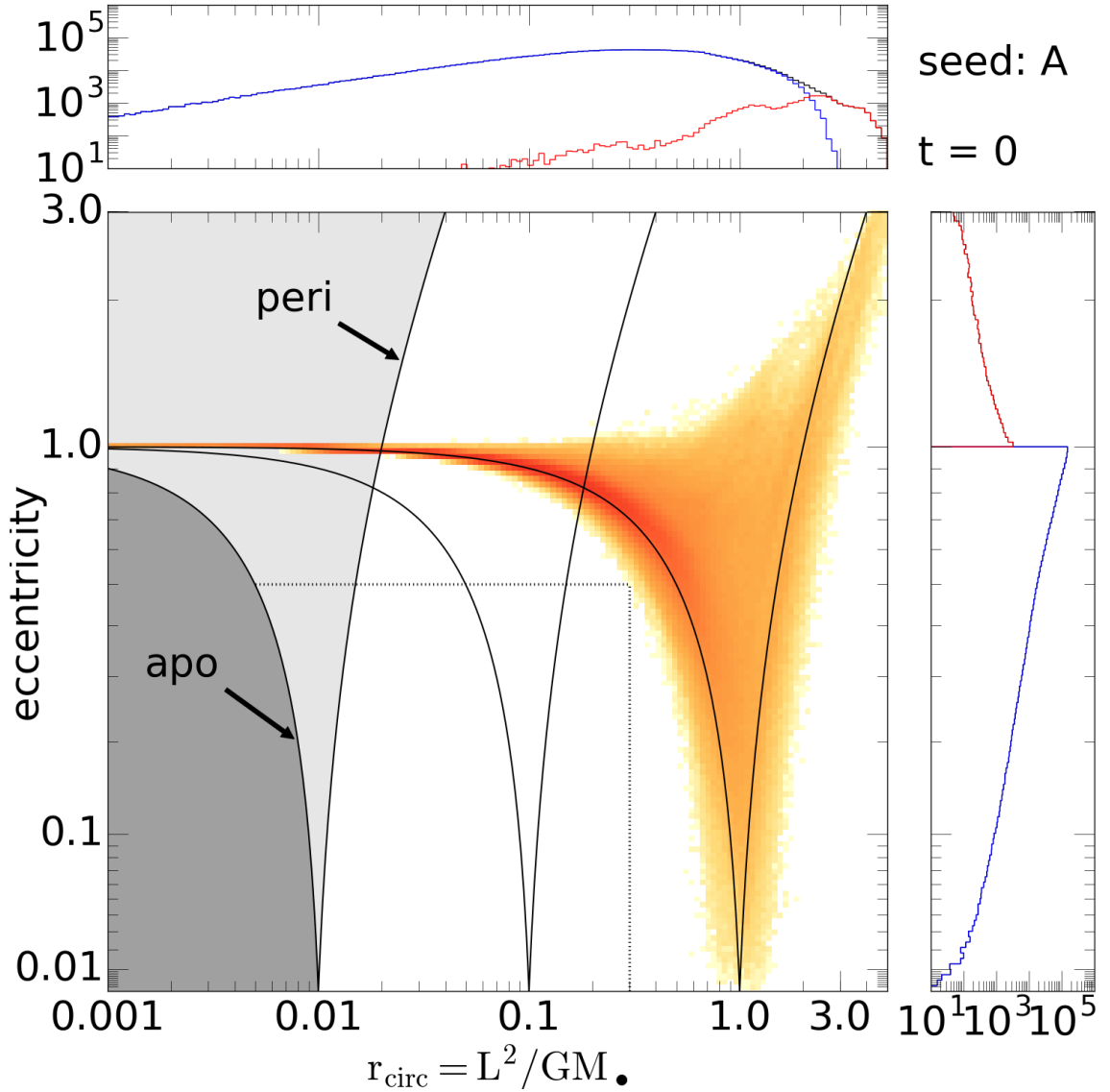


FIGURE 3.1: Distribution of the initial gas shell (at $r \approx r_{\text{shell}}$) over eccentricity e and circularisation radius $r_{\text{circ}} = L^2/GM_{\bullet}$ for the reference simulation (see Section 3.3.1). Loci of constant peri/apo-centre, $r_{\text{apo,peri}} = r_{\text{circ}}/(1 \mp e)$, are indicated by outward/inward bending curves. In particular, the dark and light grey region correspond to orbits with, respectively, apo-centre and pericentre within the absorption radius of the central sink particle: orbits in the light grey region cross into the absorption region, whereas the dark grey region is inaccessible to simulated gas. The thin rectangular box indicates orbits classified as ‘disc’ in later figures. In the distributions over e (right) and r_{circ} (top), black indicates the total, blue the bound ($e < 1$), and red the unbound ($e \geq 1$) fraction. Most gas is initially in the region $r_{\text{peri}} - \sigma_r \leq r_{\text{shell}} < r_{\text{apo}} + \sigma_r$, as expected. The tail at $e \sim 1$ and small r_{circ} originates from gas with near-zero angular momentum currently near apo-centre $r_{\text{apo}} \approx r_{\text{shell}}$.

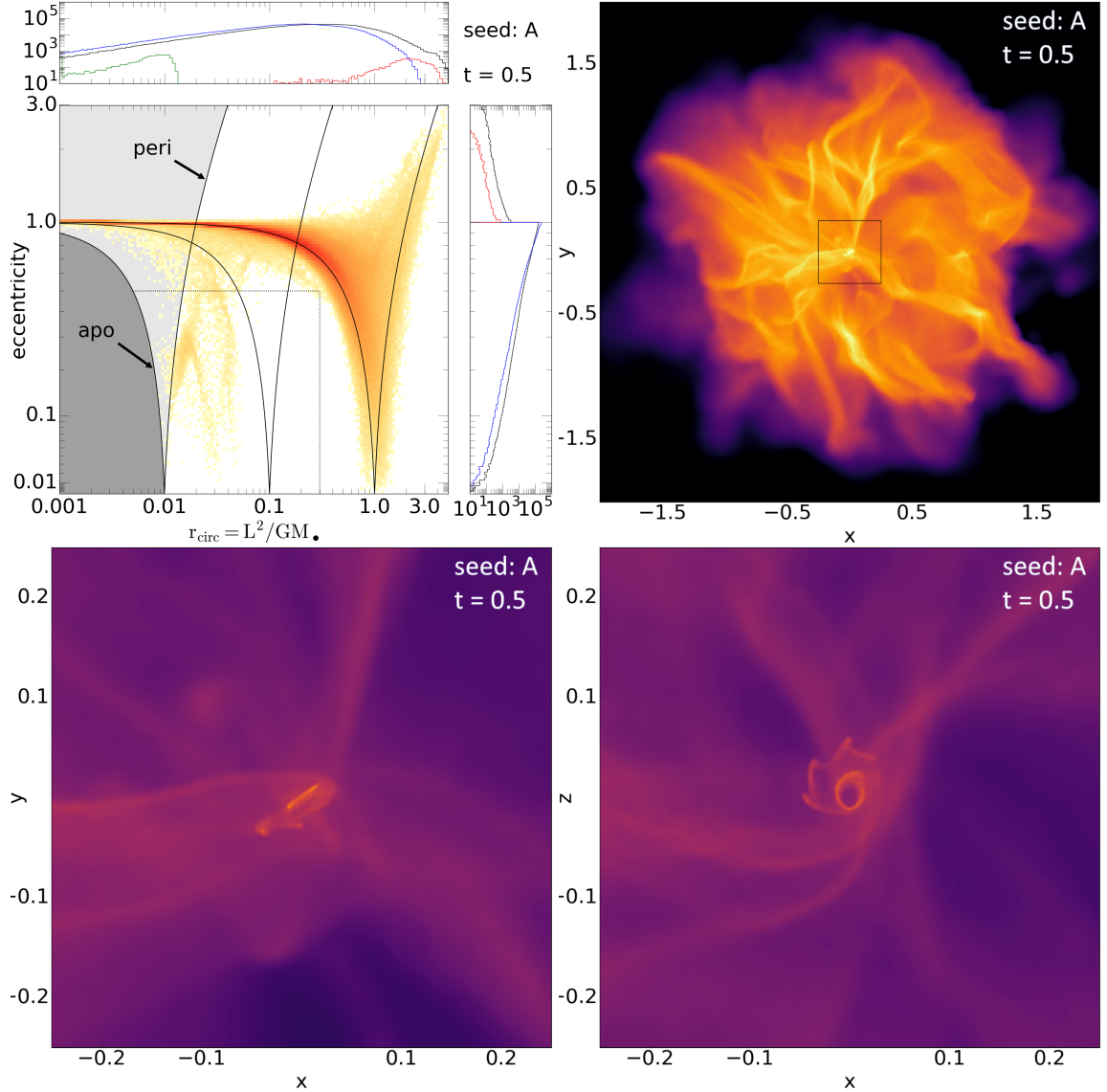


FIGURE 3.2: Snapshots for the reference simulation at $t = 0.5$. *Top left*: gas distributions over e and r_{circ} (as in Fig. 3.1). The black and green histograms in the top and right sub-panels refer, respectively, to the initial state and the absorbed gas (the bin at $r_{\text{circ}} = 0.001$ includes gas absorbed with $r_{\text{circ}} \leq 0.001$). *Top right*: gas density (log scale with range of 10^6) over (x, y) for gas near $z = 0$, centred on the sink particle. *Bottom left*: a zoom into the inner part of the plots in the top right. *Bottom right*: like the bottom left plot, but for gas near the $y = 0$ plane. The central gap in the disc visible in the bottom plots is due to the inner boundary, where gas reaching $r_{\text{sink}} = 0.01$ is absorbed into the sink. In the top left plot this disc corresponds to the structure at $e \lesssim 0.3$ and $r_{\text{circ}} \lesssim 0.1$.

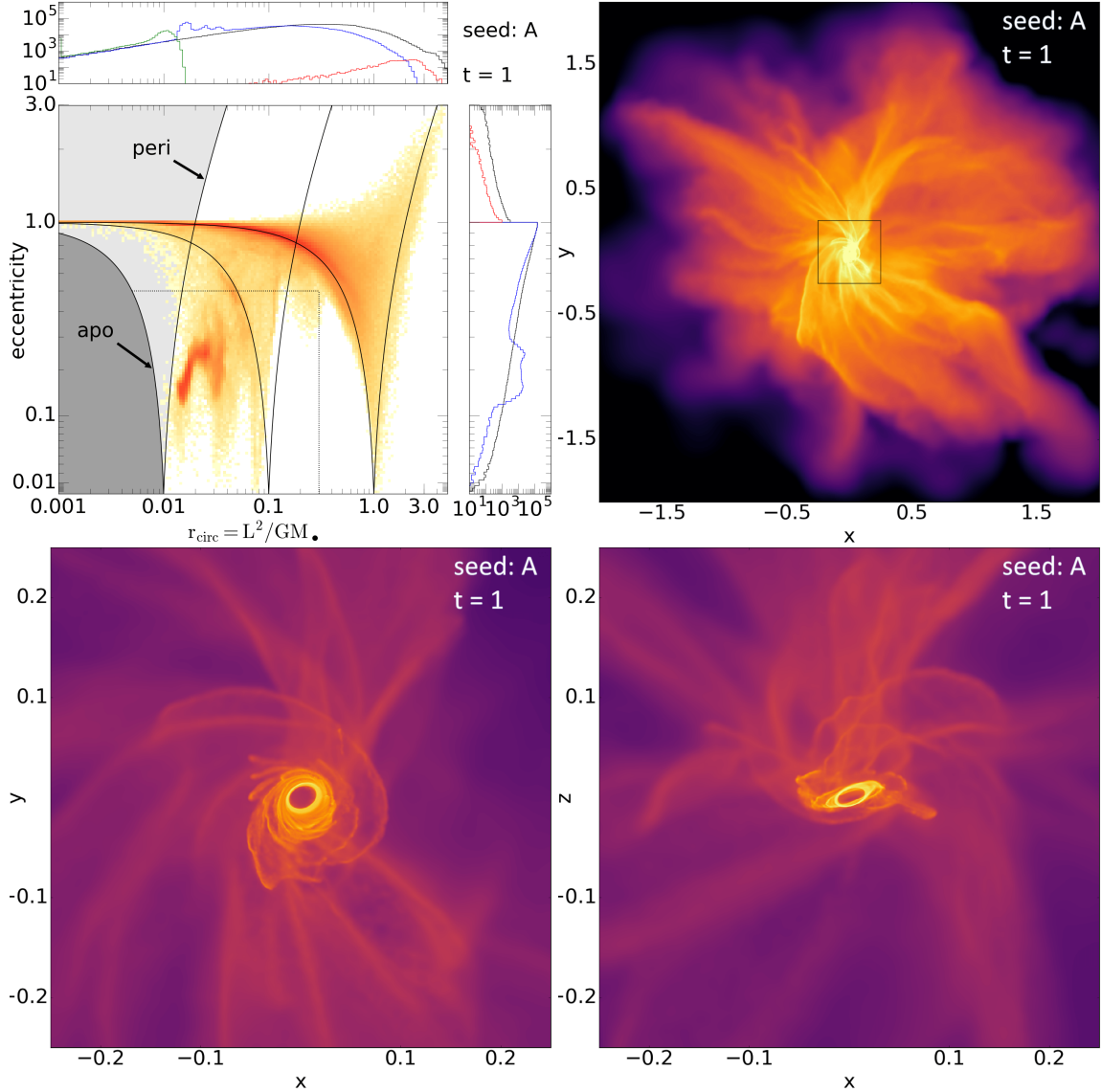


FIGURE 3.3: Snapshots for the reference simulation at $t = 1.0$. *Top left*: gas distributions over e and r_{circ} (as in Fig. 3.1). The black and green histograms in the top and right subpanels refer, respectively, to the initial state and the absorbed gas (the bin at $r_{\text{circ}} = 0.001$ includes gas absorbed with $r_{\text{circ}} \leq 0.001$). *Top right*: gas density (log scale with range of 10^6) over (x, y) for gas near $z = 0$, centred on the sink particle. *Bottom left*: a zoom into the inner part of the plots in the top right. *Bottom right*: like the bottom left plot, but for gas near the $y = 0$ plane. The central gap in the disc visible in the bottom plots is due to the inner boundary, where gas reaching $r_{\text{sink}} = 0.01$ is absorbed into the sink. In the top left plot this disc corresponds to the structure at $e \lesssim 0.3$ and $r_{\text{circ}} \lesssim 0.1$.

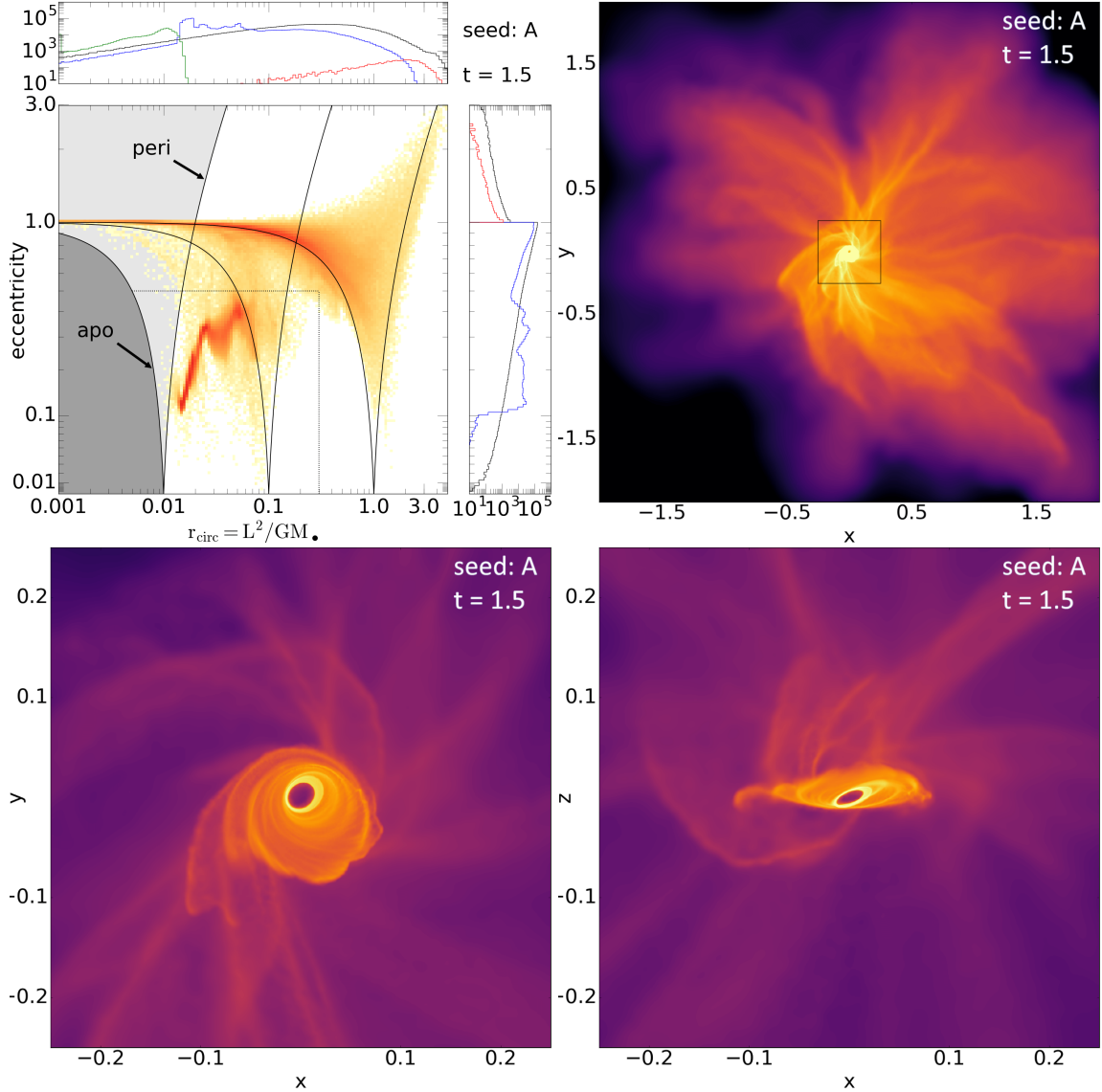


FIGURE 3.4: Snapshots for the reference simulation at $t = 1.5$. *Top left*: gas distributions over e and r_{circ} (as in Fig. 3.1). The black and green histograms in the top and right subpanels refer, respectively, to the initial state and the absorbed gas (the bin at $r_{\text{circ}} = 0.001$ includes gas absorbed with $r_{\text{circ}} \leq 0.001$). *Top right*: gas density (log scale with range of 10^6) over (x, y) for gas near $z = 0$, centred on the sink particle. *Bottom left*: a zoom into the inner part of the plots in the top right. *Bottom right*: like the bottom left plot, but for gas near the $y = 0$ plane. The central gap in the disc visible in the bottom plots is due to the inner boundary, where gas reaching $r_{\text{sink}} = 0.01$ is absorbed into the sink. In the top left plot this disc corresponds to the structure at $e \lesssim 0.3$ and $r_{\text{circ}} \lesssim 0.1$.

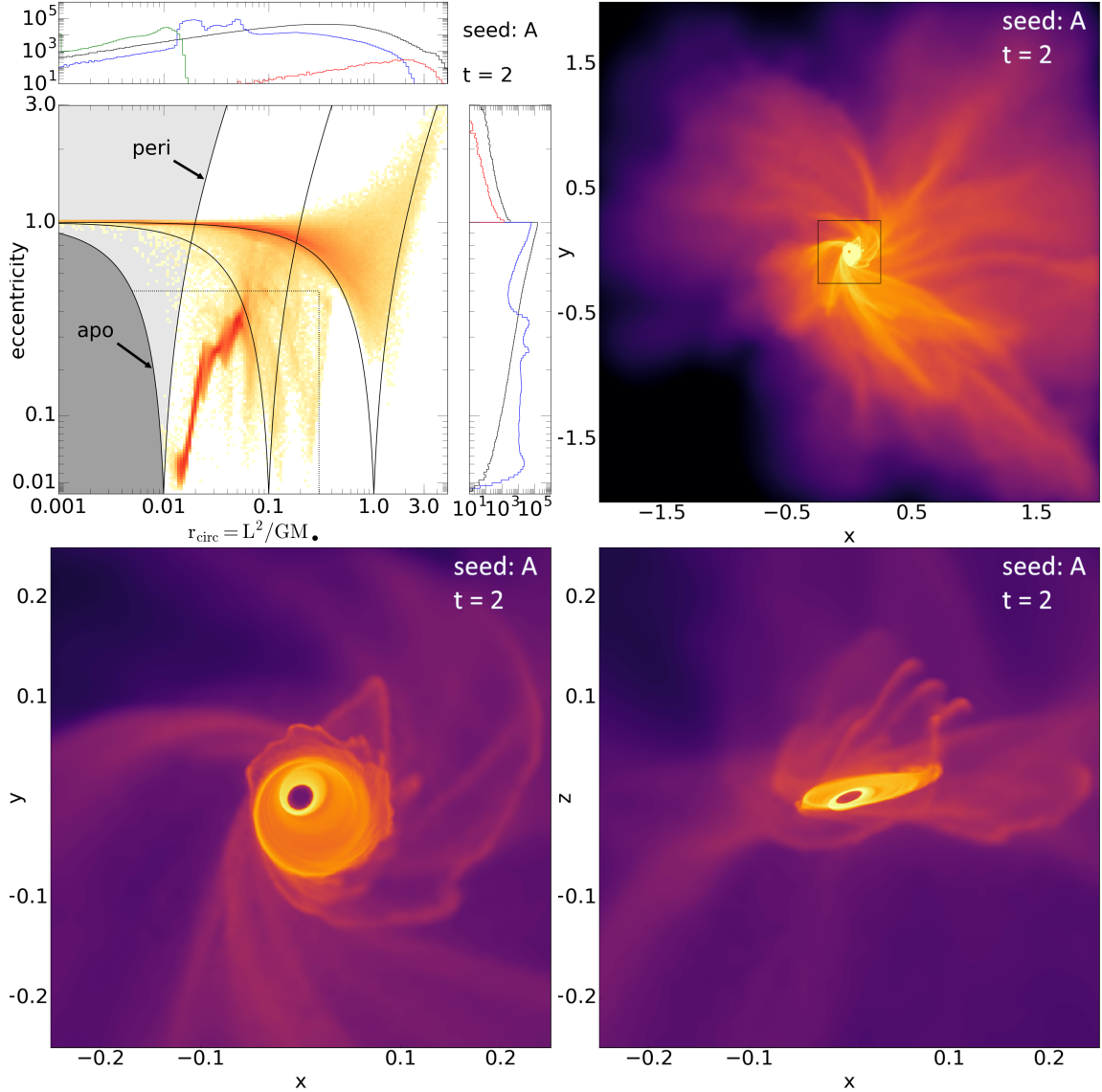


FIGURE 3.5: Snapshots for the reference simulation at $t = 2.0$. *Top left*: gas distributions over e and r_{circ} (as in Fig. 3.1). The black and green histograms in the top and right sub-panels refer, respectively, to the initial state and the absorbed gas (the bin at $r_{\text{circ}} = 0.001$ includes gas absorbed with $r_{\text{circ}} \leq 0.001$). *Top right*: gas density (log scale with range of 10^6) over (x, y) for gas near $z = 0$, centred on the sink particle. *Bottom left*: a zoom into the inner part of the plots in the top right. *Bottom right*: like the bottom left plot, but for gas near the $y = 0$ plane. The central gap in the disc visible in the bottom plots is due to the inner boundary, where gas reaching $r_{\text{sink}} = 0.01$ is absorbed into the sink. In the top left plot this disc corresponds to the structure at $e \lesssim 0.3$ and $r_{\text{circ}} \lesssim 0.1$.

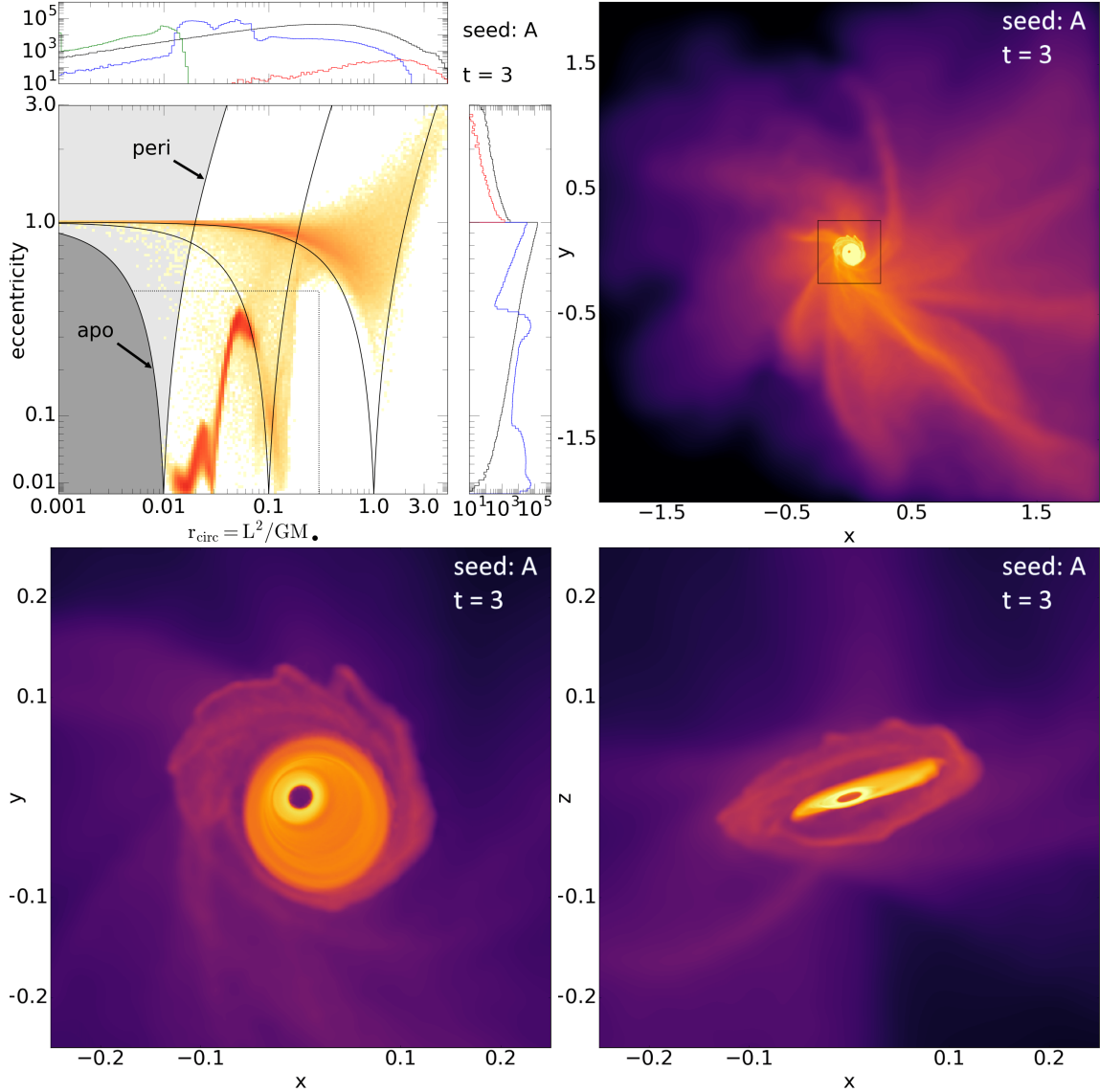


FIGURE 3.6: Snapshots for the reference simulation at $t = 3.0$. *Top left*: gas distributions over e and r_{circ} (as in Fig. 3.1). The black and green histograms in the top and right subpanels refer, respectively, to the initial state and the absorbed gas (the bin at $r_{\text{circ}} = 0.001$ includes gas absorbed with $r_{\text{circ}} \leq 0.001$). *Top right*: gas density (log scale with range of 10^6) over (x, y) for gas near $z = 0$, centred on the sink particle. *Bottom left*: a zoom into the inner part of the plots in the top right. *Bottom right*: like the bottom left plot, but for gas near the $y = 0$ plane. The central gap in the disc visible in the bottom plots is due to the inner boundary, where gas reaching $r_{\text{sink}} = 0.01$ is absorbed into the sink. In the top left plot this disc corresponds to the structure at $e \lesssim 0.3$ and $r_{\text{circ}} \lesssim 0.1$.

sisters) in detail, while in the Section 3.4 individual parameters are altered to investigate their importance. The physical parameters for the reference simulation have already been mentioned in the previous section and can also be found in the top row of Table 3.1.

3.3.1 A detailed look at a representative simulation

A representation of the initial conditions can be seen in Figure 3.1. The central panel shows the distribution of the initial gas shell over eccentricity e and the circularisation radius $r_{\text{circ}} = L^2/GM_{\bullet}$. The majority of gas is initially bound ($e < 1$) and, as $r \sim r_{\text{shell}} = 1$, resides between the curves for $r_{\text{peri}} = r_{\text{shell}}$ and $r_{\text{apo}} = r_{\text{shell}}$. Most of the unbound gas will quickly become bound due to the initial interactions caused by the turbulence imposed on the initial velocity field.

Material with $r_{\text{circ}} \ll r_{\text{shell}}$ and $e \sim 1$ has very small angular momentum, but resides near its apo-centre. As the simulation progresses, this tail of the distribution remains occupied by low-angular-momentum gas near its apo-centre (i.e. at $r \gg r_{\text{circ}}$). Individual gas particles stay only briefly (typically much shorter than a local dynamical time) in this region, because their angular momentum is altered by local hydrodynamics and minute changes in the SMBH position and velocity.

The top and right panels plot the gas distributions over r_{circ} and e , respectively, using different colours for bound (blue) and unbound (red) gas. In later versions of this plot, I distinguish the initial distributions and gas absorbed into the central sink particle as well (black).

Figure 3.2–3.6 shows snapshots at $t = 0.5, 1, 1.5, 2,$ and 3 utilising different representations. The top left graph shows the gas distribution over e and r_{circ} as in Figure 3.1, while the remaining graphs display column density plots at different scales and projections.

The time evolution of the gas happens roughly in two phases, which are approximately separated by the free-fall time

$$t_{\text{ff}} = \frac{\pi}{\sqrt{8}} \sqrt{r_{\text{shell}}^3 / GM_{\bullet}}, \quad (3.9)$$

when most of the gas reaches the inner regions around the SMBH and forms or feeds a nuclear disc. In the first $t \sim 0.1t_{\text{ff}}$ (not represented in Figure 3.1), the turbulent velocity field produces filaments and clumps, which are ~ 10 times

denser than the initial state resulting in a clumpy, weakly rotating shell of gas. During this very early phase, the amount of unbound gas decreases (as energy is dissipated), though the distribution over e and r_{circ} hardly changes otherwise.

Subsequently, the filaments and clumps fall towards the central region and are stretched into extended streams by tidal forces. The resulting focusing of material drastically enhances the chance of interactions and results in angular-momentum cancellation. This in turn reduces the average r_{circ} and increases the average e . By $t \sim 0.5$ (Figure 3.2) the first simulated gas has reached the inner region with some being absorbed into the sink and some starting to circularise and to form a disc. The orientation of this early disc is roughly edge-on if viewed along the z -axis, i.e. not aligned with the overall initial angular momentum of the shell. Further infall changes this original tilt and by $t \sim t_{\text{ff}}$ (Figure 3.3) a disc has formed, which is aligned with the overall angular momentum. This disc is clearly visible as a peak at $e \sim 0.2$ and $r_{\text{circ}} \sim 0.025$ in the distribution over e and r_{circ} (Figure 3.3, top left plot).

In the following evolution, additional infalling filaments hit the disc and may cause angular-momentum cancellation followed by circularisation resulting in the growth of the disc out to $0.1r_{\text{shell}}$, though still with substantial eccentricities of $e \sim 0.1 - 0.4$. This phase lasts roughly to $t = 1.5t_{\text{ff}}$, when further infall of filaments and clumps onto the disc ceases sufficiently for the disc to settle. In particular in its inner parts, the eccentricity drops to $e \ll 0.1$, while it remains quite eccentric in its outer parts. The disc suffers a small, but constant flow of gas into the (unresolved) inner region at $r < r_{\text{sink}}$.

Since the focus of this study is the interaction of the filaments, the simulation is stopped at $t = 3$ (Figure 3.6). A comparison of the distributions over r_{circ} (Figure 3.2–3.6, top left: top sub-panels) between the initial conditions (black) with the gravitationally bound gas (blue) and gas absorbed (green) at the end of the simulations clearly shows a considerable shift towards lower r_{circ} . At the end of the simulation $\sim 1/5$ of the gas has reached $r < r_{\text{sink}} = 0.01r_{\text{shell}}$ (at which moment gas particles are absorbed into the sink) and a further $\sim 2/3$ are inside the disc region. The majority of the remaining gas ($\sim 1/10$ of the initial amount) is bound, but on eccentric orbits.

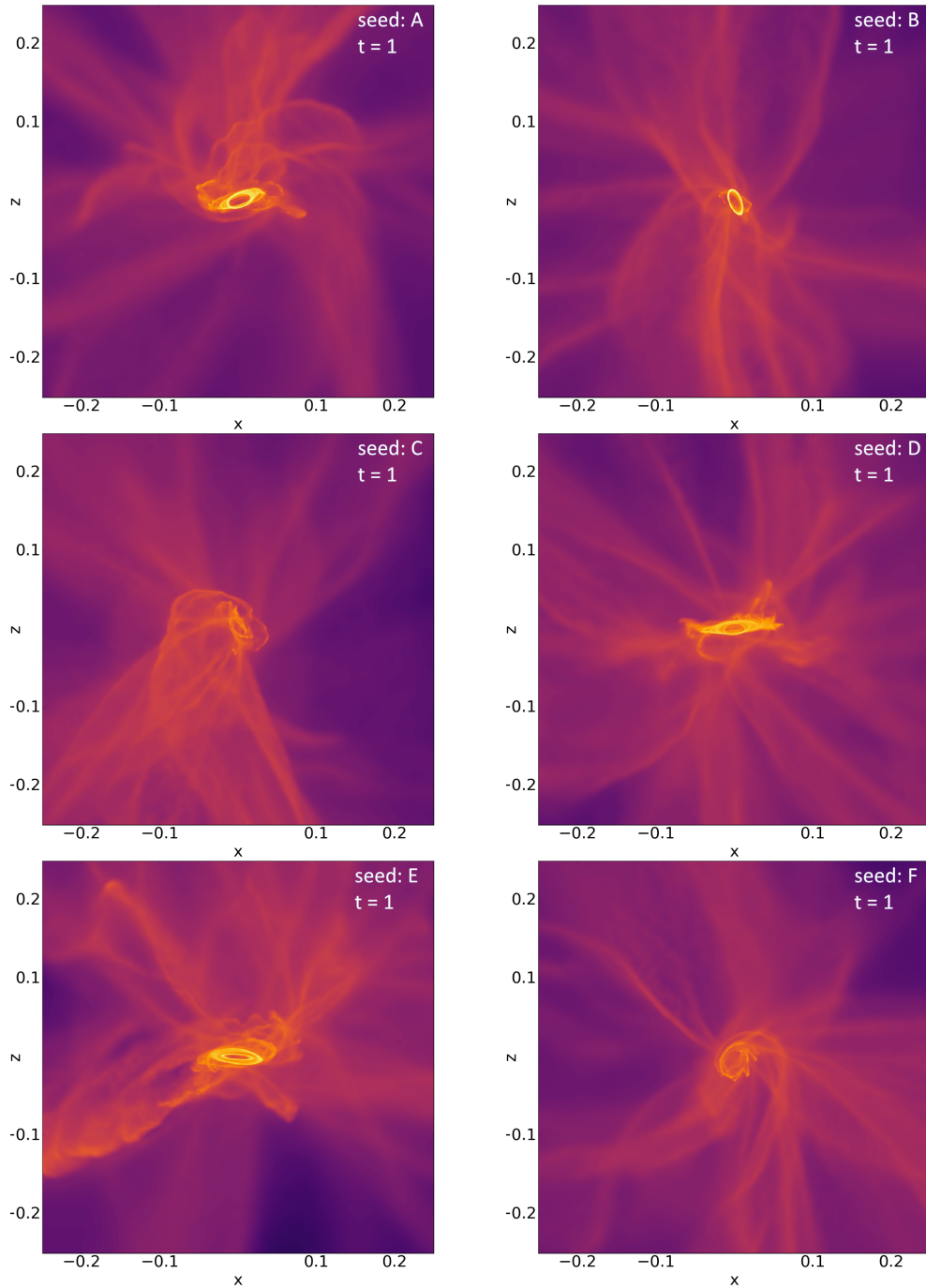


FIGURE 3.7: Density plots (as in bottom right of Figure 3.3) at time $t = 1$ for the sextet of reference simulations which differ only by the random seed used to generate the turbulent velocities and have the same parameters as the simulation presented in detail in Section 3.3.1 and Figure 3.3 (shown here in the top left). Discs orientated in accordance with the net angular momentum of the initial conditions would appear edge-on and horizontally aligned.

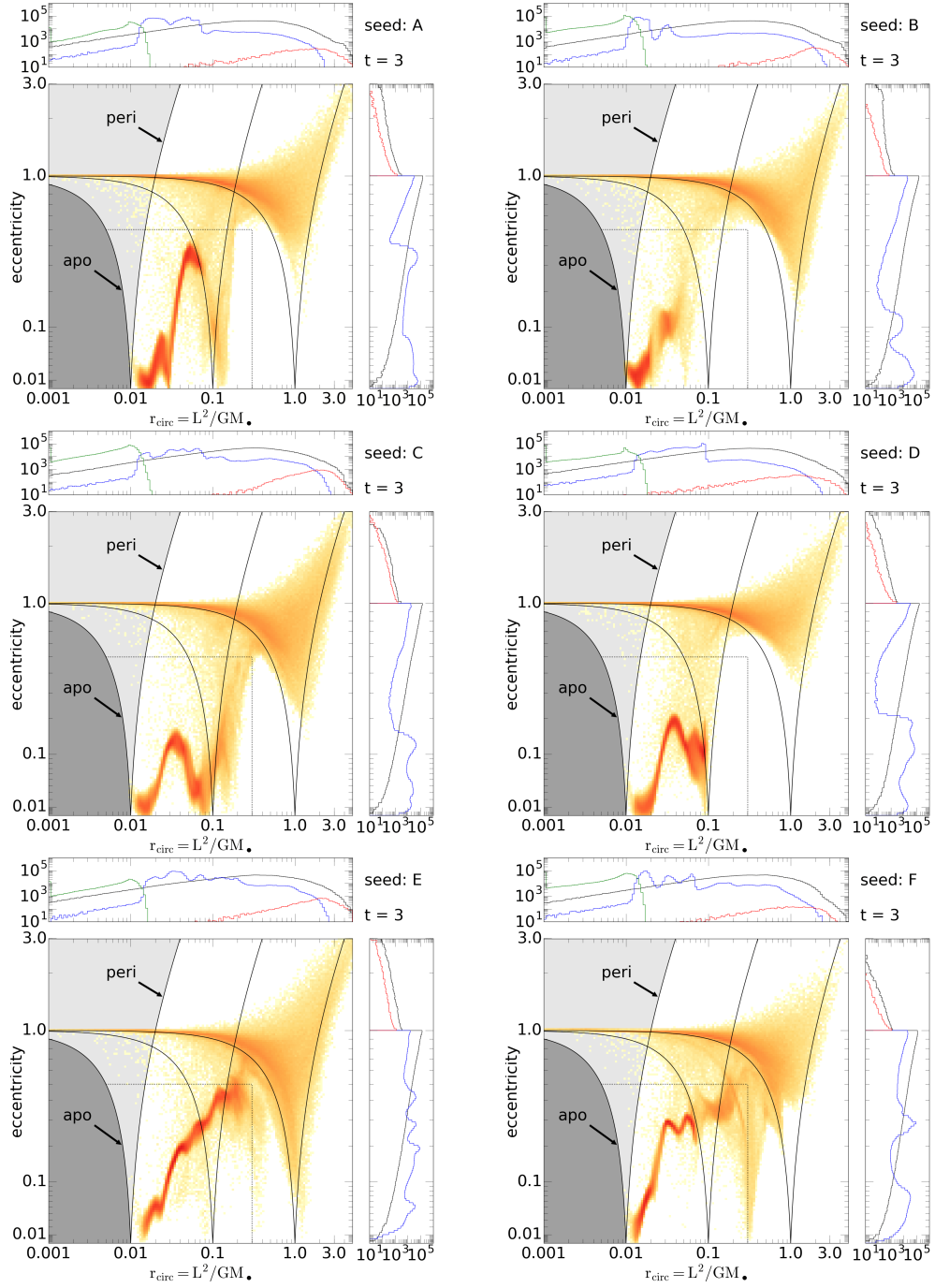


FIGURE 3.8: Distributions over e and r_{circ} (as in Figure 3.1 or Figure 3.6) at the final simulation time $t = 3$ for the sextet of reference simulations which differ only in the random components of their initial conditions (the same simulations for which Figure 3.7 shows snapshots at time $t = 1$). While there is considerable variation of the disc structure and extent, the overall distributions of circularisation radii (top histograms) are similar.

3.3.2 Simulations differing only by the random seed

The choice of the random number seed used to generate the turbulent velocity field does not affect the velocity power spectrum, but results in large local differences in the velocity and, consequently, in the emerging density distributions of the infalling gas as well. Therefore, any two simulations with different random seed may differ considerably in their details. In order to assess how much variation there is and which results are least variable, I conduct a suite of five additional simulations with the same parameters as those presented in the previous sub-section, but utilising different random seeds.

For the resulting simulation sextet, Figure 3.7 shows the density distributions near the $y = 0$ plane at time $t = 1$ (Figure 3.3, bottom right). At this early time, only three of the six simulations (A, D, E) have formed a disc that is roughly aligned with the net angular momentum imposed on the initial conditions, while one (B) has a disc that is almost perpendicular to that orientation and two (C&F) have hardly formed any well-defined disc structure at all. There is large variation in the tilt/warp and eccentricity of these discs, as well as in the filamentary structures. Over the course of these simulations, new infall can substantially disrupt any previously formed discs including re-orientation or the formation of nested, but mutually (strongly) inclined discs.

For the same six simulations, Figure 3.8 shows the distributions over e and r_{circ} at time $t = 3$, the end of the simulations. All simulations have eventually formed some sort of disc corresponding to the structures at $e \lesssim 0.5$ and $r_{\text{circ}} \lesssim 0.3$. Moreover, these discs all approach circularity ($e \lesssim 0.02$) at their inner simulated edge at $r_{\text{circ}} \sim 0.01$. At $r_{\text{circ}} \lesssim 4r_{\text{sink}}$, such circularisation is largely an artefact of the inner boundary condition, as simulations with smaller r_{sink} demonstrate (see Chapter 4). However, the general trend that the disc is less eccentric at smaller radii, (also seen in the aforementioned simulations with smaller r_{sink}) and can be understood in terms of the faster evolution (shorter dynamical time) at smaller radii. Apart from this general trend, the details of the disc structures vary considerably between the six simulations including their sizes: typically the disc edge occurs at $r_{\text{circ}} \sim 0.1$, but shows a variation of a factor ~ 10 (between 0.03 and 0.3 for simulations B and E, respectively).

Figure 3.9 shows how the averages of r_{circ} and e as well as the gas fractions

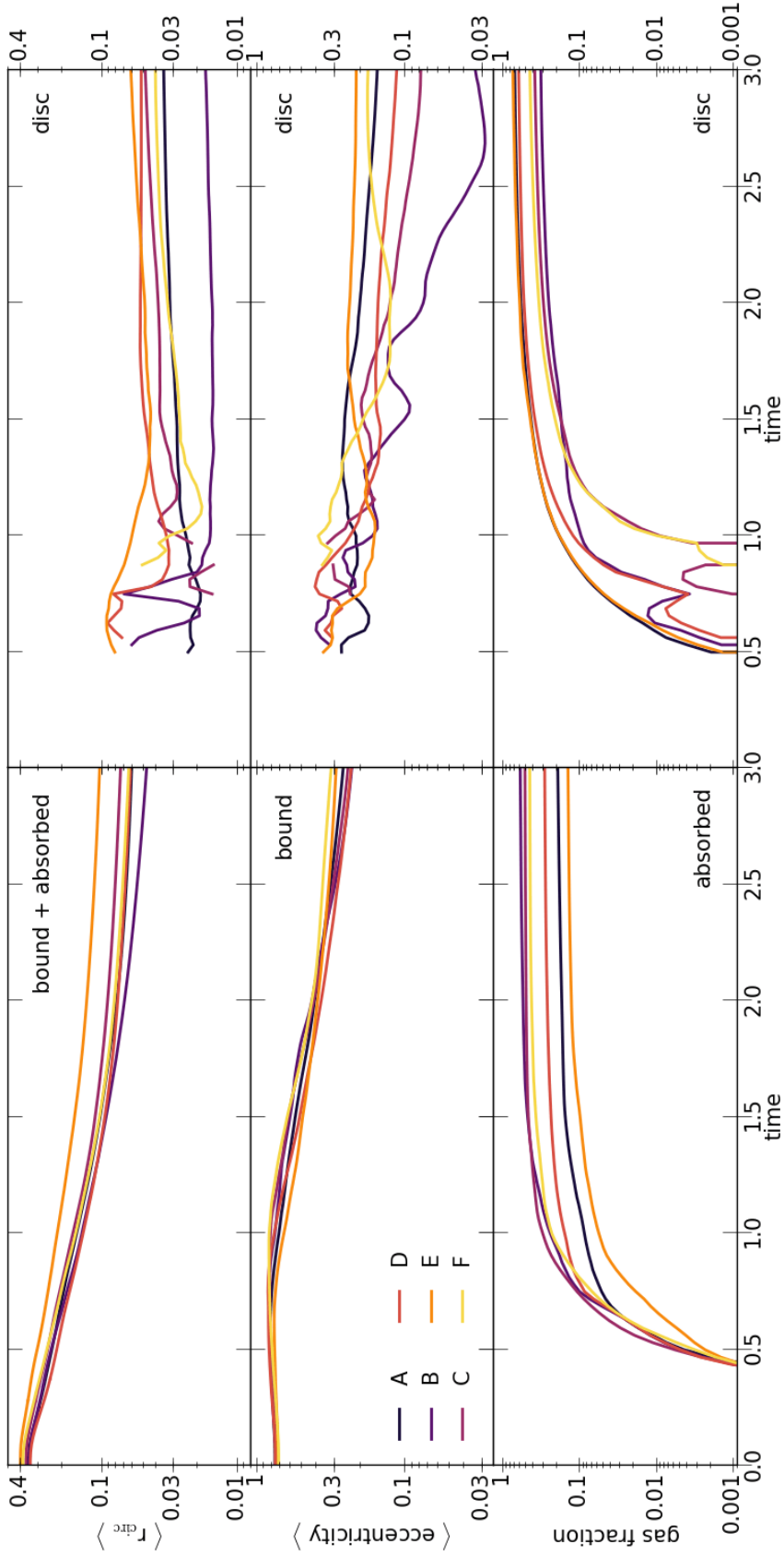


FIGURE 3.9: Time evolution of the average circularisation radius and eccentricity as well as the gas fraction for different portions of the gas and for each of the sextet of reference simulations already shown in Figs. 3.7 and 3.8. ‘Absorbed’ refers to simulated gas that at some point prior to t has reached $r < r_{\text{sink}} = 0.01$ and was absorbed into the central sink particle; ‘bound’ refers to all remaining gas that at the given time has $e < 1$, ‘disc’ represents all bound gas at $e \leq 0.5$ and $r_{\text{circ}} \leq 0.3$ indicated by a thin dotted rectangle in Figure 3.1 (which may also contain a small fraction of impacting filaments).

evolves for certain gas components (see the figure caption for the precise definition of the categories ‘bound’, ‘absorbed’ and ‘disc’). Again, I can distinguish several phases of evolution. Before $t = 0.5$ no gas has reached $r = r_{\text{sink}}$ and the formation of density filaments from the turbulent velocity field resulted in some reduction of the mean r_{circ} owing to angular-momentum cancellation between impacting gas. Between $t = 0.5$ and $t = 1$ infalling material is either directly absorbed (because it reached $r = r_{\text{sink}}$) or contributes to a forming disc. The early phases of disc formation may even involve the complete disruption of an earlier disc (simulations C & F). After $t = 1$, the disc formation consolidates, when further infalling filaments contribute to the growing disc, which prevents any significant further direct infall to $r < r_{\text{sink}}$.

The largest variations occur in the disc properties, whose mean eccentricity and circularisation radius varies by factors of ~ 5 , while the total amount of gas in the disc varies by a factor of 2-3 with less massive discs forming later. The amount of gas at $r < r_{\text{sink}}$ (particles absorbed into the sink), i.e. material that may ultimately reach the central SMBH varies by a factor ~ 4 .

3.4 Effects of varying the parameters

In this section, I vary (usually) one of the parameters of the simulations, but keep the initial conditions otherwise identical (as much as possible) to those used for the six simulations presented in the previous section. In this way, the effect of the parameter considered can be isolated in the clearest way, while at the same time ensuring that I capture any variation across the different random realisations of the same physics.

3.4.1 Sound speed

The assumed overall gas temperature or, equivalently sound speed, influences the nature of the filaments: small c_s (low temperature) leads to denser filaments with smaller cross sections for collision, which may reduce the efficiency of angular-momentum cancellations. Large c_s (higher temperature) smooths out small-scale modes of the turbulent shell and results in a lower density in the filaments. Additionally the disc structure is directly influenced by the value of c_s through the

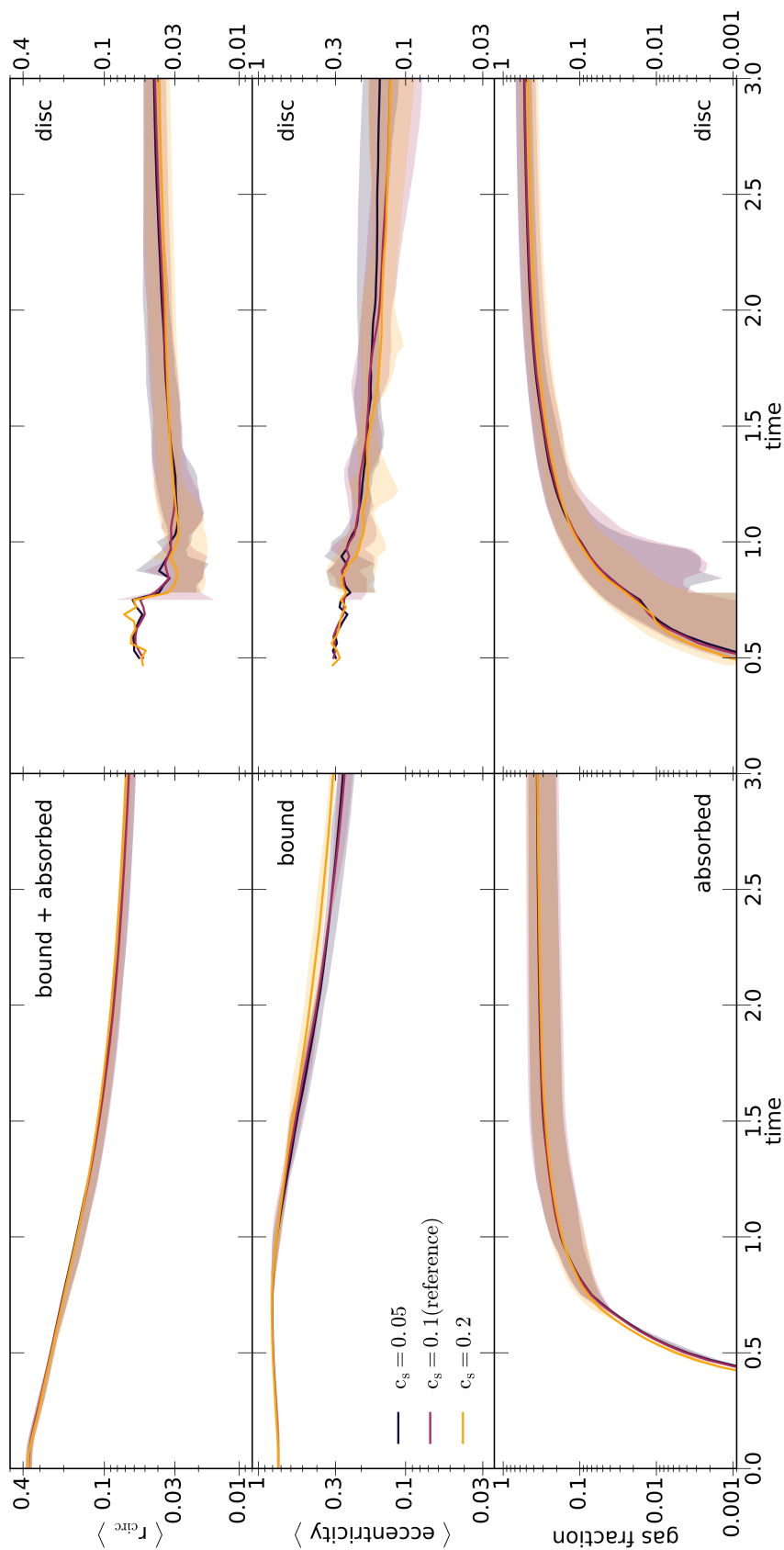


FIGURE 3.10: Similar to Figure 3.9, except that I compare three sextets of simulations, each with a different value of the gas temperature (or sound speed as indicated). Each sextet is indicated by a curve for its mean and a band covering the 17 and 83 percentiles (excluding the two most extreme simulations).

conditions for a vertical hydrostatic equilibrium with smaller values resulting in a thinner discs.

The value of the sound speed used for the reference simulation is 0.1, i.e. a tenth of the circular speed at $r = r_{\text{shell}}$. Two suites of simulations with $c_s = 0.05$ and 0.2 with the latter corresponding to an increase in temperature by a factor 4 are summarised in Figure 3.10.

Simulations $c_s = 0.05$ behave very similarly to the reference simulations. However, the slightly denser infalling filaments are more likely to form rings, which can be up to 10 times denser than the more uniform disc structure in the reference simulations. The disc is on average more eccentric than for larger c_s and the latest infall remains often visible as a ring separated by a low-density gap from the original disc.

Simulations with $c_s = 0.2$ form wider and less dense filaments, which have a higher collision cross section and form a disc earlier than the reference simulation. A larger pressure is likely to better erase the small-scale fluctuations of the initial velocity field and, consequently, simulations with $c_s = 0.2$ share some characteristics with simulations starting from velocities with a steeper power spectrum ($P \propto k^{-9/2}$ in Figure 3.11): larger mean eccentricities and circularisation radii in the bound gas and less material in the disc.

In general, however, there is very little variation in the gross statistical properties between simulations that differ by a factor 4 in the sound speed (or a factor 16 in temperature).

3.4.2 Power spectrum of the turbulent velocity field

Changing the slope of the power spectrum has a profound impact on the evolution of the simulation due to its influence on the distribution of the energy in the initial turbulent velocity field. For the reference simulation $P \propto k^{-11/3}$, bracketed by the two additional sets of simulations with $P \propto k^{-5/2}$ (shallower) and $P \propto k^{-9/2}$ (steeper), respectively, the results of these simulations are summarised in Figure 3.11. Recent observations of scattering material in the Galactic Centre have revealed a shallower spectrum than the suggested Kolmogorov spectrum of $P \propto k^{-11/3}$ and therefore providing further motivation to investigate the changes caused by a differing spectrum (Johnson et al., 2018)

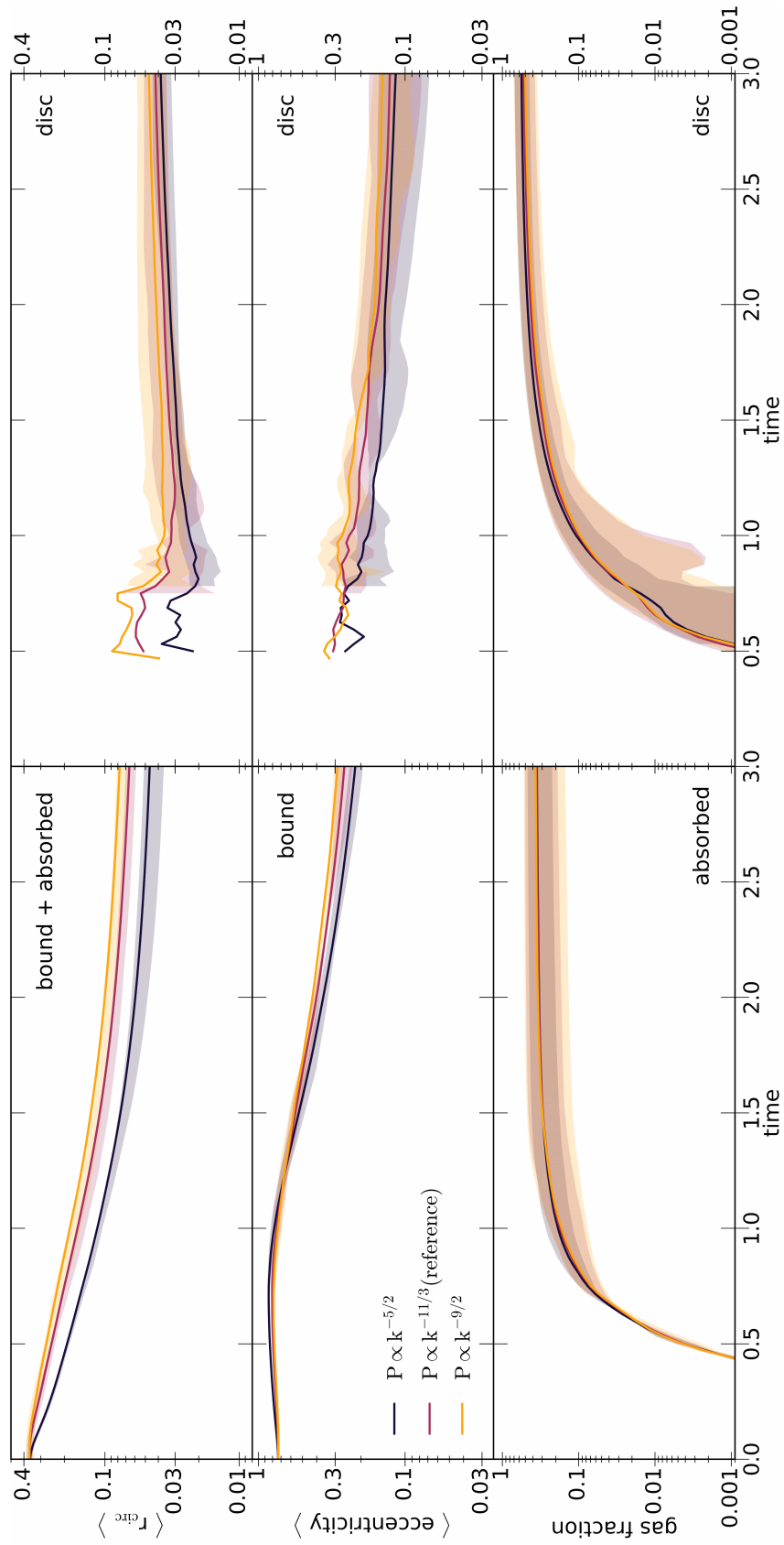


FIGURE 3.11: As Figure 3.10, but for simulations with different power spectrum of the turbulent velocity field.

For $P \propto k^{-5/2}$ there are more small-scale fluctuations in the emerging density field shortly after the start of the simulations, when compared to the reference simulations. This is reflected in more substructure in the filaments, while the maximal density remains similar. The main effect in terms of the average properties of the resulting gas flows is a stronger reduction of the average angular momentum, or r_{circ} , in the early phases. Conversely, for $P \propto k^{-9/2}$ fewer, but more pronounced large scale filaments emerge at the start of the simulations and the average r_{circ} declines less; again with the main difference being in the early phase (before $t = 1$).

There is no significant difference in the rate of gas inflow onto the inner simulation boundary (particle absorbed onto the sink particle) nor in the mass and formation rate of the gas disc. However, there is a difference in the structure of the disc: with more power on smaller scales the disc forms at slightly smaller radii. Furthermore it is slightly less eccentric, but this may simply be a consequence of the faster circularisation rate at smaller radii.

3.4.3 Balance between rotation and turbulence

The parameter χ determines the relative contributions of the turbulent velocities and solid-body rotation to the initial velocity field according to equation (3.5). For $\chi = 0$ the velocities field only contains solid-body rotation and no random (turbulent) component resulting in rather unrealistic situation, while for $\chi = 1$ there is no rotational component apart from the residual rotation of the random velocity field. For four values $\chi > 0$, Figure 3.12 summarises the time evolution of the mean properties for the emerging gas flows². There are clear trends with χ : the more rotational supported the initial velocity fields, the larger, more massive, and more circular the forming gas discs³ and the less gas is ‘absorbed’ into the sink particle.

Of particular interest are the simulations with $\chi = 1$, when the only rotational component of the initial velocity field is the small residual rotation of the random velocity component. The six simulations for this choice of χ show large variety

²The initial mean circularisation radius is minimal near $\chi = 0.5$, when the rotational and turbulent velocities are comparable. A simple analytic estimate for my initial model suggests $\langle r_{\text{circ}} \rangle \approx \frac{2}{3}\eta(\chi^2 + [1 - \chi]^2\eta)r_{\text{shell}}$, which shares this property.

³It appears from Figure 3.12 that for $\chi = 0.25$ the discs stop growing at $t = 2$, but this is an artefact of my definition of the disc region in (e, r_{circ}) , which excludes disc material at $r_{\text{circ}} > 0.3$, when in fact the discs for these simulations grow larger.

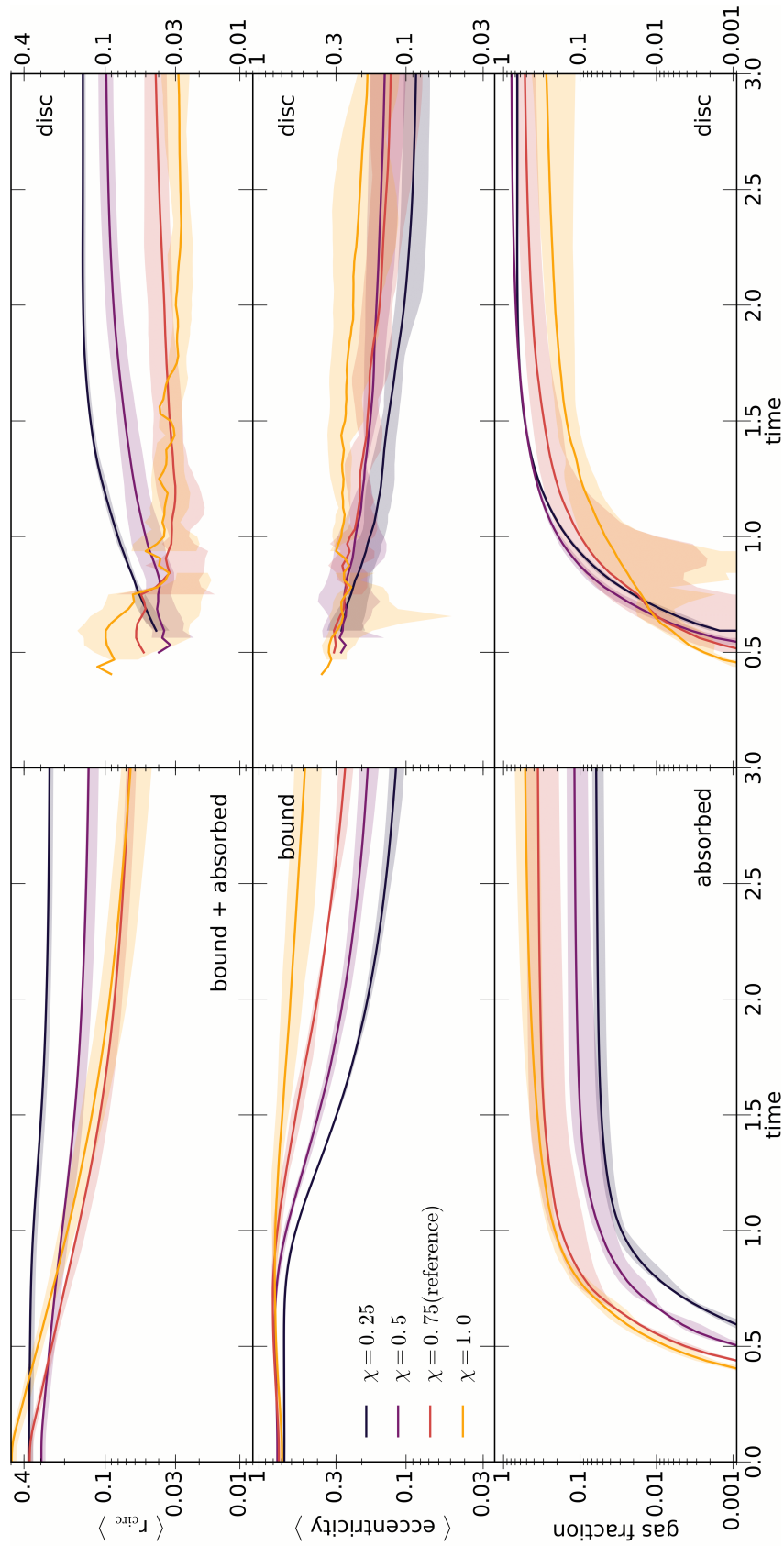


FIGURE 3.12: As Figure 3.10, but for simulations with different balance between rotation and turbulence in the initial velocity field according to equation (3.5). For $\chi = 1$ no rotation has been added to the turbulent velocities, but any random rotational component of the latter has not been removed.

in their disc properties, often including the complete destruction of an early disc by later infall. However, by the end all six of these simulations have formed some gas disc (with random orientation in line with the expectation of stochastic accretion described in Section 3.1), often exhibiting large eccentricities and warps or gaps (rings). These discs are typically much smaller than those formed in simulations with $\chi \leq 0.75$, but still significantly larger than the (artificial) sink absorption radius of 0.01. When reducing this radius to half, i.e. $r_{\text{sink}} = 0.005$, I found no significant change in the evolution, in particular the outer structure of these small discs remains hardly affected, although the inner parts are, of course, is altered by the change of r_{sink} (see Section 4.4).

3.4.4 Solenoidal velocity field

In Figure 3.13 I summarise the results of six simulations, which differ from the reference simulations only by the choice of the velocity field such that $\nabla \cdot v = 0$ everywhere. It is important to note that my method for creating such initial conditions (see Section 3.2.2) produces a different field instead of transforming a general field into a divergent-free one. Therefore the same seed numbers will produce a different asymmetric initial condition, such that a one-to-one comparison with the simulations in the reference set is not sensible, but only a comparison between either set of simulations in a statistical sense.

The overall evolution of the system is very similar to the set of reference simulations up to $t \sim 1$. Thereafter, the discs formed from divergent-free initial conditions are initially slightly smaller (but eventually equally large) and distinctly less eccentric, but equally massive than for the reference case.

3.4.5 Mass of the initial gas shell

In all simulations presented so far, the total amount of gas equals 1% of that of the SMBH, $M_{\text{shell}} = 0.01M_{\bullet}$. I also considered the cases of $M_{\text{shell}}/M_{\bullet} = 0.1$ and 1. The resulting simulated gas flows (not shown) behave very similar to the reference simulations. One difference is a slightly higher fraction of gas ‘absorbed’ onto the sink particle, i.e. removed from the simulation, because it reached $r < r_{\text{sink}} = 0.01r_{\text{shell}}$. This can be explained by the increased amplitude of the sink

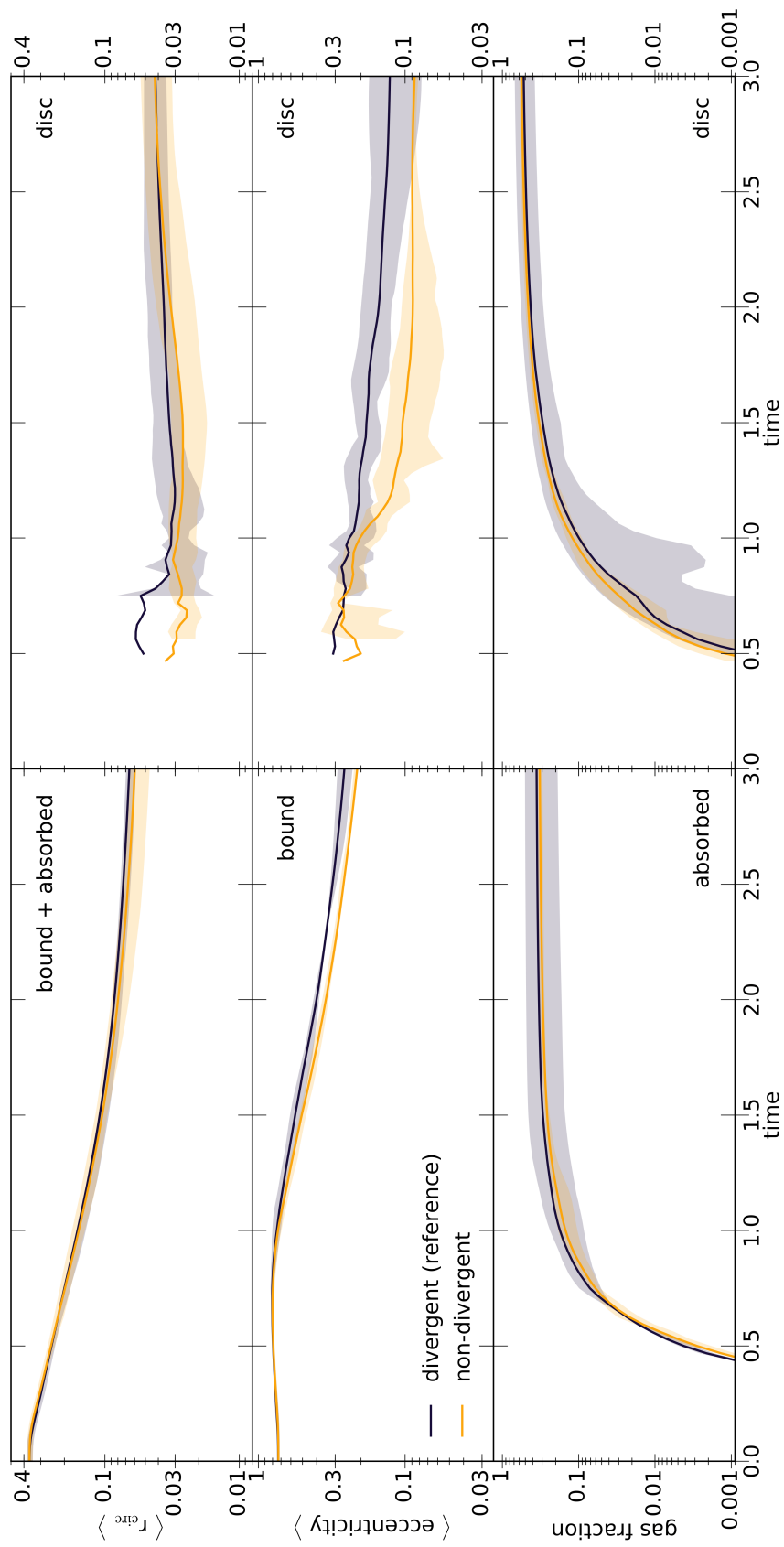


FIGURE 3.13: As Figure 3.10, but for simulations with initial velocities satisfying $\nabla \cdot v = 0$ (neither diverging nor converging).

particle’s random walk (‘Brownian motion’) owed to the relatively larger momentum it absorbs due to the increased mass of the flow⁴. For high M_{shell} the picture is quite different, if the gas self-gravity is accounted for (see Chapter 5).

3.4.6 Width of the initial gas shell

The parameter r_{width} controls the Gaussian width of the initial shell and defaults to $0.2r_{\text{shell}}$. I have also run two sets of simulations for $r_{\text{width}} = 0.1$ and 0.3 , see Fig. 3.14. A smaller (larger) width implies a smaller (larger) spread of peri-centre arrival timings across the shell. This in turn increases (decreases) the chance of collisions and hence angular-momentum cancellation and reduction of r_{circ} . I find indeed that the final averaged r_{circ} for $r_{\text{width}} = 0.1$ is almost twice as large as for $r_{\text{width}} = 0.3$, which between them bracket the result for my default simulations with $r_{\text{width}} = 0.2$.

3.4.7 The initial kinetic energy of the gas

The parameters η_{rot} and η_{turb} control the relative amount of kinetic energy and hence the deviation of the initial conditions from virial equilibrium. In all simulations so far, both were set equal to $\eta = 0.9$, when the overall virial ratio for the reference simulations is ≈ 0.74 (according to equation 3.8). Here, I report simulations with $\eta = 0.5$ and 1.1 , when the virial ratio becomes ≈ 0.35 and 0.97 , respectively.

This change in the initial velocity amplitudes directly affects the initial distribution of angular momenta such that the average initial r_{circ} is roughly proportional to η . With smaller velocities, the gas streams are on average more plunging and collide at smaller radii where collisions are more likely (due to the smaller volume). This results in more cancellation of angular momenta and hence reduction of r_{circ} for simulations with smaller η . The size and mass of any gas discs formed in the later stages of the simulations increase with the initial velocity amplitude, as expected.

Arguably, my simulations with $\eta = 0.5$ are somewhat under resolved and would have benefited from a smaller value for r_{sink} , the radius at which particles are absorbed into the central sink particle. With the value $r_{\text{sink}} = 0.01$ used, these

⁴The initial random gas velocities contain some small centre-of-mass motion with respect to the hole. When removing this small momentum, simulations show hardly differences.

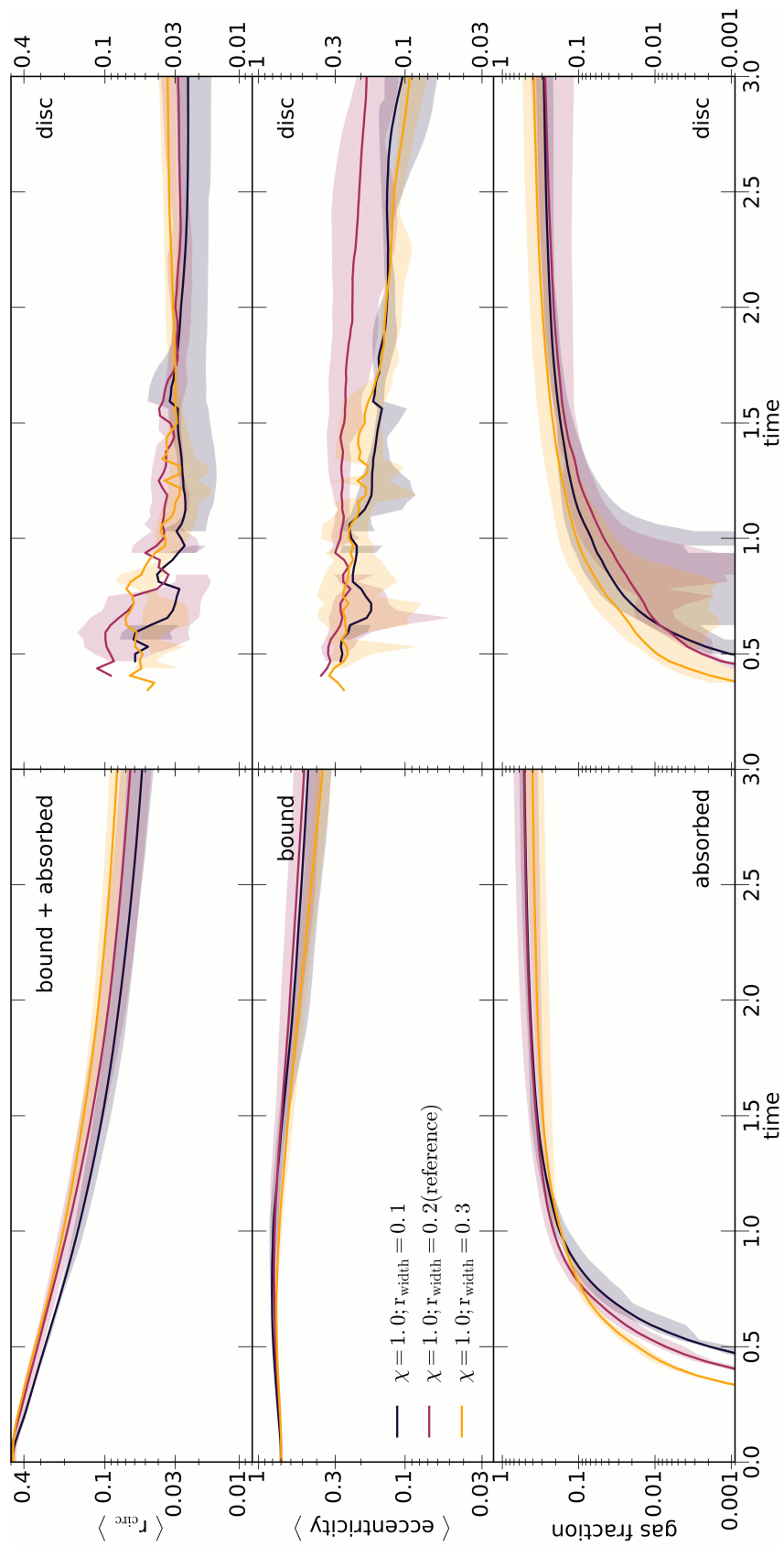


FIGURE 3.14: As Figure 3.10, but for simulations with different width r_{width} of the initial shell of gas.

simulations struggle to form continuously existing discs as most of the inflowing material is lost to absorption onto the sink particle (about twice as much as for the reference simulations).

3.5 Discussion

Our simulations do not model the feedback and sweeping-up of gas from the vicinity of the SMBH, but start from a gaseous shell of radius r_{shell} with non-uniform velocity distribution and a combination of rotational and turbulent motion. Shortly after the start of each simulation, the non-uniformity of the velocity field generates non-uniformity in the gas density, forming clumps, which subsequently fall into the cavity where tidal forces transform them into radially elongated streams. As modelling the gas flow close to the SMBH is prohibited by ever shorter dynamical time scales, I impose an inner boundary at $r_{\text{sink}} = 0.01r_{\text{shell}}$ representing the sub-parsec volume around a SMBH. This is still much larger than r_{visc} if I take $r_{\text{shell}} \sim 10 \text{ pc}$, the typical radius of a momentum-driven outflow corresponding roughly to the size of the SMBH's sphere of influence for $M_{\bullet} \approx 10^8 M_{\odot}$.

As the streams approach their orbital peri-centre, there is a good chance of collisions, which typically diminish the circularisation radius r_{circ} of the gas, with an average reduction by a factor of a few. This allows a higher portion of the gas to cross r_{sink} , while the most of the remaining gas circularises and forms disc-like structures at $\sim 0.05r_{\text{shell}}$. The earlier phases of these discs are typically randomly oriented and can be completely destroyed and subsequently reformed from impacting streams. After roughly one free-fall time, the disc dominates the further evolution of the distribution of the simulated gas over angular momentum (i.e. r_{circ}) and eccentricity e . Continued gas infall often has larger r_{circ} and extends the disc rather than destroying it. At the end of my simulations, the disc is still far from settled but possesses significant eccentricity and often warps or gaps.

Of course, the details of these gas flows are highly dependent on the details of the initial conditions. Therefore, I perform for each set of physical parameters six simulations which differ only by the random seed used to generate the turbulent velocities. Amongst simulations from such sextets no are identical or even similar in their gas flows, but differ in details like the shape of the disc, its formation

time, the fraction of gas crossing r_{sink} etc.. Despite the differences, the overall behaviours are similar and follow closely that outlined above.

In order to assess the robustness of my results, I varied the physical parameters of my simulations, such as the gas temperature (assumed to be constant), total gas mass, power-spectrum of the initial turbulent velocities, total kinetic energy, rotational support of the gas, and the width of the initial gas shell. Most of these variations have little effect on the overall reduction of the gas circularisation radii (but see Section 3.4). The one exception is the initial rotational support of the gas as compared to the turbulence. In case of significant rotation, the streams fall in a more orderly fashion, reducing the number of collisions such that only interactions with the forming disc cancel some angular momentum. Conversely, simulations without systematic rotation show the strongest average reduction of r_{circ} and the largest amount of gas crossed into $r < r_{\text{sink}}$. This result agrees with simulations presented by Hobbs et al. (2011) who used a similar setup, but focused on the gas transportation in the galactic bulge. They argue that the formation of dense material caused by the turbulence leads to ‘ballistic accretion’ whereby the angular momentum of those filaments barely mixes with the ISM and therefore the gas can reach smaller radii directly.

While the interactions of the streams with the disc are not the focus of this Chapter (see Chapter 5), it is worth commenting on the ability of some discs to resist destruction or at least major disturbance caused by the gaseous infall. One might expect that low-angular-momentum gas on plunging orbits can fall to small scales, but a number of simulations (see Sections 3.4.2 and 3.4.4) indicate that dense disc-like structures are effective at preventing gas infall to smaller scales.

The realism of my simulations is limited in various ways. One such limitation is my simple treatment of the thermodynamics, where I assumed a constant gas temperature (isothermal equation of state). While the gas may cool rapidly after stream-stream collisions, when my approach is reasonably accurate, it is insufficient for the high densities in the disc, when a detailed thermodynamics model including cooling would be desirable. However, the disc formation is not my main focus here.

A second limitation is the omission of gas self-gravity in most simulations. Even when including self-gravity, I had to suppress small-scale clumping and hence star formation, which may well occur in reality. The main effect of star

formation for the purpose of my simulation is (a) a reduction of the amount of gas available for feeding the SMBH and (b) the heating of gas by stellar feedback (driven by supernovae and winds). Both should reduce the efficiency of stream collision and disrupt the formation of the disc. The latter is indeed what I find in simulations with gas self-gravity and a larger total gas mass (see Chapter 5).

Another limitation is introduced by the (unavoidable) inner boundary, represented by a radius r_{sink} from the black hole, inside of which particles are removed from the simulation (and their mass, momentum, and angular momentum added to the SMBH particle). This inevitably introduces some artefacts near the boundary. Simulations run with up to ten times smaller r_{sink} show a larger reduction of r_{circ} and more gas in the low-angular-momentum tail of the distribution, since the collision cascade can penetrate to smaller radii. Extrapolation of these results suggest that $\gtrsim 10\%$ of the gas can circularise at $r \lesssim 10^{-3}$ pc, which is the scale of efficient viscosity-driven accretion discs (see Chapter 4).

Finally, my simulations ignore for simplicity the gravity of the host galaxy. A more accurate picture might be obtained by a static potential or even an N -body model for the stellar cusp. However, as the SMBH dominates gravity within the simulated volume, such treatment is unlikely to improve the realism of the simulations in view of the other aforementioned limitations.

3.6 Conclusion

I have presented smoothed particle hydrodynamic (SPH) simulations investigating the scenario proposed by Dehnen and King (2013) to overcome the angular momentum problem impeding SMBH feeding. In this scenario, gas swept-up by momentum-driven feedback from a previous accretion event falls back towards the hole. As this occurs near-simultaneously for most of the gas, the chances for collisions are enhanced. Such collisions promote the (partial) cancellation of angular momentum and increase the amount of material at circularisation radius $r_{\text{circ}} \lesssim r_{\text{visc}}$, the radius at which classical disc-driven viscous accretion becomes efficient. The goal of this study was to assess the efficiency of this process more quantitatively.

Our suite of simulations provides strong support for this scenario of SMBH feeding, as they demonstrate a reduction of r_{circ} by a factor of a few on average and by much larger factors for a small fraction of the gas. These reductions

are caused predominantly by stream-stream collisions but also interactions with discs that form from the infalling material. The details of each simulation depend both on the random velocity field and the physical parameters (such as gas temperature, velocity power spectrum, or velocity amplitudes), but the reduction of the specific angular momentum for most of the gas flow is hardly affected by changing these parameters. My simulations confirm the suggestions by Dehnen and King (2013) of the formation and maintenance of a near-toroidal dynamical gas structure caused by the continuous circularisation of infalling gaseous streams; the creation and destruction of randomly orientated discs; and high rates of gas passing through the inner numerical boundary, which potentially drive growth of the SMBH.

The scenario of angular-momentum reduction via a collisional cascade requires the near-simultaneous infall of gas from different trajectories. In my simulations this was provided by the fallback of a shell of gas assumed to have previously been swept up by AGN feedback. However, other initial situations are also possible, for example the collision of two massive clouds/streams of gas, resulting in a near-cancellation of their angular momenta and the subsequent infall of their shreds.

When adding star formation to this picture, one expects stars to form both from gas in the newly formed disc and from gas on plunging streams, possibly triggered by stream collisions. Of the latter some may come close enough to the SMBH to suffer from tidal disruption of binaries (Hills, 1988) and subsequent capture of one binary component into an eccentric orbit around the SMBH. This fits with the observational situation in our own Galaxy, where young stars (4-6 Myr old) are found in a disc at ~ 0.1 pc (Paumard et al., 2006), while the so-called S-stars on eccentric isotropic orbits at much smaller (~ 0.01 pc) distances from Sgr A* have a similar age (3-10 Myr, Habibi et al., 2017), which appears to coincide with the driving of the Fermi bubbles and the likely associated AGN activity (Zubovas, King, and Nayakshin, 2011; Zubovas and Nayakshin, 2012). This time span appears too short to change the initially very eccentric orbits of tidally captured stars into a thermal distribution, as observed for the S-stars (Gillessen et al., 2017), solely by stellar dynamics (in particular scalar resonant relaxation, Perets et al., 2009), for review (see Alexander, 2017). However, the S-stars may have lost their high eccentricities by gravitational interactions within the gas-rich environment during the formation of an accretion disc. Alternatively, they may

have formed in situ within a high-density AGN outflow (Nayakshin and Zubovas, 2018).

Chapter 4

Collisional cascades enhance feeding of SMBHs

Dehnen and King (2013) suggested a model of how it may be possible for gas to bridge the angular momentum barrier of material around the sphere of influence (of order pc) so it can reach scales of the order of $\sim 10^{-3}$ pc beyond which radius viscous accretion becomes short enough to be relevant to the feeding process of supermassive black holes. In Chapter 3 I quantified this model via simulating the collapse of a clumpy shell that forms interacting streams, which leads to cancellation of angular momentum. Here I present follow-up simulations that investigate the effect of the artificial, but numerically necessary, inner boundary. I show that the results can be used to extrapolate the fraction of gas undergoing collisional cascades and consequently reaching the relevant radii to at least 10%. Finally I discuss whether the reduction of the inner boundary radius can further show that these cascades change the orientation of angular momentum of the infalling gas and therefore may always cause chaotic accretion onto the black hole.

4.1 Introduction

It is widely thought that at least the majority of massive, if not all galaxies, contain a supermassive black hole (SMBH) in their central region (e.g Soltan, 1982; Kormendy and Richstone, 1995; Kormendy and Ho, 2013). Equally well established is the interaction of the SMBH with its host galaxy via outflows, both observationally (e.g Anderson and Kraft, 1969; Begelman, McKee, and Shields, 1983; Pounds et al., 2003; Tombesi et al., 2015; Reeves et al., 2016) and theoretically (e.g. Shakura

and Sunyaev, 1973; Pounds et al., 2003; King and Pounds, 2003), although various associated details are still matter of active research, e.g. as to their precise launching mechanism or how quickly the shocked outflow can cool (e.g. Silk and Rees, 1998; King and Pounds, 2003; King, 2005; King, 2010; Faucher-Giguère and Quataert, 2012; Zubovas, 2018). The interaction is thought to manifest itself in the $M_{\bullet} - \sigma$ relation (e.g. Silk and Rees, 1998; Haehnelt, Natarajan, and Rees, 1998; King, 2003; King, 2010; Zubovas and King, 2012), for which the mass of the SMBH M_{\bullet} is correlated with the velocity dispersion σ of the stellar component inside the host spheroid (e.g. Ferrarese and Merritt, 2000; Gebhardt et al., 2000; Kormendy and Ho, 2013).

In order to both launch these outflows, which are typically suggested to be the result of radiation pressure generated by the accreting gaseous material (e.g. Lucy and Solomon, 1970; Proga, Stone, and Drew, 1998; Frank, King, and Raine, 2002; King and Pounds, 2003), and grow the SMBH to large masses in relatively short time (e.g. Willott, McLure, and Jarvis, 2003; Riechers et al., 2009; Mortlock et al., 2011), gas needs to reach the scales associated with an accretion disc (Prendergast and Burbidge, 1968; Shakura and Sunyaev, 1973; Lynden-Bell and Pringle, 1974; Pringle, 1981). Such a disc is limited by the self-gravity radius ($> 10^{-2}$ pc) (e.g. Kolykhalov and Syunyaev, 1980; Pringle, 1981; King and Pringle, 2007; Lodato, 2007) and more restrictively the radius below the viscous angular momentum transport (e.g. Goldreich and Schubert, 1967; Shakura and Sunyaev, 1973) becomes short enough ($< 10^{-3}$ pc) to be relevant for typically active phases of a SMBH (King and Nixon, 2015). The differences in magnitude are considerable even if one does not consider the galaxy itself (order of kpc) as a direct source of the gaseous supply, but only the influence radius (of order pc) at which the gravitational potential generated by the SMBH dominates the volume. Consequently the fuel needs to be either "aimed" very well or there must a be mechanism that effectively cancels angular momentum of the infalling material, so it may reach the relevant scales.

In Chapter 3 I have presented a range of simulations that explore some of the potentially relevant parameters to achieve the required angular momentum reduction. The simulations are based on the concept proposed by Dehnen and King (2013) in which the previously alluded to outflows sweep out the gas, creating a non-uniform shell. As soon as the feedback event subsides, the gas will form infalling streams that will have an increasing chance to collide with each other as

they approach their respective peri-centre. The simulation show how the angular momentum distribution is shifted towards lower values (typically a factor of a few for most setups) and that the low angular momentum tail is enhanced. However, ultimately the fraction of the gas reaching these low circularisation radii (r_{circ}) is still arguably too low.

As the simulations only cover about two magnitudes in scale due to numerical requirements of an inner boundary, it is clear that that these simulations show a small part of the total sum of interactions. Indeed the interactions of the streams should continue inside the non-simulated volume described by the sink radius r_{sink} . It is worth noting that this boundary causes another, perhaps more subtle numerical effect. The gas particles, which orbit the SMBH on an elliptic orbit with an apo-centre outside of r_{sink} but a peri-centre inside are removed and thus prevented from affecting the gas flow further out. Even with sophisticated criteria for particle absorption this problem cannot be avoided, only alleviated at higher computational costs, which is equivalent to reducing r_{sink} in simulations. The problem is illustrated by Figure 4.1, where the top schematic shows a SPH particle with an eccentric orbit eventually being absorbed by the sink particle as it approaches its peri-centre. The particle is subsequently lost to the simulation even if its apo-centre is located outside this volume. The bottom schematic shows the same situation with a reduced r_{sink} allowing the particle to escape and potentially interact with other infalling particles leading to further (partial) cancellation of angular momentum.

Naturally, the reduction of the radius of the sink particle comes at a greater computational cost as the possible orbits become smaller and therefore require a smaller time step (see Section 2.2.4). As the scale of the simulation in total increases as well, the number of SPH particles needs to be increased in order to maintain a comparable resolution. This leads to further increasing computational cost and highlights why the inner boundary is used in these scenarios in the first place.

Indeed this problem is not limited to this set of simulations, but is in fact of particular importance in cosmological simulations. A typically used solution is the Bondi-Hoyle accretion (Hoyle and Lyttleton, 1941; Bondi and Hoyle, 1944; Bondi, 1952), which allows the simulations to obtain an approximate mass accretion rate onto the SMBH, which in turn impacts a feedback prescription, even if

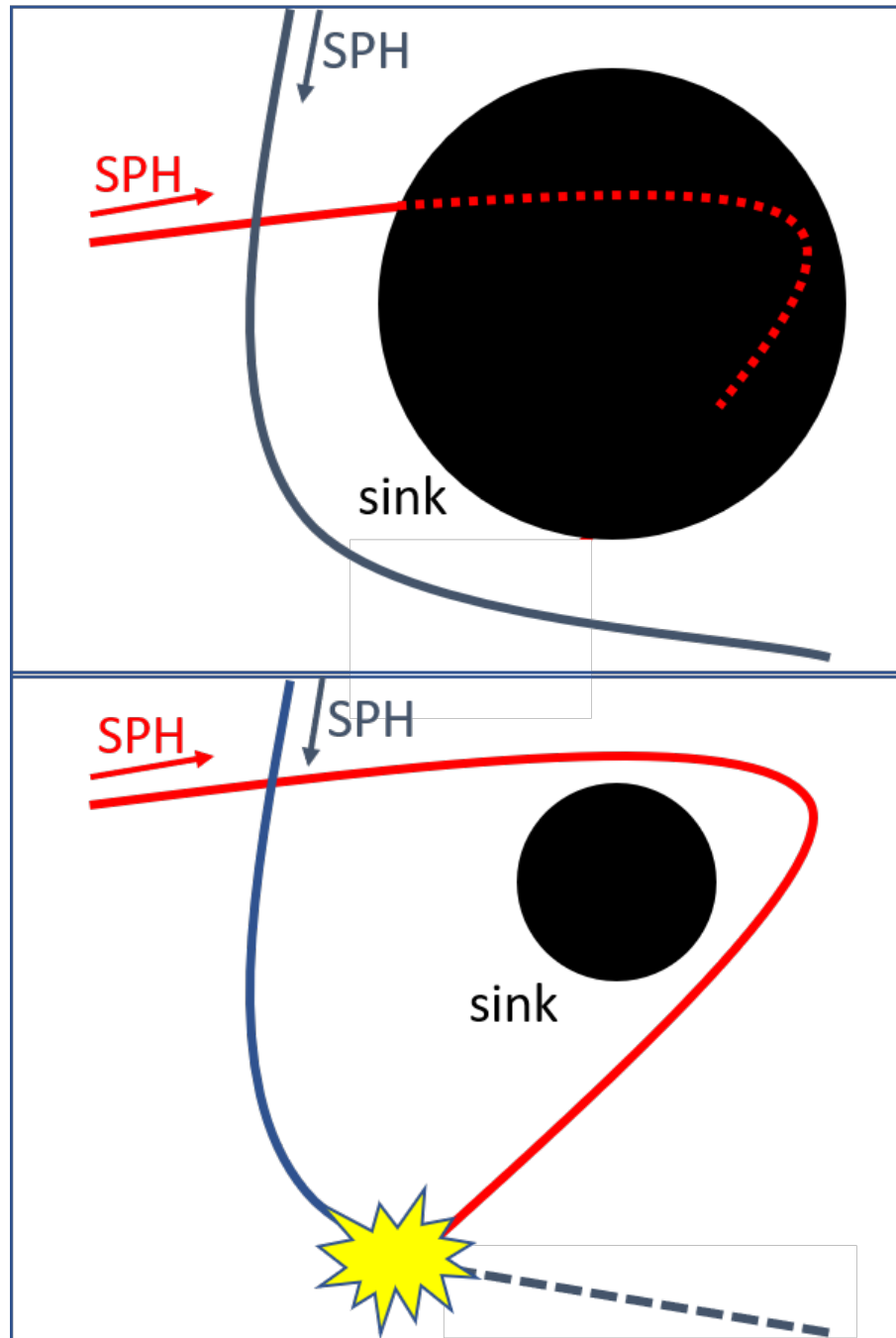


FIGURE 4.1: The top schematic shows the difference between a SPH particle (red) with a peri-centre inside the sink particle (top, black), but with an apo-centre outside. Nevertheless, the particle gets removed from the simulation. The bottom schematic show the same particle, however, the reduced sink particle radius avoids the removal of the particle and may be able to interact with other particles (blue) subsequently.

the central part of the galaxy cannot be resolved below e.g. 1kpc (e.g. Di Matteo et al., 2008; DeGraf and Sijacki, 2017; Grand et al., 2017; Stevens et al., 2017). Clearly such a sub-grid model cannot effectively account for the angular momentum exchange happening inside such a radius e.g. through collisions. As the high performance computers become more powerful and the simulations more sophisticated, the resulting numerical errors become more apparent (e.g. Negri and Volonteri, 2017; Beckmann, Slyz, and Devriendt, 2018) and require these models to utilise more detailed sub-grid models (e.g. Curtis and Sijacki, 2016; Fiacconi, Sijacki, and Pringle, 2018).

In order to investigate the behaviour of the infalling streams at lower radii than was possible in the original set of simulations, I chose not to utilise a sub-grid model, but instead to lower the sink radius r_{sink} . This allowed me to investigate the impact on the inner part of the accretion disc, how the resolution requirements may change and whether any change of the circularisation radius r_{circ} can be used to extrapolate the accretion onto the relevant scales of 10^{-3}pc .

Finally, I will consider whether we can use the same principle changes caused by the reduced r_{sink} so that the proposed cascade of infalling material may (partially) remove any original orientation leading to chaotic accretion. This type of accretion refers to the assumption of randomly aligned orientations of the gaseous infall (e.g. Sanders, 1981; Moderski, Sikora, and Lasota, 1998; King and Pringle, 2006; King, Pringle, and Livio, 2007; Dehnen and King, 2013; King and Nixon, 2015). The subsequent randomly orientated accretion onto the SMBH may keep the spin low (e.g. King et al., 2005; King and Pringle, 2006; King, Pringle, and Hofmann, 2008; Fanidakis et al., 2011; Hopkins et al., 2012) and therefore SMBHs can reach the high masses early on and hence avoid the stringent requirement for more than stellar mass sized black hole seeds (e.g. Haehnelt and Rees, 1993; Latif and Ferrara, 2016).

This Chapter is organised as follows: In Section 4.2 I briefly describe the initial setup and will show how the change of r_{sink} impacts the inner parts of the simulation. I will show evidence for the collisional cascade in Section 4.4 and discuss its impact on chaotic accretion in Section 4.5. The results are discussed and concluded in Section 4.6.

4.2 Simulation setup

Similar to the approach taken in Chapter 3, I base the initial conditions on a spherical shell modelled by 2×10^6 SPH particles that are positioned according to a quasi-random generator (e.g. Niederreiter, 1992) following a Gaussian distribution with a width of $0.2r_{\text{shell}}$, where $r_{\text{shell}} = 1$. The shell mass is $0.01M_{\bullet}$, where $M_{\bullet} = 1$.

In order to create a non-uniform gas shell, I follow the widely used method outlined by Dubinski, Narayan, and Phillips, 1995. The power spectrum is based on work by Kolmogorov, 1941; Kolmogorov, 1991 and is set to $-11/3$ accordingly. The turbulence generator is set up to take into account contributions of a solid body rotation and the turbulence itself. It is expressed by χ , where $\chi = 0$ refers to pure solid body rotation without any turbulence and $\chi = 1$ to a purely turbulent case, which, may possess a small, randomly orientated rotation. Furthermore a scaling factor η allows me to adjust the total kinetic energy with respect to the virial theorem. This leads to:

$$\frac{2E_{\text{kin}}}{-E_{\text{pot}}} = \frac{\sum_i m_i v_i^2}{\sum_i G m_i M_{\bullet} / |r_i|} \approx \chi^2 \eta_{\text{turb}} + \frac{2}{3} (1 - \chi)^2 \eta_{\text{rot}}^2 \quad (4.1)$$

where both η are set to 0.9 and χ is chosen to be either the reference value (see Section 3.3) of 0.75 or alternatively to 1, 0.25 or 0.5. However, for Section 4.4 we only utilise $\chi = 1$ as a fully turbulent shell should show the strongest signs of changes. This is due to their larger portion of lower angular momentum particles and the tendency to form elliptical disc, which are more likely to be affected by the issue outlined in Section 4.1 and displayed in Figure 4.1. While it would be worthwhile performing a similar parameter sweep as in Chapter 3, due to the apparent impact on the disc formation of at least some of the investigated parameters (e.g. changes of the sound speed or solenoidal turbulence), the computational costs are too high ($\gtrsim 4000$ CPU hours per simulation instead of $\gtrsim 100$ CPU hours) for the scope of this chapter. Therefore I decided to only investigate changes of χ with respect to changes to the inner boundary. Following a similar line of thought, I have restricted the number of seeds run at least for Section 4.5 - otherwise I utilise the same set of seeds as described in some detail in Section 3.3.2.

All my simulations must employ an inner boundary condition to avoid simulating the gas flow very close to the SMBH, where the dynamical time scales are

too short for efficient modelling. This is implemented in the usual way by a sink radius r_{sink} around the SMBH particle, such that any gas particle found at distance $r < r_{\text{sink}}$ from the SMBH is ‘absorbed’ into the latter and removed from the simulation. Of course, this is somewhat artificial and unphysical, but a necessary requirement to avoid a stalling of the simulation. I vary r_{sink} from the reference value of 0.01 to 0.005, 0.0025 and 0.001.

Finally, the runtime parameters of the simulation are identical to the ones in Chapter 3. In particular we employ an isothermal equation of state with a sound speed set to 0.1. The simulations have been computed by the SPH code (Lucy, 1977; Gingold and Monaghan, 1977) called SPHINX written by Walter Dehnen (for more information see e.g. Cullen and Dehnen, 2010; Aly et al., 2015; Faber and Dehnen, 2018).

4.3 Convergence

In order to assess the effect of the inner boundary more quantitatively, I ran three additional sets of six simulations each with $\chi = 1$ and $r_{\text{sink}} = 0.005, 0.0025,$ and 0.001 (the default value was 0.01). Figure 4.2 shows four density plots of exactly the same simulations, but with differing values for r_{sink} (0.01, 0.005, 0.0025, and 0.001 from left to right, top to bottom) at $t = 1.5$. The time corresponds roughly to the free fall time of the outer parts of the initial shell and therefore one can expect that the majority of currently infalling gas has reached the centre of the simulations. One immediately apparent difference is the structure of the inner disc. For the original reference value (top left), we see a high density filament in the process of circularising and forming a new disc as previous infall (not shown here) destroyed the predecessor. However, the remaining simulations with lower r_{sink} seem to have formed such a disc already and reveal a more circular (due to shorter orbital times) inner density ring that increases in density with decreasing r_{sink} . This can be expected as the gas has a continuous angular momentum distribution and therefore should circularise at smaller radii, if so allowed by the artificial limitation of the inner boundary. Equally expected is that the filamentary structure outside of the disc is identical.

However, without further zooming into these density plots, little quantitative information can be obtained to judge the impact of the reduced r_{sink} . Therefore

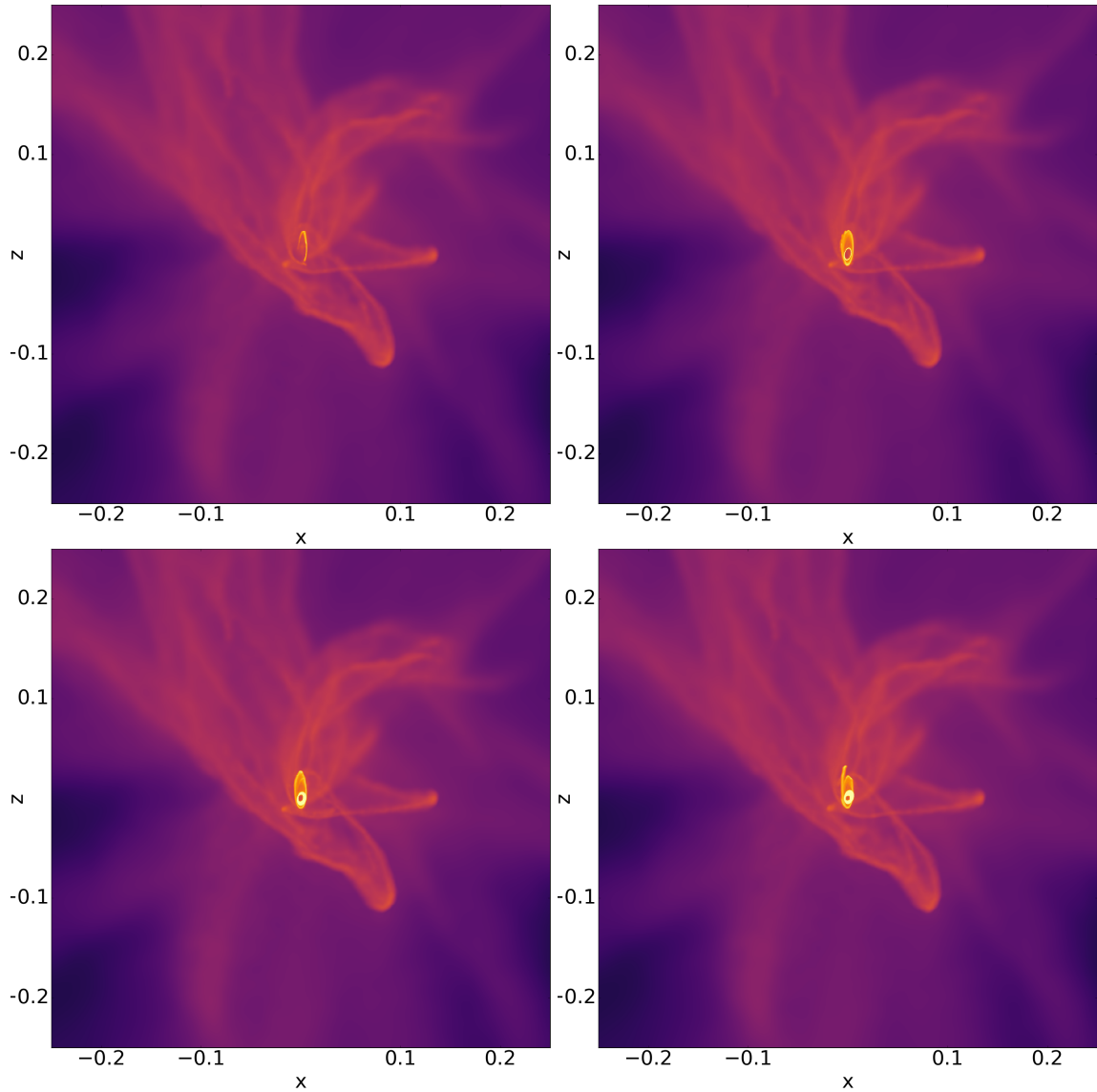


FIGURE 4.2: Density plots at time $t = 1$ for simulation with the same Seed A, which differ by size of the inner boundary radius: $r_{\text{sink}} = 0.01, 0.005, 0.0025,$ and 0.001 from left to right, top to bottom. While the original simulation with $r_{\text{sink}} = 0.01$ (top left) appears to have been disturbed by infall leaving a mere hint of newly forming accretion disc, said disc exists in the simulations with reduced r_{sink} . An inner ring increases with density for lower r_{sink} . As expected, the gaseous structure further out is identical.

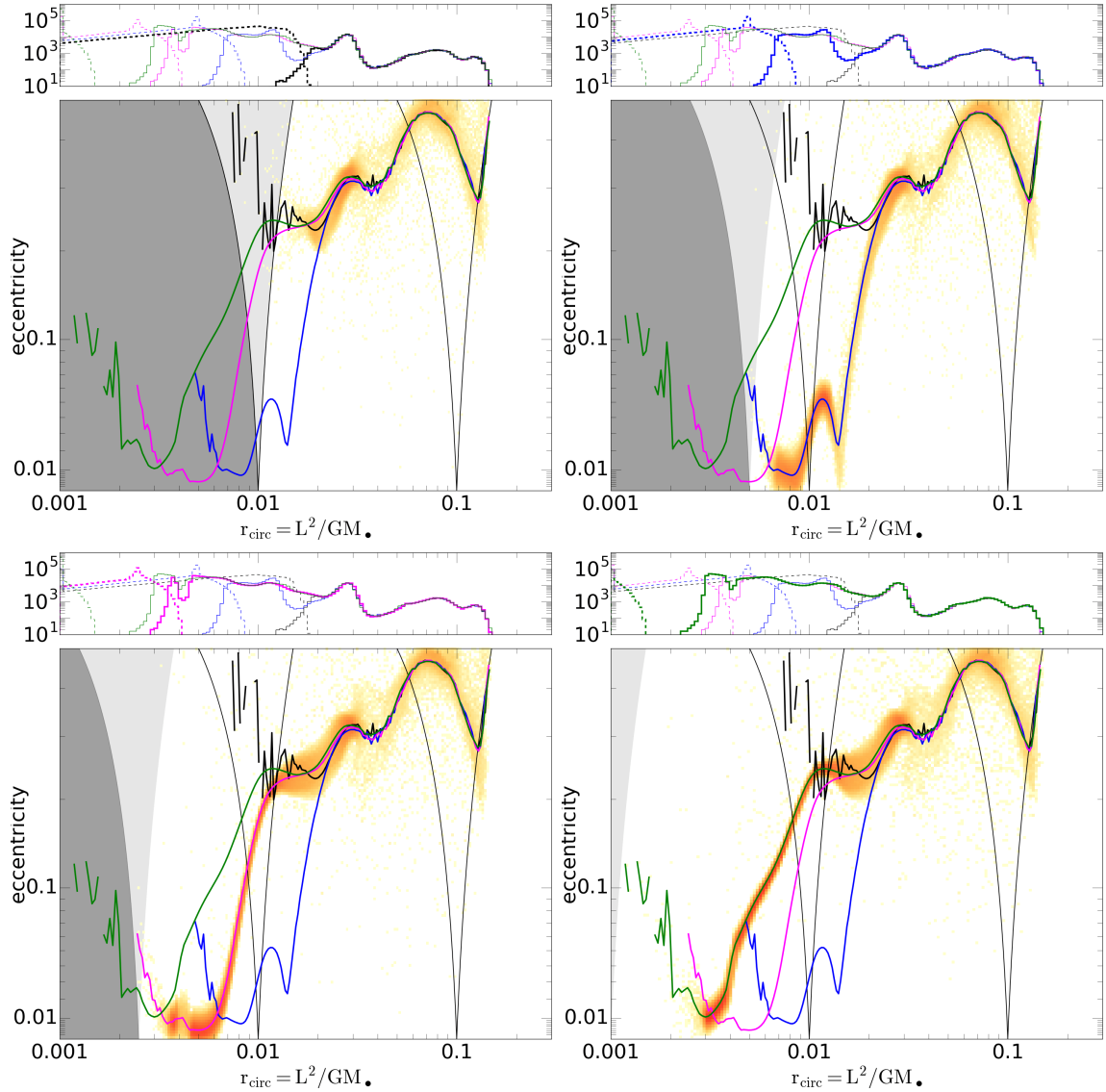


FIGURE 4.3: The distributions over r_{circ} and e in the disc region for four simulations which differ only in the choice for the inner boundary radius: $r_{\text{sink}} = 0.01, 0.005, 0.0025,$ and 0.001 from left to right, top to bottom or equivalently the black, blue, pink and green lines in each graph. For better comparison, the thin curves indicate the mean eccentricity within the disc regions of these four simulations. Similarly, the top panels show the r_{circ} distributions for all four simulations.

I employ a slightly modified version of the distribution plot over the circularisation radius $r_{\text{circ}} = GM/L^2$ and eccentricity e . Fig. 4.3 presents the resulting distributions over r_{circ} and e at the end ($t = 3$) of these simulations for Seed A. The gas flows are very similar, if not identical, at $r_{\text{circ}} \gtrsim 4r_{\text{sink}}$, but differ sometimes significantly at small angular momenta. This implies that the details of the flows at these small radii, for instance the presence and characteristics of the inner disc formed at later stages of the simulations are not reliable and confirm the suggestions made in Section 4.1.

In addition, there appears to be a difference between the convergence of the top row and the bottom row. The top row follows a steeper path at $r_{\text{circ}} \sim 0.02$ compared to simulations with even smaller r_{sink} , which appear to feature a horizontal-esque feature before the eccentricities decrease rapidly due the faster circularisation for particles with shorter orbital periods. The feature is visible in the previous Figure 4.2 as a high density ring. This highlights that any convergence is difficult to estimate as the chaotic nature of any single seeded infall may change the disc structure notably. Furthermore the difference between the green line ($r_{\text{sink}} = 0.001$) and the pink one ($r_{\text{sink}} = 0.0025$) is significantly smaller compared to the blue line ($r_{\text{sink}} = 0.005$) despite a larger reduction of the inner boundary radius. This is an artefact of lacking resolution as I should increase the number of particles in the simulation when I change the scale of it. However, this would increase the computation cost even further and therefore is not feasible (see Section 4.1).

Finally, I note the highlighted lines in the histogram at the top of each individual figure, which show a slightly increased number of absorbed particles with low angular momentum compared to the original simulation. This is despite the existence of a disc at lower radii, which naturally contains some of the otherwise absorbed particles. I will investigate this further in Section 4.4.

In order to perform a convergence test based on resolution, I first analyse how seed dependent the artificial gap is. While some small variations exist from seed to seed (see Section 3.3.2), they are negligible relative to the size of the gap - especially in the case for setting $r_{\text{sink}} = 0.001$. This allows me to focus only on a single seed (the reference Seed A, see Section 3.3.1) and consequently save valuable CPU time. Following the same notion, I further test how early the gap appears as the later stages of the simulation (e.g. $t \gtrsim 1.5$) are especially computationally expensive due to the large scale disc that typically establishes itself after roughly one

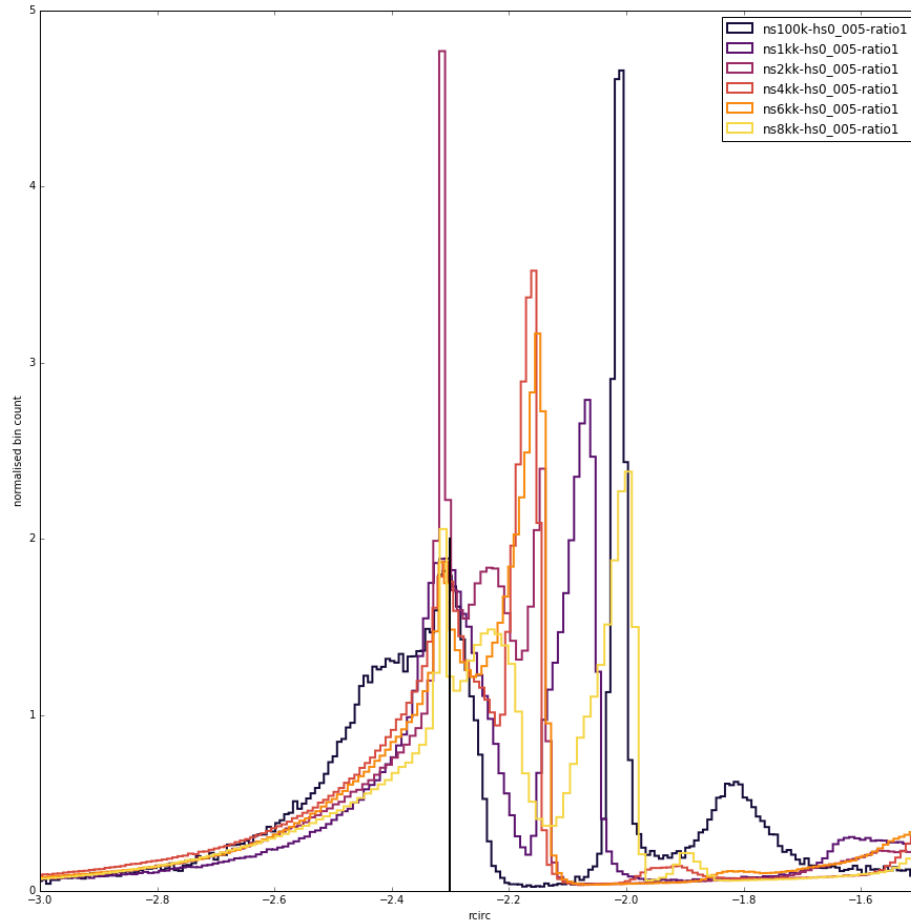


FIGURE 4.4: Normalised bin count of distributions of r_{circ} for increasing numbers of SPH particles per simulation (increasingly lighter colours) and for $r_{\text{sink}} = 0.005$ at $t = 2$. There is no artificial gap for higher numbers of particles between the coloured particle distributions and the inner boundary radius (vertical black line).

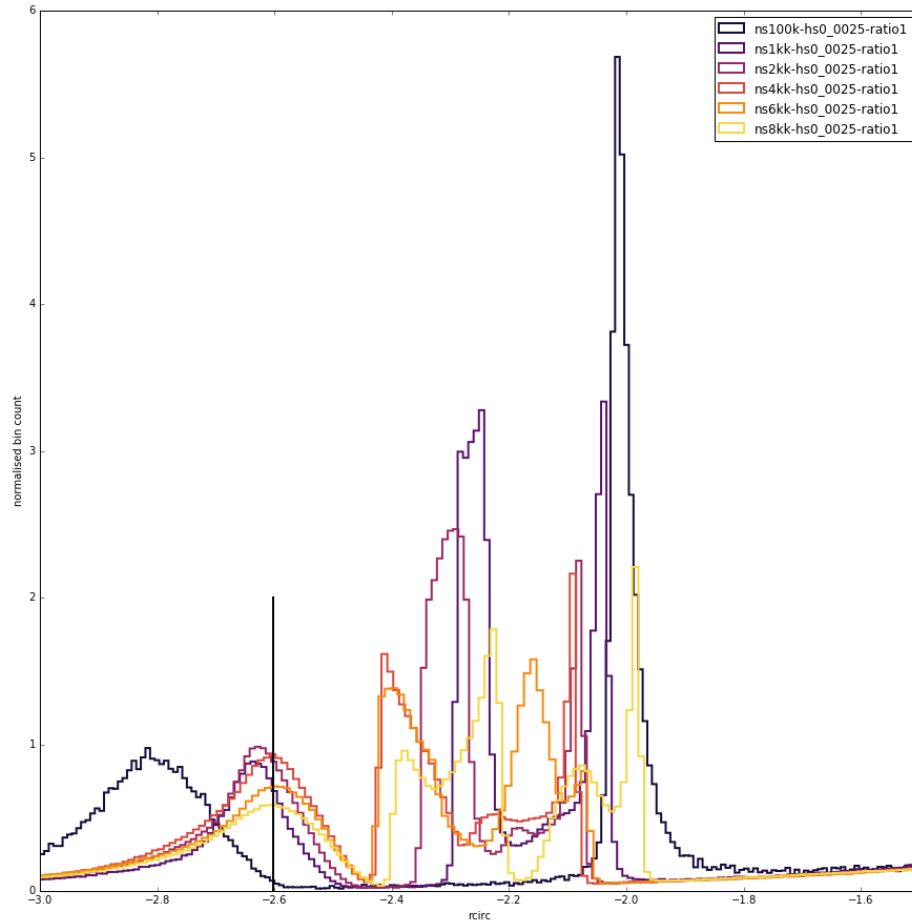


FIGURE 4.5: Normalised bin count of distributions of r_{circ} for increasing numbers of SPH particles per simulation (increasingly lighter colours) and for $r_{\text{sink}} = 0.0025$ at $t = 1.5$. There is no clear artificial gap for higher numbers of particles between the coloured particle distributions and the inner boundary radius (vertical black line).

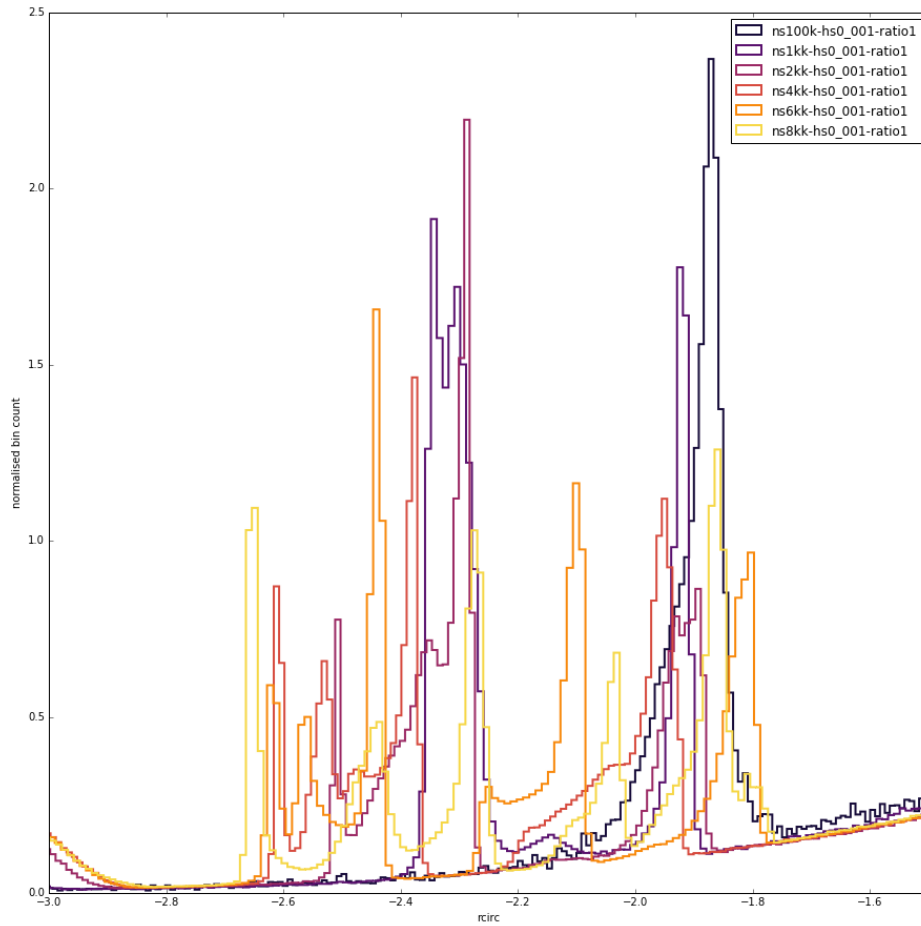


FIGURE 4.6: Normalised bin count of distributions of r_{circ} for increasing numbers of SPH particles per simulation (increasingly lighter colours) and for $r_{\text{sink}} = 0.001$ at $t = 1$. There is a clear artificial gap even for higher numbers of particles between the coloured particle distributions and the inner boundary radius (coincident with the left border of the plot).

free fall time of the outer parts of the shell. I find that the gap becomes reliably visible as early as $t \sim 0.75$. More analysis of the convergence for these early times showed scatter that I attribute to the chaotic nature of the infall, in which small changes may significantly change the appearance of e.g. the inner disc structure. Therefore I decided to restart and continue the simulations further.

The results can be seen in Figure 4.4 to 4.6. For $r_{\text{sink}} = 0.005$ (Figure 4.4) a gap only exists for the extremely low number of 1×10^5 SPH particles. The gap for $r_{\text{sink}} = 0.0025$ (Figure 4.5) appears closed for simulations with $\gtrsim 4 \times 10^6$ particles, however, more crucially for $r_{\text{sink}} = 0.001$ (Figure 4.6) even 8×10^6 particles barely start to close the gap. I note that the histograms are snapshots at different times ($t = 1, 1.5$ and 2 for Figure 4.4 to 4.6) as I found myself increasingly limited by the largest scale simulations. The simulation with $r_{\text{sink}} = 0.001$ and 8×10^6 particles took two magnitudes longer to reach $t \sim 1.2$ compared to the original simulation and appeared to grind down to a hold afterwards. Therefore it might not be possible with current means to find a convergence even for just a tenth of the original inner boundary condition for these sets of simulations.

4.4 The collisional cascade

As a direct consequence of the previous Section 4.3, my simulations cannot directly give the fraction of gas which lost sufficient angular momentum for viscous accretion to become efficient, i.e. reaching $r_{\text{circ}} \sim 10^{-4} r_{\text{shell}}$. However, I can attempt to estimate this by extrapolating to smaller r_{sink} . The time evolution plots I utilised in Section 3.4 to report the changes in e.g. r_{circ} and the number of absorbed particles allows only a rather restricted look (see Figure 4.7). This is due to the reduced absorption rate caused by the smaller inner boundary radius, giving the appearance that these simulations may be less effective in shifting the angular momentum distribution to smaller values. This is further emphasised by the little if any change to the average r_{circ} . However, while the first is a natural consequence of the change of scale in the simulation, the latter is not an effective way of presenting the difference that only appears close to the inner boundary radius, because the majority of the simulation remains unchanged.

To this end, I consider the distribution of gas over initial and final r_{circ} , which I can directly interpret as the conditional probability for gas to reach some final value for r_{circ} given its initial value. For the four sets of simulations with different

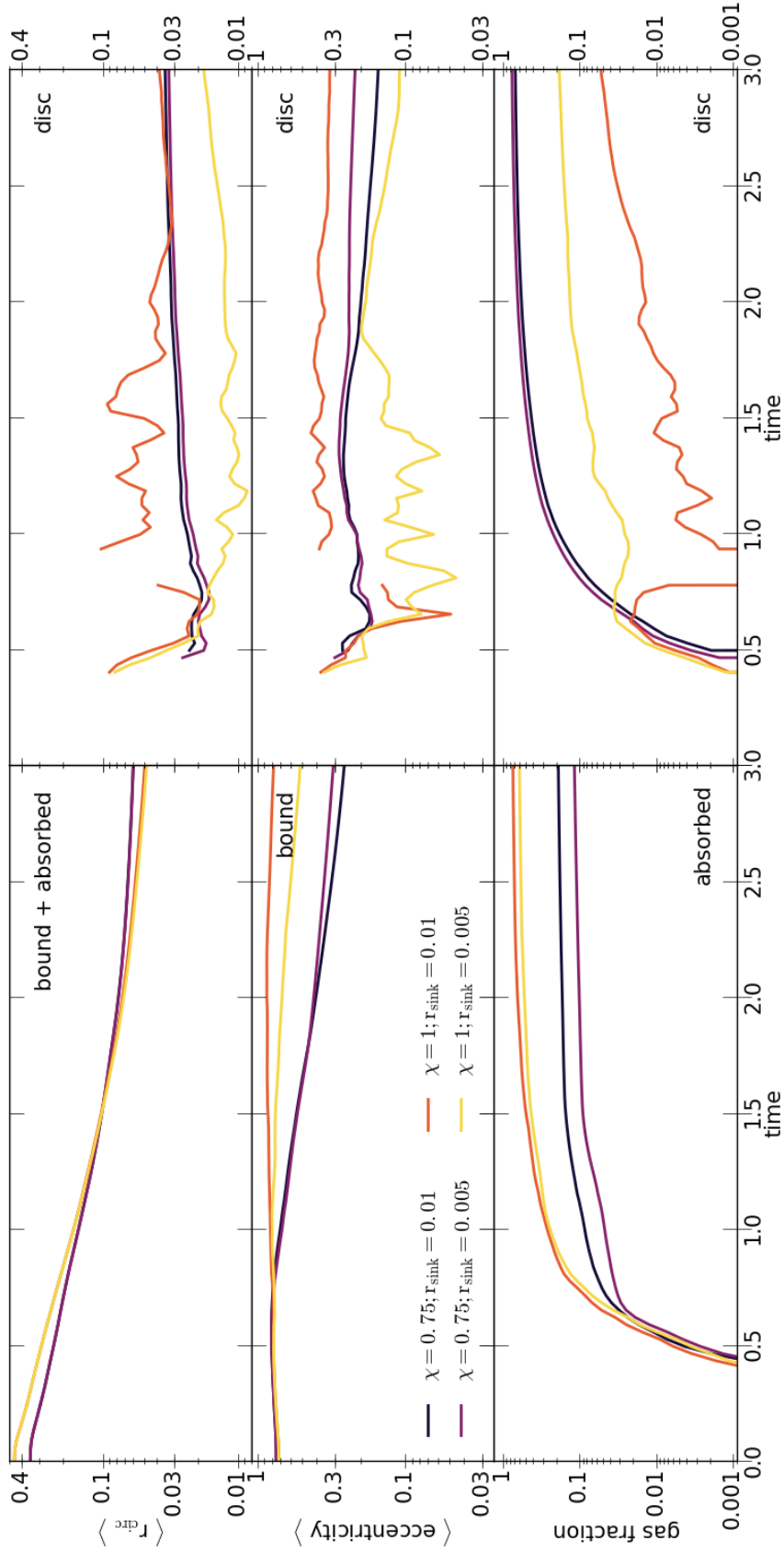


FIGURE 4.7: Time evolution of the average circularisation radius and eccentricity as well as the gas fraction for different portions of the gas and for simulations with $\chi = 0.75$ and 1 with respectively $r_{\text{sink}} = 0.01$ and 0.005 . ‘Absorbed’ refers to simulated gas that at some point prior to t has reached $r < r_{\text{sink}} = 0.01$ and was absorbed into the central sink particle; ‘bound’ refers to all remaining gas that at the given time has $e < 1$, ‘disc’ represents all bound gas at $e \leq 0.5$ and $r_{\text{circ}} \leq 0.3$ indicated by a thin dotted rectangle in Figure 3.1, Section 3.3.1 (which may also contain a small fraction of impacting filaments).

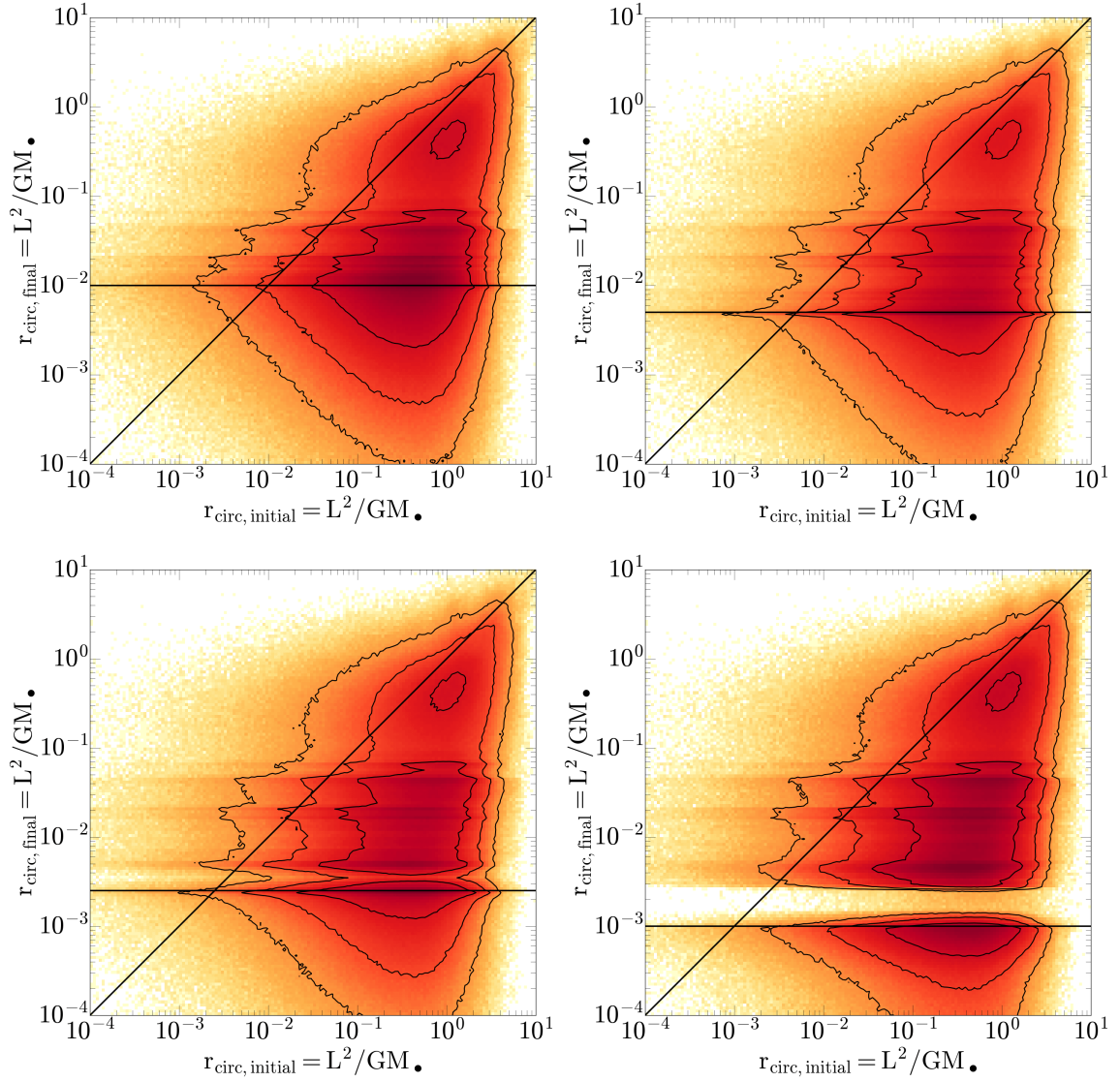


FIGURE 4.8: The distributions of the SPH particles over initial and final r_{circ} for four sets of simulations which differ only in the choice for the inner boundary radius r_{sink} as indicated by the horizontal lines. The horizontal features are gas rings/discs formed in the later stages of the simulations.

r_{sink} , Fig. 4.8 plots the combined distributions from the six simulations for each set to minimise the impact of any quirks inherent in any single seed.

These distributions are fairly wide: the range of $r_{\text{circ,final}}$ for a given $r_{\text{circ,initial}}$ spans at least four orders of magnitude and vice versa. As one would expect, $r_{\text{circ,final}} < r_{\text{circ,initial}}$ for the bulk of the distribution: most gas has lost angular momentum. Within each simulation, material with large initial r_{circ} experienced greater angular-momentum reduction. This is simply a consequence of the inner boundary: particles with larger initial r_{circ} typically require more interactions and angular-momentum reduction before they are taken out of the simulation at that boundary. Similarly, with a larger dynamic range (decreasing r_{sink}) the typical reduction of r_{circ} increases, which can be attributed to the same cause.

The simulations for $r_{\text{sink}} = 0.001$ show a gap at $r_{\text{circ}} \sim 0.002$, which is also present, to a lesser degree, at $r_{\text{sink}} = 0.0025$ or in simulations with $N_{\text{gas}} \lesssim 10^6$ and $r_{\text{sink}} = 0.01$ (not shown, see Section 4.3). As mentioned previously, this effect is an artefact of low resolution: the innermost particles' smoothing length becomes comparable to r_{sink} and I cannot expect an adequate model of the gas flow.

In order to extrapolate these trends to the even smaller values of $r_{\text{circ}} \sim 10^{-4}r_{\text{shell}}$ required for efficient viscous accretion, I plot in Fig. 4.9 the cumulative distributions over the final circularisation radius for gas with the same initial value of $r_{\text{circ}} = 0.05, 0.1, \text{ or } 1$ (top to bottom), but obtained from simulations with different r_{sink} . Simulations with smaller r_{sink} always obtain more particles at smaller $r_{\text{circ,final}}$. In the converged part, the cumulative distributions approximately follow a power law with index $\gtrsim -0.5$. Extrapolating, I estimate that at least 10 percent of the gas will reach $r_{\text{circ}} = 10^{-4}r_{\text{shell}}$.

4.5 Will gaseous infall always be chaotic?

In Figure 4.8 I have shown that the majority of the gas loses angular momentum due to collisions of streams with each other and the disc. In the previous Section 4.4 I also provided evidence that the cascade will continue to lower radii leading to more particles being shifted in to the low angular momentum tail relevant for the feeding of the SMBH. The number of random collisions in general should reduce any imprint of the original angular momentum orientation. One way of testing this is to utilise the same principle behind this whole chapter: Decreasing the artificial inner boundary keeps the simulation essentially identical

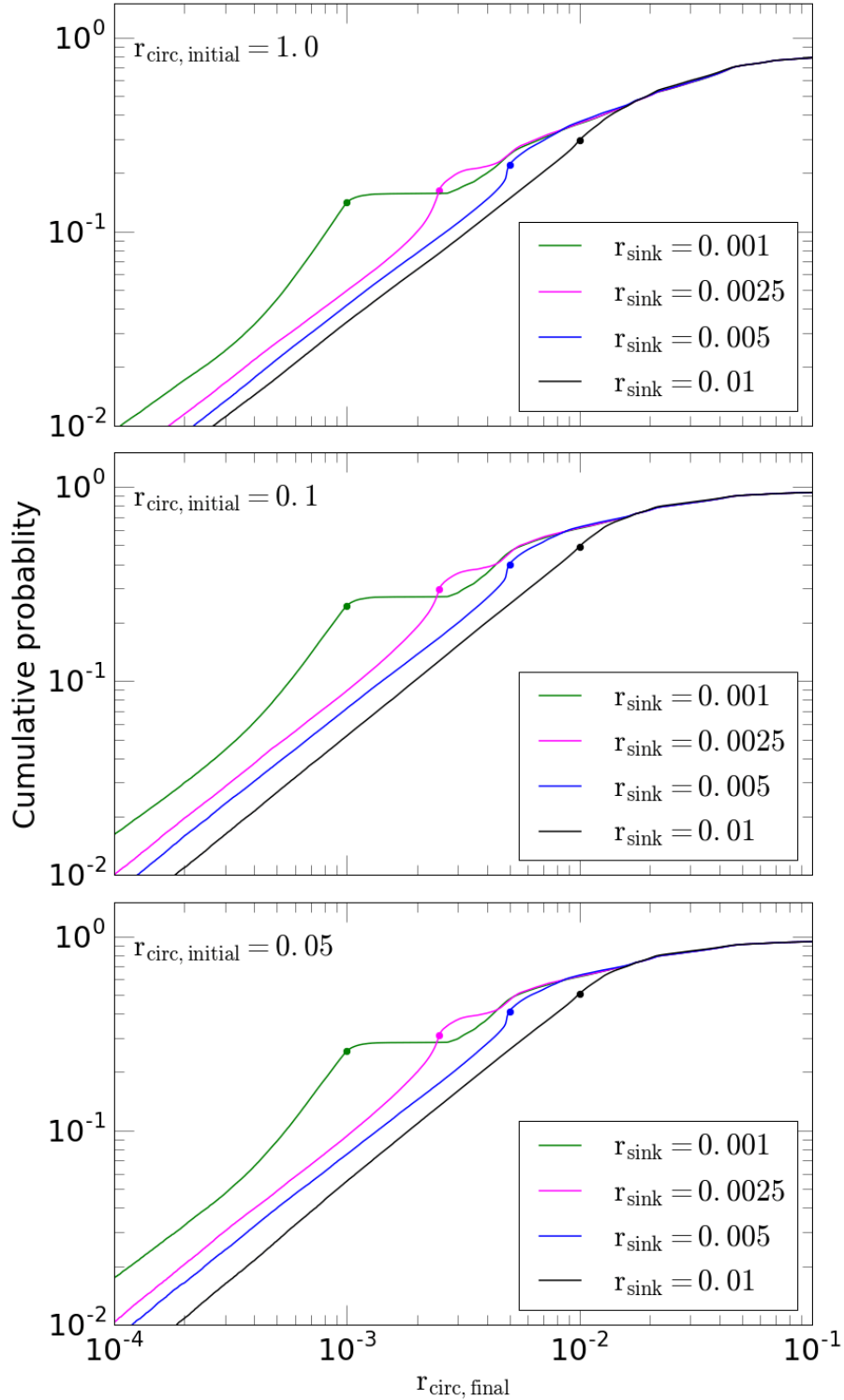


FIGURE 4.9: The cumulative distributions of SPH particles over the final circularisation radius $r_{\text{circ}} = L^2/GM$ for gas with three different initial values as indicated (gas particles within 0.1 dex of this value are included in the plots). The four distributions per panel refer to sextets of simulations with different dynamic range or r_{sink} as indicated (the solid dots are at $r_{\text{circ, final}} = r_{\text{sink}}$).

while promoting further collisions close to said boundary. In practice, this is achieved by analysing the angular momentum orientation of absorbed particles, which have their properties saved in the same timestep as they get removed from the simulation.

The following figures show the $\cos \theta = \frac{L_z}{|L|}$ over time for simulations with the Seed D. I chose this seed as it coincidentally aligns well with the z-axis (the rotation axis for simulations with $\chi \lesssim 1$) for the purely turbulent case, where $\chi = 1$ (see Figure 4.10).

Figure 4.11 shows the results for $\chi = 0.5$ with $r_{\text{sink}} = 0.01$ for the top and $r_{\text{sink}} = 0.0025$ for the bottom graph. The contribution of absorbed particles from the disc is extremely high as expected given that large contributions of solid body rotation to the initial velocity field create large discs early on that block efficiently low angular momentum infall (see Section 3.4.3). The change caused by the reduction of the inner boundary radius is marginal.

Figure 4.12 shows the results for $\chi = 0.75$ (equivalent to the reference simulation, see Section 3.3.1 with $r_{\text{sink}} = 0.01$ for the top, $r_{\text{sink}} = 0.005$ for the middle and $r_{\text{sink}} = 0.0025$ for the bottom graph). While the original simulation is still well aligned with the z-axis, the differences arising from the change of the inner boundary radius are more prominent. This is likely due to the increased contribution of turbulence towards the initial velocity field causing more erratic behaviour, which itself leads to a higher chance of collisions and consequently (partial) angular momentum cancellation. Furthermore it is worth noting that the spread in $\cos \theta$ decreases for later times. As the disc can reach smaller radii, it is capable of blocking and accreting infalling gaseous matter causing it to slightly shift. Hence, a higher fraction of absorbed particles stems from the disc.

Finally, Figure 4.13 shows the results for $\chi = 1$ with $r_{\text{sink}} = 0.01, 0.005, 0.0025$ and 0.001 from left to right, top to bottom. I remark again, that I chose this seed specifically because it aligns well with z-axis by chance. While the results for the above cases of $\chi < 1$ are comparable across all seeds, this is not true for $\chi = 1$. Some of the seeds, for example, have a positive value for $\cos \theta$ and may decrease with decreasing r_{sink} contrary to Figure 4.13. However, the distribution shifts with decreasing r_{sink} , although the changes are overall small.

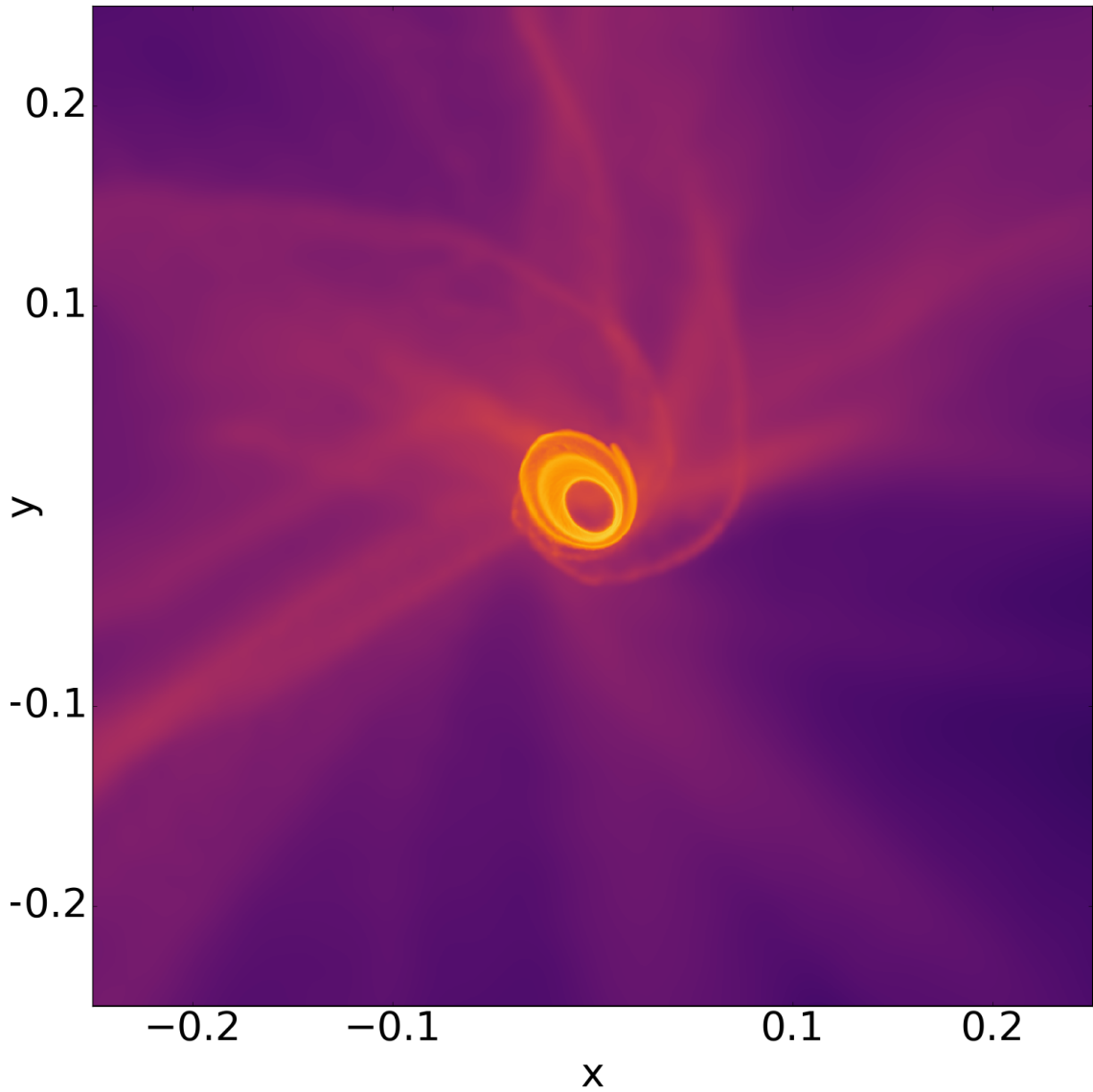


FIGURE 4.10: Density plots at time $t = 1.5$ for a simulation with the Seed D and $\chi = 1$ (fully turbulent setup). As even a fully turbulent velocity field may have some inherent (randomly orientated) rotation, Seed D happens to form a disc aligned with z-axis as is the case for simulations with increased contribution of a solid body rotation to their velocity field (e.g. $\chi < 1$).

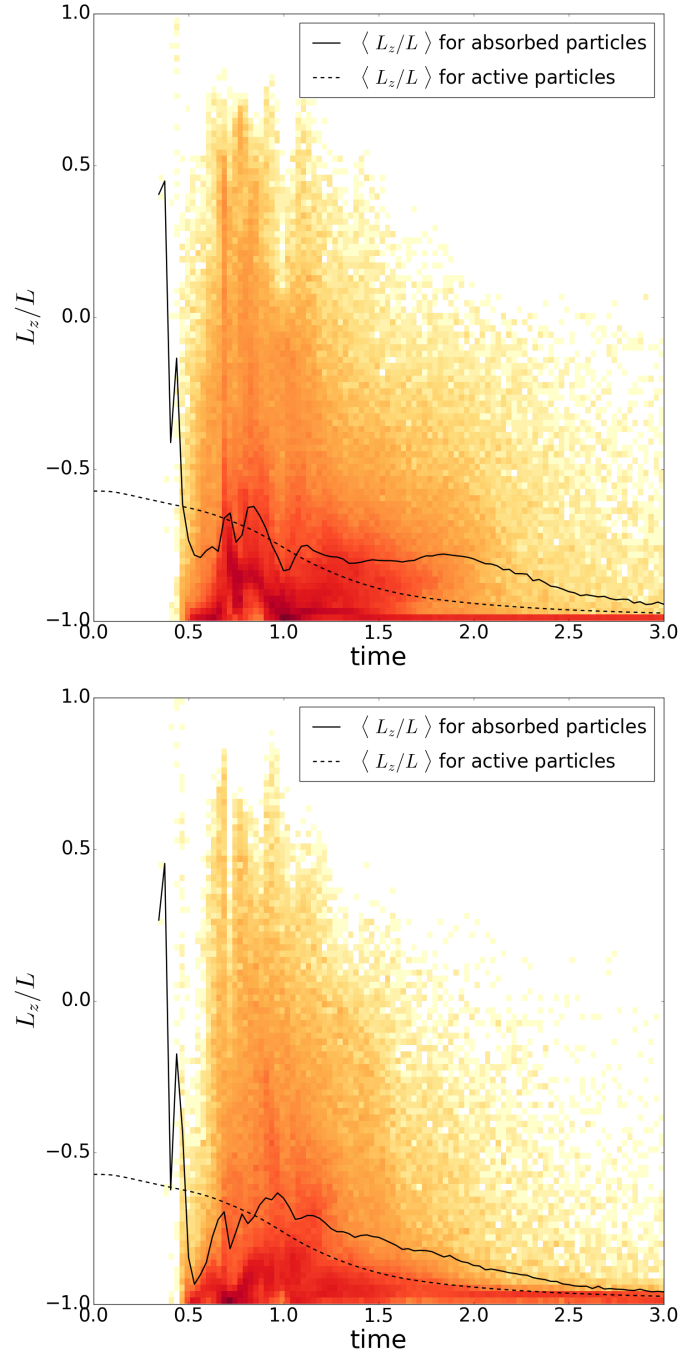


FIGURE 4.11: Distribution of $\cos \theta = L_z/|L|$ of simulation with Seed D and $\chi = 0.5$ for different $r_{\text{sink}} = 0.01$ (top) and 0.0025 (bottom). The solid line represents the average $\cos \theta$ of the absorbed particles, while the dotted line shows the same average, but for the remaining particles in the simulation (not shown in the 2D histogram). Due to the high contribution of the solid body rotation to the initial velocity field, the formation of a large disc early on is the result and subsequently a lot of the absorbed particles stem from the disc (e.g. the high density horizontal line at $\cos \theta = -1$). The disc appears to be slightly less aligned for the simulation with the reduced inner boundary.

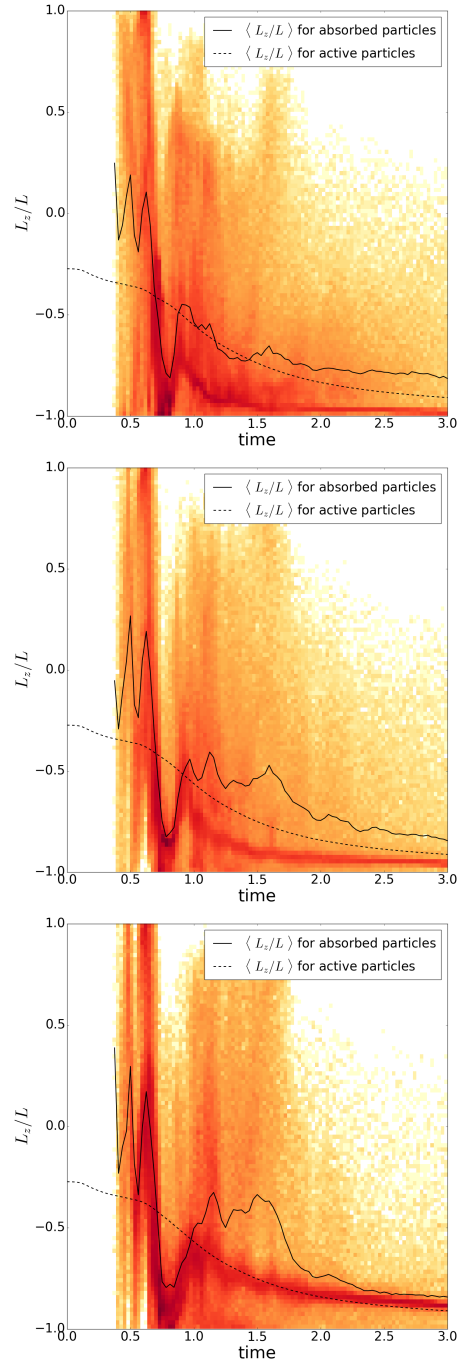


FIGURE 4.12: Distribution of $\cos \theta = L_z/|L|$ of simulation with Seed D and $\chi = 0.75$ (reference) for different $r_{\text{sink}} = 0.01$ (top), 0.005 (middle) and 0.0025 (bottom). The solid line represents the average $\cos \theta$ of the absorbed particles, while the dotted line shows the same average, but for the remaining particles in the simulation (not shown in the 2D histogram). While the original simulation (top) shows still a strong alignment with the z-axis, the changes of the inner boundary cause a more notable shift of $\cos \theta$ for lower r_{sink} compared to Figure 4.11.

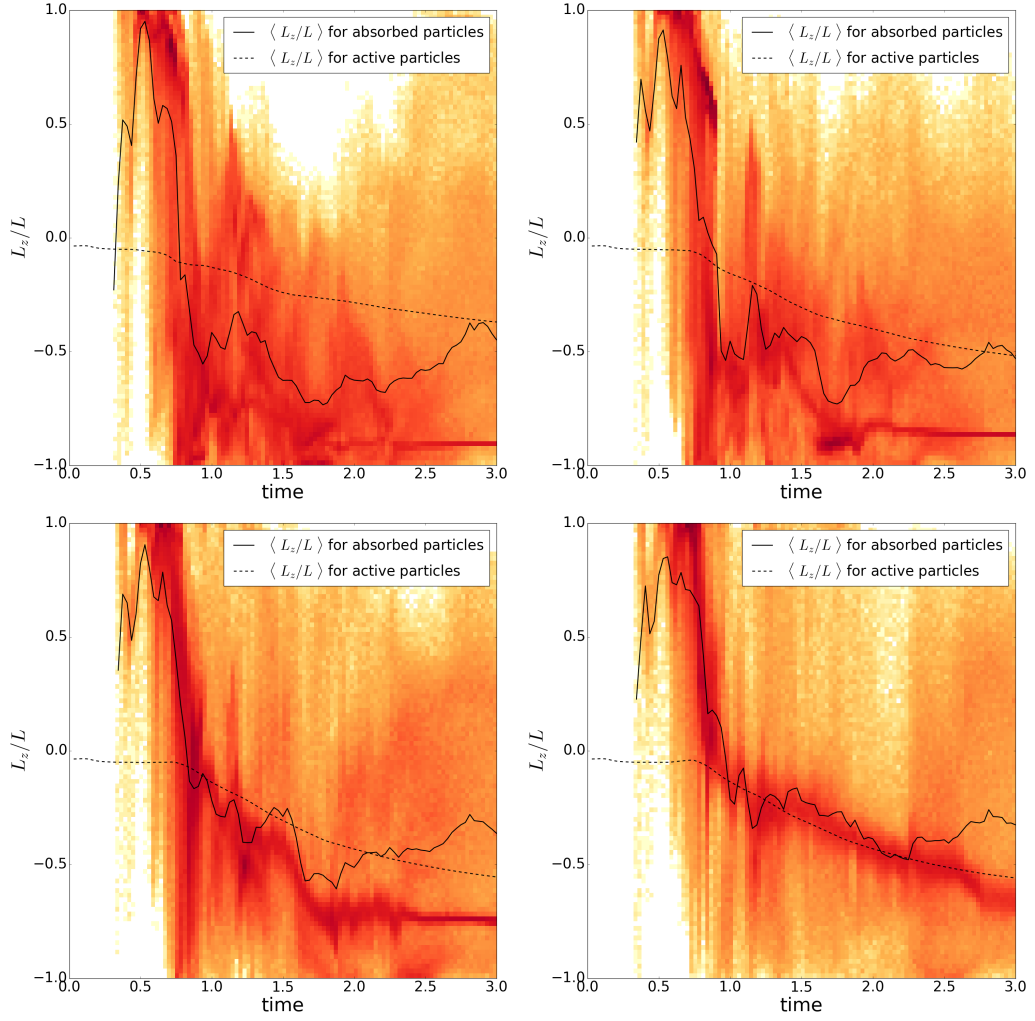


FIGURE 4.13: Distribution of $\cos \theta = L_z/|L|$ of simulation with Seed D and $\chi = 1$ for different $r_{\text{sink}} = 0.01, 0.005, 0.0025$ and 0.001 (left to right, top to bottom). The solid line represents the average $\cos \theta$ of the absorbed particles, while the dotted line shows the same average, but for the remaining particles in the simulation (not shown in the 2D histogram). The progressively smaller inner boundary radii cause a clear shift of $\cos \theta$.

4.6 Discussion and conclusion

I have detailed a number of follow-up simulations to the work done in Chapter 3 by mainly considering the affect of reducing the artificial inner boundary radius r_{sink} . This radius is a numerical necessity to avoid stalling or at least spending significant portions of the available CPU time calculating a small fraction of the gas on very small orbits as shown for the convergence test here. Instead this radius is imposed and particles that cross the boundary are removed from the simulation (however, in our simulations their properties are saved right before the absorption). This naturally causes unphysical behaviour as for example not every orbit that may cross the boundary necessarily has an apo-centre inside the boundary as well. Nevertheless, such a particle is removed. Furthermore the collisions of the streams with other streams or the disc, as shown in Chapter 3, are likely to continue beyond this radius. This potentially severely limits our interpretation of the quantitative effects of the (partial) angular momentum cancellation, which was the very focus of Chapter 3.

To this end I have run several convergence tests and found that indeed the inner structure is modified noticeably by the reduction of r_{sink} , confirming the previously made suggestions that orbits for eccentric particles are removed only for numerical reasons. While this effect converges relative to decreasing r_{sink} as one may expect, it is worth noting that "jumps" may occur, where the behaviour of the innermost structure suddenly changes. This is a result of the chaotic infall of highly eccentric particles and therefore seed dependent.

Consequently we cannot directly deduce the fraction that reaches small enough radii to become relevant for the accretion and subsequent growth process of a SMBH. However, I show by considering the initial and final circularisation radius r_{circ} that we may extrapolate such quantity based on the converged part. This suggests that at least about 10% of the total gas content that undergoes collisional cascades described in Section 3.6 will reach $r_{\text{circ}} = 10^{-4}r_{\text{shell}}$, a significantly larger value than suggested by the changes of the average r_{circ} in Chapter 3.

Finally I attempt to use a similar line of thought to investigate whether the additional collisions caused by the expanded scale of the simulation reveal a change of the orientation of the angular momentum vector. However, the changes appear small - especially for the cases with an already preexisting strongly preferred orientation, which pose the more interesting scientific case. The strongest changes

are observed for the simulations that already have an inherent chaotic movement. While the changes still exist, these results are currently too tentative and more work may be required to form a more quantitative conclusion.

Chapter 5

Application to the Galactic Centre

Zubovas and Nayakshin, 2012 suggest a model that links the formation of the O-stars that are observed inside the sphere of influence of Sgr A*, but above the self-gravity radius ($\sim 10^{-2}$ pc) with an wide-angle outflow event of comparable age that produced the Fermi bubbles. However, a corresponding disc hosting the star formation has been excluded at least for the optical thick case by observations. Furthermore, the disc could not have dissipated in the short time span based on the typical life time of the stars. Here I report on the frequency of major disc disruptions in the simulations presented in Chapter 3 and how they can enable the direct depositing of low angular momentum material that may otherwise be blocked by a disc. Finally I suggest that self-gravity has a crucial impact on disc where sufficiently massive clumps are capable of disrupting the disc completely. This both will cause further (partial) angular momentum cancellation due to the involved collisions and allows the direct infall of gas streams. I briefly discuss to which degree these simulations may be relevant to the case of the missing disc that formed the O-stars inside the central parsec of the Milky Way.

5.1 Introduction

A supermassive black hole (SMBH) named Sgr A* is located at the heart of the Milky Way galaxy in line with the commonly invoked assumption, that most galaxies contain such a massive, but compact object (Soltan, 1982; Kormendy and Richstone, 1995; Kormendy and Ho, 2013). Originally identified as a radio source (Jansky, 1933; Balick and Brown, 1974), increasingly advanced observational studies were able to first utilise the velocity dispersions from emissions (e.g. Serabyn and Lacy, 1985; Miyoshi et al., 1995) and stars (e.g. Genzel et al.,

1996) inside the sphere of influence of the SMBH and later follow the orbits of the "S-stars" (Schödel et al., 2002; Ghez et al., 2008; Boehle et al., 2016), which are composed of a set of highly eccentric stars with orbits close to the SMBH. The by the time of writing this Chapter more than two decades lasting observation campaign allowed the observation of a complete orbit of the star "S2" (Gillessen et al., 2009) and even was able to test predictions arising from the theories of relativity (Einstein, 1905; Einstein, 1915) as the star moved through its peri-centre at $\sim 120\text{AU}$ ($\sim 6 \times 10^{-4}pc$) producing a relativistic Doppler shift (Gravity Collaboration et al., 2018). The result is the most precise measurement of a SMBH mass suggesting that Sgr A* mass is $\sim 4.28 \times 10^6 M_{\odot}$ (Gillessen et al., 2017).

Therefore the centre of the Milky Way provides an unique testbed to compare the results and potential implication of the work shown in Chapter 3 and 4. To this end I shall provide a description of objects of interest ordered by radially increasing distance and discuss any likely connection between those.

I already mentioned the SMBH Sgr A* at the centre of volume of interest. A useful quantity to that respect is to determine the radius at which point not even light can escape the gravitational pull anymore -the Schwarzschild (1916), radius is:

$$R_S \sim 4 \times 10^{-7} \left(\frac{M_{\bullet}}{4.28 \times 10^6 M_{\odot}} \right) \left(\frac{2G}{c^2} \right) pc, \quad (5.1)$$

where R_S is the Schwarzschild radius, G the gravitational constant, M_{\bullet} the mass of the SMBH and c the speed of light. This equation assumes no spin.

As everything in the Universe has some angular momentum, the formation of an accretion disc around a SMBH is inevitable (e.g. Prendergast and Burbidge, 1968; Shakura and Sunyaev, 1973; Lynden-Bell and Pringle, 1974; Pringle, 1981) and in fact is argued to be the source of the emission, which allows the SMBH to be observed in the first place (e.g. Salpeter, 1964; Zel'dovich, 1964; Lynden-Bell, 1969; Wolfe and Burbidge, 1970; Lynden-Bell and Rees, 1971; Pringle and Rees, 1972; Bardeen, Press, and Teukolsky, 1972). Following the above mentioned Schwarzschild metric based on the theory of general relativity (Einstein, 1915), one can define an innermost stable circular orbit (ISCO) beyond which the gas (or in fact any object) approximately free falls into the black hole while radiating away further energy (e.g. Shklovsky, 1967; Bardeen, Press, and Teukolsky, 1972; Frank, King, and Raine, 2002):

$$R_{ISCO} \sim 1.2 \times 10^{-7} \left(\frac{M_{\bullet}}{4.28 \times 10^6 M_{\odot}} \right) \left(\frac{6G}{c^2} \right) \text{pc} \quad (5.2)$$

where R_{ISCO} is the inner most stable circular orbit. Zero spin of the SMBH is again assumed. This can be thought as the inner edge of the accretion disc.

Further out the already mentioned S-stars (not to be mistaken with the spectral type of the same name) reach peri-centre of the order of 10^{-4} pc and extend up to about 0.04pc (e.g. Gillessen et al., 2017). They are massive stars (typically B-type of about $10M_{\odot}$ with an upper age limit of 15 Myr (S2 is thought to be about 6 – 7 Myr old) on randomly orientated, high eccentric orbits (e.g. Habibi et al., 2017; Gillessen et al., 2017). These relatively young stars severely constrain dynamical migration theories like inspiralling star clusters (e.g. Portegies Zwart, McMillan, and Gerhard, 2003; Kim and Morris, 2003; Fujii et al., 2008; Mapelli and Gualandris, 2016) or the Hills mechanism (Hills, 1988). The latter describes the binary break up by the SMBH due to tidal disruptions, which lead to high eccentricities and matches the observation, if one accounts for the orbit shifts caused by resonant relaxation resulting in a thermal eccentricity distribution (e.g. Hills, 1988; Perets et al., 2009). However, it is thought that these timescale required might be too short (Perets et al., 2009; Habibi et al., 2017; Alexander, 2017). More local formation channels, e.g. fragmentation of accretion discs still require migration of the stars or Kozai-Lidov oscillations (Lidov, 1962; Kozai, 1962; Levin, 2007; Šubr and Haas, 2016; Habibi et al., 2017; Bar-Or and Fouvry, 2018), but ultimately take too long (Bar-Or and Fouvry, 2018). It has been suggested, that the S-stars might be instead formed by the fragmentation of an AGN outflow event (Nayakshin and Zubovas, 2018).

There might be further so far undetected stars or stellar black holes, that may perturb the orbits of the S-stars. So far constraints of the total mass of these objects put an upper limits of about two magnitudes less the mass of Sgr A* (Gillessen et al., 2009). These might be highly obscured by the interstellar dust in the plane of the Galactic disc as the stars mentioned here are typically observed in the infra-red that can pierce through the layer. Some of the objects are referred to as G objects, that feature high eccentricities. G2 was thought to allow a "live" observation of the disruption and subsequent feeding of the SMBH, however, the object survived the gravitational forces of the SMBH unaffected probably due to its own source of gravity in form of star (Gillessen et al., 2012; Gillessen et al., 2013; Witzel

et al., 2014; Shahzamanian et al., 2016; Calderón et al., 2016).

The angular momentum transport (and therefore the mass transport as well) in an accretion disc is thought to be caused by viscosity (e.g. Goldreich and Schubert, 1967; Shakura and Sunyaev, 1973; Smak, 1999; Dubus, Hameury, and Lasota, 2001; King, Pringle, and Livio, 2007). The viscous time scale approaches multiple times the age of the Universe for discs with a radius of ~ 1 pc and beyond (Frank, King, and Raine, 2002; King and Pringle, 2007; King, Pringle, and Hofmann, 2008). Recent observations of AGN phases suggest that such an accretion disc might be only relevant to SMBH growth if it is $R \lesssim 2 \times 10^{-3}$ pc (Schawinski et al., 2015; King and Nixon, 2015). This can be seen as an upper limit for an effective accretion disc as the disc itself may well extend beyond this radius.

Furthermore, it can be argued that a disc exceeding 10^{-2} pc (King and Pringle, 2007) is subject to self-gravity causing the fragmentation of the disc, which leads to star formation (Kolykhalov and Syunyaev, 1980; Pringle, 1981; Lodato, 2007). This radius agrees remarkably well with hundreds of early-type Wolf-Rayet and O-type stars between 0.03 and 0.4 pc with a common age of $\sim 2.5 - 6$ Myr. 20 – 50% form an approximately Keplerian, but potentially warped disc with an eccentricity of ~ 0.3 rotating clockwise, while the majority of the counter-rotating disc feature more eccentric orbits (e.g Paumard et al., 2006; Bartko et al., 2009; Do et al., 2013), however, the existence of the latter has been recently questioned (Yelda et al., 2014). Compared to the "S-stars", the formation channel is likely in-situ star formation generally thought to be the result of the circularisation of a disrupted molecular gas cloud (e.g. Nayakshin and Cuadra, 2005; Nayakshin, Cuadra, and Springel, 2007; Bonnell and Rice, 2008; Hobbs and Nayakshin, 2009; Alig et al., 2011; Mapelli et al., 2012). This requires the disc to be reasonably massive, cool quickly or be cold enough to allow local collapse, while shock heating of the infalling material avoids a runaway process and instigates an angular momentum transport (Cossins, Lodato, and Clarke, 2009). The simulations typically achieve most of the observational aspects, in particular the top heavy initial mass function and slightly eccentric orbits. In order to form multiple misaligned discs, these restrictions had to either be relaxed (Lucas et al., 2013) or invoke further gaseous infall on a pre-existing stellar disc (Mapelli, Gualandris, and Hayfield, 2013). Finally, as the disruption of the cloud either requires the cloud to get close enough to be affected by gravitational potential of the SMBH or another cloud

on similar orbits, the proposed collisions and instabilities with the further out located circum-nuclear disc (CND) may provide a more likely scenario (Alig et al., 2013; Trani et al., 2016).

A rarely considered constraint is the apparently missing disc, which is ruled out at least for an optically thick disc utilising near infrared observations (e.g. Cuadra, Nayakshin, and Sunyaev, 2003). It could have not been dispersed by viscous accretion or by the stars that formed of said disc (Alexander et al., 2012). The authors suggest, that it may have been accreted by the central SMBH -an intriguing prospect that forms the motivation for the analysis presented in this chapter and I will provide a preliminary answer to that end based on the results of new simulations featuring self-gravity.

The volume that the SMBH dominated gravitationally is referred to as the sphere of influence and can be computed as follows (Peebles, 1972; Frank, King, and Raine, 2002):

$$r_{inf} = \frac{GM_{\bullet}}{\sigma_{\bullet}^2} \sim 1.5\text{pc} \left(\frac{M_{\bullet}}{4.28 \times 10^6 M_{\odot}} \right) \left(\frac{\sigma(r_{\bullet})}{113\text{km/s}} \right)^{-2}, \quad (5.3)$$

where r_{inf} is the influence radius and σ the velocity dispersion of the central stars (Zhu et al., 2008).

The circum-nuclear disc (CND) or circum-nuclear ring (CNR) (e.g. Serabyn et al., 1986; Wright et al., 2001; Liu et al., 2013) is situated just outside the sphere of influence $\sim 1.5 - 7\text{pc}$ and is on the verge of star formation. Simulations show that a nuclear star cluster with a mass of $\sim 10^7 M_{\odot}$ and a core of up to $\sim 0.5\text{pc}$ decreasing afterwards in density up to $\sim 30\text{pc}$ (Mapelli and Trani, 2016; Trani, Mapelli, and Ballone, 2018) or an outflow event (Zubovas and Nayakshin, 2012) can lead to the formation of circum-nuclear rings outside the sphere of influence in accordance with observations of the Milky Way central region. In fact such a molecular torus of around pc size centre is reported as well in Seyfert galaxies (e.g. Krolik and Begelman, 1988). Furthermore, molecular gas streams have been observed that connect clouds around $10 - 20\text{pc}$ and the CNR providing further evidence for how the fuel may reach the galactic centre (Ho et al., 1991; Takekawa et al., 2017; Sormani and Barnes, 2019). Montero-Castaño, Herrnstein, and Ho (2009) and Blank et al. (2016) observe clumpiness in the CNR and find evidence for that this destabilised region funnels gas towards the centre as well. Those filaments (see Figure 5.1) are referred to as "mini-spirals" and reach $\lesssim 1\text{pc}$ with

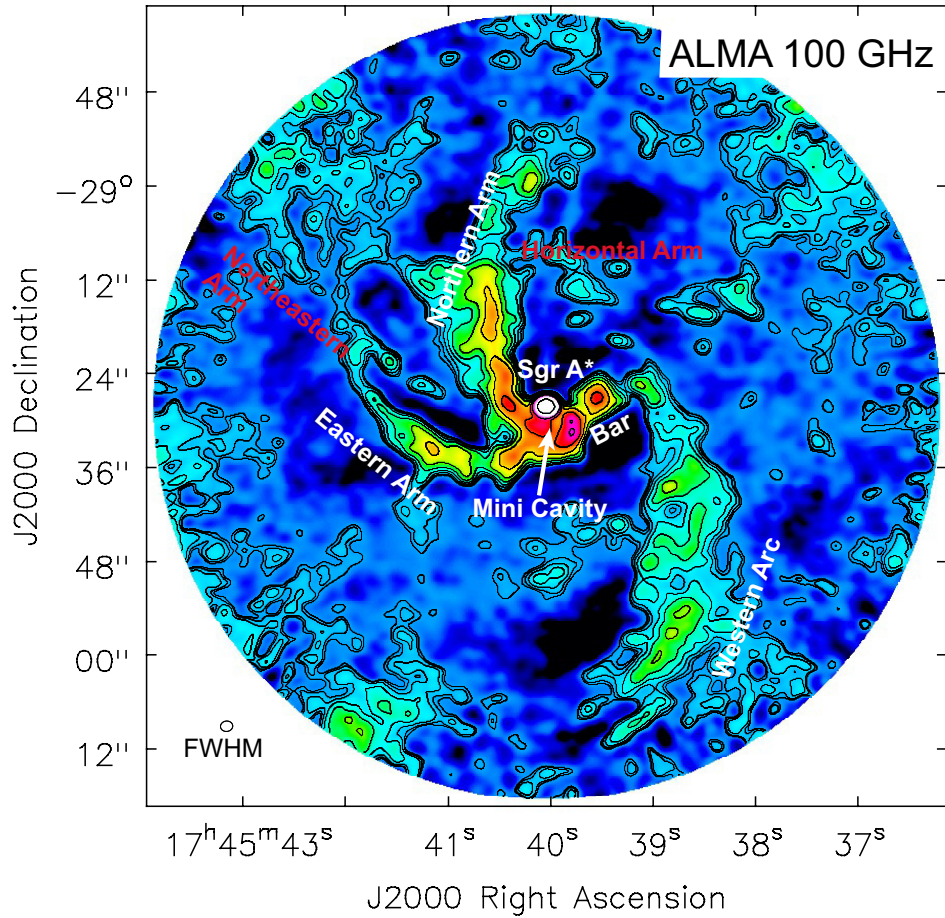


FIGURE 5.1: ALMA image at 100 GHz of the mini-spiral with labelled substructure. Taken from (Tsuboi et al., 2017).

masses of $\sim 10^2 - 10^3 M_{\odot}$ (Lacy et al., 1980; Scoville et al., 2003; Tsuboi et al., 2017).

Finally, it is worth mentioning the so called Fermi bubbles that are two symmetric pear shaped X- and gamma-ray structures centred on Sgr A* and reach from 100 to 8,000pc (Su, Slatyer, and Finkbeiner, 2010). These can be interpreted as a quasi-spherical (e.g. King and Pounds, 2003; King, 2010) AGN outflow (Zubovas, King, and Nayakshin, 2011) that appear to be connected to the above mentioned formation of stars ~ 6 Myr ago. In another paper Zubovas and Nayakshin, 2012 argue that the outflow requires a quasar phase of at least 2.5×10^5 yr duration (which is tantalising close to observational evidence of AGN phases (Schawinski et al., 2015; King and Nixon, 2015)) and that the SMBH accreted $\sim 10^5 M_{\odot}$ (which is about a magnitude more than the mass of the young stars mentioned above). The latter suggests that $\sim 90\%$ may be accreted of a

self-gravitating accretion disc.

This chapter is organised as follows: In Section 4.2 I briefly describe the initial setup. I will discuss the potential impact of disc destructions on our previous set of simulations (see Chapter 3) in Section 5.3. Section 5.4 provides some preliminary results how self-gravity fundamentally changes the disc structure. The results are discussed and concluded in Section 5.5.

5.2 Initial conditions

I utilise the same setup of a non-uniform shell produced by an initial velocity field opposed on a Gaussian distributed 2×10^6 SPH particles with a mean of $r_{shell} = 1$ and a width of $0.2r_{shell}$ (see Chapter 3). This is done by using a quasi-random number generator to avoid spurious over- and under-densities (e.g. Niederreiter, 1992)). The sink particle representing a volume encapsulating the SMBH has a radius of $r_{sink} = 0.01$, which is numerically motivated to avoid stalling the simulation by spending much of the available CPU time computing the orbits of a small fraction of particles at very small orbits (see Chapter 4). The mass of the shell is varied from its reference value of $M_{shell} = 0.01M_{\bullet}$ to $0.1M_{\bullet}$ and $1M_{\bullet}$, where $M_{\bullet} = 1$ is the mass of the sink particle, in order for self-gravity to take affect.

The velocity field is modified by contributions of a solid body rotation or turbulent velocity field, where the latter is computed based on the method proposed by Dubinski, Narayan, and Phillips (1995) and uses a Kolmogorov (1941) and Kolmogorov (1991) spectrum (see Section 3.2.2). The individual contributions are set up such that I can scale the involved kinetic energies with respect to the virial theorem:

$$\frac{2E_{kin}}{-E_{pot}} = \frac{\sum_i m_i v_i^2}{\sum_i Gm_i M_{\bullet} / |r_i|} \approx \chi^2 \eta_{turb} + \frac{2}{3}(1 - \chi)^2 \eta_{rot}^2, \quad (5.4)$$

where η is a scaling factor and is set for both instances to 0.9. χ controls the fraction of the contribution from both velocity fields, where $\chi = 0$ only considers the solid body rotation and $\chi = 1$ is equivalent to the purely turbulent velocity field. The resulting velocity field is sub-virial and forms rapidly the desired clumpy medium. I vary χ between the reference value of 0.75 and 1 and expect

that differences arise based on the typically readily formed disc for the simulation with some contribution from a solid body rotation velocity field. Such a disc may show stronger fragmentation than might be the case in the more volatile conditions generated by a purely turbulent realisation of the initial velocity field.

While once again a wider parameter sweep akin to the one performed for Chapter 3 appears desirable, the increased CPU cost of about a factor of ten incurred by the self-gravitating fragments requiring significantly shorter time steps, imposes time constraints such that I limit my analysis to the above mentioned parameters.

As I employ an isothermal equation of state for the sake of consistency with previous simulations, I note that instant and complete cooling represents somewhat a worst case scenario for self-gravity as it allows a runaway collapse (otherwise if $t_{cool} \lesssim 3/\Omega$ bound clumps can form fragmenting the disc, see e.g. Gammie, 2001; Forgan and Rice, 2011). To avoid this and to generally counter the potentially prohibitively expensive CPU times caused by the higher densities formed, I limit the gravitational softening length ϵ (and therefore the Jean mass) and hence ensure that it is always resolved (Bate and Burkert, 1997).

I vary ϵ between 0.001 and 0.005 in order to test the impact of changing the gravitational softening length on the simulations. Figure 5.2 shows a density plot at $t = 1.5$ for the two differing softening lengths. Both simulations do form self-gravitating clumps, but simulations with $\epsilon = 0.005$ are more similar in disc structure to the reference simulations. Interestingly, Figure 5.3 shows that the time evolution over the average r_{circ} and eccentricity (see Section 3.4) of both values for ϵ are remarkably equal with respect to average r_{circ} of the bound and absorbed particles and the fraction of absorbed particles itself. The latter, however, features an extremely high absorption rate ($\sim 90\%$), so small differences may not be immediately apparent. The fraction of gas particles I attribute to the disc (e.g. $e < 0.5, r_{circ} < 0.3$, see Section 3.4) reflect the visual difference apparent in Figure 5.2. Nevertheless, the similar average reduction of the circularisation radius suggest that the distribution caused by self-gravity might not be only due to the formation of high density clumps, but in general due to the increased density of the inner structure and the infalling streams (up to ~ 4 magnitudes higher density compared to the corresponding reference simulation). I note that the calculation of r_{circ} and e is flawed in the case of self-gravitating material, however, they represent only a small fraction of the particles in the disc. A more thorough

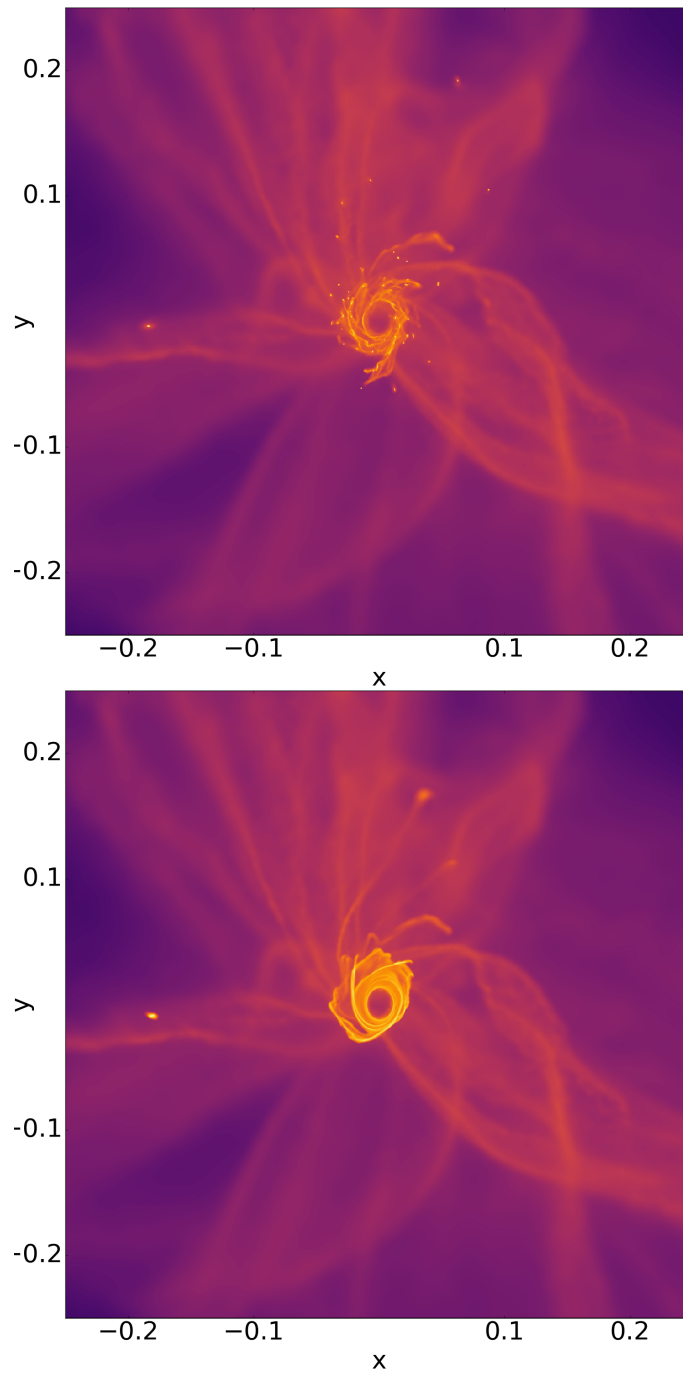


FIGURE 5.2: Density plots at time $t = 1$ for simulations with the same Seed B, $m = 1$ and $\chi = 1$, which differ by the gravitational softening length employed (top: $\epsilon = 0.001$, bottom: $\epsilon = 0.005$). While both simulation show self-gravitating clumps at various stages of the simulation, the version with $\epsilon = 0.005$ (bottom) clearly is more akin to the reference simulations.

discussion of this problem can be found in Section 5.4.

A disc with $M_{disc} \sim 0.25M_{\bullet}$ and $H/R \lesssim 0.1$ is shown to be essentially local and therefore the α (see Section 2.2.3) viscosity can be utilised (Lodato and Rice, 2004; Forgan and Rice, 2011), however, more massive discs lead to temporary spiral modes producing global perturbations that are hard to model with the α disc model (e.g. Lodato and Rice, 2005; Forgan and Rice, 2011). While I do present simulations with with a shell mass equivalent to that of the sink particle, I argue that only a fraction of the particles end up in the disc (see Figure 5.3, right side) and therefore this condition should not be reached. The isothermal equation of state ensures that the disc remains thin.

The simulation have been performed with the SPH (Lucy, 1977; Gingold and Monaghan, 1977) code SPHINX by Walter Dehnen (for more information see e.g. Cullen and Dehnen, 2010; Aly et al., 2015; Faber and Dehnen, 2018).

5.3 Disc destruction

In Chapter 3 I alluded in the discussion section (Section 3.5) that in some cases the average r_{circ} was reduced compared to the reference simulations, but the absorption rate was lower (see e.g. Sections 3.4.2 and 3.4.4). Naturally one may expect that a lower average r_{circ} and therefore angular momentum should result in more particles to enter the inner boundary radius. The simulations that propose the contrary claim have all an early developed, never strongly disrupted disc in common. Infalling clumps or streams of particles with low enough angular momentum to circularise inside the inner boundary radius may therefore interact with the disc first. However, if the disc is massive enough, the addition of a relatively small mass and an even smaller amount of angular momentum will barely affect the disc. Hence despite having potentially suitably low angular momentum, gas may be trapped by an existing disc.

Turning this conclusion around, we should observe significant absorption rates, if a disc gets disrupted enough for example to be destroyed and reformed (typically with a different orientation in line with the expectations for chaotic accretion (e.g. King and Pounds, 2003; King, 2005; Pounds et al., 2018)). Figure 5.4 shows how such a sequence may look like in the form of density plots. The time evolves from left to right, top to bottom in equally spaced periods between $t = 0.65 - 0.81$. The first snapshot (top left) displays a misaligned disc

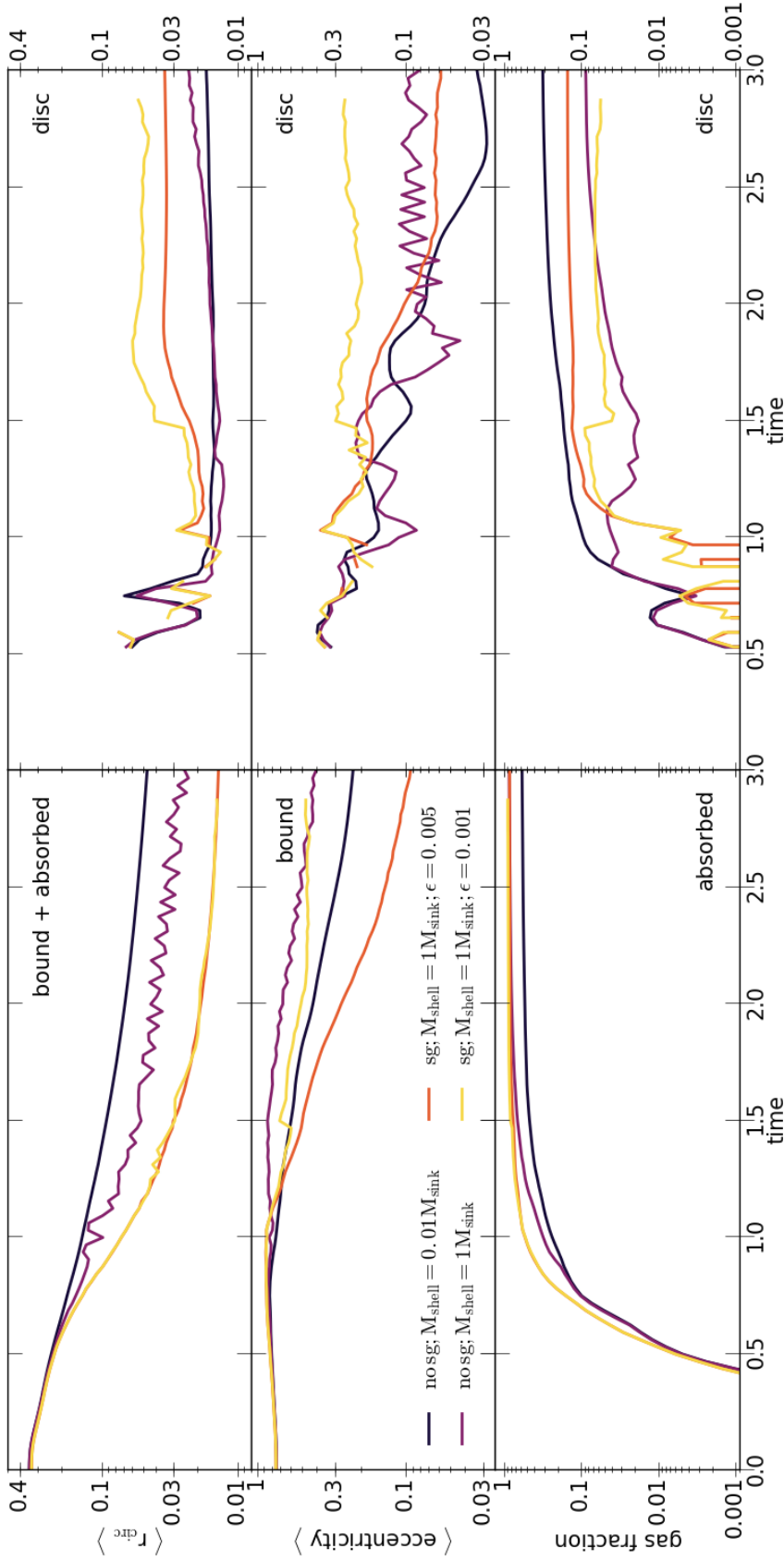


FIGURE 5.3: Time evolution of the average circularisation radius and eccentricity as well as the gas fraction for different portions of the gas and for differing ϵ . Additionally the simulations without gravity (however, with and without an increased mass) are shown as comparison. ‘Absorbed’ refers to simulated gas that at some point prior to t has reached $r < r_{\text{sink}} = 0.01$ and was absorbed into the central sink particle; ‘bound’ refers to all remaining gas that at the given time has $e < 1$, ‘disc’ represents all bound gas at $e \leq 0.5$ and $r_{\text{circ}} \leq 0.3$ indicated by a thin dotted rectangle in Figure 3.1 (which may also contain a small fraction of impacting filaments). The text details the limitation arising from the self-gravity with respect to the r_{circ} and e .

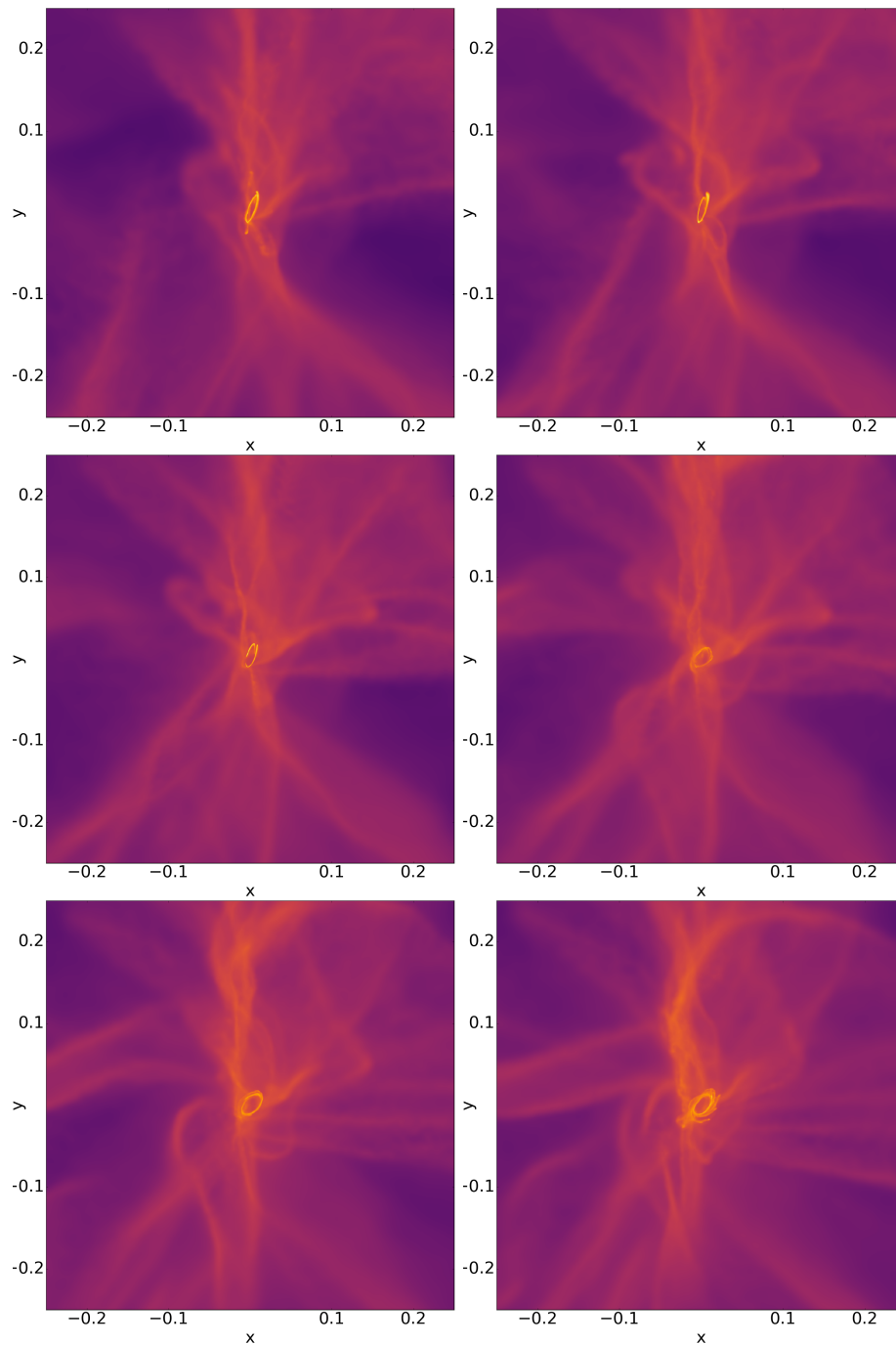


FIGURE 5.4: Density plots at the times $t = 0.65 - 0.81$ (left to right, top to bottom) of a reference simulation (see Section 3.3.2) with the Seed B. The early disc gets disrupted by gaseous infall and collapsed beyond the inner boundary radius before a new disc with a different orientation is formed.

or rather ring that is in the process of interacting with an infalling stream. The second row shows how the ring is broken up and a new disc is formed (middle right). Unfortunately the snapshot frequency does not allow to observe the absence of the disc, however, a simulation with higher data output rate confirms the suggestion. The paper format of this thesis, however, is not suitable to display these sequences in an elegant way. Finally, the bottom rows shows the formation of a disc with a different orientation as suggested above.

It is worth noting that this simulation is not based on purely turbulent initial velocity field ($\chi = 1$), but rather part of the sextet of reference simulations with $\chi = 0.75$. Indeed, the same style of density plot shows a disc at $t = 3$ that is aligned with z-axis in accordance with the contribution of the solid body rotation to the initial velocity field.

This immediately begs the questions, whether these disc destructions or at least major disruptions might occur more frequently and do not require necessarily the completely chaotic infall induced by the initial condition parameter $\chi = 1$. To this end, I analysed the set of simulations presented in Chapter 3 and looked for sudden drops in the number of particles inside the as belonging to the disc defined area e.g. $r_{\text{circ}} < 0.3$ and $e < 0.5$ (see e.g. Figure 3.1). I caution that the described frequency of the snapshot output may hide some of the disruption and that the criteria above may include infalling material as well bolstering the numbers stated and therefore may as well obscure any major impact.

Nevertheless I find that half of all simulations show either a noticeable dip as a result of disruption by infall or a complete destruction and subsequent forming of a new disc (roughly equally distributed between the two cases). While principally every choice of parameter shows at least a few such incidents, some parameters show a lower fraction. These include simulations with a shallower power spectrum of the turbulence (see Section 3.4.2), large solid body rotation contribution to the initial velocity field (see Section 3.4.3) and simulations with a solenoidal turbulent velocity field (see Section 3.4.4). As described in the corresponding section, all these simulations feature a large disc early one that is capable of blocking some of the low angular momentum infall. At the other end simulations with a fully turbulent realisation (see Section 3.4.3) and with higher shell masses (see Section 3.4.5) feature a specifically high fraction of disruptions. The latter is caused by the sink particle moving around due to the heavier infall.

In order to test whether the destruction of the disc only absorbs the associated

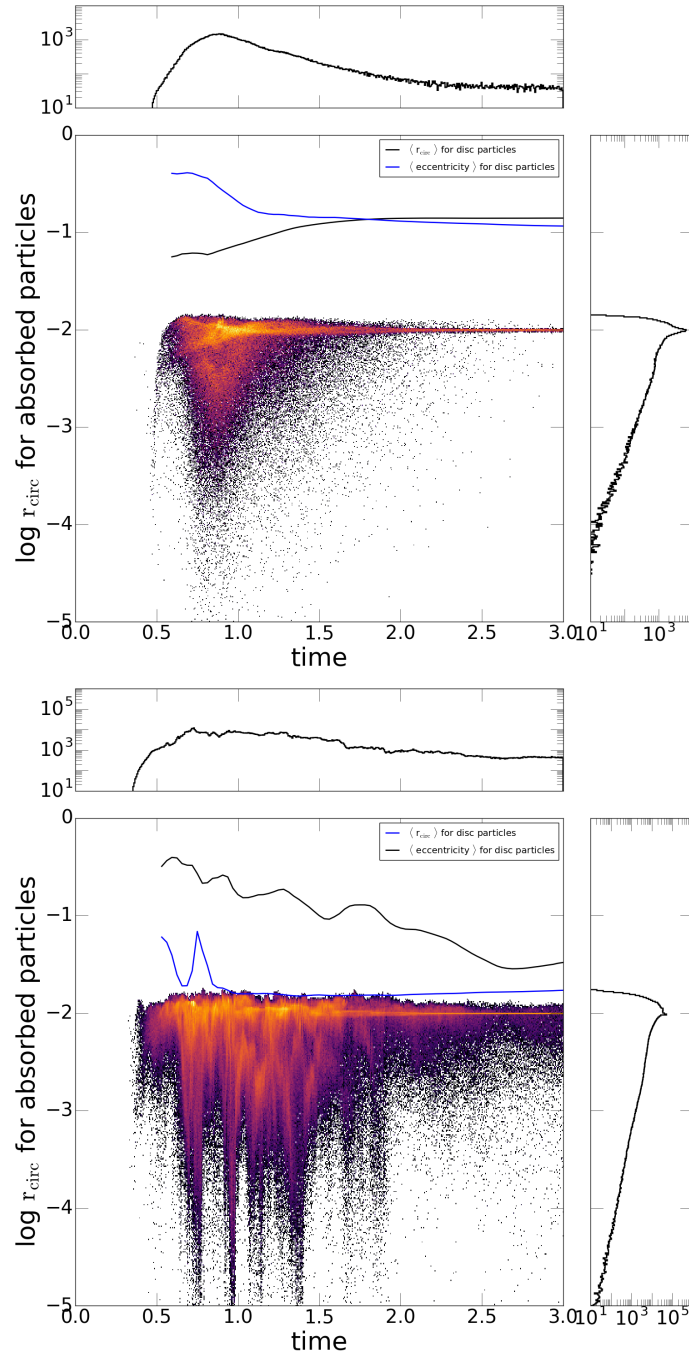


FIGURE 5.5: Distribution of r_{circ} over time for the absorbed particles. The top plot shows simulation with $\chi = 0.25$. The large contribution of the solid body rotation to the initial velocity field aids the formation of a large disc early on, which limits the angular momentum of the infalling particles to the disc. The bottom plot shows the same Seed B, but with $\chi = 0.75$. While the disc will still dominate the infall at later times, the angular momentum spread is much larger for longer time span. The blue line shows the average r_{circ} of the disc, while the black indicates the corresponding eccentricity.

particles and therefore can be treated as a numerical artefact of the inner boundary condition or allows as well the infall of low angular momentum material that potentially caused the destruction in the first place, I plot the distribution of r_{circ} over time. Figure 5.5 shows two representative examples of simulations where the disc dominates the infall (top) and where it is disrupted and/or remain eccentric (blue lines) for a longer time (bottom). Both simulations feature the same Seed B, however differ by $\chi = 0.25$ (top) and $\chi = 0.75$ (bottom). The larger rotational component causes the formation of a large disc early on for the top simulation, reducing the spread of r_{circ} of the absorbed particles to a small area close to the inner boundary radius. Therefore accretion occurs almost exclusively from the disc. On the other hand, the bottom simulation retains a portion of the rotational component that leads to the formation of a persistent disc later on. However, as the disc is significantly smaller in comparison to the top simulation, the general spread of r_{circ} across the absorbed particles is wider. For early times ($t \sim 0.7$) the average r_{circ} falls rapidly before it rises again (green line), which coincides with particular large spread of r_{circ} of the absorbed particles. These "spikes" in the plot indicate that the absorption happens often in form of clumps or streams that deposit particles in relatively short time frames. Furthermore there is a large fraction of particles that get absorbed with $r_{\text{circ}} > r_{\text{sink}}$, which represents the material from the original disc that got destroyed by the infall.

Therefore these simulations confirm that the disc can block low angular momentum infall, if it can resist it by being large and massive enough, but can also significantly contribute towards the here reported absorption rates when disrupted or even destroyed. More importantly such an event frees the way for direct low angular momentum infall. However, the conditions for such an event are less clear and their predominantly occurrence at times before the majority of the gas has reached the inner volume may suggest that is a numerical artefact caused by the struggle to resolve such an early disc properly or is simply a case of an impact of a comparable or larger mass than the disc.

5.4 Self-gravity

In the previous section I have shown that for chaotic infall some major disruption of the disc can be expected and that this may lead to the direct depositing of low angular momentum material to small radii. Recalling the introduction focusing

on the situation that present itself in the GC, one may invoke some infall event forming a disc, which fragments into the observed O-type stars that is hit by further infall probably of the same principal origin. It is able to disrupt and/or destroy the disc making large quantities of gas available to cause the outflow event that produce the Fermi bubbles eventually. The gas may undergo the collisional cascades described in Chapter 4 in order to reach the small radii required for viscous accretion. However, based on the preliminary results of the previous section this may involve a mass comparable or larger, which is more difficult to explain.

Here I present a set of simulations that vary χ between 0.75 and 1 and change the shell mass between $0.01M_{\text{sink}}$, $0.1M_{\text{sink}}$ and M_{sink} , where M_{sink} is 1, but more importantly utilise self-gravity of the gas. Of particular interest is the question whether the formation of self-gravitating clumps takes away mass from the SMBH or whether the disruption caused by the self-gravity may enhance the absorption rate similar to the case presented in Section 5.3.

Conveniently the simulation setup may be straight forwardly adapted to the condition of the GC: If we take the outer most part of the Gaussian distributed shell ($r \sim 1.5$) as the sphere of influence radius, it follows that the self-gravity radius ($\sim 10^{-2}\text{pc}$) and therefore the inner most orbit of the O-stars coincides with the inner boundary radius of our simulations. Furthermore, taken the mass of Sgr A* for the sink particle, the mass of the shell equates to $4.28 \times 10^4 M_{\odot}$, $4.28 \times 10^5 M_{\odot}$ (which is comparable to the mass claimed by Zubovas and Nayakshin, 2012) and $4.28 \times 10^6 M_{\odot}$.

Figure 5.6 and 5.7 show density density plots of simulations with Seed A and B respectively run with self-gravity turned on. The top row features a mass of the shell of $0.1M_{\text{sink}}$, while the for the bottom row it is set to $1M_{\text{sink}}$. The displayed simulations are further differentiated by χ , where the left column has χ set to 0.75 (reference value), while the right column has it set to 1 (fully turbulent realisation of the initial velocity field).

The simulation of $M_{\text{shell}} = 0.1M_{\text{sink}}$ (top row in the respective figures) bare the closest resemblance to the simulations with $M_{\text{shell}} = 0.01M_{\text{sink}}$, which is the original value used in e.g. Chapter 3. These simulations are not shown, because they are identical to the versions of the simulation run without self-gravity as they do not reach the density threshold to experience self-gravity. Despite the structural similarities, the highest densities reached is a few magnitudes higher than in their non-self-gravitating counterparts suggesting that there is still some

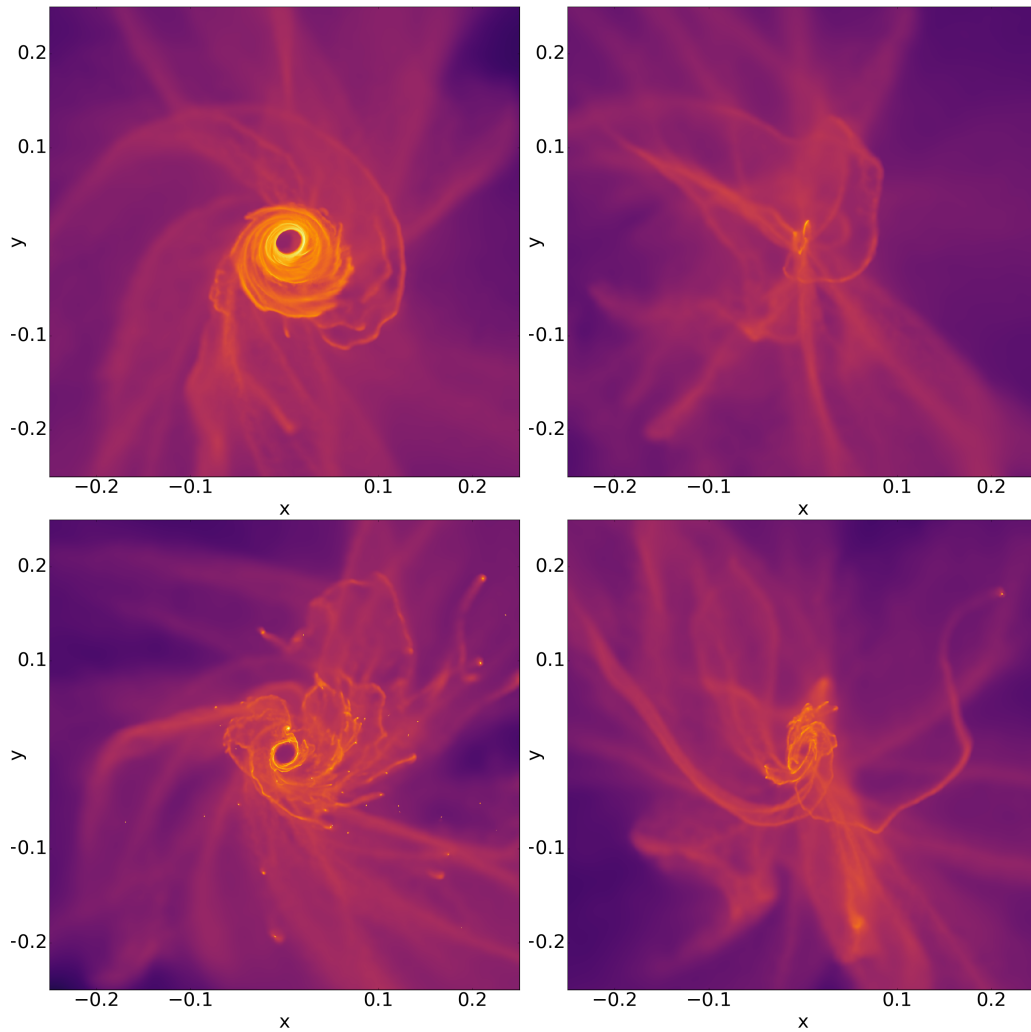


FIGURE 5.6: Density plots at the time $t = 1.21$ of Seed A with self-gravity. The top row features $M_{shell} = 0.1M_{sink}$, bottom row $M_{shell} = 1M_{sink}$. The left column shows simulation with $\chi = 0.75$, the right side with $\chi = 1$.

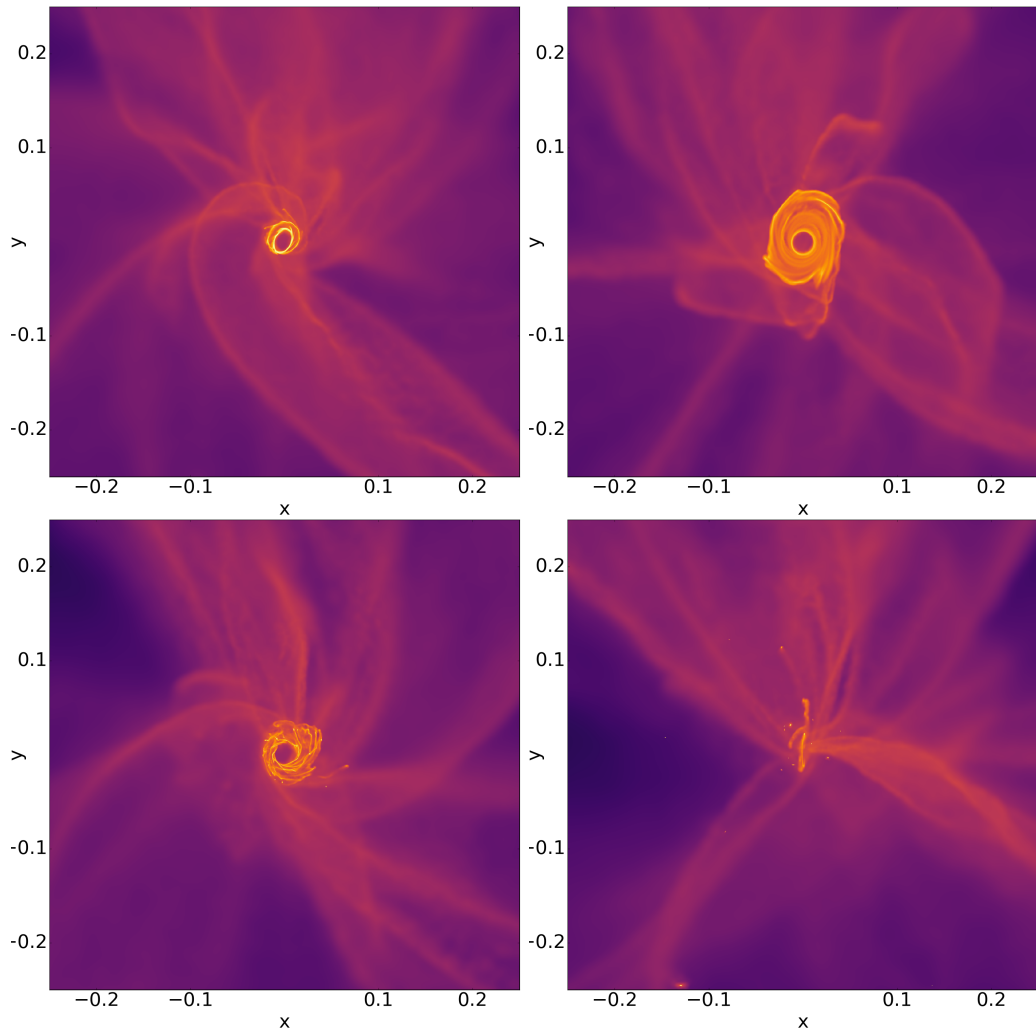


FIGURE 5.7: Density plots at the time $t = 1.21$ of Seed B with self-gravity. The top row features $M_{shell} = 0.1 M_{sink}$, bottom row $M_{shell} = 1 M_{sink}$. The left column shows simulation with $\chi = 0.75$, the right side with $\chi = 1$.

impact.

The bottom row shows simulations where the initial gas mass is equal to that of the sink particle. Here the differences are much more apparent, especially in the bottom left of Figure 5.6, where the disc is dominated by a large number of extremely dense (up to 8 magnitudes higher) clumps that -if seen in sequence- clearly show their disruptive impact upon the disc. In fact a disc may not be formed for an extended period of time ($\Delta t > 1$), if $\chi = 1$. The constant impact of massive streams destroys immediately any earlier material in the process of circularising outside the inner boundary radius. Clumps get typically absorbed by the sink particle, however, some are forced out of the central regions at high speed and many of them have their own associated mini-disc that is randomly orientated with respect to the main disc.

The large differences for each seed are in line with the reasoning in Section 3.3.2 and demand that for any quantitative assessment, it is sensible to average the results based on several simulations as done for the sextet in previous chapters. However, the associated computational cost is beyond the scope of this chapter and therefore the results here should be seen as preliminary.

I noted in Section 5.2, that my approach of considering the circularisation radius and eccentricity is flawed as soon as self-gravity creates locally gravitational dominant volumes. This will lead to particles in self-gravitating clumps to appear potentially unbound with respect to the sink particle. This affects the particles that are being sorted under the "disc" fraction as well. Nevertheless, the fraction of gas in such clumps is still low compared to the total number of particles and will have a small impact on the average r_{circ} , however, eccentricity appears to be worse affected by this. For this reason and for the sake of comparability with previous plots, I utilise the same style plot.

Figure 5.8 and 5.9 show the time evolution of the average circularisation radius and eccentricity for different fractions of the gas, but vary by their choice of χ (0.75 and 1 respectively). The simulation plotted all, but the first one (black) feature self-gravity, however, as mentioned earlier, the small, if any impact of self-gravity on simulations with $M_{\text{shell}} = 0.01M_{\text{sink}}$ renders them almost identical. While the changes r_{circ} are debatable with respect to their accuracy, they are clearly in line with the absorption rate, which is notably increased and reaches over 90% of total fraction of particles. Recalling Section 3.4.5 that points out that

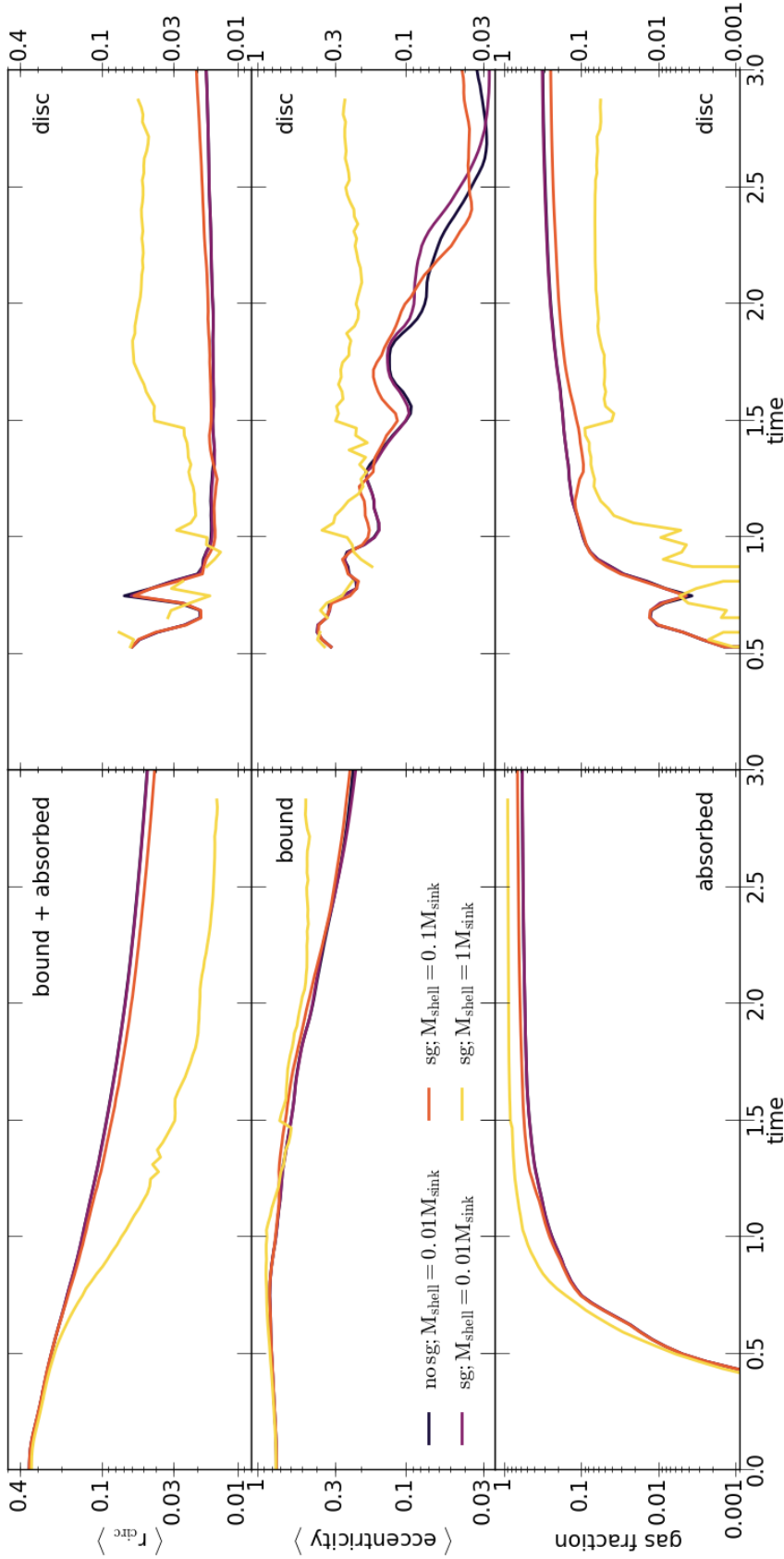


FIGURE 5.8: Time evolution of the average circularisation radius and eccentricity as well as the gas fraction for different portions of the gas and for differing M_{shell} with self gravity (besides the black line, however, it is almost identical to its self-gravity counterpart) for the same Seed B and $\chi 0.75$. ‘Absorbed’ refers to simulated gas that at some point prior to t has reached $r < r_{\text{sink}} = 0.01$ and was absorbed into the central sink particle; ‘bound’ refers to all remaining gas that at the given time has $e < 1$, ‘disc’ represents all bound gas at $e \leq 0.5$ and $r_{\text{circ}} \leq 0.3$ indicated by a thin dotted rectangle in Figure 3.1 (which may also contain a small fraction of impacting filaments). The text details the limitation arising from the self-gravity with respect to the r_{circ} and e .

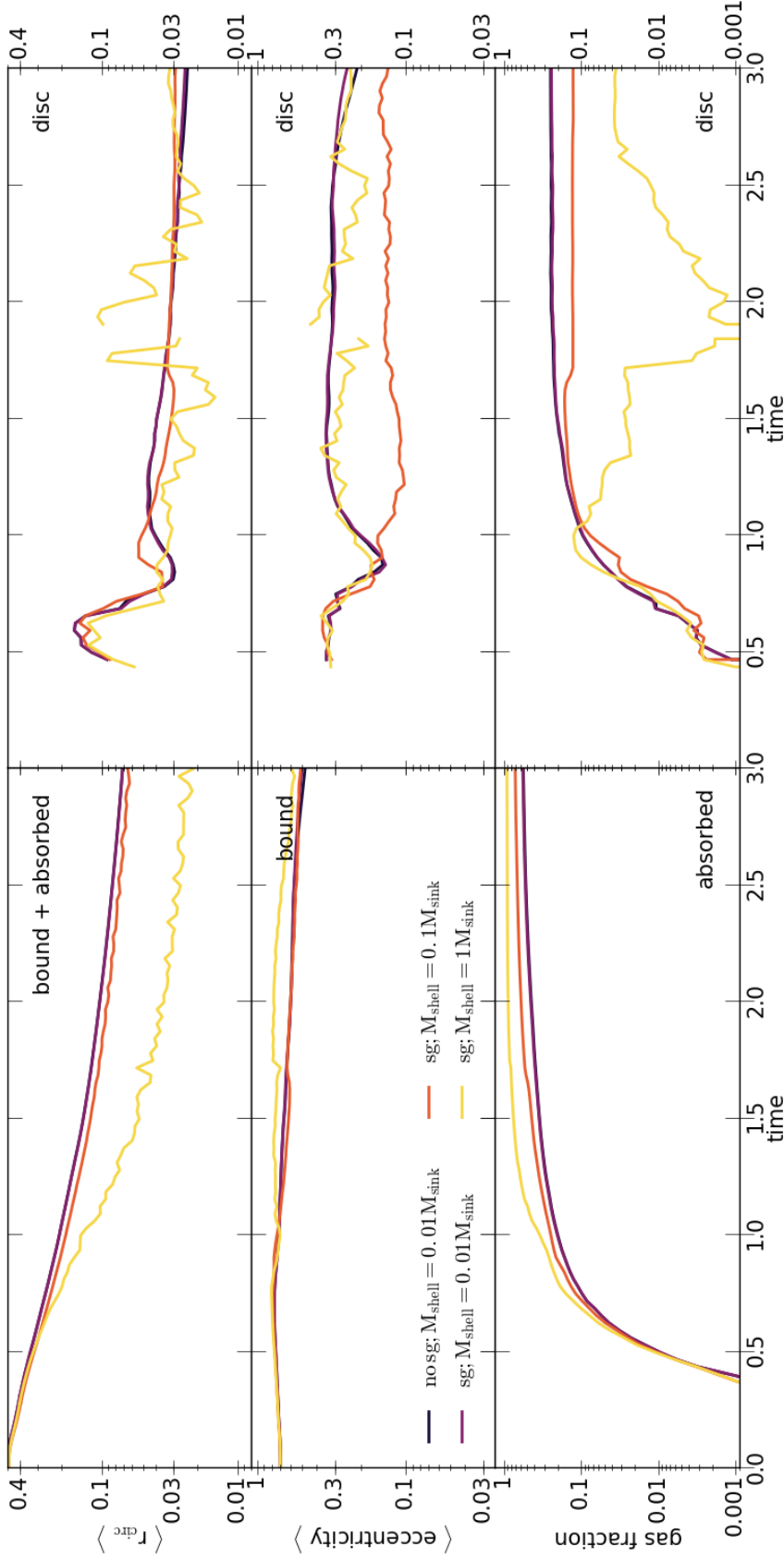


FIGURE 5.9: Time evolution of the average circularisation radius and eccentricity as well as the gas fraction for different portions of the gas and for differing M_{shell} with self gravity (besides the black line, however, it is almost identical to its self-gravity counterpart) for the same Seed B and $\chi = 1$. ‘Absorbed’ refers to simulated gas that at some point prior to t has reached $r < r_{\text{sink}} = 0.01$ and was absorbed into the central sink particle; ‘bound’ refers to all remaining gas that at the given time has $e < 1$, ‘disc’ represents all bound gas at $e \leq 0.5$ and $r_{\text{circ}} \leq 0.3$ indicated by a thin dotted rectangle in Figure 3.1 (which may also contain a small fraction of impacting filaments). The text details the limitation arising from the self-gravity with respect to the r_{circ} and e .

the movement of the sink particle caused by the more massive gas particles increases the absorption rate as well, I can confirm that these absorption rates are only marginally smaller when I artificially pin the sink particle to its coordinate origin.

Finally I present Figure 5.10 that shows the distribution of r_{circ} at the moment of absorption by the sink particle over time. Compared to the same style figures in Section 5.3, the spread of r_{circ} is larger and persists over a longer period of time. This strongly indicates that the affect of self-gravity when massive clumps form is twofold: Firstly, the clumps are capable of disturbing the disc significantly - sometimes to a degree, where no disc forms for a prolonged period of time. This allows the continued infall of potentially low angular momentum particles that would otherwise be blocked by a disc (see Section 5.3). Secondly, the interactions of the clumps itself likely causes further collisions and therefore (partial) angular momentum cancellation.

5.5 Discussion and conclusion

I have analysed the set of simulations presented in Chapter 3 to determine the impact a disc has on the rate of absorption and the spread of r_{circ} of the absorbed particles. By analysing the fraction of particles that belong to the previously defined disc region ($r_{\text{circ}} < 0.3$ and $e < 0.5$), I note which simulation encounters dips caused by major disruptions or even disappeared completely below a defined threshold of particles indicating a disc destruction. I confirm and refine these findings by comparing them both to density plots and plots showing r_{circ} over time for the absorbed particles. The latter clearly shows an increased rate of absorption in the event of disc impacts, but also a large spread of r_{circ} in short time periods. This further confirms a suggestion made in Chapter 3 that a sufficiently massive and large disc is able to resist infall and may even block low angular momentum material that would have otherwise circularised at sometimes significantly lower orbits.

However, these results should be seen as preliminary, because major disruptions of the disc tend to happen before the majority of the gas has reached the central volume. Hence the source of these disruptions may be infalling streams of comparable or larger size than that of the disc making this scenario only a temporally viable option before enough material has formed a large disc. Geometry and

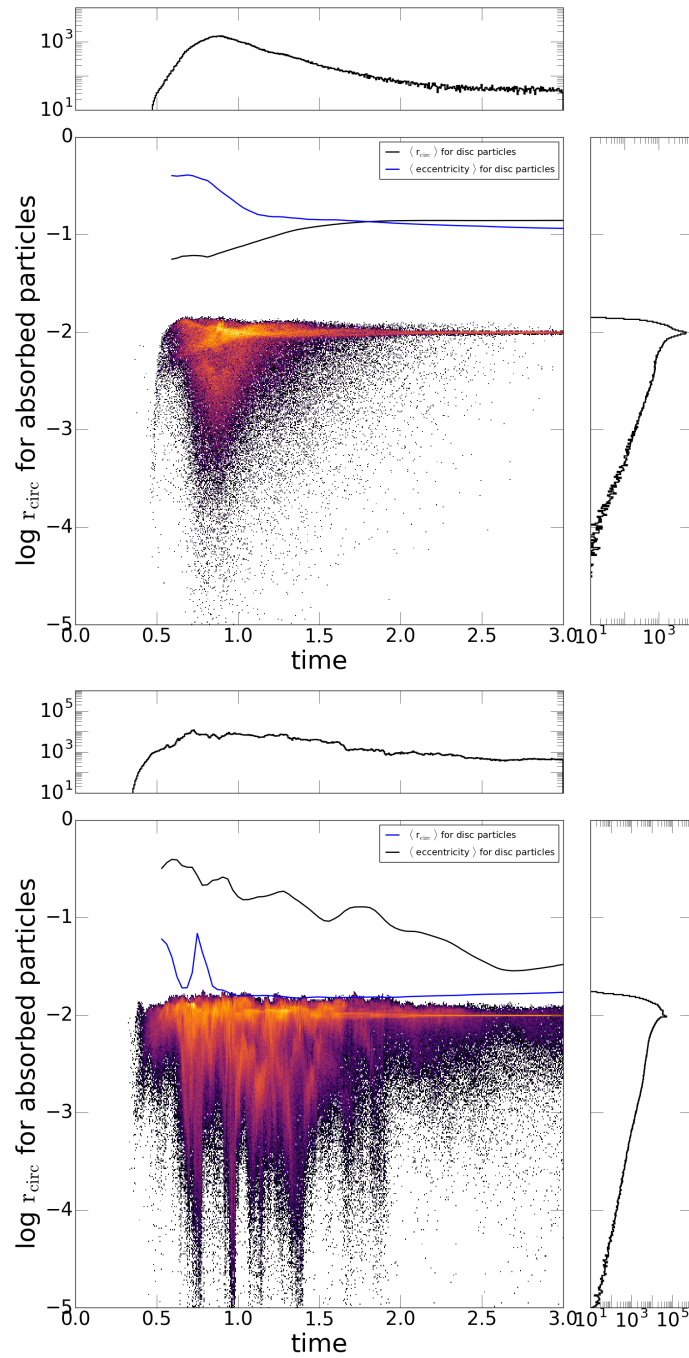


FIGURE 5.10: Distribution of r_{circ} over time for the absorbed particles. The plot shows a simulation with $\chi = 1$, $M_{\text{shell}} = 1M_{\text{sink}}$ for Seed B. The blue line shows the average r_{circ} of the disc, while the black indicates the corresponding eccentricity. The self-gravitating clumps disrupt the disc constantly allowing gaseous matter to fall in with a large spread in r_{circ} .

angular momentum of the infall relative to the disc will play at least some role as well and one may attempt to test this by placing a disc with varying properties (e.g. angular momentum orientation) inside the above described simulations. However, I argue that the nature of the chaotic infall may still prove it difficult to determine clear results especially for a wider ranges of seeds. Therefore it might be more efficient to simulate the infall of one stream and vary e.g. its position and impact angle instead. I also note that the output frequency of my simulations might not be high enough to observe every disruption to the disc. Additionally the way I define a disc may be insufficient as it may contain infalling streams that are in the process of circularising. Finally, a disc may not disappear, if we would reduce the inner boundary radius, however, Chapter 4 showed that the net effect is still a larger reduction of angular momentum. In a recent paper featuring a similar principal setup like the one here presented, the authors conclude the importance of disc instabilities (in this case triggered by impacting clouds) for the black hole growth as well and suggest it might be the reason for the episodic nature of the accretion process (Beckmann, Devriendt, and Slyz, 2019).

Nevertheless, the idea that a disrupted disc may be beneficial to the transport of gas to small scales, is appealing. As described in the introduction, our own galaxy may provide a physically motivated case to investigate this. My simulation provide a convenient, if unintentional representation of the sphere of influence radius (outer edge of the Gaussian distributed shell) down to the self-gravity radius (coinciding with the inner boundary radius).

I ran several simulations with self-gravity for the gas particles turned on. In this case, we limit the Jeans mass (such that it is always resolved) by limiting the gas softening lengths to $\epsilon \geq 10^{-3}$ (while otherwise ϵ_i is proportional to the SPH smoothing length). We experimented with self-gravity for the default gas mass $M_{\text{shell}}/M_{\bullet} = 0.01$, but also for the larger values of 0.1 and 1 and vary χ between 0.75 and 1.

The inclusion of the gas self-gravity has little effect on the gas inflow in the early phases of the simulations prior to $t \sim t_{\text{ff}}$, in particular the re-distribution of angular momenta (as reflected in the distribution of r_{circ}) and absorption onto the sink particle. However, as soon as the majority of the gas reaches the central volume of the simulation the formation of dense clumps within the gas discs starts. This is where the gas is densest and most prone to the Jeans instability (see Figure 5.6, bottom left). In particular, in simulations with $M_{\text{shell}} = M_{\bullet}$ a multitude

of such clumps form, which may be surrounded by their own mini-disc and render the smooth disc seen without self-gravity into a rather messy arrangement. For $M_{\text{shell}}/M_{\bullet} = 0.1$, the effect is much milder and virtually absent at the reference value $M_{\text{shell}}/M_{\bullet} = 0.01$. Plots detailing r_{circ} over time for absorbed particles indicate, that if self-gravity can form dense clumps these can disrupt the disc significantly up to a degree where no stable disc may exist for extended periods of time contrary to the simulations without self-gravity. This allows streams to deposit low angular momentum material directly without being blocked by a disc. Furthermore it is likely that the interactions of the clumps with the disc and infalling streams cause more collisions and hence reduce the average r_{circ} of the gas even further.

While the $M_{\text{shell}} = M_{\bullet}$ simulation show that $\gtrsim 90\%$ of the total gas mass are absorbed in line with suggestions by Zubovas and Nayakshin, 2012, the mass is more than a magnitude larger than the suggested one. However, these simulations are not in particular set up to simulate such an event and therefore these results should be taken as preliminary. Further work should assess more quantitatively the effect of the disruption caused by self-gravity by utilising more seeds and establish a more reliable measurement tool to determine the evolution of angular momentum of the gas even in the presence of self-gravitating disc. The realism of the simulations may be further improved by using for example a density dependent cooling function instead of an isothermal equation of state and implement the ability of the code to convert high density regions into a sink particle, which both will save CPU time and avoid setting a rigid gravitational softening length.

Chapter 6

Conclusions

6.1 Feeding of SMBHs via collisional cascades

At the very heart of this thesis is the question whether chaotic infall is capable of allowing gas to bridge the large gap of about four magnitudes to become relevant for the feeding of the SMBH. The scale difference stems from the fact that the viscous accretion time scale is only short enough to be effective in a typical AGN phase (Schawinski et al., 2015; King and Nixon, 2015) for accretion disc radii of order 10^{-3} pc and smaller (e.g. King and Pringle, 2006; King, Pringle, and Hofmann, 2008), while its gas reservoir must be massive enough to grow the black hole up to $10^8 M_{\odot}$ and more. Therefore the gaseous food source likely occupies a much larger volume (at least of order of the sphere of influence radius, e.g. ~ 10 pc for a $10^8 M_{\odot}$ SMBH). Wide-angle outflows, a consequence of SMBHs accreting close to their Eddington limit (e.g. King and Pounds, 2003; Zubovas, 2018), interact with the surrounding ISM and are thought to drive the scaling relations between SMBHs and their host galaxy (e.g. King, 2005; King and Pounds, 2015). However, if the above mentioned AGN phase is about 10^5 yr than the SMBH must grow in many individual feeding events. Consequently the outflows cannot drive out the gas immediately, but rather must stall after they swept up some of the ISM.

This is the starting point of the argument presented by Dehnen and King, 2013: The impact of the feedback shock wave increases the gravitational energy of the shocked material shifting the peri-centre to smaller radii and may cancel out some angular momentum as the material is swept up and condensed. When the outflow subsides, the non-uniform shell will infall and form streams. As the peri-centre of the gas is closer to the SMBH and therefore describes a smaller

volume, chances for collisions are increased, which leads to (partial) cancellation of angular momentum.

My simulations presented in this thesis do not model the feedback, but instead start right after it subsides. By imposing varying fractions of a turbulent velocity field, I ensure that the initially uniform shell forms quickly over- and under-densities in line with observations of for example giant molecular gas clouds (e.g. Larson, 1981; Sun et al., 2018). Furthermore this leads to some degree of randomisation of the velocity field resulting in a chaotic infall event. Consequently streams form that will interact with each other and the disc, which is created due to circularising gaseous infall.

As suggested by Dehnen and King (2013), the streams form a near-toroidal dynamical gas structure and cause the disc to change its orientation randomly, if no strong preferentially aligned infall is persisting. Additionally, a significant fraction of the gas crosses the inner boundary radius, which may feed the SMBH. This was of particular focus in Chapter 4, where I analysed the consequences of the purely numerically motivated inner boundary (sink particle). At the cost of significantly increased computation time, I was able to show that a reduction of sink radius affects the innermost processes significantly. In fact I found that in the presence of eccentric orbits, the simulation cannot be trusted about a factor of 4 times the radius of the inner boundary. However, the reduction of the sink radius also allowed the tracing of infalling particles further in. While the disc will reach down to smaller radii as well, it was shown that average r_{circ} was reduced beyond the values given by the references simulations. Ultimately I used these changes to extrapolate the efficiency down to radii relevant for viscous accretion and found that at least about 10% of the gas undergoing these collisional cascade reaches $r_{\text{circ}} = 10^{-4}r_{\text{shell}}$. At this point I further note tentative evidence I found that even if there is some common orientation of the angular momentum of the gas, the collisional cascades of the infalling gas streams may be able to obscure evidence of an original orientation and therefore such infall may always lead to chaotic accretion.

While it is not clear how far down the collisional cascades may continue as in principal less and less material reaches lower radii, the Lense-Thirring effect may start to become important, if the spin of the SMBH is misaligned with the accretion disc - a likely consequence of chaotic infall driven by collisional cascades.

Nixon et al., 2012 suggest about 70% of the accretion events are sufficiently misaligned to cause precession of parts of disc leading to counter-rotating gas flow that are naturally very effective at cancelling out angular momentum and potentially causing radial infall. Recent detections of an ultrafast inflow in a luminous Seyfert galaxy provide further support to this idea and can be interpreted as the first direct observed evidence of chaotic accretion (Pounds et al., 2018).

Alternatively to the feedback driven inflow triggering mechanism discussed in Chapter 3, cooling and subsequent condensation of initially pressure supported gas can lead to turbulent infall (Gaspari, Ruszkowski, and Oh, 2013). Positive feedback, where the SMBH outflow enhances the star formation rate instead of quenching it, results in instabilities that can lead to such turbulent infall as well (Nayakshin and Zubovas, 2012). In the context of simulating the formation channels of the O-type stars warped disc in the centre of the Milky Way (see Section 5.1) prolate clouds and clouds impacting the circum-nuclear ring/disc have been suggested and produce conditions similar to those investigated in the simulations. The CNR itself is thought to be on the verge of star formation (e.g. Liu et al., 2013) and those destabilised regions appear to be connected to the "mini-spirals" (e.g. Tsuboi et al., 2017), which are infalling gas streams strikingly similar in appearance to those in my simulations. Therefore they may offer another alternative to the feedback model as a molecular torus is observed in other galaxies suggesting it may be a common feature (e.g. Krolik and Begelman, 1988). However, some authors argue that the formation of the CNR itself might be caused by a feedback event (Zubovas and Nayakshin, 2012). In fact the outflowing material in the feedback event itself may condensate from the warm accretion disc wind, which could form the observed broad emission line clouds and will be too dense to be accelerated above the escape velocity (Elvis, 2017). Therefore the clouds, if they survive long enough or perhaps some part of the cloud formation coincides with the end of the feedback event, will subsequently fall back towards the SMBH, where the gravitational pull stretches them into streams that may intersect and cancel angular momentum similar to the cases discussed in this thesis.

Overall I find the results to be robust across the tested physical parameter variations despite sometimes significant changes in the details particularly caused by the seed of the turbulent component of the initial velocity field. The largest impact has the fraction of rotational support in comparison to the turbulent velocities - a result that is in line with work by Hobbs et al. (2011), who further

found that dense material is capable of resisting to mix with the ISM and therefore can reach smaller radii in form of "ballistic accretion" directly. More recently authors utilising a completely different numerical setup (RAMSES, an adaptive mesh refinement code), different thermodynamics (e.g. a tabulated cooling function) and other differences to my astrophysical setup (e.g. star formation), found similar results to the ones presented in Chapter 3 and 4. Especially noteworthy is their highlighting of the importance of resolution since in the case of not resolved infalling streams, they will be relatively less efficient at cancelling angular momentum. Furthermore they underline the importance of the disc and its impact on the growth history of the SMBH (Beckmann, Devriendt, and Slyz, 2019). A range of 1D simulations further supports the overall

6.2 Comparison to the Centre of Milky Way

In Chapter 5 I described preliminary results that indicate that major disruptions or even the destruction of a disc causes an increased accretion rate, but more importantly allows streams containing low angular momentum material to fall in directly and hence potentially reach their corresponding circularisation radius. Simulations that feature a large, stable disc early on provide evidence that they can effectively block and absorb such gas with little impact on the disc. By adding self-gravity to the simulation and increasing the mass of the gas shell, I find that in the presence of dense, self-gravitating clumps a disc will be significantly affected. Additionally, the interactions of the clumps with the surrounding gas both in streams and the disc caused further cancellation of angular momentum. Overall these simulation show that over 90% of the total amount of gas can reach the inner boundary radius representing a significant increase compared to the simulation without self-gravity.

Following the argument detailed by Zubovas and Nayakshin (2012), an event triggers gaseous infall by for example a gas cloud interacting with the circumnuclear ring. Some of the infall will circularise above the self-gravity radius, where the disc will fragment and form the observed O-star population. The fragmentation may disrupt the disc sufficiently enough, which would explain the lack of an observable thick disc, and allow most of the infalling gas to continue its path to lower scales. Ongoing collisional cascades are able to keep cancelling angular momentum and therefore feeding the SMBH, which in turn causes a wide-angle

outflow event that formed the Fermi bubble. While at this stage this line of reasoning is rather speculative, the potential of the self-gravitating clumps to cause havoc in a disc is intriguing enough to warrant further investigation.

6.3 Future work

Both in Chapter 3 and 4 I alluded to the various shortcomings of the simulations presented here. In particular the simple treatment of the thermodynamics, the lack of self-gravity (except for Chapter 5) and the issue of the inner boundary radius and the associated resolution problems suggest themselves as potential focal points of further studies. While I would argue that the discussed model setup describes a well posed problem (see for example recent work by Zubovas and King (2019)) and allows both quantitative and qualitative assessments, the most significant modifications to the result may stem from increasing the scale of the simulation. However, as shown in Chapter 4 this may require a significant amount of computational resources in order to resolve the inner structure sufficiently, and consequently may be beyond the current capabilities of supercomputers. Therefore I suggest that the implementation of a cooling function is the more practical step forward on testing chaotic infall for the described scenario. While I investigated temperature changes in Section 3.4.1 and found them to only have a marginal impact on the level of angular momentum cancellation given the here utilised isothermal equation of state, the use of a cooling function would allow a better representation of the shocking material when for example two streams intersect. As these interactions are one of the main sources for the sought after shrinking of the average circularisation radius of the gas, a more accurate modelling away from an isothermal equation of state may yield further insight.

In Section 3.4.5 I have noted that the movement of the sink particle (typically suppressed by ensuring that the total mass of the gas is a hundredth of the mass of the SMBH) can enhance the accretion rate especially if self-gravity of the gas is considered as well. Recently it was suggested that a frequent discrepancy between the location of the torus and the AGN implied that the SMBH indeed is able to wander of up to the order of 10 pc around the centre of its galaxy (Combes et al., 2019). Such an investigation should feature a more accurate modelling of the

background potential including the stellar cusp and more observationally motivated choice of the ratio of mass between the mass of the SMBH and the total mass of the simulated infalling gas.

As described in Section 3.6, the infall produces as a near-toroidal dynamical gas structure. It might be worth comparing the level of obscuration of the central region from different point of views (e.g. different angles based on the alignment of the angular momentum vector of the initial particle distribution) both time-dependent and seed-dependent. While careful arguments have to be made about the density and uniformity of the initial infalling gas, the results may yield insights how chaotic infall can be linked to the unification attempts of the different AGN types (see Section 1.2.2).

Similarly an analysis of the orbits of the infalling gas for different seeds and ratios of rotational to turbulent contributions will provide insights how the eccentricity of these typically non-Keplerian orbits are distributed and how it evolves throughout the time span simulated in this work. This could help to test and potentially refine models that consider eccentric orbits instead of the widely used assumption of circular orbits for estimations of the mass of a SMBH by observing the gas dynamics of the central part of a low redshift galaxy (see Section 1.2.2). Estimating the mass instead based on the central stellar dynamics, a systematic difference of the mass estimate is found for large early type galaxies (e.g. Gebhardt et al., 2011). Recently it was shown that moving away from the simplified assumption of the gas being on Keplerian orbits (both in line with observations of the centre of the Milky Way and what I observe in the here presented simulations, see Section 3.1 and 3.6), the discrepancy can be explained allowing more precise SMBH mass estimates (Jeter, Broderick, and McNamara, 2018, unpublished at the time of writing this). Those non-Keplerian models provide velocity curves akin to the more commonly used circular models at the very centre, while resulting in up to twice the mass for the central SMBH.

The sink radius (extensive discussion in Chapter 4) arising from the numerically motivated need to avoid calculation of particle movement far beyond the resolution limit is a natural place for further work related to the in this thesis presented results. However, I pointed out that even if one limits themselves to only calculate the particles whose trajectories should allow them to leave the numerical boundary, the slowdown would be the same as in principal this would be equivalent to reducing the sink radius. Instead the orbit of such particles might

be calculated and the position and velocity vector shifted accordingly to when the particle would appear outside of the numerical boundary again. Clearly, this assumes that no interaction inside the sink radius happened, while the particle would be available again for interaction with gas streams outside the boundary. Careful testing with simulation suites (see Section 3.3.2) should provide insight whether such a procedure would lead to an over- (the interactions of the gas particles inside the boundary are more important) or underestimate (the interaction with the otherwise removed particles with infalling streams are more important) of the amount of cancelled angular momentum. If the latter is the case, this may allow to improve the accuracy of simulations without the otherwise associated large computational costs of reducing the sink radius. While such an reintroduction of particles to the simulation will play havoc with the kernel estimations in this region and requires testing, I would argue that the error should be comparable to the one caused by parts of a group of infalling particles being accreted by the sink particle in different timesteps. This leads to a noticeable impact on the reported eccentricities, but not for the here particular relevant circularisation radius and hence may play a negligible role overall.

Improving and expanding the analysis of the disc dynamics will yield a better understanding of when and how a disc (or lack thereof) influences subsequent gaseous infall. Especially being able to distinguish between gas particles belonging to the disc and to the infalling streams will be helpful as the so far used method based solely on an eccentricity and circularisation threshold is not precise enough for a focus on the disc. Furthermore, the frequency of how often the data is written out needs to be drastically increased to capture properly the interactions with the streams -specifically when the mass of the disc is low compared to the infalling stream. A more detailed look at the disc dynamics may also reveal counter-rotating discs, that are suggested to enhance the accretion rate noticeably (Nixon, King, and Price, 2012). The inclusion of self-gravity for the gas particles adds another important dimension to how a disc influences the infall rate of gas towards a SMBH. This requires a complete rethink of how to assess the effectiveness of a simulation with respect to the cancellation of angular momentum given that an individual gas particle will be dominated by a local gas clump instead of the SMBH. The importance of the connection between chaotic accretion and a self-gravitating disc was recently highlighted by Bustamante and Springel (2019), whose paper is unpublished at the time of writing this. The paper stresses as well

the importance of the consideration of the spin of the SMBH for its growth and resulting feedback.

Finally, a more targeted approach to the scenario presented itself in the central region of the Milky Way will likely yield further insights, if the disc disruptions holds up to more physically motivated initial conditions and setup (e.g. including a density dependent cooling function or sink particle conversion of dense clumps). This may take the form of simulating the collision of a gas cloud with an already existing disc representing the CND.

Bibliography

- Abbott, B. P. et al. (2016). “Astrophysical Implications of the Binary Black-hole Merger GW150914”. In: *ApJL* 818, L22, p. L22. DOI: [10.3847/2041-8205/818/2/L22](https://doi.org/10.3847/2041-8205/818/2/L22). arXiv: [1602.03846](https://arxiv.org/abs/1602.03846) [astro-ph.HE].
- Alexander, R. D. et al. (2012). “Galactic Centre star formation: the case of the missing gas disc”. In: *MNRAS* 419, pp. 1970–1976. DOI: [10.1111/j.1365-2966.2011.19849.x](https://doi.org/10.1111/j.1365-2966.2011.19849.x). arXiv: [1109.4148](https://arxiv.org/abs/1109.4148) [astro-ph.GA].
- Alexander, T. (2017). “Stellar Dynamics and Stellar Phenomena Near a Massive Black Hole”. In: *ARA&A* 55, pp. 17–57. DOI: [10.1146/annurev-astro-091916-055306](https://doi.org/10.1146/annurev-astro-091916-055306). arXiv: [1701.04762](https://arxiv.org/abs/1701.04762).
- Alig, C. et al. (2011). “Simulations of direct collisions of gas clouds with the central black hole”. In: *MNRAS* 412, pp. 469–486. DOI: [10.1111/j.1365-2966.2010.17915.x](https://doi.org/10.1111/j.1365-2966.2010.17915.x). arXiv: [0908.1100](https://arxiv.org/abs/0908.1100) [astro-ph.GA].
- Alig, C. et al. (2013). “Numerical Simulations of the Possible Origin of the Two Sub-parsec Scale and Counterrotating Stellar Disks around SgrA*”. In: *ApJ* 771, 119, p. 119. DOI: [10.1088/0004-637X/771/2/119](https://doi.org/10.1088/0004-637X/771/2/119). arXiv: [1305.2953](https://arxiv.org/abs/1305.2953) [astro-ph.GA].
- Allen, L. R. et al. (1962). “Observations of 384 radio sources at a frequency of 158 Mc/s with a long baseline interferometer”. In: *MNRAS* 124, p. 477. DOI: [10.1093/mnras/124.6.477](https://doi.org/10.1093/mnras/124.6.477).
- Aly, H. et al. (2015). “Misaligned gas discs around eccentric black hole binaries and implications for the final-parsec problem”. In: *MNRAS* 449, pp. 65–76. DOI: [10.1093/mnras/stv128](https://doi.org/10.1093/mnras/stv128). arXiv: [1501.04623](https://arxiv.org/abs/1501.04623) [astro-ph.HE].
- Anderson, K. S. and R. P. Kraft (1969). “Evidence for the Ejection of Matter from the Nucleus of the Seyfert Galaxy NGC 4151”. In: *ApJ* 158, p. 859. DOI: [10.1086/150246](https://doi.org/10.1086/150246).
- Angulo, R. E. et al. (2012). “Scaling relations for galaxy clusters in the Millennium-XXL simulation”. In: *MNRAS* 426, pp. 2046–2062. DOI: [10.1111/j.1365-2966.2012.21830.x](https://doi.org/10.1111/j.1365-2966.2012.21830.x). arXiv: [1203.3216](https://arxiv.org/abs/1203.3216).

- Antonucci, R. (1993). "Unified models for active galactic nuclei and quasars". In: *ARA&A* 31, pp. 473–521. DOI: [10.1146/annurev.aa.31.090193.002353](https://doi.org/10.1146/annurev.aa.31.090193.002353).
- Armitage, P. J. and B. M. S. Hansen (1999). "Early planet formation as a trigger for further planet formation". In: *NATURE* 402, pp. 633–635. DOI: [10.1038/45179](https://doi.org/10.1038/45179). eprint: [astro-ph/9912147](https://arxiv.org/abs/astro-ph/9912147).
- Baade, W. and R. Minkowski (1954). "Identification of the Radio Sources in Cassiopeia, Cygnus A, and Puppis A." In: *ApJ* 119, p. 206. DOI: [10.1086/145812](https://doi.org/10.1086/145812).
- Bahcall, J. N., S. Kirhakos, and D. P. Schneider (1994). "HST images of nearby luminous quasars". In: *ApJL* 435, pp. L11–L14. DOI: [10.1086/187582](https://doi.org/10.1086/187582). eprint: [astro-ph/9409028](https://arxiv.org/abs/astro-ph/9409028).
- Balbus, S. A. and J. F. Hawley (1991). "A powerful local shear instability in weakly magnetized disks. I - Linear analysis. II - Nonlinear evolution". In: *ApJ* 376, pp. 214–233. DOI: [10.1086/170270](https://doi.org/10.1086/170270).
- Baldry, I. K., K. Glazebrook, and S. P. Driver (2008). "On the galaxy stellar mass function, the mass-metallicity relation and the implied baryonic mass function". In: *MNRAS* 388, pp. 945–959. DOI: [10.1111/j.1365-2966.2008.13348.x](https://doi.org/10.1111/j.1365-2966.2008.13348.x). arXiv: [0804.2892](https://arxiv.org/abs/0804.2892).
- Baldry, I. K. et al. (2012). "Galaxy And Mass Assembly (GAMA): the galaxy stellar mass function at $z = 0.06$ ". In: *MNRAS* 421, pp. 621–634. DOI: [10.1111/j.1365-2966.2012.20340.x](https://doi.org/10.1111/j.1365-2966.2012.20340.x). arXiv: [1111.5707](https://arxiv.org/abs/1111.5707).
- Balick, B. and R. L. Brown (1974). "Intense sub-arcsecond structure in the galactic center". In: *ApJ* 194, pp. 265–270. DOI: [10.1086/153242](https://doi.org/10.1086/153242).
- Bar-Or, Ben and Jean-Baptiste Fouvy (2018). "Scalar Resonant Relaxation of Stars around a Massive Black Hole". In: *ApJ* 860, L23, p. L23. DOI: [10.3847/2041-8213/aac88e](https://doi.org/10.3847/2041-8213/aac88e).
- Bardeen, J. M. (1970). "Kerr Metric Black Holes". In: *NATURE* 226, pp. 64–65. DOI: [10.1038/226064a0](https://doi.org/10.1038/226064a0).
- Bardeen, J. M. and J. A. Petterson (1975). "The Lense-Thirring Effect and Accretion Disks around Kerr Black Holes". In: *ApJL* 195, p. L65. DOI: [10.1086/181711](https://doi.org/10.1086/181711).
- Bardeen, J. M., W. H. Press, and S. A. Teukolsky (1972). "Rotating Black Holes: Locally Nonrotating Frames, Energy Extraction, and Scalar Synchrotron Radiation". In: *ApJ* 178, pp. 347–370. DOI: [10.1086/151796](https://doi.org/10.1086/151796).
- Barnes, J. E. and L. E. Hernquist (1991). "Fueling starburst galaxies with gas-rich mergers". In: *ApJL* 370, pp. L65–L68. DOI: [10.1086/185978](https://doi.org/10.1086/185978).

- Barnes, Josh and Piet Hut (1986). “A hierarchical $O(N \log N)$ force-calculation algorithm”. In: *NATURE* 324, pp. 446–449. DOI: [10.1038/324446a0](https://doi.org/10.1038/324446a0).
- Baron, D. et al. (2018). “Direct evidence of AGN feedback: a post-starburst galaxy stripped of its gas by AGN-driven winds”. In: *MNRAS* 480, pp. 3993–4016. DOI: [10.1093/mnras/sty2113](https://doi.org/10.1093/mnras/sty2113). arXiv: [1804.03150](https://arxiv.org/abs/1804.03150).
- Barrow, K. S. S., A. Aykotalp, and J. H. Wise (2018). “Observational signatures of massive black hole formation in the early universe”. In: *ArXiv e-prints*. arXiv: [1809.03526](https://arxiv.org/abs/1809.03526).
- Barthel, P. D. (1989). “Is every quasar beamed?” In: *ApJ* 336, pp. 606–611. DOI: [10.1086/167038](https://doi.org/10.1086/167038).
- Bartko, H. et al. (2009). “Evidence for Warped Disks of Young Stars in the Galactic Center”. In: *ApJ* 697, pp. 1741–1763. DOI: [10.1088/0004-637X/697/2/1741](https://doi.org/10.1088/0004-637X/697/2/1741). arXiv: [0811.3903](https://arxiv.org/abs/0811.3903) [astro-ph].
- Bate, M. R. and A. Burkert (1997). “Resolution requirements for smoothed particle hydrodynamics calculations with self-gravity”. In: *MNRAS* 288, pp. 1060–1072. DOI: [10.1093/mnras/288.4.1060](https://doi.org/10.1093/mnras/288.4.1060).
- Bate, N. F. et al. (2008). “A microlensing study of the accretion disc in the quasar MG 0414+0534”. In: *MNRAS* 391, pp. 1955–1960. DOI: [10.1111/j.1365-2966.2008.14020.x](https://doi.org/10.1111/j.1365-2966.2008.14020.x). arXiv: [0810.1092](https://arxiv.org/abs/0810.1092).
- Beckmann, R. S., J. Devriendt, and A. Slyz (2019). “Zooming in on supermassive black holes: how resolving their gas cloud host renders their accretion episodic”. In: *MNRAS* 483, pp. 3488–3509. DOI: [10.1093/mnras/sty2890](https://doi.org/10.1093/mnras/sty2890). arXiv: [1810.01649](https://arxiv.org/abs/1810.01649).
- Beckmann, R. S., A. Slyz, and J. Devriendt (2018). “Bondi or not Bondi: the impact of resolution on accretion and drag force modelling for supermassive black holes”. In: *MNRAS* 478, pp. 995–1016. DOI: [10.1093/mnras/sty931](https://doi.org/10.1093/mnras/sty931). arXiv: [1803.03014](https://arxiv.org/abs/1803.03014) [astro-ph.HE].
- Begelman, M. C., R. D. Blandford, and M. J. Rees (1980). “Massive black hole binaries in active galactic nuclei”. In: *NATURE* 287, pp. 307–309. DOI: [10.1038/287307a0](https://doi.org/10.1038/287307a0).
- Begelman, M. C., C. F. McKee, and G. A. Shields (1983). “Compton heated winds and coronae above accretion disks. I Dynamics”. In: *ApJ* 271, pp. 70–88. DOI: [10.1086/161178](https://doi.org/10.1086/161178).
- Begelman, M. C. and M. J. Rees (1978). “The fate of dense stellar systems”. In: *MNRAS* 185, pp. 847–860. DOI: [10.1093/mnras/185.4.847](https://doi.org/10.1093/mnras/185.4.847).

- Begelman, M. C., M. Volonteri, and M. J. Rees (2006). "Formation of supermassive black holes by direct collapse in pre-galactic haloes". In: *MNRAS* 370, pp. 289–298. DOI: [10.1111/j.1365-2966.2006.10467.x](https://doi.org/10.1111/j.1365-2966.2006.10467.x). eprint: [astro-ph/0602363](https://arxiv.org/abs/astro-ph/0602363).
- Bentz, M. C. and E. Manne-Nicholas (2018). "Black Hole - Galaxy Scaling Relationships for Active Galactic Nuclei with Reverberation Masses". In: *ArXiv e-prints*. arXiv: [1808.01329](https://arxiv.org/abs/1808.01329).
- Berti, E. and M. Volonteri (2008). "Cosmological Black Hole Spin Evolution by Mergers and Accretion". In: *ApJ* 684, pp. 822–828. DOI: [10.1086/590379](https://doi.org/10.1086/590379). arXiv: [0802.0025](https://arxiv.org/abs/0802.0025).
- Bieri, R. et al. (2016). "External pressure-triggering of star formation in a disc galaxy: a template for positive feedback". In: *MNRAS* 455, pp. 4166–4182. DOI: [10.1093/mnras/stv2551](https://doi.org/10.1093/mnras/stv2551). arXiv: [1507.00730](https://arxiv.org/abs/1507.00730).
- Bland-Hawthorn, J. et al. (2013). "Fossil Imprint of a Powerful Flare at the Galactic Center along the Magellanic Stream". In: *ApJ* 778, 58, p. 58. DOI: [10.1088/0004-637X/778/1/58](https://doi.org/10.1088/0004-637X/778/1/58). arXiv: [1309.5455](https://arxiv.org/abs/1309.5455).
- Blandford, R. D. and C. F. McKee (1982). "Reverberation mapping of the emission line regions of Seyfert galaxies and quasars". In: *ApJ* 255, pp. 419–439. DOI: [10.1086/159843](https://doi.org/10.1086/159843).
- Blandford, R. D. and D. G. Payne (1982). "Hydromagnetic flows from accretion discs and the production of radio jets". In: *MNRAS* 199, pp. 883–903. DOI: [10.1093/mnras/199.4.883](https://doi.org/10.1093/mnras/199.4.883).
- Blank, M. et al. (2016). "The inner cavity of the circumnuclear disc". In: *MNRAS* 459, pp. 1721–1736. DOI: [10.1093/mnras/stw771](https://doi.org/10.1093/mnras/stw771).
- Boehle, A. et al. (2016). "An Improved Distance and Mass Estimate for Sgr A* from a Multistar Orbit Analysis". In: *ApJ* 830, 17, p. 17. DOI: [10.3847/0004-637X/830/1/17](https://doi.org/10.3847/0004-637X/830/1/17). arXiv: [1607.05726](https://arxiv.org/abs/1607.05726).
- Bogdán, Á. and A. D. Goulding (2015). "Connecting Dark Matter Halos with the Galaxy Center and the Supermassive Black Hole". In: *ApJ* 800, 124, p. 124. DOI: [10.1088/0004-637X/800/2/124](https://doi.org/10.1088/0004-637X/800/2/124). arXiv: [1502.05043](https://arxiv.org/abs/1502.05043).
- Bolton, C. T. (1972). "Identification of Cygnus X-1 with HDE 226868". In: *NATURE* 235, pp. 271–273. DOI: [10.1038/235271b0](https://doi.org/10.1038/235271b0).
- Bond, J. R., W. D. Arnett, and B. J. Carr (1984). "The evolution and fate of Very Massive Objects". In: *ApJ* 280, pp. 825–847. DOI: [10.1086/162057](https://doi.org/10.1086/162057).
- Bondi, H. (1952). "On spherically symmetrical accretion". In: *MNRAS* 112, p. 195. DOI: [10.1093/mnras/112.2.195](https://doi.org/10.1093/mnras/112.2.195).

- Bondi, H. and F. Hoyle (1944). "On the mechanism of accretion by stars". In: *MNRAS* 104, p. 273. DOI: [10.1093/mnras/104.5.273](https://doi.org/10.1093/mnras/104.5.273).
- Bonnell, I. A. and W. K. M. Rice (2008). "Star Formation Around Supermassive Black Holes". In: *Science* 321, p. 1060. DOI: [10.1126/science.1160653](https://doi.org/10.1126/science.1160653). arXiv: [0810.2723](https://arxiv.org/abs/0810.2723) [astro-ph].
- Booth, C. M. and J. Schaye (2010). "Dark matter haloes determine the masses of supermassive black holes". In: *MNRAS* 405, pp. L1–L5. DOI: [10.1111/j.1745-3933.2010.00832.x](https://doi.org/10.1111/j.1745-3933.2010.00832.x). arXiv: [0911.0935](https://arxiv.org/abs/0911.0935).
- Bourne, M. A. and S. Nayakshin (2013). "Inverse Compton X-ray signature of AGN feedback". In: *MNRAS* 436, pp. 2346–2351. DOI: [10.1093/mnras/stt1739](https://doi.org/10.1093/mnras/stt1739). arXiv: [1306.2636](https://arxiv.org/abs/1306.2636).
- Bower, R. G. et al. (2006). "Breaking the hierarchy of galaxy formation". In: *MNRAS* 370, pp. 645–655. DOI: [10.1111/j.1365-2966.2006.10519.x](https://doi.org/10.1111/j.1365-2966.2006.10519.x). eprint: [astro-ph/0511338](https://arxiv.org/abs/astro-ph/0511338).
- Bowyer, C. S. et al. (1970). "Detection of X-Ray Emission from 3c 273 and NGC 5128". In: *ApJL* 161, p. L1. DOI: [10.1086/180559](https://doi.org/10.1086/180559).
- Boylan-Kolchin, M., C.-P. Ma, and E. Quataert (2006). "Red mergers and the assembly of massive elliptical galaxies: the fundamental plane and its projections". In: *MNRAS* 369, pp. 1081–1089. DOI: [10.1111/j.1365-2966.2006.10379.x](https://doi.org/10.1111/j.1365-2966.2006.10379.x). eprint: [astro-ph/0601400](https://arxiv.org/abs/astro-ph/0601400).
- Broderick, A. E. et al. (2016). "Modeling Seven Years of Event Horizon Telescope Observations with Radiatively Inefficient Accretion Flow Models". In: *ApJ* 820, 137, p. 137. DOI: [10.3847/0004-637X/820/2/137](https://doi.org/10.3847/0004-637X/820/2/137). arXiv: [1602.07701](https://arxiv.org/abs/1602.07701) [astro-ph.HE].
- Bromm, V. and A. Loeb (2003). "Formation of the First Supermassive Black Holes". In: *ApJ* 596, pp. 34–46. DOI: [10.1086/377529](https://doi.org/10.1086/377529). eprint: [astro-ph/0212400](https://arxiv.org/abs/astro-ph/0212400).
- Burbidge, E. M. and G. R. Burbidge (1962). "Nature of the Peculiar Galaxy NGC 5128". In: *NATURE* 194, pp. 367–368. DOI: [10.1038/194367a0](https://doi.org/10.1038/194367a0).
- Burbidge, E. M., G. R. Burbidge, and K. H. Prendergast (1963). "The Rotation and Physical Conditions in the Seyfert Galaxy NGC 7469." In: *ApJ* 137, p. 1022. DOI: [10.1086/147580](https://doi.org/10.1086/147580).
- Burbidge, E. M. et al. (1957). "Synthesis of the Elements in Stars". In: *Reviews of Modern Physics* 29, pp. 547–650. DOI: [10.1103/RevModPhys.29.547](https://doi.org/10.1103/RevModPhys.29.547).
- Burbidge, G. R. (1956). "On Synchrotron Radiation from Messier 87." In: *ApJ* 124, p. 416. DOI: [10.1086/146237](https://doi.org/10.1086/146237).

- Burbidge, G. R. (1958). “Possible Sources of Radio Emission in Clusters of Galaxies.” In: *ApJ* 128, p. 1. DOI: [10.1086/146509](https://doi.org/10.1086/146509).
- (1961). “Galactic Explosions as Sources of Radio Emission”. In: *NATURE* 190, pp. 1053–1056. DOI: [10.1038/1901053a0](https://doi.org/10.1038/1901053a0).
- Burbidge, G. R., E. M. Burbidge, and A. R. Sandage (1963). “Evidence for the Occurrence of Violent Events in the Nuclei of Galaxies”. In: *Reviews of Modern Physics* 35, pp. 947–972. DOI: [10.1103/RevModPhys.35.947](https://doi.org/10.1103/RevModPhys.35.947).
- Bustamante, S. and V. Springel (2019). “Spin evolution and feedback of supermassive black holes in cosmological simulations”. In: *arXiv e-prints*. arXiv: [1902.04651](https://arxiv.org/abs/1902.04651).
- Calderón, D. et al. (2016). “Clump formation through colliding stellar winds in the Galactic Centre”. In: *MNRAS* 455, pp. 4388–4398. DOI: [10.1093/mnras/stv2644](https://doi.org/10.1093/mnras/stv2644).
- Cameron, A. G. W. (1962). “Star Formation in Elliptical Galaxies and Intense Radio Sources”. In: *NATURE* 194, pp. 963–964. DOI: [10.1038/194963a0](https://doi.org/10.1038/194963a0).
- (1978). “Physics of the primitive solar accretion disk”. In: *Moon and Planets* 18, pp. 5–40. DOI: [10.1007/BF00896696](https://doi.org/10.1007/BF00896696).
- Chadwick, J. (1932). “Possible Existence of a Neutron”. In: *NATURE* 129, p. 312. DOI: [10.1038/129312a0](https://doi.org/10.1038/129312a0).
- Chandrasekhar, S. (1931). “The Maximum Mass of Ideal White Dwarfs”. In: *ApJ* 74, p. 81. DOI: [10.1086/143324](https://doi.org/10.1086/143324).
- Chen, Y. et al. (2015). “Jet/accretion and unification for FSRQs/FRII and BL Lac objects/FRI radio galaxies”. In: *APSS* 357, 100, p. 100. DOI: [10.1007/s10509-015-2303-x](https://doi.org/10.1007/s10509-015-2303-x). arXiv: [1504.05638](https://arxiv.org/abs/1504.05638) [astro-ph.HE].
- Cho, A. (2018). “A weight limit emerges for neutron stars”. In: *Science* 359, pp. 724–725. DOI: [10.1126/science.359.6377.724](https://doi.org/10.1126/science.359.6377.724).
- Cicone, C. et al. (2014). “Massive molecular outflows and evidence for AGN feedback from CO observations”. In: *A&A* 562, A21, A21. DOI: [10.1051/0004-6361/201322464](https://doi.org/10.1051/0004-6361/201322464). arXiv: [1311.2595](https://arxiv.org/abs/1311.2595).
- Clauwens, B. et al. (2018). “The three phases of galaxy formation”. In: *MNRAS* 478, pp. 3994–4009. DOI: [10.1093/mnras/sty1229](https://doi.org/10.1093/mnras/sty1229). arXiv: [1711.00030](https://arxiv.org/abs/1711.00030).
- Clowes, R. G. et al. (1979). “Two optically selected QSOs with very broad-lined absorption systems”. In: *MNRAS* 189, pp. 175–182. DOI: [10.1093/mnras/189.2.175](https://doi.org/10.1093/mnras/189.2.175).

- Cohen, B. (1940). "Roemer and the First Determination of the Velocity of Light (1676)". In: *Isis* 31.2, pp. 327–379. DOI: [10.1086/347594](https://doi.org/10.1086/347594). eprint: <https://doi.org/10.1086/347594>. URL: <https://doi.org/10.1086/347594>.
- Cole, Shaun et al. (2000). "Hierarchical galaxy formation". In: *Monthly Notices of the Royal Astronomical Society* 319.1, pp. 168–204. DOI: [10.1046/j.1365-8711.2000.03879.x](https://doi.org/10.1046/j.1365-8711.2000.03879.x). eprint: [/oup/backfile/content_public/journal/mnras/319/1/10.1046/j.1365-8711.2000.03879.x/2/319-1-168.pdf](http://oup/backfile/content_public/journal/mnras/319/1/10.1046/j.1365-8711.2000.03879.x/2/319-1-168.pdf). URL: <http://dx.doi.org/10.1046/j.1365-8711.2000.03879.x>.
- Combes, F. et al. (2019). "ALMA observations of molecular tori around massive black holes". In: *A&A* 623, A79, A79. DOI: [10.1051/0004-6361/201834560](https://doi.org/10.1051/0004-6361/201834560). arXiv: [1811.00984](https://arxiv.org/abs/1811.00984).
- Contopoulos, J. and R. V. E. Lovelace (1994). "Magnetically driven jets and winds: Exact solutions". In: *ApJ* 429, pp. 139–152. DOI: [10.1086/174307](https://doi.org/10.1086/174307).
- Cossins, Peter, Giuseppe Lodato, and C. J. Clarke (2009). "Characterizing the gravitational instability in cooling accretion discs". In: *MNRAS* 393, pp. 1157–1173. DOI: [10.1111/j.1365-2966.2008.14275.x](https://doi.org/10.1111/j.1365-2966.2008.14275.x). arXiv: [0811.3629](https://arxiv.org/abs/0811.3629) [astro-ph].
- Costa, T. et al. (2018). "Driving gas shells with radiation pressure on dust in radiation-hydrodynamic simulations". In: *MNRAS* 473, pp. 4197–4219. DOI: [10.1093/mnras/stx2598](https://doi.org/10.1093/mnras/stx2598). arXiv: [1703.05766](https://arxiv.org/abs/1703.05766).
- Costa, Tiago, Debora Sijacki, and Martin G. Haehnelt (2014). "Feedback from active galactic nuclei: energy- versus momentum-driving". In: *MNRAS* 444, pp. 2355–2376. DOI: [10.1093/mnras/stu1632](https://doi.org/10.1093/mnras/stu1632). arXiv: [1406.2691](https://arxiv.org/abs/1406.2691) [astro-ph.GA].
- Crenshaw, D. M., S. B. Kraemer, and I. M. George (2003). "Mass Loss from the Nuclei of Active Galaxies". In: *ARA&A* 41, pp. 117–167. DOI: [10.1146/annurev.astro.41.082801.100328](https://doi.org/10.1146/annurev.astro.41.082801.100328).
- Cuadra, J., S. Nayakshin, and R. Sunyaev (2003). "Bright stars and an optically thick inactive disk in Sgr A* and other dormant galaxy centers". In: *A&A* 411, pp. 405–416. DOI: [10.1051/0004-6361:20031350](https://doi.org/10.1051/0004-6361:20031350). arXiv: [astro-ph/0304533](https://arxiv.org/abs/astro-ph/0304533) [astro-ph].
- Cullen, L. and W. Dehnen (2010). "Inviscid smoothed particle hydrodynamics". In: *MNRAS* 408, pp. 669–683. DOI: [10.1111/j.1365-2966.2010.17158.x](https://doi.org/10.1111/j.1365-2966.2010.17158.x). arXiv: [1006.1524](https://arxiv.org/abs/1006.1524) [astro-ph.IM].
- Curtis, H. D. (1988). "Novae in Spiral Nebulae and the Island Universe Theory". In: *PASP* 100, p. 6. DOI: [10.1086/132128](https://doi.org/10.1086/132128).

- Curtis, M. and D. Sijacki (2016). “Resolving flows around black holes: the impact of gas angular momentum”. In: *MNRAS* 463, pp. 63–77. DOI: [10.1093/mnras/stw1944](https://doi.org/10.1093/mnras/stw1944). arXiv: [1606.02729](https://arxiv.org/abs/1606.02729).
- DeGraf, C. and D. Sijacki (2017). “Black hole clustering and duty cycles in the Illustris simulation”. In: *MNRAS* 466, pp. 3331–3343. DOI: [10.1093/mnras/stw3267](https://doi.org/10.1093/mnras/stw3267). arXiv: [1609.06727](https://arxiv.org/abs/1609.06727).
- DeGraf, C. et al. (2015). “Scaling relations between black holes and their host galaxies: comparing theoretical and observational measurements, and the impact of selection effects”. In: *MNRAS* 454, pp. 913–932. DOI: [10.1093/mnras/stv2002](https://doi.org/10.1093/mnras/stv2002). arXiv: [1412.4133](https://arxiv.org/abs/1412.4133).
- Dehnen, W. and H. Aly (2012). “Improving convergence in smoothed particle hydrodynamics simulations without pairing instability”. In: *MNRAS* 425, pp. 1068–1082. DOI: [10.1111/j.1365-2966.2012.21439.x](https://doi.org/10.1111/j.1365-2966.2012.21439.x). arXiv: [1204.2471](https://arxiv.org/abs/1204.2471) [astro-ph.IM].
- Dehnen, W. and A. King (2013). “Black Hole Foraging: Feedback Drives Feeding”. In: *ApJL* 777, L28, p. L28. DOI: [10.1088/2041-8205/777/2/L28](https://doi.org/10.1088/2041-8205/777/2/L28). arXiv: [1310.2039](https://arxiv.org/abs/1310.2039) [astro-ph.CO].
- Dehnen, W. and J. I. Read (2011). “N-body simulations of gravitational dynamics”. In: *European Physical Journal Plus* 126, 55, p. 55. DOI: [10.1140/epjp/i2011-11055-3](https://doi.org/10.1140/epjp/i2011-11055-3). arXiv: [1105.1082](https://arxiv.org/abs/1105.1082) [astro-ph.IM].
- Di Matteo, T. et al. (2008). “Direct Cosmological Simulations of the Growth of Black Holes and Galaxies”. In: *ApJ* 676, pp. 33–53. DOI: [10.1086/524921](https://doi.org/10.1086/524921). arXiv: [0705.2269](https://arxiv.org/abs/0705.2269).
- Dipierro, G. et al. (2015). “On planet formation in HL Tau”. In: *MNRAS* 453, pp. L73–L77. DOI: [10.1093/mnrasl/slv105](https://doi.org/10.1093/mnrasl/slv105). arXiv: [1507.06719](https://arxiv.org/abs/1507.06719) [astro-ph.EP].
- Do, T. et al. (2013). “Three-dimensional Stellar Kinematics at the Galactic Center: Measuring the Nuclear Star Cluster Spatial Density Profile, Black Hole Mass, and Distance”. In: *ApJ* 779, L6, p. L6. DOI: [10.1088/2041-8205/779/1/L6](https://doi.org/10.1088/2041-8205/779/1/L6). arXiv: [1311.0886](https://arxiv.org/abs/1311.0886) [astro-ph.GA].
- Doeleman, S. S. et al. (2008). “Event-horizon-scale structure in the supermassive black hole candidate at the Galactic Centre”. In: *NATURE* 455, pp. 78–80. DOI: [10.1038/nature07245](https://doi.org/10.1038/nature07245). arXiv: [0809.2442](https://arxiv.org/abs/0809.2442).
- Dressler, A. (1989). “Observational Evidence for Supermassive Black Holes”. In: *Active Galactic Nuclei*. Ed. by D. E. Osterbrock and J. S. Miller. Vol. 134. IAU Symposium, p. 217.

- Dressler, A. and D. O. Richstone (1988). "Stellar dynamics in the nuclei of M31 and M32 - Evidence for massive black holes?" In: *ApJ* 324, pp. 701–713. DOI: [10.1086/165930](https://doi.org/10.1086/165930).
- (1990). "New measurements of stellar kinematics in the core of M87". In: *ApJ* 348, pp. 120–126. DOI: [10.1086/168218](https://doi.org/10.1086/168218).
- Drew, J. E. and A. Boksenberg (1984). "Optical spectroscopy of two broad absorption line QSOs and implications for spherical-symmetric absorbing wind models". In: *MNRAS* 211, pp. 813–831. DOI: [10.1093/mnras/211.4.813](https://doi.org/10.1093/mnras/211.4.813).
- Dubinski, J. (1998). "The Origin of the Brightest Cluster Galaxies". In: *ApJ* 502, pp. 141–149. DOI: [10.1086/305901](https://doi.org/10.1086/305901). eprint: [astro-ph/9709102](https://arxiv.org/abs/astro-ph/9709102).
- Dubinski, J., R. Narayan, and T. G. Phillips (1995). "Turbulence in Molecular Clouds". In: *apj* 448, p. 226. DOI: [10.1086175954](https://doi.org/10.1086175954). eprint: [astro-ph9501032](https://arxiv.org/abs/astro-ph9501032).
- Dubois, Y. et al. (2012). "Self-regulated growth of supermassive black holes by a dual jet-heating active galactic nucleus feedback mechanism: methods, tests and implications for cosmological simulations". In: *MNRAS* 420, pp. 2662–2683. DOI: [10.1111/j.1365-2966.2011.20236.x](https://doi.org/10.1111/j.1365-2966.2011.20236.x). arXiv: [1108.0110](https://arxiv.org/abs/1108.0110).
- Dubrulle, B. (1992). "A turbulent closure model for thin accretion disks". In: *A&A* 266, pp. 592–604.
- Dubus, G., J.-M. Hameury, and J.-P. Lasota (2001). "The disc instability model for X-ray transients: Evidence for truncation and irradiation". In: *A&A* 373, pp. 251–271. DOI: [10.1051/0004-6361:20010632](https://doi.org/10.1051/0004-6361:20010632). eprint: [astro-ph/0102237](https://arxiv.org/abs/astro-ph/0102237).
- Ebisuzaki, T. et al. (2001). "Missing Link Found? The "Runaway" Path to Supermassive Black Holes". In: *ApJL* 562, pp. L19–L22. DOI: [10.1086/338118](https://doi.org/10.1086/338118). eprint: [astro-ph/0106252](https://arxiv.org/abs/astro-ph/0106252).
- Eddington, A. S. (1916). "On the radiative equilibrium of the stars". In: *MNRAS* 77, pp. 16–35. DOI: [10.1093/mnras/77.1.16](https://doi.org/10.1093/mnras/77.1.16).
- Efstathiou, G. et al. (1985). "Numerical techniques for large cosmological N-body simulations". In: *ApJS* 57, pp. 241–260. DOI: [10.1086/191003](https://doi.org/10.1086/191003).
- Eggen, O. J., D. Lynden-Bell, and A. R. Sandage (1962). "Evidence from the motions of old stars that the Galaxy collapsed." In: *ApJ* 136, p. 748. DOI: [10.1086/147433](https://doi.org/10.1086/147433).
- Einstein, A. (1905). "Zur Elektrodynamik bewegter Körper". In: *Annalen der Physik* 322, pp. 891–921. DOI: [10.1002/andp.19053221004](https://doi.org/10.1002/andp.19053221004).
- (1915). "Die Feldgleichungen der Gravitation". In: *Sitzungsberichte der Königlich Preussischen Akademie der Wissenschaften (Berlin)*, Seite 844-847.

- Elder, F. R. et al. (1947). “Radiation from Electrons in a Synchrotron”. In: *Physical Review* 71, pp. 829–830. DOI: [10.1103/PhysRev.71.829.5](https://doi.org/10.1103/PhysRev.71.829.5).
- Elvis, M. (2017). “Quasar Rain: The Broad Emission Line Region as Condensations in the Warm Accretion Disk Wind”. In: *ApJ* 847, 56, p. 56. DOI: [10.3847/1538-4357/aa82b6](https://doi.org/10.3847/1538-4357/aa82b6). arXiv: [1703.02956](https://arxiv.org/abs/1703.02956).
- Elvis, M., G. Risaliti, and G. Zamorani (2002). “Most Supermassive Black Holes Must Be Rapidly Rotating”. In: *ApJL* 565, pp. L75–L77. DOI: [10.1086/339197](https://doi.org/10.1086/339197). eprint: [astro-ph/0112413](https://arxiv.org/abs/astro-ph/0112413).
- Faber, C. and W. Dehnen (2018). “Feeding supermassive black holes by collisional cascades”. In: *MNRAS* 478, pp. 852–866. DOI: [10.1093/mnras/sty1076](https://doi.org/10.1093/mnras/sty1076). arXiv: [1804.08499](https://arxiv.org/abs/1804.08499).
- Fabian, A. C. (1999). “The obscured growth of massive black holes”. In: *MNRAS* 308, pp. L39–L43. DOI: [10.1046/j.1365-8711.1999.03017.x](https://doi.org/10.1046/j.1365-8711.1999.03017.x). eprint: [astro-ph/9908064](https://arxiv.org/abs/astro-ph/9908064).
- (2012). “Observational Evidence of Active Galactic Nuclei Feedback”. In: *ARA&A* 50, pp. 455–489. DOI: [10.1146/annurev-astro-081811-125521](https://doi.org/10.1146/annurev-astro-081811-125521). arXiv: [1204.4114](https://arxiv.org/abs/1204.4114).
- Falcke, H., E. Körding, and S. Markoff (2004). “A scheme to unify low-power accreting black holes. Jet-dominated accretion flows and the radio/X-ray correlation”. In: *A&A* 414, pp. 895–903. DOI: [10.1051/0004-6361:20031683](https://doi.org/10.1051/0004-6361:20031683). eprint: [astro-ph/0305335](https://arxiv.org/abs/astro-ph/0305335).
- Falcke, H., F. Melia, and E. Agol (2000). “Viewing the Shadow of the Black Hole at the Galactic Center”. In: *ApJL* 528, pp. L13–L16. DOI: [10.1086/312423](https://doi.org/10.1086/312423). eprint: [astro-ph/9912263](https://arxiv.org/abs/astro-ph/9912263).
- Fanaroff, B. L. and J. M. Riley (1974). “The morphology of extragalactic radio sources of high and low luminosity”. In: *MNRAS* 167, 31P–36P. DOI: [10.1093/mnras/167.1.31P](https://doi.org/10.1093/mnras/167.1.31P).
- Fanidakis, N. et al. (2011). “Grand unification of AGN activity in the Λ CDM cosmology”. In: *MNRAS* 410, pp. 53–74. DOI: [10.1111/j.1365-2966.2010.17427.x](https://doi.org/10.1111/j.1365-2966.2010.17427.x). arXiv: [0911.1128](https://arxiv.org/abs/0911.1128).
- Fath, E. A. (1909). “The Spectra of Some Spiral Nebulae and Globular Star Clusters”. In: *PASP* 21, pp. 138–143. DOI: [10.1086/121907](https://doi.org/10.1086/121907).
- Faucher-Giguère, C.-A. and E. Quataert (2012). “The physics of galactic winds driven by active galactic nuclei”. In: *MNRAS* 425, pp. 605–622. DOI: [10.1111/j.1365-2966.2012.21512.x](https://doi.org/10.1111/j.1365-2966.2012.21512.x). arXiv: [1204.2547](https://arxiv.org/abs/1204.2547).

- Ferrarese, L. (2002). “Beyond the Bulge: A Fundamental Relation between Supermassive Black Holes and Dark Matter Halos”. In: *ApJ* 578, pp. 90–97. DOI: [10.1086/342308](https://doi.org/10.1086/342308). eprint: [astro-ph/0203469](https://arxiv.org/abs/astro-ph/0203469).
- Ferrarese, L., H. C. Ford, and W. Jaffe (1996). “Evidence for a Massive Black Hole in the Active Galaxy NGC 4261 from Hubble Space Telescope Images and Spectra”. In: *ApJ* 470, p. 444. DOI: [10.1086/177876](https://doi.org/10.1086/177876).
- Ferrarese, L. and D. Merritt (2000). “A Fundamental Relation between Supermassive Black Holes and Their Host Galaxies”. In: *ApJL* 539, pp. L9–L12. DOI: [10.1086/312838](https://doi.org/10.1086/312838). eprint: [astro-ph/0006053](https://arxiv.org/abs/astro-ph/0006053).
- Feruglio, C. et al. (2010). “Quasar feedback revealed by giant molecular outflows”. In: *A&A* 518, L155, p. L155. DOI: [10.1051/0004-6361/201015164](https://doi.org/10.1051/0004-6361/201015164). arXiv: [1006.1655](https://arxiv.org/abs/1006.1655).
- Fiacconi, D., D. Sijacki, and J. E. Pringle (2018). “Galactic nuclei evolution with spinning black holes: method and implementation”. In: *MNRAS* 477, pp. 3807–3835. DOI: [10.1093/mnras/sty893](https://doi.org/10.1093/mnras/sty893). arXiv: [1712.00023](https://arxiv.org/abs/1712.00023).
- Fish, V. L. et al. (2011). “1.3 mm Wavelength VLBI of Sagittarius A*: Detection of Time-variable Emission on Event Horizon Scales”. In: *ApJL* 727, L36, p. L36. DOI: [10.1088/2041-8205/727/2/L36](https://doi.org/10.1088/2041-8205/727/2/L36). arXiv: [1011.2472](https://arxiv.org/abs/1011.2472).
- Fish, V. L. et al. (2016). “Persistent Asymmetric Structure of Sagittarius A* on Event Horizon Scales”. In: *ApJ* 820, 90, p. 90. DOI: [10.3847/0004-637X/820/2/90](https://doi.org/10.3847/0004-637X/820/2/90). arXiv: [1602.05527](https://arxiv.org/abs/1602.05527).
- Floyd, D. J. E., N. F. Bate, and R. L. Webster (2009). “The accretion disc in the quasar SDSS J0924+0219”. In: *MNRAS* 398, pp. 233–239. DOI: [10.1111/j.1365-2966.2009.15045.x](https://doi.org/10.1111/j.1365-2966.2009.15045.x). arXiv: [0905.2651](https://arxiv.org/abs/0905.2651) [[astro-ph](https://arxiv.org/abs/astro-ph).HE].
- Ford, H. C. et al. (1994). “Narrowband HST images of M87: Evidence for a disk of ionized gas around a massive black hole”. In: *ApJL* 435, pp. L27–L30. DOI: [10.1086/187586](https://doi.org/10.1086/187586).
- Forgan, Duncan and Ken Rice (2011). “The Jeans mass as a fundamental measure of self-gravitating disc fragmentation and initial fragment mass”. In: *MNRAS* 417, pp. 1928–1937. DOI: [10.1111/j.1365-2966.2011.19380.x](https://doi.org/10.1111/j.1365-2966.2011.19380.x). arXiv: [1107.0831](https://arxiv.org/abs/1107.0831) [[astro-ph](https://arxiv.org/abs/astro-ph).EP].
- Fosbury, R. A. E. et al. (2003). “Massive Star Formation in a Gravitationally Lensed H II Galaxy at $z = 3.357$ ”. In: *ApJ* 596, pp. 797–809. DOI: [10.1086/378228](https://doi.org/10.1086/378228). eprint: [astro-ph/0307162](https://arxiv.org/abs/astro-ph/0307162).

- Frank, J., A. King, and D. J. Raine (2002). *Accretion Power in Astrophysics: Third Edition*. Cambridge University Press. ISBN: 9780521629577.
- Friedmann, A. (1922). “Über die Krümmung des Raumes”. In: *Zeitschrift für Physik* 10, pp. 377–386. DOI: [10.1007/BF01332580](https://doi.org/10.1007/BF01332580).
- Fujii, M. et al. (2008). “Evolution of Star Clusters near the Galactic Center: Fully Self-Consistent N-Body Simulations”. In: *ApJ* 686, pp. 1082–1093. DOI: [10.1086/591483](https://doi.org/10.1086/591483). arXiv: [0708.3719](https://arxiv.org/abs/0708.3719).
- Fukumura, K. et al. (2010). “Magnetohydrodynamic Accretion Disk Winds as X-ray Absorbers in Active Galactic Nuclei”. In: *ApJ* 715, pp. 636–650. DOI: [10.1088/0004-637X/715/1/636](https://doi.org/10.1088/0004-637X/715/1/636). arXiv: [0910.3001](https://arxiv.org/abs/0910.3001) [astro-ph.HE].
- Gammie, C. F. (1996). “Layered Accretion in T Tauri Disks”. In: *ApJ* 457, p. 355. DOI: [10.1086/176735](https://doi.org/10.1086/176735).
- Gammie, C. F., S. L. Shapiro, and J. C. McKinney (2004). “Black Hole Spin Evolution”. In: *ApJ* 602, pp. 312–319. DOI: [10.1086/380996](https://doi.org/10.1086/380996). eprint: [astro-ph/0310886](https://arxiv.org/abs/astro-ph/0310886).
- Gammie, Charles F. (2001). “Nonlinear Outcome of Gravitational Instability in Cooling, Gaseous Disks”. In: *ApJ* 553, pp. 174–183. DOI: [10.1086/320631](https://doi.org/10.1086/320631). arXiv: [astro-ph/0101501](https://arxiv.org/abs/astro-ph/0101501) [astro-ph].
- Gaspari, M., M. Ruszkowski, and S. P. Oh (2013). “Chaotic cold accretion on to black holes”. In: *MNRAS* 432, pp. 3401–3422. DOI: [10.1093/mnras/stt692](https://doi.org/10.1093/mnras/stt692). arXiv: [1301.3130](https://arxiv.org/abs/1301.3130).
- Gebhardt, K. et al. (2000). “A Relationship between Nuclear Black Hole Mass and Galaxy Velocity Dispersion”. In: *ApJL* 539, pp. L13–L16. DOI: [10.1086/312840](https://doi.org/10.1086/312840). eprint: [astro-ph/0006289](https://arxiv.org/abs/astro-ph/0006289).
- Gebhardt, K. et al. (2011). “The Black Hole Mass in M87 from Gemini/NIFS Adaptive Optics Observations”. In: *ApJ* 729, 119, p. 119. DOI: [10.1088/0004-637X/729/2/119](https://doi.org/10.1088/0004-637X/729/2/119). arXiv: [1101.1954](https://arxiv.org/abs/1101.1954).
- Geller, M. J. and J. P. Huchra (1989). “Mapping the universe”. In: *Science* 246, pp. 897–903. DOI: [10.1126/science.246.4932.897](https://doi.org/10.1126/science.246.4932.897).
- Genzel, R. et al. (1996). “The Dark Mass Concentration in the Central Parsec of the Milky Way”. In: *ApJ* 472, p. 153. DOI: [10.1086/178051](https://doi.org/10.1086/178051).
- Ghez, A. M. et al. (2008). “Measuring Distance and Properties of the Milky Way’s Central Supermassive Black Hole with Stellar Orbits”. In: *ApJ* 689, pp. 1044–1062. DOI: [10.1086/592738](https://doi.org/10.1086/592738). arXiv: [0808.2870](https://arxiv.org/abs/0808.2870).

- Gibson, R. R. et al. (2009). "A Catalog of Broad Absorption Line Quasars in Sloan Digital Sky Survey Data Release 5". In: *ApJ* 692, pp. 758–777. DOI: [10.1088/0004-637X/692/1/758](https://doi.org/10.1088/0004-637X/692/1/758). arXiv: [0810.2747](https://arxiv.org/abs/0810.2747).
- Gillessen, S. et al. (2009). "Monitoring Stellar Orbits Around the Massive Black Hole in the Galactic Center". In: *ApJ* 692, pp. 1075–1109. DOI: [10.1088/0004-637X/692/2/1075](https://doi.org/10.1088/0004-637X/692/2/1075). arXiv: [0810.4674](https://arxiv.org/abs/0810.4674).
- Gillessen, S. et al. (2012). "A gas cloud on its way towards the supermassive black hole at the Galactic Centre". In: *NATURE* 481, pp. 51–54. DOI: [10.1038/nature10652](https://doi.org/10.1038/nature10652). arXiv: [1112.3264](https://arxiv.org/abs/1112.3264) [astro-ph.GA].
- Gillessen, S. et al. (2013). "New Observations of the Gas Cloud G2 in the Galactic Center". In: *ApJ* 763, 78, p. 78. DOI: [10.1088/0004-637X/763/2/78](https://doi.org/10.1088/0004-637X/763/2/78). arXiv: [1209.2272](https://arxiv.org/abs/1209.2272) [astro-ph.GA].
- Gillessen, S. et al. (2017). "An Update on Monitoring Stellar Orbits in the Galactic Center". In: *ApJ* 837, 30, p. 30. DOI: [10.3847/1538-4357/aa5c41](https://doi.org/10.3847/1538-4357/aa5c41). arXiv: [1611.09144](https://arxiv.org/abs/1611.09144).
- Gingold, R. A. and J. J. Monaghan (1977). "Smoothed particle hydrodynamics - Theory and application to non-spherical stars". In: *MNRAS* 181, pp. 375–389.
- Glassgold, A. E., J. Najita, and J. Igea (2004). "Heating Protoplanetary Disk Atmospheres". In: *ApJ* 615, pp. 972–990. DOI: [10.1086/424509](https://doi.org/10.1086/424509).
- Goldreich, P. and G. Schubert (1967). "Differential Rotation in Stars". In: *ApJ* 150, p. 571. DOI: [10.1086/149360](https://doi.org/10.1086/149360).
- Goldreich, P. and S. Tremaine (1979). "The excitation of density waves at the Lindblad and corotation resonances by an external potential". In: *ApJ* 233, pp. 857–871. DOI: [10.1086/157448](https://doi.org/10.1086/157448).
- Goodman, A. A. et al. (1993). "Dense cores in dark clouds. VIII - Velocity gradients". In: *ApJ* 406, pp. 528–547. DOI: [10.1086/172465](https://doi.org/10.1086/172465).
- Grand, R. J. J. et al. (2017). "The Auriga Project: the properties and formation mechanisms of disc galaxies across cosmic time". In: *MNRAS* 467, pp. 179–207. DOI: [10.1093/mnras/stx071](https://doi.org/10.1093/mnras/stx071). arXiv: [1610.01159](https://arxiv.org/abs/1610.01159).
- Gravity Collaboration et al. (2018). "Detection of the gravitational redshift in the orbit of the star S2 near the Galactic centre massive black hole". In: *A&A* 615, L15, p. L15. DOI: [10.1051/0004-6361/201833718](https://doi.org/10.1051/0004-6361/201833718). arXiv: [1807.09409](https://arxiv.org/abs/1807.09409).
- Greene, J. E. and L. C. Ho (2004). "Active Galactic Nuclei with Candidate Intermediate-Mass Black Holes". In: *ApJ* 610, pp. 722–736. DOI: [10.1086/421719](https://doi.org/10.1086/421719). eprint: [astro-ph/0404110](https://arxiv.org/abs/astro-ph/0404110).

- Greenstein, J. L. (1963). "Red-Shift of the Unusual Radio Source: 3C 48". In: *NATURE* 197, pp. 1041–1042. DOI: [10.1038/1971041a0](https://doi.org/10.1038/1971041a0).
- Greif, T. H. et al. (2011). "Simulations on a Moving Mesh: The Clustered Formation of Population III Protostars". In: *ApJ* 737, 75, p. 75. DOI: [10.1088/0004-637X/737/2/75](https://doi.org/10.1088/0004-637X/737/2/75). arXiv: [1101.5491](https://arxiv.org/abs/1101.5491).
- Gressel, O. et al. (2013). "Global Hydromagnetic Simulations of a Planet Embedded in a Dead Zone: Gap Opening, Gas Accretion, and Formation of a Protoplanetary Jet". In: *ApJ* 779, 59, p. 59. DOI: [10.1088/0004-637X/779/1/59](https://doi.org/10.1088/0004-637X/779/1/59). arXiv: [1309.2871](https://arxiv.org/abs/1309.2871) [astro-ph.EP].
- Gullbring, E. et al. (1998). "Disk Accretion Rates for T Tauri Stars". In: *ApJ* 492, pp. 323–341. DOI: [10.1086/305032](https://doi.org/10.1086/305032).
- Habibi, M. et al. (2017). "Twelve Years of Spectroscopic Monitoring in the Galactic Center: The Closest Look at S-stars near the Black Hole". In: *ApJ* 847, 120, p. 120. DOI: [10.3847/1538-4357/aa876f](https://doi.org/10.3847/1538-4357/aa876f). arXiv: [1708.06353](https://arxiv.org/abs/1708.06353) [astro-ph.SR].
- Haehnelt, M. G., P. Natarajan, and M. J. Rees (1998). "High-redshift galaxies, their active nuclei and central black holes". In: *MNRAS* 300, pp. 817–827. DOI: [10.1046/j.1365-8711.1998.01951.x](https://doi.org/10.1046/j.1365-8711.1998.01951.x). eprint: [astro-ph/9712259](https://arxiv.org/abs/astro-ph/9712259).
- Haehnelt, M. G. and M. J. Rees (1993). "The formation of nuclei in newly formed galaxies and the evolution of the quasar population". In: *MNRAS* 263, pp. 168–178. DOI: [10.1093/mnras/263.1.168](https://doi.org/10.1093/mnras/263.1.168).
- Halpern, J. P. (1984). "Variable X-ray absorption in the QSO MR 2251 - 178". In: *ApJ* 281, pp. 90–94. DOI: [10.1086/162077](https://doi.org/10.1086/162077).
- Harms, R. J. et al. (1994). "HST FOS spectroscopy of M87: Evidence for a disk of ionized gas around a massive black hole". In: *ApJL* 435, pp. L35–L38. DOI: [10.1086/187588](https://doi.org/10.1086/187588).
- Harrower, G. A. (1960). "Cosmic Radio Sources as Intergalactic Collisions." In: *ApJ* 132, p. 22. DOI: [10.1086/146895](https://doi.org/10.1086/146895).
- Hartmann, L. et al. (1998). "Accretion and the Evolution of T Tauri Disks". In: *ApJ* 495, pp. 385–400. DOI: [10.1086/305277](https://doi.org/10.1086/305277).
- Hashimoto, G. L. et al. (2008). "Felsic highland crust on Venus suggested by Galileo Near-Infrared Mapping Spectrometer data". In: *Journal of Geophysical Research (Planets)* 113, E00B24, E00B24. DOI: [10.1029/2008JE003134](https://doi.org/10.1029/2008JE003134).
- Hawley, J. F., C. F. Gammie, and S. A. Balbus (1995). "Local Three-dimensional Magnetohydrodynamic Simulations of Accretion Disks". In: *ApJ* 440, p. 742. DOI: [10.1086/175311](https://doi.org/10.1086/175311).

- Hayli, A. (1967). "The N-Body Gravitational Problem and the Simulation of Galactic Clusters". In: *NASA Special Publication* 153, p. 315.
- Heckman, T. M. (1980). "An optical and radio survey of the nuclei of bright galaxies - Activity in normal galactic nuclei". In: *A&A* 87, pp. 152–164.
- Heckman, T. M. et al. (1986). "Galaxy collisions and mergers - The genesis of very powerful radio sources?" In: *ApJ* 311, pp. 526–547. DOI: [10.1086/164793](https://doi.org/10.1086/164793).
- Heger, A. and S. E. Woosley (2002). "The Nucleosynthetic Signature of Population III". In: *ApJ* 567, pp. 532–543. DOI: [10.1086/338487](https://doi.org/10.1086/338487). eprint: [astro-ph/0107037](https://arxiv.org/abs/astro-ph/0107037).
- Herbig, G. H. (1960). "The Spectra of Be- and Ae-Type Stars Associated with Nebulosity". In: *ApJS* 4, p. 337. DOI: [10.1086/190050](https://doi.org/10.1086/190050).
- Hernquist, L. and J. C. Mihos (1995). "Excitation of Activity in Galaxies by Minor Mergers". In: *ApJ* 448, p. 41. DOI: [10.1086/175940](https://doi.org/10.1086/175940). eprint: [astro-ph/9501090](https://arxiv.org/abs/astro-ph/9501090).
- Hills, J. G. (1988). "Hyper-velocity and tidal stars from binaries disrupted by a massive Galactic black hole". In: *NATURE* 331, pp. 687–689. DOI: [10.1038/331687a0](https://doi.org/10.1038/331687a0).
- Hirschmann, M. et al. (2010). "On the evolution of the intrinsic scatter in black hole versus galaxy mass relations". In: *MNRAS* 407, pp. 1016–1032. DOI: [10.1111/j.1365-2966.2010.17006.x](https://doi.org/10.1111/j.1365-2966.2010.17006.x). arXiv: [1005.2100](https://arxiv.org/abs/1005.2100).
- Ho, L. C., A. V. Filippenko, and W. L. W. Sargent (1997). "A Search for "Dwarf" Seyfert Nuclei. V. Demographics of Nuclear Activity in Nearby Galaxies". In: *ApJ* 487, pp. 568–578. DOI: [10.1086/304638](https://doi.org/10.1086/304638). eprint: [astro-ph/9704108](https://arxiv.org/abs/astro-ph/9704108).
- Ho, P. T. P. et al. (1991). "A molecular gas streamer feeding the Galactic Centre". In: *NATURE* 350, pp. 309–312. DOI: [10.1038/350309a0](https://doi.org/10.1038/350309a0).
- Hobbs, A. et al. (2011). "Feeding supermassive black holes through supersonic turbulence and ballistic accretion". In: *MNRAS* 413, pp. 2633–2650. DOI: [10.1111/j.1365-2966.2011.18333.x](https://doi.org/10.1111/j.1365-2966.2011.18333.x). arXiv: [1001.3883](https://arxiv.org/abs/1001.3883) [[astro-ph](https://arxiv.org/abs/astro-ph).HE].
- Hobbs, Alexander and Sergei Nayakshin (2009). "Simulations of the formation of stellar discs in the Galactic Centre via cloud-cloud collisions". In: *MNRAS* 394, pp. 191–206. DOI: [10.1111/j.1365-2966.2008.14359.x](https://doi.org/10.1111/j.1365-2966.2008.14359.x). arXiv: [0809.3752](https://arxiv.org/abs/0809.3752) [[astro-ph](https://arxiv.org/abs/astro-ph)].
- Holmberg, Erik (1941). "On the Clustering Tendencies among the Nebulae. II. a Study of Encounters Between Laboratory Models of Stellar Systems by a New Integration Procedure." In: *ApJ* 94, p. 385. DOI: [10.1086/144344](https://doi.org/10.1086/144344).

- Homayouni, Y. et al. (2018). “The Sloan Digital Sky Survey Reverberation Mapping Project: Accretion-Disk Sizes from Continuum Lags”. In: *arXiv e-prints*. arXiv: [1806.08360](https://arxiv.org/abs/1806.08360).
- Hopkins, P. F. et al. (2012). “Why are active galactic nuclei and host galaxies misaligned?” In: *MNRAS* 425, pp. 1121–1128. DOI: [10.1111/j.1365-2966.2012.21449.x](https://doi.org/10.1111/j.1365-2966.2012.21449.x). arXiv: [1111.1236](https://arxiv.org/abs/1111.1236) [astro-ph.CO].
- Hoyle, F. (1953). “On the Fragmentation of Gas Clouds Into Galaxies and Stars.” In: *ApJ* 118, p. 513. DOI: [10.1086/145780](https://doi.org/10.1086/145780).
- Hoyle, F. and W. A. Fowler (1963). “On the nature of strong radio sources”. In: *MNRAS* 125, p. 169. DOI: [10.1093/mnras/125.2.169](https://doi.org/10.1093/mnras/125.2.169).
- Hoyle, F. and R. A. Lyttleton (1941). “On the accretion theory of stellar evolution”. In: *MNRAS* 101, p. 227. DOI: [10.1093/mnras/101.4.227](https://doi.org/10.1093/mnras/101.4.227).
- Hoyle, F. and R. J. Tayler (1964). “The Mystery of the Cosmic Helium Abundance”. In: *NATURE* 203, pp. 1108–1110. DOI: [10.1038/2031108a0](https://doi.org/10.1038/2031108a0).
- Hubble, E. (1929). “A Relation between Distance and Radial Velocity among Extra-Galactic Nebulae”. In: *Proceedings of the National Academy of Science* 15, pp. 168–173. DOI: [10.1073/pnas.15.3.168](https://doi.org/10.1073/pnas.15.3.168).
- Hughes, S. A. and R. D. Blandford (2003). “Black Hole Mass and Spin Coevolution by Mergers”. In: *ApJL* 585, pp. L101–L104. DOI: [10.1086/375495](https://doi.org/10.1086/375495). eprint: [astro-ph/0208484](https://arxiv.org/abs/astro-ph/0208484).
- Israel, W. (1967). “Event Horizons in Static Vacuum Space-Times”. In: *Physical Review* 164, pp. 1776–1779. DOI: [10.1103/PhysRev.164.1776](https://doi.org/10.1103/PhysRev.164.1776).
- Ives, J. C., P. W. Sanford, and M. V. Penston (1976). “The variability and absorption of the X-ray emission from NGC 4151”. In: *ApJL* 207, pp. L159–L162. DOI: [10.1086/182203](https://doi.org/10.1086/182203).
- Jahnke, K. and A. V. Macciò (2011). “The Non-causal Origin of the Black-hole-galaxy Scaling Relations”. In: *ApJ* 734, 92, p. 92. DOI: [10.1088/0004-637X/734/2/92](https://doi.org/10.1088/0004-637X/734/2/92). arXiv: [1006.0482](https://arxiv.org/abs/1006.0482).
- Jansky, K. G. (1933). “Electrical phenomena that apparently are of interstellar origin”. In: *Popular Astronomy* 41, pp. 548–555.
- Jeter, Britton, Avery E. Broderick, and B. R. McNamara (2018). “Impact of Accretion Flow Dynamics on Gas Dynamical Black Hole Mass Estimates”. In: *arXiv e-prints*, arXiv:1810.05238, arXiv:1810.05238. arXiv: [1810.05238](https://arxiv.org/abs/1810.05238) [astro-ph.HE].

- Jog, C. J. and P. M. Solomon (1992). “A triggering mechanism for enhanced star formation in colliding galaxies”. In: *ApJ* 387, pp. 152–161. DOI: [10 . 1086 / 171067](https://doi.org/10.1086/171067).
- Johnson, M. D. et al. (2015). “Resolved magnetic-field structure and variability near the event horizon of Sagittarius A*”. In: *Science* 350, pp. 1242–1245. DOI: [10.1126/science.aac7087](https://doi.org/10.1126/science.aac7087). arXiv: [1512.01220](https://arxiv.org/abs/1512.01220) [[astro-ph.HE](https://arxiv.org/abs/1512.01220)].
- Johnson, M. D. et al. (2018). “The Scattering and Intrinsic Structure of Sagittarius A* at Radio Wavelengths”. In: *ArXiv e-prints*. arXiv: [1808.08966](https://arxiv.org/abs/1808.08966).
- Joy, A. H. (1945). “T Tauri Variable Stars.” In: *ApJ* 102, p. 168. DOI: [10 . 1086 / 144749](https://doi.org/10.1086/144749).
- Kardashev, N. S. et al. (2017). “RadioAstron Science Program Five Years after Launch: Main Science Results”. In: *Solar System Research* 51, pp. 535–554. DOI: [10.1134/S0038094617070085](https://doi.org/10.1134/S0038094617070085).
- Kennicutt Jr., R. C. (1998). “Star Formation in Galaxies Along the Hubble Sequence”. In: *ARA&A* 36, pp. 189–232. DOI: [10.1146/annurev.astro.36.1.189](https://doi.org/10.1146/annurev.astro.36.1.189). eprint: [astro-ph/9807187](https://arxiv.org/abs/astro-ph/9807187).
- Kepler, J. and W.H. Donahue (1992). *New Astronomy*.
- Kerr, R. P. (1963). “Gravitational Field of a Spinning Mass as an Example of Algebraically Special Metrics”. In: *Physical Review Letters* 11, pp. 237–238. DOI: [10.1103/PhysRevLett.11.237](https://doi.org/10.1103/PhysRevLett.11.237).
- Keto, E., L. C. Ho, and K.-Y. Lo (2005). “M82, Starbursts, Star Clusters, and the Formation of Globular Clusters”. In: *ApJ* 635, pp. 1062–1076. DOI: [10 . 1086 / 497575](https://doi.org/10.1086/497575). eprint: [astro-ph/0508519](https://arxiv.org/abs/astro-ph/0508519).
- Kim, S. S. and M. Morris (2003). “Dynamical Friction on Star Clusters near the Galactic Center”. In: *ApJ* 597, pp. 312–322. DOI: [10.1086/378347](https://doi.org/10.1086/378347). eprint: [astro-ph/0307271](https://arxiv.org/abs/astro-ph/0307271).
- King, A. (2003). “Black Holes, Galaxy Formation, and the $M_{BH}-\sigma$ Relation”. In: *ApJL* 596, pp. L27–L29. DOI: [10.1086/379143](https://doi.org/10.1086/379143). eprint: [astro-ph/0308342](https://arxiv.org/abs/astro-ph/0308342).
- (2005). “The AGN-Starburst Connection, Galactic Superwinds, and $M_{\bullet}-\sigma$ ”. In: *ApJL* 635, pp. L121–L123. DOI: [10.1086/499430](https://doi.org/10.1086/499430). eprint: [astro-ph/0511034](https://arxiv.org/abs/astro-ph/0511034).
- King, A. and C. Nixon (2015). “AGN flickering and chaotic accretion”. In: *MNRAS* 453, pp. L46–L47. DOI: [10 . 1093 / mnrasl / slv098](https://doi.org/10.1093/mnrasl/slv098). arXiv: [1507 . 05960](https://arxiv.org/abs/1507.05960) [[astro-ph.HE](https://arxiv.org/abs/1507.05960)].

- King, A. and K. Pounds (2015). "Powerful Outflows and Feedback from Active Galactic Nuclei". In: *ARA&A* 53, pp. 115–154. DOI: [10.1146/annurev-astro-082214-122316](https://doi.org/10.1146/annurev-astro-082214-122316). arXiv: [1503.05206](https://arxiv.org/abs/1503.05206).
- King, A. R. (2010). "Black hole outflows". In: *MNRAS* 402, pp. 1516–1522. DOI: [10.1111/j.1365-2966.2009.16013.x](https://doi.org/10.1111/j.1365-2966.2009.16013.x). arXiv: [0911.1639](https://arxiv.org/abs/0911.1639).
- King, A. R. and K. A. Pounds (2003). "Black hole winds". In: *MNRAS* 345, pp. 657–659. DOI: [10.1046/j.1365-8711.2003.06980.x](https://doi.org/10.1046/j.1365-8711.2003.06980.x). eprint: [astro-ph/0305541](https://arxiv.org/abs/astro-ph/0305541).
- King, A. R. and J. E. Pringle (2006). "Growing supermassive black holes by chaotic accretion". In: *MNRAS* 373, pp. L90–L92. DOI: [10.1111/j.1745-3933.2006.00249.x](https://doi.org/10.1111/j.1745-3933.2006.00249.x). eprint: [astro-ph/0609598](https://arxiv.org/abs/astro-ph/0609598).
- (2007). "Fuelling active galactic nuclei". In: *MNRAS* 377, pp. L25–L28. DOI: [10.1111/j.1745-3933.2007.00296.x](https://doi.org/10.1111/j.1745-3933.2007.00296.x). eprint: [astro-ph/0701679](https://arxiv.org/abs/astro-ph/0701679).
- King, A. R., J. E. Pringle, and J. A. Hofmann (2008). "The evolution of black hole mass and spin in active galactic nuclei". In: *MNRAS* 385, pp. 1621–1627. DOI: [10.1111/j.1365-2966.2008.12943.x](https://doi.org/10.1111/j.1365-2966.2008.12943.x). arXiv: [0801.1564](https://arxiv.org/abs/0801.1564).
- King, A. R., J. E. Pringle, and M. Livio (2007). "Accretion disc viscosity: how big is alpha?" In: *MNRAS* 376, pp. 1740–1746. DOI: [10.1111/j.1365-2966.2007.11556.x](https://doi.org/10.1111/j.1365-2966.2007.11556.x). eprint: [astro-ph/0701803](https://arxiv.org/abs/astro-ph/0701803).
- King, A. R., K. Zubovas, and C. Power (2011). "Large-scale outflows in galaxies". In: *MNRAS* 415, pp. L6–L10. DOI: [10.1111/j.1745-3933.2011.01067.x](https://doi.org/10.1111/j.1745-3933.2011.01067.x). arXiv: [1104.3682](https://arxiv.org/abs/1104.3682).
- King, A. R. et al. (2005). "Aligning spinning black holes and accretion discs". In: *MNRAS* 363, pp. 49–56. DOI: [10.1111/j.1365-2966.2005.09378.x](https://doi.org/10.1111/j.1365-2966.2005.09378.x). eprint: [astro-ph/0507098](https://arxiv.org/abs/astro-ph/0507098).
- Kızıltan, B., H. Baumgardt, and A. Loeb (2017). "An intermediate-mass black hole in the centre of the globular cluster 47 Tucanae". In: *NATURE* 542, pp. 203–205. DOI: [10.1038/nature21361](https://doi.org/10.1038/nature21361). arXiv: [1702.02149](https://arxiv.org/abs/1702.02149).
- Kolmogorov, A. N. (1991). "The local structure of turbulence in incompressible viscous fluid for very large Reynolds numbers". In: *Proceedings of the Royal Society of London Series A* 434, pp. 9–13. DOI: [10.1098/rspa.1991.0075](https://doi.org/10.1098/rspa.1991.0075).
- Kolmogorov, A.N. (1941). "The Local Structure of Turbulence in Incompressible Viscous Fluid for Very Large Reynolds' Numbers". In: *Akademiia Nauk SSSR Doklady* 30, pp. 301–305.

- Kolykhalov, P. I. and R. A. Syunyaev (1980). "The Outer Parts of the Accretion Disks around Supermassive Black Holes in Galaxy Nuclei and Quasars". In: *Soviet Astronomy Letters* 6, pp. 357–361.
- Kormendy, J., R. Bender, and M. E. Cornell (2011). "Supermassive black holes do not correlate with galaxy disks or pseudobulges". In: *NATURE* 469, pp. 374–376. DOI: [10.1038/nature09694](https://doi.org/10.1038/nature09694). arXiv: [1101.3781](https://arxiv.org/abs/1101.3781).
- Kormendy, J. and L. C. Ho (2013). "Coevolution (Or Not) of Supermassive Black Holes and Host Galaxies". In: *ARA&A* 51, pp. 511–653. DOI: [10.1146/annurev-astro-082708-101811](https://doi.org/10.1146/annurev-astro-082708-101811). arXiv: [1304.7762](https://arxiv.org/abs/1304.7762).
- Kormendy, J. and D. Richstone (1992). "Evidence for a supermassive black hole in NGC 3115". In: *ApJ* 393, pp. 559–578. DOI: [10.1086/171528](https://doi.org/10.1086/171528).
- (1995). "Inward Bound—The Search For Supermassive Black Holes In Galactic Nuclei". In: *ARA&A* 33, p. 581. DOI: [10.1146/annurev.aa.33.090195.003053](https://doi.org/10.1146/annurev.aa.33.090195.003053).
- Koushiappas, S. M., J. S. Bullock, and A. Dekel (2004). "Massive black hole seeds from low angular momentum material". In: *MNRAS* 354, pp. 292–304. DOI: [10.1111/j.1365-2966.2004.08190.x](https://doi.org/10.1111/j.1365-2966.2004.08190.x). eprint: [astro-ph/0311487](https://arxiv.org/abs/astro-ph/0311487).
- Kozai, Y. (1962). "Secular perturbations of asteroids with high inclination and eccentricity". In: *AJ* 67, p. 591. DOI: [10.1086/108790](https://doi.org/10.1086/108790).
- Kraemer, S. B., F. Tombesi, and M. C. Bottorff (2018). "Physical Conditions in Ultra-fast Outflows in AGN". In: *ApJ* 852, 35, p. 35. DOI: [10.3847/1538-4357/aa9ce0](https://doi.org/10.3847/1538-4357/aa9ce0). arXiv: [1711.07965](https://arxiv.org/abs/1711.07965).
- Krolik, J. H. and M. C. Begelman (1988). "Molecular tori in Seyfert galaxies - Feeding the monster and hiding it". In: *ApJ* 329, pp. 702–711. DOI: [10.1086/166414](https://doi.org/10.1086/166414).
- Lacy, J. H. et al. (1980). "Observations of the motion and distribution of the ionized gas in the central parsec of the Galaxy. II." In: *ApJ* 241, pp. 132–146. DOI: [10.1086/158324](https://doi.org/10.1086/158324).
- Larkin, A. C. and D. E. McLaughlin (2016). "Dark-matter haloes and the $M-\sigma$ relation for supermassive black holes". In: *MNRAS* 462, pp. 1864–1881. DOI: [10.1093/mnras/stw1749](https://doi.org/10.1093/mnras/stw1749). arXiv: [1607.05478](https://arxiv.org/abs/1607.05478).
- Larson, R. B. (1981). "Turbulence and star formation in molecular clouds". In: *MNRAS* 194, pp. 809–826. DOI: [10.1093/mnras/194.4.809](https://doi.org/10.1093/mnras/194.4.809).
- Lasota, J.-P. (2001). "The disc instability model of dwarf novae and low-mass X-ray binary transients". In: *NAR* 45, pp. 449–508. DOI: [10.1016/S1387-6473\(01\)00112-9](https://doi.org/10.1016/S1387-6473(01)00112-9). eprint: [astro-ph/0102072](https://arxiv.org/abs/astro-ph/0102072).

- Latif, M. A. and A. Ferrara (2016). "Formation of Supermassive Black Hole Seeds". In: *PASA* 33, e051, e051. DOI: [10.1017/pasa.2016.41](https://doi.org/10.1017/pasa.2016.41). arXiv: [1605.07391](https://arxiv.org/abs/1605.07391).
- Latif, M. A. et al. (2016). "Impact of Dust Cooling on Direct-collapse Black Hole Formation". In: *ApJ* 823, 40, p. 40. DOI: [10.3847/0004-637X/823/1/40](https://doi.org/10.3847/0004-637X/823/1/40). arXiv: [1509.07034](https://arxiv.org/abs/1509.07034).
- Lauer, T. R. et al. (1995). "The Centers of Early-Type Galaxies with HST.I.An Observational Survey". In: *AJ* 110, p. 2622. DOI: [10.1086/117719](https://doi.org/10.1086/117719).
- Lemaître, A. G. (1931). "Contributions to a British Association Discussion on the Evolution of the Universe." In: *NATURE* 128, pp. 704–706. DOI: [10.1038/128704a0](https://doi.org/10.1038/128704a0).
- Levin, Yuri (2007). "Starbursts near supermassive black holes: young stars in the Galactic Centre, and gravitational waves in LISA band". In: *MNRAS* 374, pp. 515–524. DOI: [10.1111/j.1365-2966.2006.11155.x](https://doi.org/10.1111/j.1365-2966.2006.11155.x). arXiv: [astro-ph/0603583](https://arxiv.org/abs/astro-ph/0603583) [astro-ph].
- Lidov, M. L. (1962). "The evolution of orbits of artificial satellites of planets under the action of gravitational perturbations of external bodies". In: *Planetary and Space Science* 9, pp. 719–759. DOI: [10.1016/0032-0633\(62\)90129-0](https://doi.org/10.1016/0032-0633(62)90129-0).
- Lin, D. N. C. and J. Papaloizou (1980). "On the structure and evolution of the primordial solar nebula". In: *MNRAS* 191, pp. 37–48. DOI: [10.1093/mnras/191.1.37](https://doi.org/10.1093/mnras/191.1.37).
- Liu, Haoyu Baobab et al. (2013). "Interstellar Medium Processing in the Inner 20 pc in Galactic Center". In: *ApJ* 770, 44, p. 44. DOI: [10.1088/0004-637X/770/1/44](https://doi.org/10.1088/0004-637X/770/1/44). arXiv: [1304.7573](https://arxiv.org/abs/1304.7573) [astro-ph.GA].
- Lodato, G. (2007). "Self-gravitating accretion discs". In: *Nuovo Cimento Rivista Serie* 30. DOI: [10.1393/ncr/i2007-10022-x](https://doi.org/10.1393/ncr/i2007-10022-x). arXiv: [0801.3848](https://arxiv.org/abs/0801.3848).
- Lodato, G. and P. Natarajan (2006). "Supermassive black hole formation during the assembly of pre-galactic discs". In: *MNRAS* 371, pp. 1813–1823. DOI: [10.1111/j.1365-2966.2006.10801.x](https://doi.org/10.1111/j.1365-2966.2006.10801.x). eprint: [astro-ph/0606159](https://arxiv.org/abs/astro-ph/0606159).
- Lodato, G. and W. K. M. Rice (2004). "Testing the locality of transport in self-gravitating accretion discs". In: *MNRAS* 351, pp. 630–642. DOI: [10.1111/j.1365-2966.2004.07811.x](https://doi.org/10.1111/j.1365-2966.2004.07811.x). arXiv: [astro-ph/0403185](https://arxiv.org/abs/astro-ph/0403185) [astro-ph].
- (2005). "Testing the locality of transport in self-gravitating accretion discs - II. The massive disc case". In: *MNRAS* 358, pp. 1489–1500. DOI: [10.1111/j.1365-2966.2005.08875.x](https://doi.org/10.1111/j.1365-2966.2005.08875.x). arXiv: [astro-ph/0501638](https://arxiv.org/abs/astro-ph/0501638) [astro-ph].

- Loeb, A. and F. A. Rasio (1994). "Collapse of primordial gas clouds and the formation of quasar black holes". In: *ApJ* 432, pp. 52–61. DOI: [10.1086/174548](https://doi.org/10.1086/174548). eprint: [astro-ph/9401026](https://arxiv.org/abs/astro-ph/9401026).
- Longinotti, A. L. et al. (2018). "Early Science with the Large Millimeter Telescope: An Energy-driven Wind Revealed by Massive Molecular and Fast X-Ray Outflows in the Seyfert Galaxy IRAS 17020+4544". In: *ApJL* 867, L11, p. L11. DOI: [10.3847/2041-8213/aae5fd](https://doi.org/10.3847/2041-8213/aae5fd). arXiv: [1810.01941](https://arxiv.org/abs/1810.01941).
- Lovelace, R. V. E. (1976). "Dynamo model of double radio sources". In: *NATURE* 262, pp. 649–652. DOI: [10.1038/262649a0](https://doi.org/10.1038/262649a0).
- Lucas, W. E. et al. (2013). "Misaligned streamers around a Galactic Centre black hole from a single cloud's infall". In: *MNRAS* 433, pp. 353–365. DOI: [10.1093/mnras/stt727](https://doi.org/10.1093/mnras/stt727). arXiv: [1305.0012](https://arxiv.org/abs/1305.0012) [[astro-ph](https://arxiv.org/abs/astro-ph).GA].
- Lucy, L. B. (1977). "A numerical approach to the testing of the fission hypothesis". In: *AJ* 82, pp. 1013–1024. DOI: [10.1086/112164](https://doi.org/10.1086/112164).
- Lucy, L. B. and P. M. Solomon (1970). "Mass Loss by Hot Stars". In: *ApJ* 159, p. 879. DOI: [10.1086/150365](https://doi.org/10.1086/150365).
- Lynden-Bell, D. (1969). "Galactic Nuclei as Collapsed Old Quasars". In: *NATURE* 223, pp. 690–694. DOI: [10.1038/223690a0](https://doi.org/10.1038/223690a0).
- Lynden-Bell, D. and J. E. Pringle (1974). "The evolution of viscous discs and the origin of the nebular variables." In: *MNRAS* 168, pp. 603–637. DOI: [10.1093/mnras/168.3.603](https://doi.org/10.1093/mnras/168.3.603).
- Lynden-Bell, D. and M. J. Rees (1971). "On quasars, dust and the galactic centre". In: *MNRAS* 152, p. 461. DOI: [10.1093/mnras/152.4.461](https://doi.org/10.1093/mnras/152.4.461).
- Maccarone, T. J., E. Gallo, and R. Fender (2003). "The connection between radio-quiet active galactic nuclei and the high/soft state of X-ray binaries". In: *MNRAS* 345, pp. L19–L24. DOI: [10.1046/j.1365-8711.2003.07161.x](https://doi.org/10.1046/j.1365-8711.2003.07161.x). eprint: [astro-ph/0309137](https://arxiv.org/abs/astro-ph/0309137).
- Magorrian, J. et al. (1998). "The Demography of Massive Dark Objects in Galaxy Centers". In: *AJ* 115, pp. 2285–2305. DOI: [10.1086/300353](https://doi.org/10.1086/300353). eprint: [astro-ph/9708072](https://arxiv.org/abs/astro-ph/9708072).
- Maiolino, R. and G. H. Rieke (1995). "Low-Luminosity and Obscured Seyfert Nuclei in Nearby Galaxies". In: *ApJ* 454, p. 95. DOI: [10.1086/176468](https://doi.org/10.1086/176468).
- Maiolino, R. et al. (1998). "Heavy obscuration in X-ray weak AGNs". In: *A&A* 338, pp. 781–794. eprint: [astro-ph/9806055](https://arxiv.org/abs/astro-ph/9806055).

- Makino, J. (1991). "Optimal order and time-step criterion for Aarseth-type N-body integrators". In: *ApJ* 369, pp. 200–212. DOI: [10.1086/169751](https://doi.org/10.1086/169751).
- Malizia, A. et al. (2009). "The fraction of Compton-thick sources in an INTEGRAL complete AGN sample". In: *MNRAS* 399, pp. 944–951. DOI: [10.1111/j.1365-2966.2009.15330.x](https://doi.org/10.1111/j.1365-2966.2009.15330.x). arXiv: [0906.5544](https://arxiv.org/abs/0906.5544) [astro-ph.HE].
- Manwell, T. and M. Simon (1966). "Spectral Density of the Possibly Random Fluctuations of 3C 273". In: *NATURE* 212, pp. 1224–1225. DOI: [10.1038/2121224a0](https://doi.org/10.1038/2121224a0).
- Mapelli, M. and A. Gualandris (2016). "Star Formation and Dynamics in the Galactic Centre". In: *Lecture Notes in Physics, Berlin Springer Verlag*. Ed. by F. Haardt et al. Vol. 905. Lecture Notes in Physics, Berlin Springer Verlag, p. 205. DOI: [10.1007/978-3-319-19416-5_6](https://doi.org/10.1007/978-3-319-19416-5_6). arXiv: [1505.05473](https://arxiv.org/abs/1505.05473).
- Mapelli, M. et al. (2012). "In Situ Formation of SgrA* Stars Via Disk Fragmentation: Parent Cloud Properties and Thermodynamics". In: *ApJ* 749, 168, p. 168. DOI: [10.1088/0004-637X/749/2/168](https://doi.org/10.1088/0004-637X/749/2/168). arXiv: [1202.0555](https://arxiv.org/abs/1202.0555) [astro-ph.GA].
- Mapelli, Michela, Alessia Gualandris, and Tristen Hayfield (2013). "Perturbations induced by a molecular cloud on the young stellar disc in the Galactic Centre". In: *MNRAS* 436, pp. 3809–3819. DOI: [10.1093/mnras/stt1858](https://doi.org/10.1093/mnras/stt1858). arXiv: [1310.0024](https://arxiv.org/abs/1310.0024) [astro-ph.GA].
- Mapelli, Michela and Alessandro A. Trani (2016). "Modelling the formation of the circumnuclear ring in the Galactic centre". In: *A&A* 585, A161, A161. DOI: [10.1051/0004-6361/201527195](https://doi.org/10.1051/0004-6361/201527195).
- Martin, R. G. et al. (2018). "Circumbinary discs around merging stellar-mass black holes". In: *MNRAS* 480, pp. 4732–4737. DOI: [10.1093/mnras/sty2178](https://doi.org/10.1093/mnras/sty2178). arXiv: [1808.06023](https://arxiv.org/abs/1808.06023) [astro-ph.HE].
- Mayer, C. H., T. P. McCullough, and R. M. Sloanaker (1958). "Observations of Venus at 3.15-CM Wave Length." In: *ApJ* 127, p. 1. DOI: [10.1086/146433](https://doi.org/10.1086/146433).
- McConnell, N. J. and C.-P. Ma (2013). "Revisiting the Scaling Relations of Black Hole Masses and Host Galaxy Properties". In: *ApJ* 764, 184, p. 184. DOI: [10.1088/0004-637X/764/2/184](https://doi.org/10.1088/0004-637X/764/2/184). arXiv: [1211.2816](https://arxiv.org/abs/1211.2816).
- McHardy, I. M. et al. (2006). "Active galactic nuclei as scaled-up Galactic black holes". In: *NATURE* 444, pp. 730–732. DOI: [10.1038/nature05389](https://doi.org/10.1038/nature05389). eprint: [astro-ph/0612273](https://arxiv.org/abs/astro-ph/0612273).

- McKernan, B., T. Yaqoob, and C. S. Reynolds (2007). "A soft X-ray study of type I active galactic nuclei observed with Chandra high-energy transmission grating spectrometer". In: *MNRAS* 379, pp. 1359–1372. DOI: [10.1111/j.1365-2966.2007.11993.x](https://doi.org/10.1111/j.1365-2966.2007.11993.x). arXiv: [0705.2542](https://arxiv.org/abs/0705.2542).
- McLure, R. J. and J. S. Dunlop (2002). "On the black hole-bulge mass relation in active and inactive galaxies". In: *MNRAS* 331, pp. 795–804. DOI: [10.1046/j.1365-8711.2002.05236.x](https://doi.org/10.1046/j.1365-8711.2002.05236.x). eprint: [astro-ph/0108417](https://arxiv.org/abs/astro-ph/0108417).
- McNamara, B. R. et al. (2005). "The heating of gas in a galaxy cluster by X-ray cavities and large-scale shock fronts". In: *NATURE* 433, pp. 45–47. DOI: [10.1038/nature03202](https://doi.org/10.1038/nature03202).
- Merritt, D. (2004). "Single and Binary Black Holes and their Influence on Nuclear Structure". In: *Coevolution of Black Holes and Galaxies*, p. 263. eprint: [astro-ph/0301257](https://arxiv.org/abs/astro-ph/0301257).
- Merritt, D. and L. Ferrarese (2001). "The $M_{\text{BH}}-\sigma$ Relation for Supermassive Black Holes". In: *ApJ* 547, pp. 140–145. DOI: [10.1086/318372](https://doi.org/10.1086/318372). eprint: [astro-ph/0008310](https://arxiv.org/abs/astro-ph/0008310).
- Mezcua, M. et al. (2018). "Intermediate-mass black holes in dwarf galaxies out to redshift 2.4 in the Chandra COSMOS-Legacy Survey". In: *MNRAS* 478, pp. 2576–2591. DOI: [10.1093/mnras/sty1163](https://doi.org/10.1093/mnras/sty1163). arXiv: [1802.01567](https://arxiv.org/abs/1802.01567).
- Miyoshi, M. et al. (1995). "Evidence for a black hole from high rotation velocities in a sub-parsec region of NGC4258". In: *NATURE* 373, pp. 127–129. DOI: [10.1038/373127a0](https://doi.org/10.1038/373127a0).
- Moderski, R., M. Sikora, and J.-P. Lasota (1998). "On the spin paradigm and the radio dichotomy of quasars". In: *MNRAS* 301, pp. 142–148. DOI: [10.1046/j.1365-8711.1998.02009.x](https://doi.org/10.1046/j.1365-8711.1998.02009.x). eprint: [astro-ph/9804140](https://arxiv.org/abs/astro-ph/9804140).
- Moe, M. et al. (2009). "Quasar Outflow Contribution to AGN Feedback: Observations of QSO SDSS J0838+2955". In: *ApJ* 706, pp. 525–534. DOI: [10.1088/0004-637X/706/1/525](https://doi.org/10.1088/0004-637X/706/1/525). arXiv: [0911.3332](https://arxiv.org/abs/0911.3332).
- Monaghan, J. J. (2012). "Smoothed Particle Hydrodynamics and Its Diverse Applications". In: *Annual Review of Fluid Mechanics* 44, pp. 323–346. DOI: [10.1146/annurev-fluid-120710-101220](https://doi.org/10.1146/annurev-fluid-120710-101220).
- Monaghan, J. J. and J. C. Lattanzio (1985). "A refined particle method for astrophysical problems". In: *A&A* 149, pp. 135–143.

- Montero-Castaño, María, Robeson M. Herrnstein, and Paul T. P. Ho (2009). “Gas Infall Toward Sgr A* from the Clumpy Circumnuclear Disk”. In: *ApJ* 695, pp. 1477–1494. DOI: [10.1088/0004-637X/695/2/1477](https://doi.org/10.1088/0004-637X/695/2/1477). arXiv: [0903.0886](https://arxiv.org/abs/0903.0886) [astro-ph.GA].
- Morris, D., H. P. Palmer, and A. R. Thompson (1957). “Five radio sources of small angular diameter”. In: *The Observatory* 77, pp. 103–106.
- Mortlock, D. J. et al. (2011). “A luminous quasar at a redshift of $z = 7.085$ ”. In: *NATURE* 474, pp. 616–619. DOI: [10.1038/nature10159](https://doi.org/10.1038/nature10159). arXiv: [1106.6088](https://arxiv.org/abs/1106.6088) [astro-ph.CO].
- Murphy, J. W. et al. (2018). “The Progenitor Age and Mass of the Black Hole Formation Candidate N6946-BH1”. In: *ApJ* 860, 117, p. 117. DOI: [10.3847/1538-4357/aac2be](https://doi.org/10.3847/1538-4357/aac2be). arXiv: [1803.00024](https://arxiv.org/abs/1803.00024) [astro-ph.SR].
- Nayakshin, S. (2014). “Two-phase model for black hole feeding and feedback”. In: *MNRAS* 437, pp. 2404–2411. DOI: [10.1093/mnras/stt2059](https://doi.org/10.1093/mnras/stt2059). arXiv: [1311.4492](https://arxiv.org/abs/1311.4492).
- Nayakshin, S. and J. Cuadra (2005). “A self-gravitating accretion disk in Sgr A* a few million years ago: Is Sgr A* a failed quasar?” In: *A&A* 437, pp. 437–445. DOI: [10.1051/0004-6361:20042052](https://doi.org/10.1051/0004-6361:20042052). arXiv: [astro-ph/0409541](https://arxiv.org/abs/astro-ph/0409541) [astro-ph].
- Nayakshin, S. and K. Zubovas (2012). “Quasar feedback: accelerated star formation and chaotic accretion”. In: *MNRAS* 427, pp. 372–378. DOI: [10.1111/j.1365-2966.2012.21950.x](https://doi.org/10.1111/j.1365-2966.2012.21950.x). arXiv: [1207.7200](https://arxiv.org/abs/1207.7200).
- (2018). “Sgr A* envelope explosion and the young stars in the centre of the Milky Way”. In: *ArXiv e-prints*. arXiv: [1804.02914](https://arxiv.org/abs/1804.02914).
- Nayakshin, Sergei, Jorge Cuadra, and Volker Springel (2007). “Simulations of star formation in a gaseous disc around Sgr A* - a failed active galactic nucleus”. In: *MNRAS* 379, pp. 21–33. DOI: [10.1111/j.1365-2966.2007.11938.x](https://doi.org/10.1111/j.1365-2966.2007.11938.x). arXiv: [astro-ph/0701141](https://arxiv.org/abs/astro-ph/0701141) [astro-ph].
- Negri, A. and M. Volonteri (2017). “Black hole feeding and feedback: the physics inside the ‘sub-grid’”. In: *MNRAS* 467, pp. 3475–3492. DOI: [10.1093/mnras/stx362](https://doi.org/10.1093/mnras/stx362). arXiv: [1610.04753](https://arxiv.org/abs/1610.04753).
- Nelson, E. J. et al. (2016). “Where Stars Form: Inside-out Growth and Coherent Star Formation from HST H α Maps of 3200 Galaxies across the Main Sequence at $0.7 < z < 1.5$ ”. In: *ApJ* 828, 27, p. 27. DOI: [10.3847/0004-637X/828/1/27](https://doi.org/10.3847/0004-637X/828/1/27). arXiv: [1507.03999](https://arxiv.org/abs/1507.03999).
- Newman, E. T. and A. I. Janis (1965). “Note on the Kerr Spinning-Particle Metric”. In: *Journal of Mathematical Physics* 6, pp. 915–917. DOI: [10.1063/1.1704350](https://doi.org/10.1063/1.1704350).

- Newton, I., A. Motte, and F. Cajori (1966). *The mathematical principles of natural philosophy and his system of the world*.
- Niederreiter, Harald (1992). *Random Number Generation and quasi-Monte Carlo Methods*. Philadelphia, PA, USA: Society for Industrial and Applied Mathematics. ISBN: 0-89871-295-5.
- Nixon, C. J. et al. (2011). “Retrograde accretion and merging supermassive black holes”. In: *MNRAS* 412, pp. 1591–1598. DOI: [10.1111/j.1365-2966.2010.17952.x](https://doi.org/10.1111/j.1365-2966.2010.17952.x). arXiv: [1011.1914](https://arxiv.org/abs/1011.1914) [astro-ph.HE].
- Nixon, Chris et al. (2012). “Tearing up the Disk: How Black Holes Accrete”. In: *ApJ* 757, L24, p. L24. DOI: [10.1088/2041-8205/757/2/L24](https://doi.org/10.1088/2041-8205/757/2/L24). arXiv: [1209.1393](https://arxiv.org/abs/1209.1393) [astro-ph.HE].
- Nixon, Christopher J., Andrew R. King, and Daniel J. Price (2012). “Rapid AGN accretion from counter-rotating discs”. In: *MNRAS* 422, pp. 2547–2552. DOI: [10.1111/j.1365-2966.2012.20814.x](https://doi.org/10.1111/j.1365-2966.2012.20814.x). arXiv: [1203.0008](https://arxiv.org/abs/1203.0008) [astro-ph.HE].
- Noguchi, M. (1999). “Early Evolution of Disk Galaxies: Formation of Bulges in Clumpy Young Galactic Disks”. In: *ApJ* 514, pp. 77–95. DOI: [10.1086/306932](https://doi.org/10.1086/306932). eprint: [astro-ph/9806355](https://arxiv.org/abs/astro-ph/9806355).
- Nordström, G. (1918). “On the Energy of the Gravitation field in Einstein’s Theory”. In: *Koninklijke Nederlandse Akademie van Wetenschappen Proceedings Series B Physical Sciences* 20, pp. 1238–1245.
- Novak, G. S., J. P. Ostriker, and L. Ciotti (2011). “Feedback from Central Black Holes in Elliptical Galaxies: Two-dimensional Models Compared to One-dimensional Models”. In: *ApJ* 737, 26, p. 26. DOI: [10.1088/0004-637X/737/1/26](https://doi.org/10.1088/0004-637X/737/1/26). arXiv: [1007.3505](https://arxiv.org/abs/1007.3505).
- Oesch, P. A. et al. (2015). “A Spectroscopic Redshift Measurement for a Luminous Lyman Break Galaxy at $z = 7.730$ Using Keck/MOSFIRE”. In: *ApJL* 804, L30, p. L30. DOI: [10.1088/2041-8205/804/2/L30](https://doi.org/10.1088/2041-8205/804/2/L30). arXiv: [1502.05399](https://arxiv.org/abs/1502.05399).
- Oesch, P. A. et al. (2016). “A Remarkably Luminous Galaxy at $z=11.1$ Measured with Hubble Space Telescope Grism Spectroscopy”. In: *ApJ* 819, 129, p. 129. DOI: [10.3847/0004-637X/819/2/129](https://doi.org/10.3847/0004-637X/819/2/129). arXiv: [1603.00461](https://arxiv.org/abs/1603.00461).
- Oldham, L. J. and M. W. Auger (2016). “Galaxy structure from multiple tracers - II. M87 from parsec to megaparsec scales”. In: *MNRAS* 457, pp. 421–439. DOI: [10.1093/mnras/stv2982](https://doi.org/10.1093/mnras/stv2982). arXiv: [1601.01323](https://arxiv.org/abs/1601.01323).

- Oppenheimer, B. D. et al. (2018). “Flickering AGN can explain the strong circumgalactic O VI observed by COS-Halos”. In: *MNRAS* 474, pp. 4740–4755. DOI: [10.1093/mnras/stx2967](https://doi.org/10.1093/mnras/stx2967). arXiv: [1705.07897](https://arxiv.org/abs/1705.07897).
- Oppenheimer, J. R. and H. Snyder (1939). “On Continued Gravitational Contraction”. In: *Physical Review* 56, pp. 455–459. DOI: [10.1103/PhysRev.56.455](https://doi.org/10.1103/PhysRev.56.455).
- Oppenheimer, J. R. and G. M. Volkoff (1939). “On Massive Neutron Cores”. In: *Physical Review* 55, pp. 374–381. DOI: [10.1103/PhysRev.55.374](https://doi.org/10.1103/PhysRev.55.374).
- Orosz, J. A. et al. (2011). “The Mass of the Black Hole in Cygnus X-1”. In: *ApJ* 742, 84, p. 84. DOI: [10.1088/0004-637X/742/2/84](https://doi.org/10.1088/0004-637X/742/2/84). arXiv: [1106.3689](https://arxiv.org/abs/1106.3689) [[astro-ph.HE](#)].
- Pacucci, F. et al. (2018). “Glimmering in the Dark: Modeling the Low-mass End of the $M_{\text{BH}}-\sigma$ Relation and of the Quasar Luminosity Function”. In: *ApJL* 864, L6, p. L6. DOI: [10.3847/2041-8213/aad8b2](https://doi.org/10.3847/2041-8213/aad8b2). arXiv: [1808.09452](https://arxiv.org/abs/1808.09452).
- Paumard, T. et al. (2006). “The Two Young Star Disks in the Central Parsec of the Galaxy: Properties, Dynamics, and Formation”. In: *ApJ* 643, pp. 1011–1035. DOI: [10.1086/503273](https://doi.org/10.1086/503273). eprint: [astro-ph/0601268](https://arxiv.org/abs/astro-ph/0601268).
- Peebles, P. J. E. (1972). “Star Distribution Near a Collapsed Object”. In: *ApJ* 178, pp. 371–376. DOI: [10.1086/151797](https://doi.org/10.1086/151797).
- Peng, C. Y. (2007). “How Mergers May Affect the Mass Scaling Relation between Gravitationally Bound Systems”. In: *ApJ* 671, pp. 1098–1107. DOI: [10.1086/522774](https://doi.org/10.1086/522774). arXiv: [0704.1860](https://arxiv.org/abs/0704.1860).
- Peng, Y.-j. et al. (2010). “Mass and Environment as Drivers of Galaxy Evolution in SDSS and zCOSMOS and the Origin of the Schechter Function”. In: *ApJ* 721, pp. 193–221. DOI: [10.1088/0004-637X/721/1/193](https://doi.org/10.1088/0004-637X/721/1/193). arXiv: [1003.4747](https://arxiv.org/abs/1003.4747) [[astro-ph.CO](#)].
- Penzias, A. A. and R. W. Wilson (1965). “A Measurement of Excess Antenna Temperature at 4080 Mc/s.” In: *ApJ* 142, pp. 419–421. DOI: [10.1086/148307](https://doi.org/10.1086/148307).
- Perets, H. B. et al. (2009). “Dynamical Evolution of the Young Stars in the Galactic Center: N-body Simulations of the S-Stars”. In: *ApJ* 702, pp. 884–889. DOI: [10.1088/0004-637X/702/2/884](https://doi.org/10.1088/0004-637X/702/2/884). arXiv: [0903.2912](https://arxiv.org/abs/0903.2912) [[astro-ph.GA](#)].
- Perna, R., D. Lazzati, and B. Giacomazzo (2016). “Short Gamma-Ray Bursts from the Merger of Two Black Holes”. In: *ApJL* 821, L18, p. L18. DOI: [10.3847/2041-8205/821/1/L18](https://doi.org/10.3847/2041-8205/821/1/L18). arXiv: [1602.05140](https://arxiv.org/abs/1602.05140) [[astro-ph.HE](#)].
- Peterson, B. M. et al. (2002). “Steps toward Determination of the Size and Structure of the Broad-Line Region in Active Galactic Nuclei. XVI. A 13 Year Study

- of Spectral Variability in NGC 5548". In: *ApJ* 581, pp. 197–204. DOI: [10.1086/344197](https://doi.org/10.1086/344197). eprint: [astro-ph/0208064](https://arxiv.org/abs/astro-ph/0208064).
- Planck Collaboration et al. (2014). "Planck 2013 results. I. Overview of products and scientific results". In: *A&A* 571, A1, A1. DOI: [10.1051/0004-6361/201321529](https://doi.org/10.1051/0004-6361/201321529). arXiv: [1303.5062](https://arxiv.org/abs/1303.5062).
- Planck Collaboration et al. (2016). "Planck 2015 results. XIII. Cosmological parameters". In: *A&A* 594, A13, A13. DOI: [10.1051/0004-6361/201525830](https://doi.org/10.1051/0004-6361/201525830). arXiv: [1502.01589](https://arxiv.org/abs/1502.01589).
- Podigachoski, P. et al. (2015). "The Unification of Powerful Quasars and Radio Galaxies and Their Relation to Other Massive Galaxies". In: *ApJL* 806, L11, p. L11. DOI: [10.1088/2041-8205/806/1/L11](https://doi.org/10.1088/2041-8205/806/1/L11). arXiv: [1505.03569](https://arxiv.org/abs/1505.03569).
- Poindexter, S., N. Morgan, and C. S. Kochanek (2008). "The Spatial Structure of an Accretion Disk". In: *ApJ* 673, pp. 34–38. DOI: [10.1086/524190](https://doi.org/10.1086/524190). arXiv: [0707.0003](https://arxiv.org/abs/0707.0003).
- Portegies Zwart, S. F. and S. L. W. McMillan (2002). "The Runaway Growth of Intermediate-Mass Black Holes in Dense Star Clusters". In: *ApJ* 576, pp. 899–907. DOI: [10.1086/341798](https://doi.org/10.1086/341798). eprint: [astro-ph/0201055](https://arxiv.org/abs/astro-ph/0201055).
- Portegies Zwart, S. F., S. L. W. McMillan, and O. Gerhard (2003). "The Origin of IRS 16: Dynamically Driven In-Spiral of a Dense Star Cluster to the Galactic Center?" In: *ApJ* 593, pp. 352–357. DOI: [10.1086/376439](https://doi.org/10.1086/376439). eprint: [astro-ph/0303599](https://arxiv.org/abs/astro-ph/0303599).
- Portegies Zwart, S. F. et al. (2004). "Formation of massive black holes through runaway collisions in dense young star clusters". In: *NATURE* 428, pp. 724–726. DOI: [10.1038/nature02448](https://doi.org/10.1038/nature02448). eprint: [astro-ph/0402622](https://arxiv.org/abs/astro-ph/0402622).
- Potter, Douglas, Joachim Stadel, and Romain Teyssier (2017). "PKDGRAV3: beyond trillion particle cosmological simulations for the next era of galaxy surveys". In: *Computational Astrophysics and Cosmology* 4.1, p. 2. ISSN: 2197-7909. DOI: [10.1186/s40668-017-0021-1](https://doi.org/10.1186/s40668-017-0021-1). URL: <https://doi.org/10.1186/s40668-017-0021-1>.
- Pounds, K. A. and J. N. Reeves (2009). "Quantifying the fast outflow in the luminous Seyfert galaxy PG1211+143". In: *MNRAS* 397, pp. 249–257. DOI: [10.1111/j.1365-2966.2009.14971.x](https://doi.org/10.1111/j.1365-2966.2009.14971.x). arXiv: [0811.3108](https://arxiv.org/abs/0811.3108).
- Pounds, K. A. et al. (2003). "Evidence of a high-velocity ionized outflow in a second narrow-line quasar PG 0844+349". In: *MNRAS* 346, pp. 1025–1030. DOI: [10.1111/j.1365-2966.2003.07164.x](https://doi.org/10.1111/j.1365-2966.2003.07164.x). eprint: [astro-ph/0305571](https://arxiv.org/abs/astro-ph/0305571).

- Pounds, K. A. et al. (2018). “An ultrafast inflow in the luminous Seyfert PG1211+143”. In: *MNRAS* 481, pp. 1832–1838. DOI: [10.1093/mnras/sty2359](https://doi.org/10.1093/mnras/sty2359). arXiv: [1808.09373](https://arxiv.org/abs/1808.09373) [astro-ph.HE].
- Prendergast, K. H. and G. R. Burbidge (1968). “On the Nature of Some Galactic X-Ray Sources”. In: *ApJL* 151, p. L83. DOI: [10.1086/180148](https://doi.org/10.1086/180148).
- Price, D. J. (2012). “Smoothed particle hydrodynamics and magnetohydrodynamics”. In: *Journal of Computational Physics* 231, pp. 759–794. DOI: [10.1016/j.jcp.2010.12.011](https://doi.org/10.1016/j.jcp.2010.12.011). arXiv: [1012.1885](https://arxiv.org/abs/1012.1885) [astro-ph.IM].
- Pringle, J. E. (1981). “Accretion discs in astrophysics”. In: *ARA&A* 19, pp. 137–162. DOI: [10.1146/annurev.aa.19.090181.001033](https://doi.org/10.1146/annurev.aa.19.090181.001033).
- Pringle, J. E. and M. J. Rees (1972). “Accretion Disc Models for Compact X-Ray Sources”. In: *A&A* 21, p. 1.
- Proga, D., J. M. Stone, and J. E. Drew (1998). “Radiation-driven winds from luminous accretion discs”. In: *MNRAS* 295, p. 595. DOI: [10.1046/j.1365-8711.1998.01337.x](https://doi.org/10.1046/j.1365-8711.1998.01337.x). eprint: [astro-ph/9710305](https://arxiv.org/abs/astro-ph/9710305).
- Pu, H.-Y. and A. E. Broderick (2018). “Probing the Innermost Accretion Flow Geometry of Sgr A* with Event Horizon Telescope”. In: *ApJ* 863, 148, p. 148. DOI: [10.3847/1538-4357/aad086](https://doi.org/10.3847/1538-4357/aad086). arXiv: [1807.01817](https://arxiv.org/abs/1807.01817) [astro-ph.HE].
- Quilis, V., R. G. Bower, and M. L. Balogh (2001). “Bubbles, feedback and the intracluster medium: three-dimensional hydrodynamic simulations”. In: *MNRAS* 328, pp. 1091–1097. DOI: [10.1046/j.1365-8711.2001.04927.x](https://doi.org/10.1046/j.1365-8711.2001.04927.x). eprint: [astro-ph/0109022](https://arxiv.org/abs/astro-ph/0109022).
- Read, J. I. and T. Hayfield (2012). “SPHS: smoothed particle hydrodynamics with a higher order dissipation switch”. In: *MNRAS* 422, pp. 3037–3055. DOI: [10.1111/j.1365-2966.2012.20819.x](https://doi.org/10.1111/j.1365-2966.2012.20819.x). arXiv: [1111.6985](https://arxiv.org/abs/1111.6985) [astro-ph.CO].
- Rees, M. J. (1967). “Studies in radio source structure-III. Inverse Compton radiation from radio sources”. In: *MNRAS* 137, p. 429. DOI: [10.1093/mnras/137.4.429](https://doi.org/10.1093/mnras/137.4.429).
- (1975). “Quasars and radio galaxies”. In: *Seventh Texas Symposium on Relativistic Astrophysics*. Ed. by P. G. Bergman, E. J. Fenyves, and L. Motz. Vol. 262. Annals of the New York Academy of Sciences, pp. 449–461. DOI: [10.1111/j.1749-6632.1975.tb31462.x](https://doi.org/10.1111/j.1749-6632.1975.tb31462.x).
- Rees, M. J. and J. P. Ostriker (1977). “Cooling, dynamics and fragmentation of massive gas clouds - Clues to the masses and radii of galaxies and clusters”. In: *MNRAS* 179, pp. 541–559. DOI: [10.1093/mnras/179.4.541](https://doi.org/10.1093/mnras/179.4.541).

- Reeves, J. N. et al. (2009). “A Compton-thick Wind in the High-luminosity Quasar, PDS 456”. In: *ApJ* 701, pp. 493–507. DOI: [10.1088/0004-637X/701/1/493](https://doi.org/10.1088/0004-637X/701/1/493). arXiv: [0906.0312](https://arxiv.org/abs/0906.0312) [astro-ph.HE].
- Reeves, J. N. et al. (2016). “Discovery of Broad Soft X-ray Absorption Lines from the Quasar Wind in PDS 456”. In: *ApJ* 824, 20, p. 20. DOI: [10.3847/0004-637X/824/1/20](https://doi.org/10.3847/0004-637X/824/1/20). arXiv: [1604.04196](https://arxiv.org/abs/1604.04196) [astro-ph.HE].
- Reines, A. E., J. E. Greene, and M. Geha (2013). “Dwarf Galaxies with Optical Signatures of Active Massive Black Holes”. In: *ApJ* 775, 116, p. 116. DOI: [10.1088/0004-637X/775/2/116](https://doi.org/10.1088/0004-637X/775/2/116). arXiv: [1308.0328](https://arxiv.org/abs/1308.0328).
- Reissner, H. (1916). “Über die Eigengravitation des elektrischen Feldes nach der Einsteinschen Theorie”. In: *Annalen der Physik* 355, pp. 106–120. DOI: [10.1002/andp.19163550905](https://doi.org/10.1002/andp.19163550905).
- Reynolds, C. S. and A. C. Fabian (1995). “Warm absorbers in active galactic nuclei”. In: *MNRAS* 273, pp. 1167–1176. DOI: [10.1093/mnras/273.4.1167](https://doi.org/10.1093/mnras/273.4.1167). eprint: [astro-ph/9502006](https://arxiv.org/abs/astro-ph/9502006).
- Ricarte, A. and P. Natarajan (2018). “The Observational Signatures of Supermassive Black Hole Seeds”. In: *ArXiv e-prints*. arXiv: [1809.01177](https://arxiv.org/abs/1809.01177).
- Rice, W. K. M. et al. (2003). “The effect of cooling on the global stability of self-gravitating protoplanetary discs”. In: *MNRAS* 339, pp. 1025–1030. DOI: [10.1046/j.1365-8711.2003.06253.x](https://doi.org/10.1046/j.1365-8711.2003.06253.x). eprint: [astro-ph/0211088](https://arxiv.org/abs/astro-ph/0211088).
- Richstone, D. et al. (1998). “Supermassive black holes and the evolution of galaxies.” In: *NATURE* 395, A14. eprint: [astro-ph/9810378](https://arxiv.org/abs/astro-ph/9810378).
- Riechers, D. A. et al. (2009). “Imaging The Molecular Gas in a $z = 3.9$ Quasar Host Galaxy at 0farcs3 Resolution: A Central, Sub-Kiloparsec Scale Star Formation Reservoir in APM 08279+5255”. In: *ApJ* 690, pp. 463–485. DOI: [10.1088/0004-637X/690/1/463](https://doi.org/10.1088/0004-637X/690/1/463). arXiv: [0809.0754](https://arxiv.org/abs/0809.0754).
- Risaliti, G., R. Maiolino, and M. Salvati (1999). “The Distribution of Absorbing Column Densities among Seyfert 2 Galaxies”. In: *ApJ* 522, pp. 157–164. DOI: [10.1086/307623](https://doi.org/10.1086/307623). eprint: [astro-ph/9902377](https://arxiv.org/abs/astro-ph/9902377).
- Robinson, D. C. (1975). “Uniqueness of the Kerr black hole”. In: *Physical Review Letters* 34, p. 905. DOI: [10.1103/PhysRevLett.34.905](https://doi.org/10.1103/PhysRevLett.34.905).
- Ruiz, M., S. L. Shapiro, and A. Tsokaros (2018). “GW170817, general relativistic magnetohydrodynamic simulations, and the neutron star maximum mass”. In: *PRD* 97.2, 021501, p. 021501. DOI: [10.1103/PhysRevD.97.021501](https://doi.org/10.1103/PhysRevD.97.021501). arXiv: [1711.00473](https://arxiv.org/abs/1711.00473) [astro-ph.HE].

- Runes, D.D. (2001). *The Dictionary of Philosophy*. Philosophical Library: Concise Dictionaries. Kensington Publishing Corporation. ISBN: 9780806522890. URL: <https://books.google.co.uk/books?id=jipt8dB9licC>.
- Ryu, D. and J. Goodman (1992). "Convective instability in differentially rotating disks". In: *ApJ* 388, pp. 438–450. DOI: [10.1086/171165](https://doi.org/10.1086/171165).
- Salpeter, E. E. (1964). "Accretion of Interstellar Matter by Massive Objects." In: *ApJ* 140, pp. 796–800. DOI: [10.1086/147973](https://doi.org/10.1086/147973).
- Sandage, A. (1965). "The Existence of a Major New Constituent of the Universe: the Quasistellar Galaxies." In: *ApJ* 141, p. 1560. DOI: [10.1086/148245](https://doi.org/10.1086/148245).
- Sanders, R. H. (1970). "The Effects of Stellar Collisions in Dense Stellar Systems". In: *ApJ* 162, p. 791. DOI: [10.1086/150711](https://doi.org/10.1086/150711).
- (1981). "Recurrent Seyfert activity in spiral galaxy nuclei". In: *NATURE* 294, pp. 427–429. DOI: [10.1038/294427a0](https://doi.org/10.1038/294427a0).
- Sargent, W. L. W. et al. (1978). "Dynamical evidence for a central mass concentration in the galaxy M87". In: *ApJ* 221, pp. 731–744. DOI: [10.1086/156077](https://doi.org/10.1086/156077).
- Schaffer, S. (1979). "John Mitchell and Black Holes". In: *Journal for the History of Astronomy* 10, p. 42. DOI: [10.1177/002182867901000104](https://doi.org/10.1177/002182867901000104).
- Schawinski, K. et al. (2015). "Active galactic nuclei flicker: an observational estimate of the duration of black hole growth phases of 10^5 yr". In: *MNRAS* 451, pp. 2517–2523. DOI: [10.1093/mnras/stv1136](https://doi.org/10.1093/mnras/stv1136). arXiv: [1505.06733](https://arxiv.org/abs/1505.06733).
- Schaye, J. et al. (2015). "The EAGLE project: simulating the evolution and assembly of galaxies and their environments". In: *MNRAS* 446, pp. 521–554. DOI: [10.1093/mnras/stu2058](https://doi.org/10.1093/mnras/stu2058). arXiv: [1407.7040](https://arxiv.org/abs/1407.7040).
- Schechter, P. (1976). "An analytic expression for the luminosity function for galaxies." In: *ApJ* 203, pp. 297–306. DOI: [10.1086/154079](https://doi.org/10.1086/154079).
- Scheuer, P. A. G. and R. Feiler (1996). "The realignment of a black hole misaligned with its accretion disc". In: *MNRAS* 282, p. 291. DOI: [10.1093/mnras/282.1.291](https://doi.org/10.1093/mnras/282.1.291).
- Schmidt, M. (1963). "3C 273 : A Star-Like Object with Large Red-Shift". In: *NATURE* 197, p. 1040. DOI: [10.1038/1971040a0](https://doi.org/10.1038/1971040a0).
- Schmidt, M. and T. A. Matthews (1964). "Redshift of the Quasi-Stellar Radio Sources 3c 47 and 3c 147." In: *ApJ* 139, p. 781. DOI: [10.1086/147815](https://doi.org/10.1086/147815).

- Schneider, R. et al. (2006). "Fragmentation of star-forming clouds enriched with the first dust". In: *MNRAS* 369, pp. 1437–1444. DOI: [10.1111/j.1365-2966.2006.10391.x](https://doi.org/10.1111/j.1365-2966.2006.10391.x). eprint: [astro-ph/0603766](https://arxiv.org/abs/astro-ph/0603766).
- Schödel, R. et al. (2002). "A star in a 15.2-year orbit around the supermassive black hole at the centre of the Milky Way". In: *NATURE* 419, pp. 694–696. DOI: [10.1038/nature01121](https://doi.org/10.1038/nature01121). eprint: [astro-ph/0210426](https://arxiv.org/abs/astro-ph/0210426).
- Schwarzschild, K. (1916). "Über das Gravitationsfeld eines Massenpunktes nach der Einsteinschen Theorie". In: *Sitzungsberichte der Königlich Preußischen Akademie der Wissenschaften (Berlin), 1916, Seite 189-196*, pp. 189–196.
- Scoville, N. Z. et al. (2003). "Hubble Space Telescope Pa α and 1.9 Micron Imaging of Sagittarius A West". In: *ApJ* 594, pp. 294–311. DOI: [10.1086/376790](https://doi.org/10.1086/376790). arXiv: [astro-ph/0305350](https://arxiv.org/abs/astro-ph/0305350) [[astro-ph](https://arxiv.org/abs/astro-ph)].
- Searle, L. and R. Zinn (1978). "Compositions of halo clusters and the formation of the galactic halo". In: *ApJ* 225, pp. 357–379. DOI: [10.1086/156499](https://doi.org/10.1086/156499).
- Serabyn, E. and J. H. Lacy (1985). "Forbidden NE II observations of the galactic center - Evidence for a massive block hole". In: *ApJ* 293, pp. 445–458. DOI: [10.1086/163250](https://doi.org/10.1086/163250).
- Serabyn, E. et al. (1986). "CO 1 - 0 and CS 2 - 1 observations of the neutral disk around the Galactic Center." In: *A&A* 169, pp. 85–94.
- Seyfert, C. K. (1943). "Nuclear Emission in Spiral Nebulae." In: *ApJ* 97, p. 28. DOI: [10.1086/144488](https://doi.org/10.1086/144488).
- Shahzamanian, B. et al. (2016). "Polarized near-infrared light of the Dusty S-cluster Object (DSO/G2) at the Galactic center". In: *A&A* 593, A131, A131. DOI: [10.1051/0004-6361/201628994](https://doi.org/10.1051/0004-6361/201628994).
- Shakura, N. I. and R. A. Sunyaev (1973). "Black holes in binary systems. Observational appearance." In: *A&A* 24, pp. 337–355.
- Shakura, N. I., R. A. Sunyaev, and S. S. Zilitinkevich (1978). "On the turbulent energy transport in accretion discs". In: *A&A* 62, pp. 179–187.
- Shaltout, Mosalam and Juan Antonio Belmonte (2005). "On the Orientation of Ancient Egyptian Temples: (1) Upper Egypt and Lower Nubia". In: 36, pp. 273–298.
- Shapiro, S. L. (2005). "Spin, Accretion, and the Cosmological Growth of Supermassive Black Holes". In: *ApJ* 620, pp. 59–68. DOI: [10.1086/427065](https://doi.org/10.1086/427065). eprint: [astro-ph/0411156](https://arxiv.org/abs/astro-ph/0411156).

- Shibata, M. et al. (2017). “Modeling GW170817 based on numerical relativity and its implications”. In: *PRD* 96.12, 123012, p. 123012. DOI: [10.1103/PhysRevD.96.123012](https://doi.org/10.1103/PhysRevD.96.123012). arXiv: [1710.07579](https://arxiv.org/abs/1710.07579) [astro-ph.HE].
- Shklovsky, I. S. (1967). “On the Nature of the Source of X-Ray Emission of Sco XR-1.” In: *ApJL* 148, p. L1. DOI: [10.1086/180001](https://doi.org/10.1086/180001).
- Shlosman, I., J. Frank, and M. C. Begelman (1989). “Bars within bars - A mechanism for fuelling active galactic nuclei”. In: *NATURE* 338, pp. 45–47. DOI: [10.1038/338045a0](https://doi.org/10.1038/338045a0).
- Sijacki, D. and V. Springel (2006). “Hydrodynamical simulations of cluster formation with central AGN heating”. In: *MNRAS* 366, pp. 397–416. DOI: [10.1111/j.1365-2966.2005.09860.x](https://doi.org/10.1111/j.1365-2966.2005.09860.x). eprint: [astro-ph/0509506](https://arxiv.org/abs/astro-ph/0509506).
- Sijacki, D. et al. (2015). “The Illustris simulation: the evolving population of black holes across cosmic time”. In: *MNRAS* 452, pp. 575–596. DOI: [10.1093/mnras/stv1340](https://doi.org/10.1093/mnras/stv1340). arXiv: [1408.6842](https://arxiv.org/abs/1408.6842).
- Silk, J. (1977). “On the fragmentation of cosmic gas clouds. I - The formation of galaxies and the first generation of stars”. In: *ApJ* 211, pp. 638–648. DOI: [10.1086/154972](https://doi.org/10.1086/154972).
- Silk, J. and M. J. Rees (1998). “Quasars and galaxy formation”. In: *A&A* 331, pp. L1–L4. eprint: [astro-ph/9801013](https://arxiv.org/abs/astro-ph/9801013).
- Slipher, V. M. (1917). “Nebulae”. In: *Proceedings of the American Philosophical Society* 56, pp. 403–409.
- Smak, J. (1999). “Dwarf Nova Outbursts. III. The Viscosity Parameter alpha”. In: *ACTAA* 49, pp. 391–401.
- Smith, H. J. and D. Hoffleit (1961). “Photographic History and Suggested Nature of the Radio Source 3C 48”. In: *PASP* 73, p. 292. DOI: [10.1086/127682](https://doi.org/10.1086/127682).
- (1963). “Light Variations in the Superluminous Radio Galaxy 3C273”. In: *NATURE* 198, pp. 650–651. DOI: [10.1038/198650a0](https://doi.org/10.1038/198650a0).
- Sobral, D. et al. (2015). “Evidence for PopIII-like Stellar Populations in the Most Luminous Lyman- α Emitters at the Epoch of Reionization: Spectroscopic Confirmation”. In: *ApJ* 808, 139, p. 139. DOI: [10.1088/0004-637X/808/2/139](https://doi.org/10.1088/0004-637X/808/2/139). arXiv: [1504.01734](https://arxiv.org/abs/1504.01734).
- Soltan, A. (1982). “Masses of quasars”. In: *MNRAS* 200, pp. 115–122. DOI: [10.1093/mnras/200.1.115](https://doi.org/10.1093/mnras/200.1.115).
- Sormani, M. C. and A. T. Barnes (2019). “Mass inflow rate into the Central Molecular Zone: observational determination and evidence of episodic accretion”.

- In: *MNRAS* 484, pp. 1213–1219. DOI: [10.1093/mnras/stz046](https://doi.org/10.1093/mnras/stz046). arXiv: [1901.00867](https://arxiv.org/abs/1901.00867).
- Sparre, M. and V. Springel (2016). “Zooming in on major mergers: dense, starbursting gas in cosmological simulations”. In: *MNRAS* 462, pp. 2418–2430. DOI: [10.1093/mnras/stw1793](https://doi.org/10.1093/mnras/stw1793). arXiv: [1604.08205](https://arxiv.org/abs/1604.08205).
- Spilker, J. S. et al. (2018). “Fast Molecular Outflow from a Dusty Star-Forming Galaxy in the Early Universe”. In: *ArXiv e-prints*. arXiv: [1809.01676](https://arxiv.org/abs/1809.01676).
- Springel, V., T. Di Matteo, and L. Hernquist (2005a). “Black Holes in Galaxy Mergers: The Formation of Red Elliptical Galaxies”. In: *ApJL* 620, pp. L79–L82. DOI: [10.1086/428772](https://doi.org/10.1086/428772). eprint: [astro-ph/0409436](https://arxiv.org/abs/astro-ph/0409436).
- (2005b). “Modelling feedback from stars and black holes in galaxy mergers”. In: *MNRAS* 361, pp. 776–794. DOI: [10.1111/j.1365-2966.2005.09238.x](https://doi.org/10.1111/j.1365-2966.2005.09238.x). eprint: [astro-ph/0411108](https://arxiv.org/abs/astro-ph/0411108).
- Springel, Volker (2010a). “E pur si muove: Galilean-invariant cosmological hydrodynamical simulations on a moving mesh”. In: *MNRAS* 401, pp. 791–851. DOI: [10.1111/j.1365-2966.2009.15715.x](https://doi.org/10.1111/j.1365-2966.2009.15715.x). arXiv: [0901.4107](https://arxiv.org/abs/0901.4107) [[astro-ph.CO](https://arxiv.org/abs/astro-ph)].
- (2010b). “Smoothed Particle Hydrodynamics in Astrophysics”. In: *Annual Review of Astronomy and Astrophysics* 48, pp. 391–430. DOI: [10.1146/annurev-astro-081309-130914](https://doi.org/10.1146/annurev-astro-081309-130914). arXiv: [1109.2219](https://arxiv.org/abs/1109.2219) [[astro-ph.CO](https://arxiv.org/abs/astro-ph)].
- Stacy, A., T. H. Greif, and V. Bromm (2012). “The first stars: mass growth under protostellar feedback”. In: *MNRAS* 422, pp. 290–309. DOI: [10.1111/j.1365-2966.2012.20605.x](https://doi.org/10.1111/j.1365-2966.2012.20605.x). arXiv: [1109.3147](https://arxiv.org/abs/1109.3147).
- Steinborn, L. K. et al. (2018). “Cosmological simulations of black hole growth II: how (in)significant are merger events for fuelling nuclear activity?” In: *MNRAS* 481, pp. 341–360. DOI: [10.1093/mnras/sty2288](https://doi.org/10.1093/mnras/sty2288). arXiv: [1805.06902](https://arxiv.org/abs/1805.06902).
- Stevens, A. R. H. et al. (2017). “How to get cool in the heat: comparing analytic models of hot, cold, and cooling gas in haloes and galaxies with EAGLE”. In: *MNRAS* 467, pp. 2066–2084. DOI: [10.1093/mnras/stx243](https://doi.org/10.1093/mnras/stx243). arXiv: [1608.04389](https://arxiv.org/abs/1608.04389).
- Stone, J. M. et al. (1996). “Three-dimensional Magnetohydrodynamical Simulations of Vertically Stratified Accretion Disks”. In: *ApJ* 463, p. 656. DOI: [10.1086/177280](https://doi.org/10.1086/177280).
- Stone, N. C., A. H. W. Küpper, and J. P. Ostriker (2017). “Formation of massive black holes in galactic nuclei: runaway tidal encounters”. In: *MNRAS* 467, pp. 4180–4199. DOI: [10.1093/mnras/stx097](https://doi.org/10.1093/mnras/stx097). arXiv: [1606.01909](https://arxiv.org/abs/1606.01909).

- Stoner, E. (1930). "The Equilibrium of Dense Stars". In: *The London, Edinburgh, and Dublin Philosophical Magazine and Journal of Science: Series 7, Volume 9, Issue 60*, p. 944-963 9, pp. 944-963.
- Su, Meng, Tracy R. Slatyer, and Douglas P. Finkbeiner (2010). "Giant Gamma-ray Bubbles from Fermi-LAT: Active Galactic Nucleus Activity or Bipolar Galactic Wind?" In: *ApJ* 724, pp. 1044-1082. DOI: [10.1088/0004-637X/724/2/1044](https://doi.org/10.1088/0004-637X/724/2/1044). arXiv: [1005.5480](https://arxiv.org/abs/1005.5480) [astro-ph.HE].
- Sun, Jiayi et al. (2018). "Cloud-scale Molecular Gas Properties in 15 Nearby Galaxies". In: *ApJ* 860, 172, p. 172. DOI: [10.3847/1538-4357/aac326](https://doi.org/10.3847/1538-4357/aac326).
- Sunyaev, R. A. and Y. B. Zeldovich (1972). "Formation of Clusters of Galaxies; Procluster Fragmentation and Intergalactic Gas Heating". In: *A&A* 20, p. 189.
- Swanick, Lois Ann (2006). "An analysis of navigational instruments in the Age of Exploration: 15th century to mid-17th century". PhD thesis. Texas A&M University.
- Tadhunter, C. et al. (2014). "Jet acceleration of the fast molecular outflows in the Seyfert galaxy IC 5063". In: *NATURE* 511, pp. 440-443. DOI: [10.1038/nature13520](https://doi.org/10.1038/nature13520). arXiv: [1407.1332](https://arxiv.org/abs/1407.1332).
- Takekawa, Shunya et al. (2017). "Discovery of Two Small High-velocity Compact Clouds in the Central 10 pc of Our Galaxy". In: *ApJ* 843, L11, p. L11. DOI: [10.3847/2041-8213/aa79ee](https://doi.org/10.3847/2041-8213/aa79ee).
- Tanaka, H., T. Takeuchi, and W. R. Ward (2002). "Three-Dimensional Interaction between a Planet and an Isothermal Gaseous Disk. I. Corotation and Lindblad Torques and Planet Migration". In: *ApJ* 565, pp. 1257-1274. DOI: [10.1086/324713](https://doi.org/10.1086/324713).
- Tegmark, M. et al. (1997). "How Small Were the First Cosmological Objects?" In: *ApJ* 474, p. 1. DOI: [10.1086/303434](https://doi.org/10.1086/303434). eprint: [astro-ph/9603007](https://arxiv.org/abs/astro-ph/9603007).
- Terlevich, R. and J. Melnick (1985). "Warmers - The missing link between Starburst and Seyfert galaxies". In: *MNRAS* 213, pp. 841-856. DOI: [10.1093/mnras/213.4.841](https://doi.org/10.1093/mnras/213.4.841).
- Tombesi, F. et al. (2015). "Wind from the black-hole accretion disk driving a molecular outflow in an active galaxy". In: *NATURE* 519, pp. 436-438. DOI: [10.1038/nature14261](https://doi.org/10.1038/nature14261). arXiv: [1501.07664](https://arxiv.org/abs/1501.07664) [astro-ph.HE].
- Tonini, C. et al. (2016). "The growth of discs and bulges during hierarchical galaxy formation - I. Fast evolution versus secular processes". In: *MNRAS* 459, pp. 4109-4129. DOI: [10.1093/mnras/stw956](https://doi.org/10.1093/mnras/stw956). arXiv: [1604.02192](https://arxiv.org/abs/1604.02192).

- Toomre, A. (1977). "Mergers and Some Consequences". In: *Evolution of Galaxies and Stellar Populations*. Ed. by B. M. Tinsley and R. B. G. Larson D. Campbell, p. 401.
- Trani, A. A., M. Mapelli, and A. Ballone (2018). "Forming Circumnuclear Disks and Rings in Galactic Nuclei: A Competition Between Supermassive Black Hole and Nuclear Star Cluster". In: *ApJ* 864, 17, p. 17. DOI: [10.3847/1538-4357/aad414](https://doi.org/10.3847/1538-4357/aad414). arXiv: [1807.09780](https://arxiv.org/abs/1807.09780).
- Trani, Alessandro A. et al. (2016). "The Influence of Dense Gas Rings on the Dynamics of a Stellar Disk in the Galactic Center". In: *ApJ* 818, 29, p. 29. DOI: [10.3847/0004-637X/818/1/29](https://doi.org/10.3847/0004-637X/818/1/29).
- Treuthardt, P. et al. (2012). "On the link between central black holes, bar dynamics and dark matter haloes in spiral galaxies". In: *MNRAS* 423, pp. 3118–3133. DOI: [10.1111/j.1365-2966.2012.21118.x](https://doi.org/10.1111/j.1365-2966.2012.21118.x). arXiv: [1204.4210](https://arxiv.org/abs/1204.4210).
- Tsuboi, M. et al. (2017). "ALMA View of the Galactic Center Minispiral: Ionized Gas Flows around Sagittarius A". In: *ApJ* 842, 94, p. 94. DOI: [10.3847/1538-4357/aa74e3](https://doi.org/10.3847/1538-4357/aa74e3). arXiv: [1608.08714](https://arxiv.org/abs/1608.08714).
- Turnshek, D. A. et al. (1988). "QSOs with PHL 5200-like broad absorption line profiles". In: *ApJ* 325, pp. 651–670. DOI: [10.1086/166036](https://doi.org/10.1086/166036).
- Ulrich, M.-H., L. Maraschi, and C. M. Urry (1997). "Variability of Active Galactic Nuclei". In: *ARA&A* 35, pp. 445–502. DOI: [10.1146/annurev.astro.35.1.445](https://doi.org/10.1146/annurev.astro.35.1.445).
- Umebayashi, T. and T. Nakano (1988). "Chapter 13. Ionization State and Magnetic Fields in the Solar Nebula". In: *Progress of Theoretical Physics Supplement* 96, pp. 151–160. DOI: [10.1143/PTPS.96.151](https://doi.org/10.1143/PTPS.96.151).
- Umeda, H. and K. Nomoto (2003). "First-generation black-hole-forming supernovae and the metal abundance pattern of a very iron-poor star". In: *NATURE* 422, pp. 871–873. DOI: [10.1038/nature01571](https://doi.org/10.1038/nature01571). eprint: [astro-ph/0301315](https://arxiv.org/abs/astro-ph/0301315).
- Urry, C. M. and P. Padovani (1995). "Unified Schemes for Radio-Loud Active Galactic Nuclei". In: *PASP* 107, p. 803. DOI: [10.1086/133630](https://doi.org/10.1086/133630). eprint: [astro-ph/9506063](https://arxiv.org/abs/astro-ph/9506063).
- Urry, C. M. et al. (2000). "The Hubble Space Telescope Survey of BL Lacertae Objects. II. Host Galaxies". In: *ApJ* 532, pp. 816–829. DOI: [10.1086/308616](https://doi.org/10.1086/308616). eprint: [astro-ph/9911109](https://arxiv.org/abs/astro-ph/9911109).
- Usher, P. D. et al. (1969). "Long-Term Behavior of the Seyfert Galaxy 3c 120". In: *ApJ* 158, p. 535. DOI: [10.1086/150217](https://doi.org/10.1086/150217).

- van der Marel, R. P. and F. C. van den Bosch (1998). "Evidence for a $3 \times 10^8 M_{\odot}$ Black Hole in NGC 7052 from Hubble Space Telescope Observations of the Nuclear Gas Disk". In: *AJ* 116, pp. 2220–2236. DOI: [10.1086/300593](https://doi.org/10.1086/300593). eprint: [astro-ph/9804194](https://arxiv.org/abs/astro-ph/9804194).
- van der Marel, R. P. et al. (1997). "A massive black hole at the centre of the quiescent galaxy M32". In: *NATURE* 385, pp. 610–612. DOI: [10.1038/385610a0](https://doi.org/10.1038/385610a0). eprint: [astro-ph/9702106](https://arxiv.org/abs/astro-ph/9702106).
- Vogelsberger, M. et al. (2014). "Introducing the Illustris Project: simulating the co-evolution of dark and visible matter in the Universe". In: *MNRAS* 444, pp. 1518–1547. DOI: [10.1093/mnras/stu1536](https://doi.org/10.1093/mnras/stu1536). arXiv: [1405.2921](https://arxiv.org/abs/1405.2921).
- Volonteri, M. (2010). "Formation of supermassive black holes". In: *AAPR* 18, pp. 279–315. DOI: [10.1007/s00159-010-0029-x](https://doi.org/10.1007/s00159-010-0029-x). arXiv: [1003.4404](https://arxiv.org/abs/1003.4404).
- Volonteri, M. et al. (2005). "The Distribution and Cosmic Evolution of Massive Black Hole Spins". In: *ApJ* 620, pp. 69–77. DOI: [10.1086/426858](https://doi.org/10.1086/426858). eprint: [astro-ph/0410342](https://arxiv.org/abs/astro-ph/0410342).
- von Hoerner, S. (1960). "Die numerische Integration des n-Ku r Sternhaufen. I". In: *Zeitschrift fur Astrophysik* 50, pp. 184–214.
- Šubr, Ladislav and Jaroslav Haas (2016). "The Properties of Hypervelocity Stars and S-stars Originating from an Eccentric Disk around a Supermassive Black Hole". In: *ApJ* 828, 1, p. 1. DOI: [10.3847/0004-637X/828/1/1](https://doi.org/10.3847/0004-637X/828/1/1).
- Wang, J.-M. et al. (2009). "Episodic Random Accretion and the Cosmological Evolution of Supermassive Black Hole Spins". In: *ApJL* 697, pp. L141–L144. DOI: [10.1088/0004-637X/697/2/L141](https://doi.org/10.1088/0004-637X/697/2/L141). arXiv: [0904.1896](https://arxiv.org/abs/0904.1896) [[astro-ph](https://arxiv.org/abs/astro-ph).GA].
- Waziry, Ayman (2016). "Probability Hypothesis and Evidence of Astronomical Observatories in ancient Egypt". In: Vol.2, pp. 31–50.
- Webster, B. L. and P. Murdin (1972). "Cygnus X-1-a Spectroscopic Binary with a Heavy Companion ?" In: *NATURE* 235, pp. 37–38. DOI: [10.1038/235037a0](https://doi.org/10.1038/235037a0).
- Wendland, Holger (1995). "Piecewise polynomial, positive definite and compactly supported radial functions of minimal degree". In: *Advances in computational Mathematics* 4.1, pp. 389–396.
- Willott, C. J., R. J. McLure, and M. J. Jarvis (2003). "A $3 \times 10^9 M_{\text{solar}}$ Black Hole in the Quasar SDSS J1148+5251 at $z=6.41$ ". In: *ApJL* 587, pp. L15–L18. DOI: [10.1086/375126](https://doi.org/10.1086/375126). eprint: [astro-ph/0303062](https://arxiv.org/abs/astro-ph/0303062).

- Witzel, G. et al. (2014). “Detection of Galactic Center Source G2 at 3.8 μm during Periapase Passage”. In: *ApJ* 796, L8, p. L8. DOI: [10.1088/2041-8205/796/1/L8](https://doi.org/10.1088/2041-8205/796/1/L8). arXiv: [1410.1884](https://arxiv.org/abs/1410.1884) [astro-ph.HE].
- Wolfe, A. M. and G. R. Burbidge (1970). “Black Holes in Elliptical Galaxies”. In: *ApJ* 161, p. 419. DOI: [10.1086/150549](https://doi.org/10.1086/150549).
- Wright, Melvyn C. H. et al. (2001). “Molecular Tracers of the Central 12 Parsecs of the Galactic Center”. In: *ApJ* 551, pp. 254–268. DOI: [10.1086/320089](https://doi.org/10.1086/320089). arXiv: [astro-ph/0011331](https://arxiv.org/abs/astro-ph/0011331) [astro-ph].
- Yang, G. et al. (2016). “Long-term X-Ray Variability of Typical Active Galactic Nuclei in the Distant Universe”. In: *ApJ* 831, 145, p. 145. DOI: [10.3847/0004-637X/831/2/145](https://doi.org/10.3847/0004-637X/831/2/145). arXiv: [1608.08224](https://arxiv.org/abs/1608.08224) [astro-ph.HE].
- Yelda, S. et al. (2014). “Properties of the Remnant Clockwise Disk of Young Stars in the Galactic Center”. In: *ApJ* 783, 131, p. 131. DOI: [10.1088/0004-637X/783/2/131](https://doi.org/10.1088/0004-637X/783/2/131). arXiv: [1401.7354](https://arxiv.org/abs/1401.7354) [astro-ph.GA].
- Young, P. J. et al. (1978). “Evidence for a supermassive object in the nucleus of the galaxy M87 from SIT and CCD area photometry”. In: *ApJ* 221, pp. 721–730. DOI: [10.1086/156076](https://doi.org/10.1086/156076).
- Yu, Q. and S. Tremaine (2002). “Observational constraints on growth of massive black holes”. In: *MNRAS* 335, pp. 965–976. DOI: [10.1046/j.1365-8711.2002.05532.x](https://doi.org/10.1046/j.1365-8711.2002.05532.x). eprint: [astro-ph/0203082](https://arxiv.org/abs/astro-ph/0203082).
- Zel’dovich, Y. B. (1964). “The Fate of a Star and the Evolution of Gravitational Energy Upon Accretion”. In: *Soviet Physics Doklady* 9, p. 195.
- Zhu, Qingfeng et al. (2008). “Radial Velocities of Stars in the Galactic Center”. In: *ApJ* 681, pp. 1254–1278. DOI: [10.1086/588135](https://doi.org/10.1086/588135). arXiv: [0803.1826](https://arxiv.org/abs/0803.1826) [astro-ph].
- Zitrin, A. et al. (2015). “Lyman α Emission from a Luminous $z = 8.68$ Galaxy: Implications for Galaxies as Tracers of Cosmic Reionization”. In: *ApJL* 810, L12, p. L12. DOI: [10.1088/2041-8205/810/1/L12](https://doi.org/10.1088/2041-8205/810/1/L12). arXiv: [1507.02679](https://arxiv.org/abs/1507.02679).
- Zubovas, K. (2015). “AGN activity and nuclear starbursts: Sgr A* activity shapes the Central Molecular Zone”. In: *MNRAS* 451, pp. 3627–3642. DOI: [10.1093/mnras/stv1173](https://doi.org/10.1093/mnras/stv1173). arXiv: [1505.05464](https://arxiv.org/abs/1505.05464).
- (2018). “AGN must be very efficient at powering outflows”. In: *MNRAS* 479, pp. 3189–3196. DOI: [10.1093/mnras/sty1679](https://doi.org/10.1093/mnras/sty1679). arXiv: [1806.08914](https://arxiv.org/abs/1806.08914).
- Zubovas, K. and A. King (2013). “BAL QSOs and Extreme UFOs: The Eddington Connection”. In: *ApJ* 769, 51, p. 51. DOI: [10.1088/0004-637X/769/1/51](https://doi.org/10.1088/0004-637X/769/1/51). arXiv: [1304.1691](https://arxiv.org/abs/1304.1691).

- Zubovas, K. and A. King (2019). “Warm absorbers: supermassive black hole feeding and Compton-thick AGN”. In: *MNRAS* 484, pp. 1829–1837. DOI: [10.1093/mnras/stz105](https://doi.org/10.1093/mnras/stz105). arXiv: [1901.02224](https://arxiv.org/abs/1901.02224).
- Zubovas, K. and A. R. King (2012). “The M - σ relation in different environments”. In: *MNRAS* 426, pp. 2751–2757. DOI: [10.1111/j.1365-2966.2012.21845.x](https://doi.org/10.1111/j.1365-2966.2012.21845.x). arXiv: [1208.1380](https://arxiv.org/abs/1208.1380).
- Zubovas, K., A. R. King, and S. Nayakshin (2011). “The Milky Way’s Fermi bubbles: echoes of the last quasar outburst?” In: *MNRAS* 415, pp. L21–L25. DOI: [10.1111/j.1745-3933.2011.01070.x](https://doi.org/10.1111/j.1745-3933.2011.01070.x). arXiv: [1104.5443](https://arxiv.org/abs/1104.5443).
- Zubovas, K. and S. Nayakshin (2012). “Fermi bubbles in the Milky Way: the closest AGN feedback laboratory courtesy of Sgr A*?” In: *MNRAS* 424, pp. 666–683. DOI: [10.1111/j.1365-2966.2012.21250.x](https://doi.org/10.1111/j.1365-2966.2012.21250.x). arXiv: [1203.3060](https://arxiv.org/abs/1203.3060).
- Zubovas, K. et al. (2013). “AGN outflows trigger starbursts in gas-rich galaxies”. In: *MNRAS* 433, pp. 3079–3090. DOI: [10.1093/mnras/stt952](https://doi.org/10.1093/mnras/stt952). arXiv: [1306.0684](https://arxiv.org/abs/1306.0684).
- Šprajc, Ivan (2016). “Astronomy and power in Mesoamerica”. In: pp. 185–192.